

Closed-Cycle, High-Temperature Central Receiver Concept for Solar Electric Power

ER-629
Research Project 377-1

Final Report, January 1978

Prepared by

BOEING ENGINEERING AND CONSTRUCTION
A Division of The Boeing Company
P.O. Box 3707
Seattle, Washington 98124

Program Manager
John R. Gintz

Prepared for

Electric Power Research Institute
3412 Hillview Avenue
Palo Alto, California 94304

EPRI Project Manager
John E. Cummings
Fossil Fuel and Advanced Systems Division

LEGAL NOTICE

This report was prepared by Boeing Engineering and Construction (BEC), a division of The Boeing Company, as an account of work sponsored by the Electric Power Research Institute, Inc. (EPRI). Neither EPRI, members of EPRI, BEC, nor any person acting on behalf of either: (a) makes any warranty or representation, express or implied, with respect to the accuracy, completeness, or usefulness of the information contained in this report, or that the use of any information, apparatus, method, or process disclosed in this report may not infringe privately owned rights; or (b) assumes any liabilities with respect to the use of, or for damages resulting from the use of, any information, apparatus, method, or process disclosed in this report.

ABSTRACT

Conversion of solar energy to electrical energy has assumed increasing significance resulting from expanded energy requirements and the potential resource and cost constraints of conventional fossil-fuel sources. Energy conversion in conjunction with a turbine-generator set is the subject of this report.

In December 1974 the Electric Power Research Institute (EPRI) contracted Boeing to examine the technical feasibility of a high-temperature, gas-cooled central receiver for solar energy in conjunction with a closed helium Brayton cycle for collecting the receiver thermal energy and converting that energy to electrical power. These choices were based upon the following rationale: (1) previous studies have identified the central receiver system as the most economically attractive concept; (2) the Brayton gas cycle operation precludes the two-phase flow problems of water/steam Rankine cycles; (3) gas operation at high temperatures promises the highest power conversion efficiencies and lowest cost; and (4) the minimum cooling water requirements facilitate plant siting.

The technical feasibility of a high-temperature central receiver in a solar plant employing closed-cycle helium as a heat transport fluid was examined in terms of system life, efficiency, cost, and technology requirements. These considerations have been implemented in the conceptual design of a receiver and its components for utilization in a solar plant of 100 megawatts of electrical power output. The rationale is provided that supports the configuration, equipment arrangement, and material choices. Thermal cycling tests simulating 30-year lifetime of the receiver's heat exchangers at temperatures to 816°C ($1,500^{\circ}\text{F}$) and at 3.45-MN/m^2 (500 psi) helium pressure, confirmed material choices. Preliminary design considerations are presented for a 1 megawatt thermal test receiver and for a 10 megawatt electrical pilot plant.

The report also contains system/supporting-subsystem definition for employing the central receiver design in a solar plant. This includes conceptual design of several thermal energy storage devices and their integration into plant operation.

The information developed during the study is presented in this final technical report. The final report selectively includes and expands the content of interim reports produced for EPRI that covered study results through August 1975. These reports and a final summary report are available from EPRI.

ACKNOWLEDGMENTS

The constructive program guidance afforded by Mr. Piet B. Bos, Solar Energy Program Director at EPRI, and by Dr. John E. Cummings and Mr. John E. Bigger, Project Managers, is gratefully acknowledged. The EPRI support provided in specialist areas by Mr. Robert Jaffe, Mr. Roger Richman, Mr. John Stringer, Mr. Michael Miller, and Mr. Gordon Sheridan is also appreciated.

The efforts of the Boeing people who made major contributions to this study are also acknowledged. These include: Mr. Fred Baisch, Mr. Don Bartlett, Mr. William Beverly, Mr. Tom Cunningham, Mr. William Engle, Mr. Mark Rubeck, Mr. Roger Shannon, Mr. Ernest Valley, Mr. Gary Vieth, Mr. William Walker, and Mr. Ronald Zentner. Mr. John Lowe, Solar Energy Systems Manager, and Mr. John Gintz, Program Manager, provided the necessary program direction and resources. This report was prepared by Mr. Keith Halvorson, Technical Leader.

Sincere appreciation is expressed to Mr. Paul Kogita and Mr. Mark Martin, who, with the Boeing Aerospace graphics staff, produced the tables, figures, report design and layout, and coordinated report production, and to Ms. Lorraine Healy for the typing and secretarial assistance.

CONTENTS

<u>Section</u>		<u>Page</u>
1.0	INTRODUCTION	1-1
	1.1 Study Objectives	1-1
	1.2 Study Ground Rules	1-2
	1.3 Study Schedules	1-5
	1.4 Report Organization	1-5
2.0	SUMMARY OF RESULTS	2-1
	2.1 Receiver Concept	2-1
	2.2 Receiver Life	2-3
	2.3 System Performance	2-4
	2.4 Technology Requirements	2-9
	2.5 Receiver Verification	2-9
	2.6 Cost	2-9
3.0	BASELINE CENTRAL RECEIVER CONCEPT	3-1
	3.1 Receiver Requirements and Implementation	3-1
	3.2 Receiver Characteristics	3-2
	3.3 Receiver Technology Requirements	3-13
	3.4 Receiver Cost	3-13
4.0	CENTRAL RECEIVER ANALYSES AND TRADES	4-1
	4.1 Configuration Trades	4-1
	4.2 Thermal Analysis	4-11
	4.3 Structural Considerations	4-31
	4.4 Receiver Cost Trades	4-41
5.0	TURBOMACHINERY/CYCLE ANALYSIS	5-1
	5.1 System Baseline (Closed Cycle Helium)	5-1
	5.2 Helium Turbomachinery Availability	5-8
	5.3 System Design Alternatives	5-11
	5.4 Adaptations for Plant Operation and Control	5-26
6.0	ENERGY STORAGE	6-1
	6.1 Storage Concepts Screening	6-2
	6.2 TES System Conceptual Design	6-6

<u>Section</u>	<u>Page</u>
6.3 Storage and Power Plant Integration	6-41
6.4 References	6-53
7.0 MATERIAL SELECTION AND TEST	7-1
7.1 Material Selection	7-1
7.2 Material Tests	7-1
7.3 Thermal-Cycle Tests	7-3
7.4 Elevated-Temperature Rupture Tests	7-17
7.5 Material Test Results	7-33
8.0 PLANT IMPLEMENTATION	8-1
8.1 Plant Concept	8-1
8.2 Plant Operation and Integration	8-5
8.3 Plant Transients	8-17
8.4 Plant Costs	8-27
9.0 RECEIVER SCALE MODEL	9-1
9.1 Introduction	9-1
9.2 Model Receiver Configuration and Test Plan	9-2
9.3 Model Design	9-12
10.0 10-MW _e SCALE PILOT PLANT	10-1
10.1 Conceptual Design of Pilot Plant Receiver	10-1
10.2 Pilot Plant Turbomachinery	10-4
10.3 Pilot Plant Schedule	10-6
11.0 CONCLUSIONS AND RECOMMENDATIONS	11-1
11.1 Conclusions	11-1
11.2 Recommendations	11-4
APPENDIX A: RECEIVER/TOWER INTEGRATION	A-1

FIGURES

<u>Figure</u>		<u>Page</u>
1-1	"Strawman" Plant/Field Concept	1-3
1-2	Subsystem Efficiencies	1-4
1-3	100-MWe Rated Intermediate Load Plants	1-4
1-4	Initial Study Schedule	1-6
1-5	Continuation Study Task Schedule	1-6
2-1	Receiver Upper Tower Configuration	2-1
2-2	Receiver Concept/Schematic	2-2
2-3	Receiver with Roof Removed Exposing Heat Exchanger Panels	2-3
2-4	Selected Thermal Cycle	2-5
2-5	Performance of Intermediate Load Plants	2-8
2-6	Relative Cost of System Elements	2-10
3-1	Insolation Profiles--Inyokern, California	3-2
3-2	External Structural Arrangement	3-3
3-3	Support Structural Concept to Traverse Field Flux	3-4
3-4	Heat Exchanger Panel	3-6
3-5	Heat Exchanger Panel Detail	3-6
3-6	Receiver Piping Concept	3-7
3-7	Receiver Heat Input	3-10
3-8	Representative Receiver Temperatures	3-11
3-9	Insulation Concept	3-12
4-1	Typical Central Receiver Configuration	4-2
4-2	Receiver Support Structure Candidates	4-3
4-3	Solar Heat Flux on Outboard Support Strut	4-4
4-4	Cavity Efficiency	4-5
4-5	Distribution of Solar Flux in Cavity Receiver	4-5
4-6	Heat Flux to Receiver Walls	4-7
4-7	Cavity Receiver Evaluation	4-8
4-8	Original and Current Structural Design Concepts	4-9
4-9	Receiver Support Structure Design/Temperature	4-10

<u>Figure</u>		<u>Page</u>
4-10	Heat Flux Distribution--Horizontal Circular Aperture	4-12
4-11	Receiver Thermal Efficiency at Part-Load Conditions	4-12
4-12	Thermal Design and Analysis Activity	4-13
4-13	Heat Exchanger Tube Performance	4-14
4-14	Receiver Cooldown at Night--No Doors	4-16
4-15	Receiver Cooldown at Night--With Doors	4-16
4-16	Receiver Thermal Model	4-18
4-17	Thermal Conductivity of Kaowool (Alumina-Silica) and Mineral Wool Products	4-19
4-18	Normal Spectral Reflectance of $[Al_2O_3 + SiO_2]$ Powders	4-21
4-19	Normal Spectral Emittance of $[Al_2O_3 + SiO_2]$ Powders	4-21
4-20	Heat Exchanger Thermal Model for Initial Studies	4-23
4-21	Temperature Data--Heat Exchanger Thermal Model	4-24
4-22	Performance Data--Heat Exchanger Thermal Model	4-24
4-23	Revision of Standard Heat Exchanger Panel	4-25
4-24	Heat Exchanger Tube Performance	4-27
4-25	Receiver Temperature Required to Achieve Heat Transfer	4-28
4-26	Performance Comparison--Heat Transfer per Tube	4-29
4-27	Performance Comparison--Peak Tubing Temperature	4-30
4-28	Heat Exchanger Panel Requirements Using New Configuration	4-31
4-29	Seismic Risk Map--Algermissen	4-32
4-30	Alternate Shapes--Structural Arrangements	4-33
4-31	Tower Configuration	4-35
4-32	Tower Seismic Analysis Results	4-36
4-33	Equipment at Lower Tower Location	4-36
4-34	Haynes 188 Material Characteristics	4-38
4-35	Tube Wall Thickness Selection	4-40
4-36	Tube Configuration Selection	4-41
4-37	Receiver Cost Economies	4-42
5-1	Pressure Ratio Effect on Efficiency	5-3
5-2	Pressure Ratio Effect on Work/Mass Flow	5-3
5-3	Helium Cycle Efficiency	5-5
5-4	Helium Precooler Surface Area	5-5
5-5	Helium Recuperator Surface Area	5-6
5-6	Helium Cycle Pressure Ratio	5-7
5-7	Helium Mass Flow	5-7
5-8	Helium Turbine Installation at Oberhausen, Germany	5-8

<u>Figure</u>		<u>Page</u>
5-9	100 MW He-Turbine	5-10
5-10	Closed Air Cycle Efficiency	5-12
5-11	Closed Cycle Air Recuperator Surface Area	5-13
5-12	Open Air Cycle Efficiency	5-13
5-13	Open Cycle Air Recuperator Surface Area	5-14
5-14	Cycle Thermal Efficiency	5-14
5-15	Recuperator Volume	5-16
5-16	Engine Diameter	5-16
5-17	Helium versus Air-Recuperator Volume	5-17
5-18	Helium versus Air-Recuperator Pressure Loss	5-17
5-19	Relative Size of Turbomachinery	5-19
5-20	Relative Sizes of Recuperators	5-19
5-21	Precooler Costs	5-20
5-22	Recuperator Costs	5-21
5-23	Turbomachinery Costs	5-22
5-24	100 MWe Brayton Cycle Costs	5-22
5-25	Recuperator Costs for 982 ^o C (1800 ^o F) System	5-24
5-26	Turbomachinery Costs for 982 ^o C (1800 ^o F) System	5-24
5-27	100-MWe Brayton-Cycle Costs for 982 ^o C (1800 ^o F) System	5-25
5-28	Cycle Thermal Efficiency	5-25
5-29	Cycle Performance	5-28
5-30	Pressure Level	5-28
6-1	Energy Storage Investment Cost Comparison	6-5
6-2	Candidate Sensible Heat TES	6-7
6-3	Candidate Fusion Salts	6-9
6-4	Candidate Fluoride Salts	6-10
6-5	Candidate Thermochemical Reactions	6-10
6-6	Sensible Heat TES	6-13
6-7	Sensible Heat TES Tank Schematic	6-14
6-8	Phase Change TES	6-17
6-9	Thermochemical Energy Storage System	6-22
6-10	Chemical Energy Storage System--Reactant Generation Cycle	6-30
6-11	Chemical Energy Storage System--Heat Generation Cycle	6-31
6-12	Cutaway View of Catalytic Reactor	6-32
6-13	Cutaway Sketch of Fractionation Column	6-34
6-14	Exothermic Reactor Startup Transient	6-39

<u>Figure</u>		<u>Page</u>
6-15	Thermal Energy Storage System Performance	6-42
6-16	Latent Heat TES Roundtrip Efficiency	6-44
6-17	TES Performance Model	6-45
6-18	TES Temperature Profile (Sensible Heat)	6-47
6-19	TES Temperature Profile (Phase Change)	6-47
6-20	Transmission of Fluoride Salts	6-48
6-21	Thermochemical Energy Storage Requirements and Performance	6-49
6-22	Storage/Plant Schematic	6-52
7-1	Stress Rupture Properties at 1600 ⁰ F (870 ⁰ C)	7-2
7-2	Header/Tube Weld (Haynes 188)	7-4
7-3	Weld Joint Microstructure (Haynes 188)	7-5
7-4	Heat Exchanger Test Specimen	7-6
7-5	Thermal Cycle Test Schematic	7-7
7-6	Thermocouple Locations	7-8
7-7	Test Specimen Assembly	7-9
7-8	Thermal Cycle Test Conditions (Simulated 30-Year Life)	7-10
7-9	Specimen in Test	7-11
7-10	Test Cycle Data Sheet-Helium	7-12
7-11	Test Cycle Data Sheet-Air	7-13
7-12	Test Results-Specimen Dimensional Changes	7-15
7-13	Wall Bending Effects	7-16
7-14	Haynes 188 Tube Header Weld Joint After Test	7-18
7-15	Outer Wall of 180 ⁰ Bend Microstructure for Haynes 188 After Cycling	7-19
7-16	Haynes 188 Tubine-Microstructure, 500 x Kallings Etch	7-20
7-17	Inconel 617 Tubine-Microstructure, 500 x, Kallings Etch	7-21
7-18	Elevated Temperature Rupture Test Specimens	7-22
7-19	Test Bed and IR Lamp Arrays	7-23
7-20	Specimen in One Test Bed	7-24
7-21	Longitudinal Temperature Gradients	7-25
7-22	Tube Ballooning After Rupture	7-27
7-23	Tube Rupture Sites	7-28
7-24(a)	Haynes 188 Microstructure (Previously Cycled Material)	7-29
7-24(b)	Inconel 617 Microstructure (Previously Cycled Material)	7-30
7-24(c)	Haynes 188 Microstructure (New Material)	7-31
7-24(d)	Inconel 617 Microstructure (New Material)	7-32

<u>Figure</u>		<u>Page</u>
8-1	Plant Operation Computer Program Schematic	8-6
8-2	Thermodynamic State Points	8-7
8-3	Storage/Plant Schematic	8-10
8-4	Plant Operation-Representative Daily Cycle (Power Distribution) (Latent Heat TES System)	8-11
8-5	4-Day Performance Summary (Sensible Heat TES System)	8-13
8-6	4-Day Performance Summary (Latent Heat TES System)	8-14
8-7	4-Day Performance Summary (Thermochemical TES System)	8-15
8-8	100 MW _e Solar Power Plant Cost Accounts	8-16
8-9	Plant Performance Sensitivity	8-17
8-10	Closed Cycle Helium Plant Performance	8-18
8-11	Plant Response Chain	8-19
8-12	Receiver Heat Exchanger Tube and Helium Temperature in Steady Operation	8-22
8-13	Receiver Heat Exchanger Tube Response to Input Heat Removal	8-23
8-14	Downcomer Responses to Inlet Temperature Drop	8-25
8-15	Temperature Profiles in 750 Ft (229 M) Downcomer as Response to Sudden Inlet Temperature Drop in Helium	8-26
8-16	Plant Cost Comparisons	8-28
8-17	100 MWe Plant Cost	8-29
9-1	Features of Proposed Test Program	9-3
9-2	Test Model Configuration	9-6
9-3	Model Configuration for ERDA Thermal Test Facility	9-6
9-4	Model Test Gas Flow Schematic	9-8
9-6	Test Facility Requirements/Test Data Acquisition	9-10
9-8	Receiver Heat Transfer Functions and Characteristics	9-13
9-9	Analytical Models, Gas in Tube Heat Transfer	9-15
9-10	Exact Geometric Scaling-Scale Ratio = 0.0577	9-21
9-11	Tubing Distortions Considered for Scale Model	9-21
9-12	Feasible 1-MW _{th} Bench Model Heat Exchanger Designs with Helium	9-23
9-13	Acceptable Designs for the 1-MW _{th} Bench Model Heat Exchanger with Helium	9-24
9-14	Feasible 1-MW _{th} Bench Model Heat Exchanger Designs Using Air, Exact Temperature Matching	9-25
9-15	Feasible 1-MW _{th} Bench Model Heat Exchanger Designs with 500 psia Superheated Steam	9-25
9-16	Acceptable 1-MW _{th} Bench Model Designs Using Air or Superheated Steam as Working Fluid	9-27

<u>Figure</u>		<u>Page</u>
9-17	Gas Velocity and Pressure Loss for Candidate Heat Exchanger Design	9-27
9-18	Effect of Tubing Distortion for Reduced Pressure Drop on Gas Temperatures and Gradients	9-29
9-19	Distortion of Model Temperatures to Accommodate Low Pressure Flow	9-30
10-1	Relative Performance of Air-in-Tube versus High Pressure Helium-in-Tube Heat Exchangers	10-3
10-2	Commercial Plant Development Program	10-6
A-1	Equipment at Upper Tower Location	A-1
A-2	Tower Configuration	A-3
A-3	Seismic Response Spectra	A-4
A-4	Tower Seismic Analysis Results	A-5
A-5	Seismic and Wind Load Comparisons	A-6
A-6	Equipment at Lower Tower Location	A-6

TABLES

<u>Table</u>		<u>Page</u>
4-1	Radiant Surface Properties for Receiver Thermal Model	4-19
5-1	Qualitative Assessment of Alternate Systems	5-26
6-1	Energy Storage Systems Economic Data Near Term Technology	6-3
6-2	Energy Storage Systems Economic Data Long Term Technology	6-3
6-3	CES Parasitic Power Requirements	6-50
7-1	Heat Exchanger Material Selection	7-2
7-2	Material Fabrication Characteristics	7-3
7-3	Test Specimen Tube Dimensions	7-6
7-4	Oxidation Sample Weights	7-15
7-5	Material Property Summary	7-15
7-6	Cycles to Failure	7-26
7-7	New Material Specimen Diameter Data	7-26

Section 1.0 INTRODUCTION

This report presents the results of a study of the technical and economic feasibility of a high-temperature central receiver utilizing closed-cycle helium for heat absorption in the receiver and heat conversion in a turbine-generator. The report encompasses the work performed for the Electric Power Research Institute (EPRI) from December 1974 through June 1976.

Figure 1-1 illustrates a central receiver system and shows a receiver mounted on top of a tower located centrally in a heliostat field. Reflected solar energy from the heliostats is directed through an aperture in the bottom of the receiver. The energy is reflected from the receiver walls onto high-temperature heat exchangers through which the working fluid, helium, is circulated. The heated helium is transported to a turbine located either at the top or the base of the tower. The high-temperature and thermal properties of helium combine to provide the potential for highly efficient conversion of the thermal energy to electrical power.

1.1 STUDY OBJECTIVES

The study objectives, established at contract initiation, include central receiver conceptual design; system integration and costs; and a materials test program to verify receiver design. Specifically, the study was directed to:

- Determine technical feasibility of a high-temperature central receiver utilizing a closed-cycle helium system, considering lifetime, efficiency, cost, and technology requirements
- Provide a general system definition and system performance parameters for a central receiver concept to produce 100-MW_e output
- Perform supporting thermal-cycle tests of representative receiver heat exchanger elements to verify operational lifetime at high temperature
- Provide a concept definition of a 1-MW_{th} test model receiver to simulate the 100-MW_e concept, including a development plan and cost estimate

These objectives have been met during the contract period and are documented in this report.

1.2 STUDY GROUND RULES

The major ground rules have been cited in paragraph 1.1. Other initial ground rules were to:

- Size the receiver to produce 100 MW_e at the generator.
- Utilize state-of-the-art high-temperature materials.
- Design for 30-year life for major components.
- Design to the Inyokern, California, location and for insolation load and seismic risk.
- Design to operate in winds of 18 meters per second (40 miles per hour) and to survive winds of 36 meters per second (80 miles per hour), with gusts to 54 meters per second (120 miles per hour).
- Assume tower height could not exceed 315 meters (1,000 feet).
- Assume storage is available, but is not a factor in the initial conceptual design.

The last two items were modified by contract redirection received from EPRI after completion of the initial study phase in August 1975. Tower height was defined at a maximum 260 meters. Energy storage concepts were to be screened, a preliminary selection made, and thermal energy storage integrated into the plant conceptual design, performance, and operations.

The EPRI redirection for the study continuation after August 1975 was extensive enough to have a major impact on study orientation. The major changes, instituted to permit EPRI to make comparative evaluations of alternative central receiver concepts, are described in subsequent paragraphs.

Plant and field descriptions were provided to put the major contract emphasis on receiver design and performance. The two 100-MW_e intermediate load plants to be examined were the stand-alone plant, consisting of two 50-MW_e plant modules with 6 hours of thermal storage, and a 100-MW_e hybrid plant, consisting of one module with 1/2 hour of thermal storage and fossil fuel backup.

The basic module (EPRI "strawman") consisted of a centrally located 260-meter tower and a collector field with characteristics as described on figure 1-1.

Subsystems	Central receiver	
Collector		
Tracking	}	0.703
Aiming		
Shading		
Blocking		
First reflectivity		0.880
Second reflectivity		—
Receiver		
Absorptivity	0.900	◀
Thermal losses	0.970	◀
Distribution pump losses	0.985	◀
Distribution line thermal losses	1.000	◀
Turbine/generator	0.360	◀
Overall efficiency (1)	0.192	◀

◀ Boeing Study Emphasis

(1) Does not include waste heat or storage losses

Figure 1-2. Subsystem Efficiencies

Plant type	Stand-alone	Hybrid
Collector area (km ²)	1.0	0.5
Storage time (hour)	6	0.5
Account		
Land	2	1
Structures and facilities	44	51
Heliostats*	600	300
Central receiver/tower**/heat exchanger	95	68
Storage/tanks***	180	15
Boiler plant	—	73
Turbine plant equipment	80	80
Electric plant equipment	21	21
Misc plant equipment	4	4
Allowance for cooling towers	20	20
Total direct cost	1,046	633
Contingency allowance and spare parts allowance (5%)	52	33
Indirect costs (10%)	105	63
Total capital investment (1975)	1,203	728
Interest during construction 15%	180	109
Total cost at year of commercial option	1,383	837

*Collector cost—\$60/m²

**Tower height—260m (2, and 1 tower(s), respectively)

***Thermal storage cost—\$30/kWh

Figure 1-3. 100-MWe Rated Intermediate Load Plants (\$/kWe)

1.3 STUDY SCHEDULES

To accomplish the objectives cited in section 1.1, the initial study was organized into the six major tasks shown on figure 1-4. Pertinent task milestones are included to indicate major task content. When the study was expanded into a continuation phase in August 1975, the major objectives were retained and new tasks were written to describe the changing emphasis of the study. Figure 1-5 lists the tasks and the significant task milestones. The new storage work, operational analyses, and the refined receiver design were included under task 1. A new task, task 2, was written to make qualitative comparisons between closed-cycle helium and alternative cycles. The other tasks expanded the interim study efforts in areas of test model receiver design and planning, materials testing, and cost estimation.

1.4 REPORT ORGANIZATION

Sections of this final technical report are organized to respond to the study objectives stated in section 1.1. Section 2.0 provides a summary of major results. Section 3.0 defines the central receiver design concept selected during the study. The central receiver analyses and trades made to arrive at that definition are contained in section 4.0. Section 5.0 details the cycle analyses and turbomachinery selection process, section 6.0 treats thermal energy storage. Section 7.0 details material selection, the high-temperature material testing performed, and the subsequent evaluations.

Plant implementation operations and costs are covered in section 8.0. The 1-MW_{th} bench model receiver concept to simulate the receiver design concept in a 100-MW_e system is discussed in section 9.0 and covers model scaling, design, a development plan, and preliminary cost estimates. A 10-MW_e pilot plant is discussed in section 10.0. The report is completed with the conclusions and recommendations for further emphasis contained in section 11.0.

Section 2.0

SUMMARY OF RESULTS

Study results confirm a high-temperature central receiver, employing closed-cycle helium, to be a promising choice for solar thermal conversion plants. The concept is technically feasible and has the potential to be cost effective because of the high thermal engine efficiency obtainable with helium and the simplicity of associated plant equipment. The concept, its operation, and the significant results for each of the major feasibility criteria are summarized in this section. The applicability also extends to closed-cycle air.

2.1 RECEIVER CONCEPT

The most promising configuration is shown by the scale model photo of figure 2-1. The receiver configuration features a lower hemispherical section and an upper cylindrical section to facilitate internal heat containment and distribution. An aperture to admit reflected energy from the collector field is located at the bottom of the receiver.

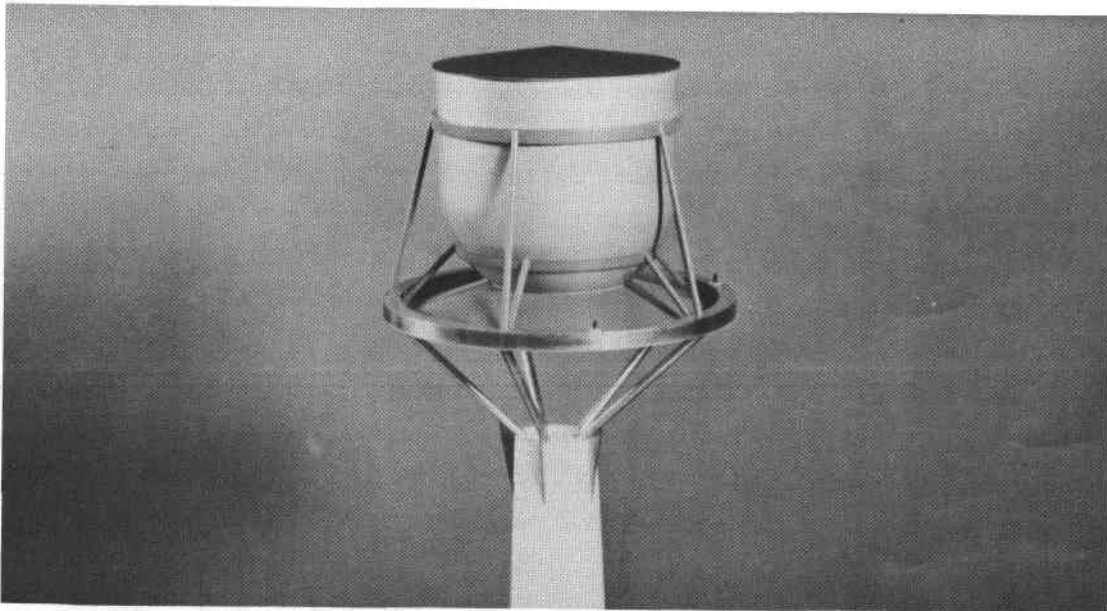


Figure 2-1. Receiver Upper Tower Configuration

The receiver is externally supported above the tower top. All associated helium plant equipment is located at the base of the tower.

Figure 2-2 illustrates the receiver concept, major equipment, and concept schematic operation. The picture on the left-hand side again shows the receiver and

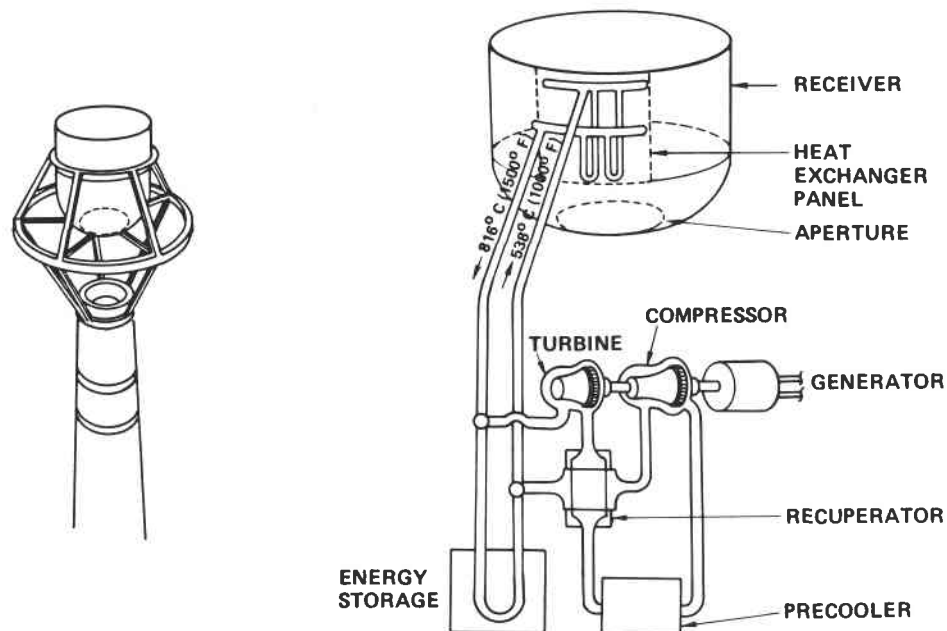


Figure 2-2. Receiver Concept/Schematic

the support structure from the tower. The right-hand side schematic identifies the major components of the receiver/solar-plant concept. Heat exchanger panels are mounted within the receiver's upper cylindrical section to transfer receiver heat to the circulating helium. Helium inlet and outlet temperatures are 538°C (1,000°F) and 816°C (1,500°F) respectively. The upper limit of 816°C (1,500°F) was chosen to increase helium-cycle efficiency while remaining within the state of the art of practical high-temperature metals. Operating pressure was chosen at 3.45 MN/m² (500 psi), consistent with helium turbine operational experience and mass flow requirements. The associated energy-conversion and helium-processing equipment shown below the receiver is located at the base of the tower. The primary flow circuit from the receiver is through the turbine(s), the recuperator (low-pressure side), the precooler, the compressor(s), the recuperator (high-pressure side), and back to the receiver. An alternative thermal energy storage

loop is shown from the receiver to extend solar plant electrical power production into noninsolation hours.

The photograph on figure 2-3 of the scale model receiver with the roof removed illustrates the routing arrangement of the heat exchanger panels in the upper half of the receiver. There are three rows of these panels with 70 panels in each row.

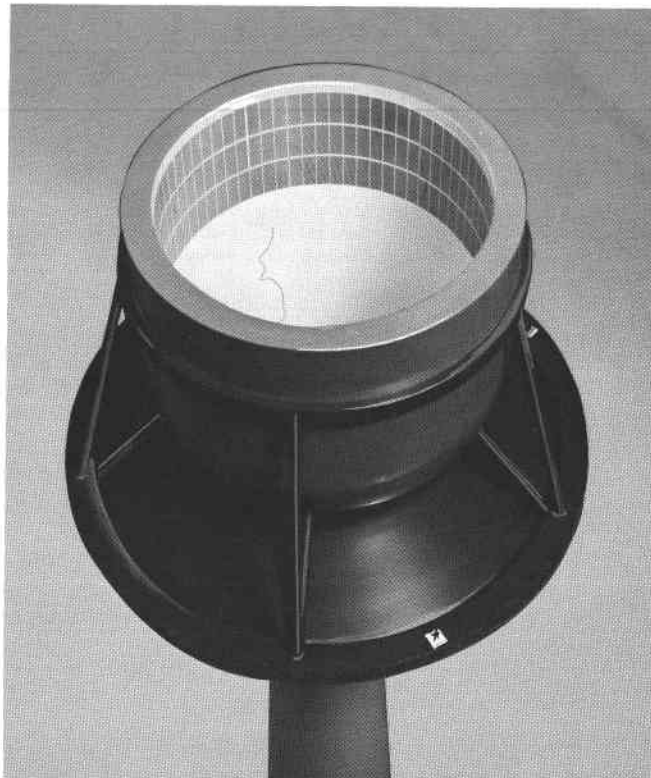


Figure 2-3. Receiver With Roof Removed Exposing Heat Exchanger Panels

2.2 RECEIVER LIFE

Materials are available to withstand the high temperatures encountered under repeated thermal cycling of the receiver and heat exchanger tubes in daily operation. Thermal cycling tests simulating 30-year lifetime at expected temperatures and pressure have been completed on two candidate material, Haynes H-188 and Inconel 617 alloys. No adverse effects were detected for the design temperature limitation chosen of 816°C ($1,500^{\circ}\text{F}$) or the 3.45-MN/m^2 (500-psi) internal pressure.

The initial material concerns were the large number of thermal cycles to be experienced in 30 years of operational life and the large thermal swing of each daily cycle up to 816°C ($1,500^{\circ}\text{F}$). To accommodate these factors, an original

concept had included receiver aperture doors, as well as a "keep warm" circuit to reduce the magnitude of the thermal cycle. However, as more in-depth data for candidate materials were reviewed, it became evident that thermal cycling stress over the number of cycles was not the only problem. The time at high temperature, particularly temperatures in excess of 760°C (1,400°F), was determined to be an important constraint due to material creep properties. Accordingly, the provisions for aperture doors and "keep warm" circuitry were deleted, significantly simplifying the receiver and helium circuit configurations, as well as reducing the operating time at high temperatures.

A subsequent concern with the wide temperature range of materials was for increased surface loss through oxidation and scaling. This has been proven by test to be insignificant with no measurable evidence of oxide layer loss.

An additional test was performed to determine the capability of Haynes H-188 and Inconel 617 to withstand temperatures considerably higher than the operational limit of 816°C (1,500°F). All the tubes were able to sustain temperatures of 1,037° to 1,092°C (1,900° to 2,000°F) at 3.45-MN/m² (500-psi) pressure before rupture occurred.

2.3 SYSTEM PERFORMANCE

2.3.1 Receiver Performance

A thermal balance of the selected receiver concept for noontime operation in summer and winter is summarized below.

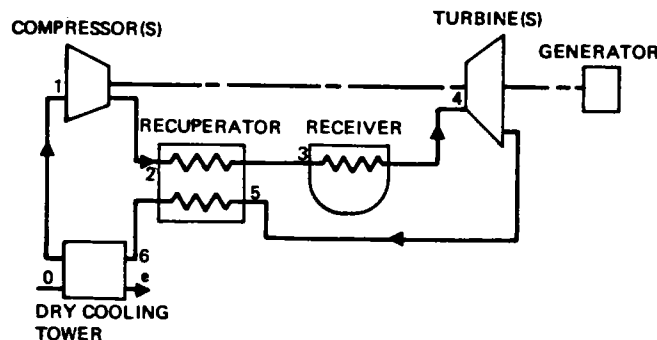
THERMAL MEGAWATTS		
	<u>Summer</u>	<u>Winter</u>
Solar input to receiver	315.0	259.0
Receiver losses:		
● Reflection out aperture	11.9	9.7
● Reradiation out aperture	33.1	29.5
● Convection to air	2.5	2.4
● Conduction through walls	6.0	5.7
Total losses	53.5	47.3
Heat removed by helium	261.5	211.7

The heat removed by the helium gives the receiver an 83% efficiency in summer, 81.7% in winter. The largest loss at both time periods is due to reradiation of the energy back out of the aperture, an unavoidable circumstance of high-temperature cavities. The reflection losses, minimized by the receiver shape, are due to those portions of entering energy that never get absorbed before escaping through the aperture. Convection and conduction losses are small. For a hybrid plant the receiver has to supply $230 \text{ MW}_{\text{th}}$ to produce $100 \text{ MW}_{\text{e}}$. The summer-noon condition exceeds this requirement, while the winter-noon condition is slightly deficient.

2.3.2 Closed-Cycle Performance

The study of closed gas cycles for a solar plant was predicated on the advantages offered by the higher power conversion efficiencies and lower costs of such systems. This has been exemplified in the helium cycle selected for use with the receiver/plant concept documented herein. Similar considerations apply to closed air cycles as well.

The design cycle selected provides an estimated thermodynamic efficiency of 0.44. The cycle schematic and parameter are displayed on figure 2-4.



BASELINE:

T_4 - TURBINE INLET TEMP	816°C (1,500°F)
T_1 - COMPRESSOR INLET TEMP	49°C (120°F)
T_0 - AMBIENT TEMP	27°C (80°F)
P_2/P_1 - PRESSURE RATIO	1.9
P_2 - MAXIMUM PRESSURE	3.45 MN/m ² (500 psi)
η_e - RECUPERATOR EFFECTIVENESS	0.94
η_t - CYCLE EFFICIENCY	0.44

Figure 2-4. Selected Thermal Cycle

The turbine inlet temperature of 816°C ($1,500^{\circ}\text{F}$) corresponds to helium temperature at the receiver operational limit. The high compressor inlet temperature of 49°C (120°F) keeps the size of the precooler to a minimum. The compressor pressure ratio of 1.9 was selected on the basis of cycle efficiency sensitivity studies. The pressure level of 3.45 MN/m^2 (500 psi) improves heat exchanger performance, reduces the size (and, therefore, cost) of the system, and corresponds to a near-optimum pressure level for a 100-MW_e helium turbine running at synchronous speed (3,600 r/min). The closed-cycle system provides higher flexibility in control and output than can be offered by other cycles. This is an important advantage due to the diversity of environmental and operational conditions and the power product options possible in a solar plant.

Recuperator effectiveness was found to be the dominant factor in both cycle efficiency and cost. The decision was made to design to a high thermodynamic cycle efficiency of 0.44, which required a recuperator effectiveness of 0.94, and significantly increased cycle costs. However, cycle costs are only a small portion of total plant costs. The reduction in heliostat field costs possible at the 0.44 cycle efficiency results in minimum plant costs.

2.3.3 Energy Storage

The requirement for 6 hours of thermal energy storage for the 100-MW_e stand-alone intermediate plant has been incorporated into the design concept. Unlike other concepts where energy is stored after power generation, the storage concepts selected are utilized upstream of the turbine generator where storage can serve the dual purpose of running the turbine during noninsolation hours and also as a short-term buffer for periods of intermittent or total cloud cover during daylight hours. Such thermal energy storage has been included in the size and performance of the receiver and in the overall plant performance. Thermal storage concepts examined and compared during the study were phase change, sensible heat, and thermochemical systems. The leading candidate, the fusible salt-phase change system, has 6-hour storage system costs within the cost definition provided for the storage account by EPRI. Math models of complete solar power plant operation have been developed and exercised to predict plant performance on an hour-by-hour basis for the thermal energy storage concepts. Effects and performance of all other major powerplant subsystems have been included. Charging to the 6-hour limit can be met over 50% of the year. Some insolation must

be rejected during summer days with all three thermal energy storage concepts due to the 6-hour storage limit.

2.3.4 Plant Performance

The baseline solar plant subsystems and the selected thermal cycle were combined with the "strawman" field to determine plant performance and operational characteristics for two intermediate plant concepts. The results are typified by the two bar charts shown on figure 2-5. Both charts show the efficiency losses in going from the direct insolation through the plant subsystems to the generator output for a summer daily cycle.

The performance of a stand-alone plant with 6 hours of thermal storage over a summer-day cycle is shown by the upper chart of figure 2-5. A phase-change thermal energy storage device is shown here, but it is representative of the results obtained using each thermal energy storage concept. For a summer day, the integrated insolation from the "strawman" field is in excess of the requirements for direct energy production and 6 hours' storage. The plant produces approximately 1,700 MWH_e of electrical power for a capacity factor of 71%. Overall plant efficiencies of 16.5% are typical for summer-day performance. Efficiencies drop to 14%-15% for winter operation with storage availability reduced to 3-4 hours. Results have also been determined for sensible heat and thermochemical energy storage; for winter, fall, and spring days; and for yearly averages.

The lower chart represents the performance of a hybrid plant with fossil-fuel backup over a summer day. This chart is similar to the upper chart prior to taking the receiver losses. Operating from insolation, the plant produces 1,200 MWH_e of fuel displacement power for a capacity factor of approximately 50%.

The performance of hybrid and stand-alone intermediate plants over a daily cycle can be compared by determining the total thermal Btu's to be supplied by an alternate mode (fossil fuel) source to match the energy production of the intermediate plant. For a summer day, energy to produce approximately 500 MWH_e must be added to match the 1,700 MWH_e of a stand-alone plant operating 17 hours. Energy to produce an additional 540 MWH_e would be required for a winter-day comparison (1,170 MWH_e).

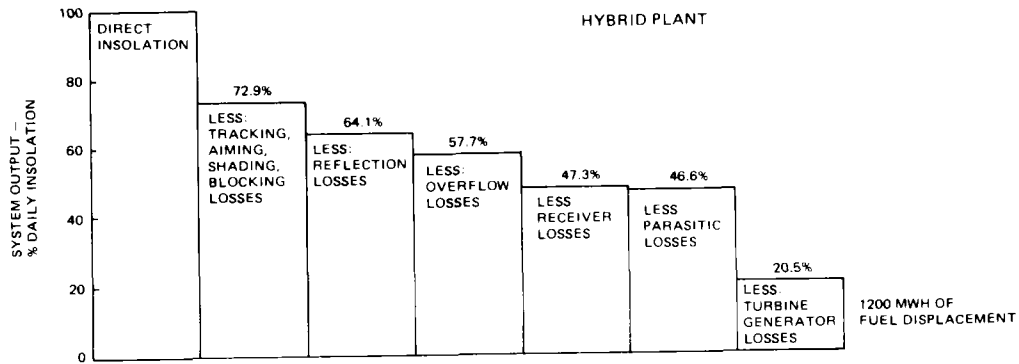
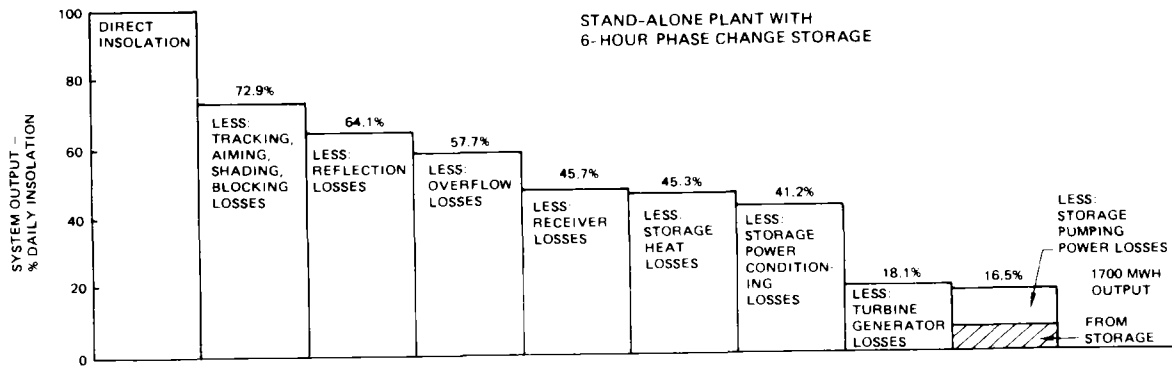


Figure 2-5. Performance of Intermediate Load Plants

2.4 TECHNOLOGY REQUIREMENTS

All the required technology is available for the design and development of the high-temperature central receiver. Technology problems of the collector field will be resolved outside of this contract. Helium turbomachinery of 50 - 100-MW_e capacity can become available with commitment to the necessary long-lead development program. The existing 50-MW_e helium turbine, such as is under test in Oberhausen, Germany, typifies the turbomachinery required either to be utilized directly in the 50-MW_e intermediate plant module or scaled up for the 100-MW_e hybrid plant usage.

For the thermal energy storage concept selected, the technology is available but has never been implemented in the size required for 50-100 MW_e. Again, a long-lead design, development, and test program should be an early commitment.

2.5 RECEIVER VERIFICATION

A test model receiver design of 1 MW_{th} has been accomplished that simulates the 100-MW_e receiver prototype in function, performance, and materials. Provision for minor configuration changes makes the design readily adaptable to the planned or existing facilities such as the U.S. ERDA Solar Thermal Test Facility at Albuquerque, New Mexico; the Centre de la Recherche Scientifique (CNRS) Solar Energy Laboratory at Odeillo, France; or IR facilities. Furthermore, it is adaptable to various test gas options and operational pressures. The necessary model test programs to verify prototype receiver design and performance have been formulated.

In addition, preliminary considerations have been included for a 10-MW_e pilot plant and for a 2.5-MW_e plant using one quadrant of a collector field. For this option, 2-2.5-MW_e air turbine availability has been assessed with reassuring results. A quotation has also been received for a 10-MW_e helium turbine.

2.6 COST

Receiver cost for the 100-MW_e stand-alone plant has been estimated at \$15.7 million. This cost comprises the two receivers required (one for each 50-MW_e module) and their heat exchangers, the supports required to mount the receivers above their towers, and the risers/downcomers to transport the helium between the receivers and the tower tops. The main supply and return lines in each tower are not included in this budget, but are accounted for in the miscellaneous plant equipment budget.

The relative cost of all helium system elements is contained on figure 2-6 with accounts arrayed against the cost model (strawman) provided by EPRI. It is assumed that the stand-alone and hybrid plants described have the same megawatt rating, overall storage capability, and total power production. Using the strawman plants as a baseline, the major reductions are in the field cost of the helium plants, directly attributable to the higher efficiency. Storage costs are slightly lower for the helium stand-alone plant, but turbine and miscellaneous plant equipment costs are higher. The direct cost dollars are comparable. For the hybrid plant the disproportionately higher storage cost for the helium plant and the riser/downcomer costs in the tower (miscellaneous plant equipment) provide the major differences.

Plant type	Stand-alone		Hybrid	
	Strawman	Helium	Strawman	Helium
Collector area (km ²)	1.0	0.84	0.5	0.42
Storage time (hour)	6	6	0.5	0.5
Account				
Land	2	2	1	1
Structures and facilities	44	44	51	51
Heliostats*	600	505	300	258
Central receiver/tower**/heat exchanger	95	197	68	98
Storage tanks	180 ***	164	15 ***	74
Boiler plant	-	-	73	73
Turbine plant equipment	80	119	80	105
Electric plant equipment	21	20	21	20
Misc plant equipment	4	28	4	16
Allowance for cooling towers	20	15	20	15
Total direct cost	1,046	1,094	633	711
Contingency allowance and spare parts allowance (5%)	52	55	32	36
Indirect costs (10%)	105	109	63	71
Total capital investment (1975)	1,203	1,258	728	818
Interest during construction (15%)	180	189	109	123
Total cost at year of comm'l operation (1975 \$)	1,383	1,447	837	941

*Collector cost—\$60/m²

**Tower height—260m (2 and 1 tower(s), respectively)

***Thermal storage cost—\$30/kWh

Figure 2-6. Relative Cost of System Elements (\$/kWe)

Section 3.0

BASELINE CENTRAL RECEIVER CONCEPT

The major study objective of determining the technical feasibility of a high-temperature central receiver for a closed-cycle helium system has been accomplished. The baseline receiver described in this section fulfills the feasibility criteria of performance life, cost, and technical practicability. It also surpassed other receiver candidates studied, when all major factors were evaluated.

3.1 RECEIVER REQUIREMENTS AND IMPLEMENTATION

3.1.1 Requirements and Assumptions

Initial study requirements called for design of a high-temperature central receiver appropriate to 100-MW_e output and the use of closed-cycle helium as the working fluid. The site for the central receiver/solar plant was specified as Inyokern, California. Other requirements were to use high-temperature materials consistent with the state of the art; to achieve 30-year equipment lifetimes; to accommodate winds gusting to 54 meters per second (120 mph); and to design structure to the seismic risk appropriate to the Inyokern site.

The requirements and assumptions stated above were particularized by EPRI guidelines to design for 50 MW_e with 6 hours' storage for each intermediate load, stand-alone plant module (two modules/plant), and for 100 MW_e with 0.5 hour storage for a hybrid plant. Associated tower height was specified at 260 meters (855 feet).

3.1.2 Requirements Implementation

The interim design requirements stated in section 3.1.1 require practical high-temperature materials for the helium turbomachinery and the receiver heat exchanger tubing. The closed-cycle helium system efficiency improves with temperature; however, 816°C (1,500°F) was initially selected as the upper helium working fluid temperature, due to potential material limitations for metals over a 30-year lifetime. The 816°C (1,500°F) nominal temperature limitation has been

proven an excellent choice. A choice of two superalloys with temperature life-time capability is available. Insolation materials to limit receiver conductive heat loss have also been identified. The insolation data for Inyokern were obtained from the Aerospace Corporation. Figure 3-1 shows the mean insolation profiles for four solstice conditions. Design insolation loading on the collector field supplying energy to the receiver was taken for noon, June 21, as 870 watts/meter² (276 Btu/hour-foot²).

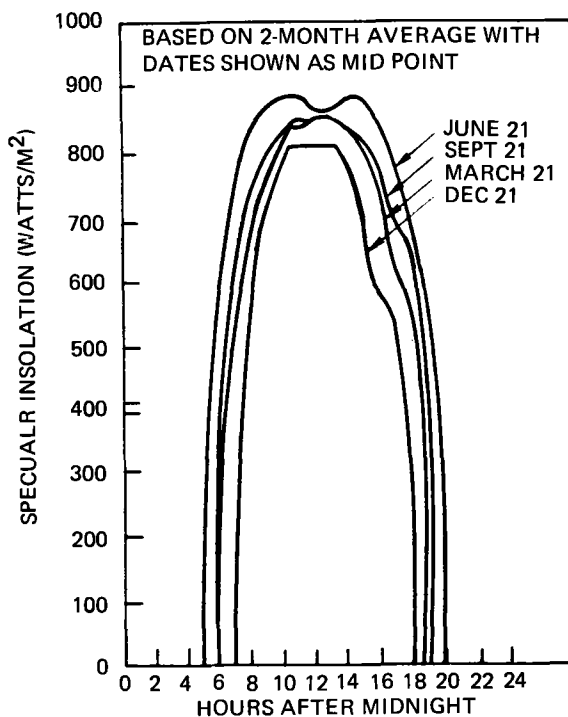


Figure 3-1. Insolation Profiles—Inyokern, California

Structural design requirements related to wind and seismic risk have been accommodated in the study. The specification of the plant site at Inyokern, California, defined the plant as being in the maximum seismic risk zone, Zone 3. While the primary impact of seismic risk Zone 3 is on tower design, increased strength is also required for the receiver, supports, and mounted equipment.

3.2 RECEIVER CHARACTERISTICS

3.2.1 Configuration

Exterior Arrangement. The baseline receiver configuration has been shown on figure 2-1. It is shown again on the external structural arrangement drawing, figure 3-2. The receiver configuration has an upper cylindrical section and a lower hemispherical section with a receiver aperture at the bottom.

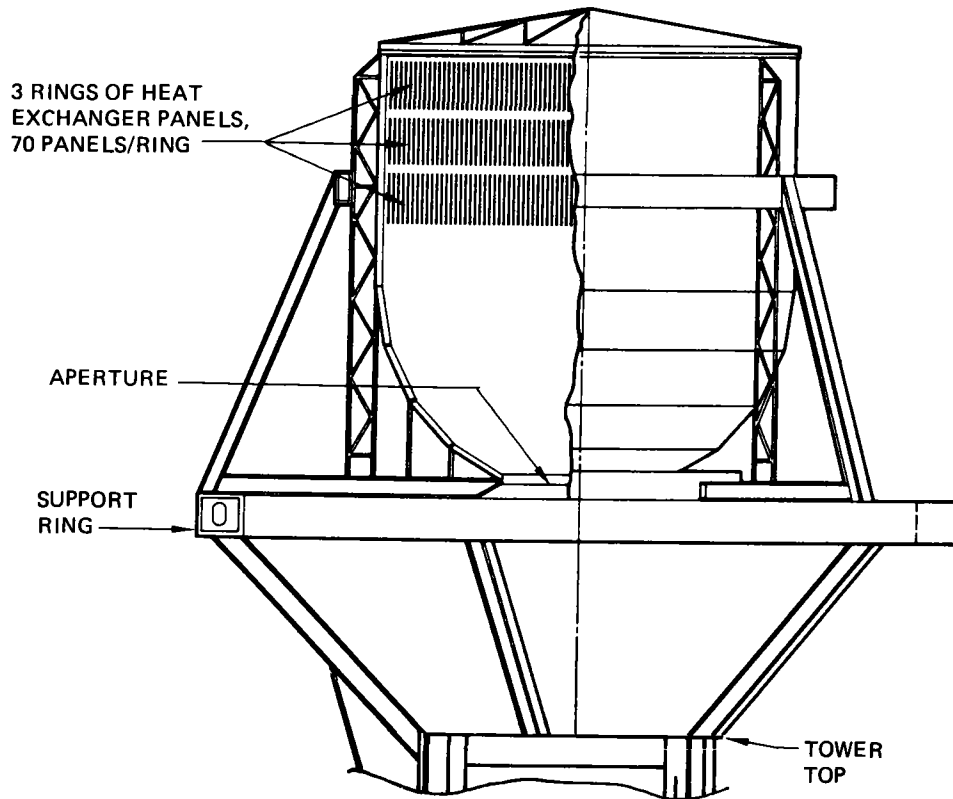


Figure 3-2. External Structural Arrangement

The distance to the aperture is taken at the specified tower height of 260 meters (855 feet). The upper cylindrical section of the receiver facilitates mounting rows of heat exchanger panels in three rings, as illustrated in the cutaway. The lower hemispherical section has insulation panels supported from the exterior wall.

The receiver is mounted approximately 30 meters (98 feet) above the tower to allow the field energy to enter the aperture. Five support legs extend up and out from the tower top to the main support ring. These supports are located away from the aperture to minimize heating by direct radiation from the field and to reduce field blockage. Vertical members extend into the receiver stringer support ring. The size of the support members just described is such that the risers and downcomers carrying the helium flow between the tower top and the receiver are mounted within the supports. There are two risers and two downcomers, each of these four pipes in an individual support. Figure 3-3 shows cross sections of the support struts at the position of maximum field flux intercept.

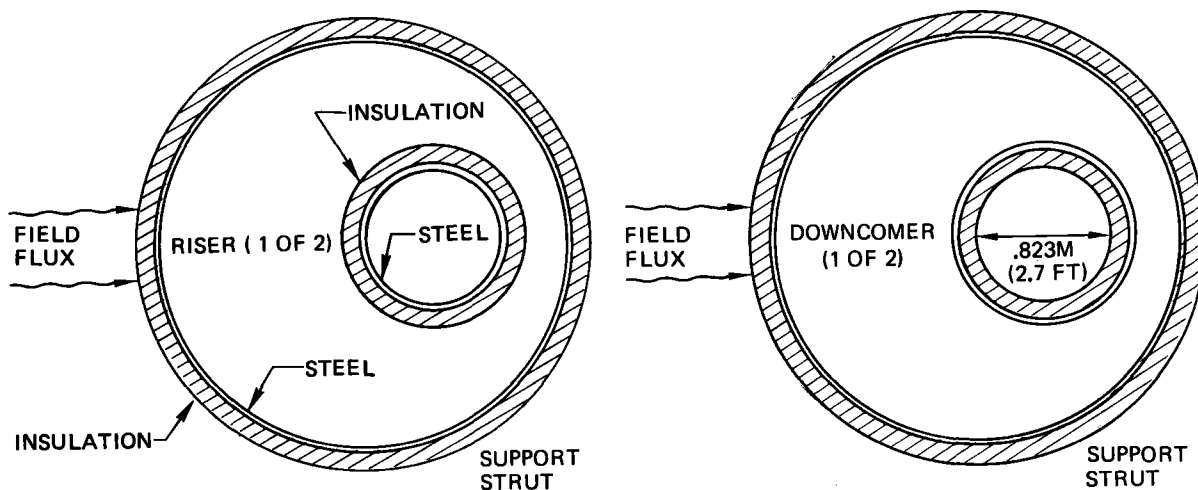


Figure 3-3. Support Structural Concept to Traverse Field Flux

The riser inside the strut on the left, carrying 538°C ($1,000^{\circ}\text{F}$) helium to the receiver, is of stainless steel externally insulated. The downcomer for the 816°C ($1,500^{\circ}\text{F}$) helium return line will be internally insulated so that carbon steel can be used for its case. Thus, the use of the more expensive superalloys can be avoided in the helium lines that traverse the 70 meters (230 feet) to the receiver. The supports are ventilated for natural convection cooling of the interior. For the region of intense field radiation, the support is protected as shown in figure 3-3 by a high-temperature insulation shield.

The vertical stringers on the receiver support the roof section, the receiver heat exchangers, and the manifolds supplying helium to the heat exchanger panels.

Interior Arrangement. The internal configuration has a cylindrical/hemispherical shape dictated by thermal and structural considerations. The success of any receiver cavity operation depends upon the effectiveness of heat transfer to the "working fluid" from the solar energy admitted to the receiver interior through the aperture.

The heat transfer to the helium, in the selected receiver concept, is by use of heat exchanger panels in the upper (cylindrical) half of the receiver interior. In this position, the direct energy impingement on the heat exchangers that could cause local "hot spots" on the tubing is minimized or eliminated. Three rows of heat exchanger panels with 70 panels per row constitute the effective heat transfer surface. All panel modules are identical in size and construction. The lower hemispherical section has panels of insulation to minimize heat loss through its surface.

The receiver interior dimensions are approximately 39 meters (128 feet) cylinder diameter and 39 meters high. Aperture diameter is 19 meters (62.5 feet).

3.2.2 Equipment Characteristics

Figure 3-4 illustrates a modularized heat exchanger panel and its structural supports. Each panel consists of two offset columns of heat exchanger tubing, insulation, tubing loops to the helium manifolds, and the support structure to the outside wall. The loops behind the insulation are to enable proper expansion and contraction during thermal cycles to keep the interior tubes in proper position. Panels are designed to be removable to facilitate easy maintenance.

The heat exchanger panel module is shown again on figure 3-5. Panel and tube dimensions are displayed. Each of the 20 tubes mounted on the panel has a U-shape, one leg going from the inlet down to the bend and the other leg returning close to the insulation. This leg is offset from the outer pass as shown by the upper diagram of figure 3-5. The staggered arrangement provides a more uniform exposure of tube surface area to the radiation flux.

Panel insulation behind the tubes consists of three successive layers of 2.54 centimeters (1 inch) alumina-silica blanket, 5 centimeters (2 inches) alumina-silica block, and 7.6 centimeters (3 inches) mineral-wool block. Total thickness is 15 centimeters (6 inches).

Helium mass flow rate for each panel has been established nominally at 0.91 kilogram/second (2.0 pounds/second) to ensure turbulent flow in each tube and the best heat transfer characteristics. At these conditions, there is only a modest temperature difference between the tube wall and the helium of about 36°C (65°F).

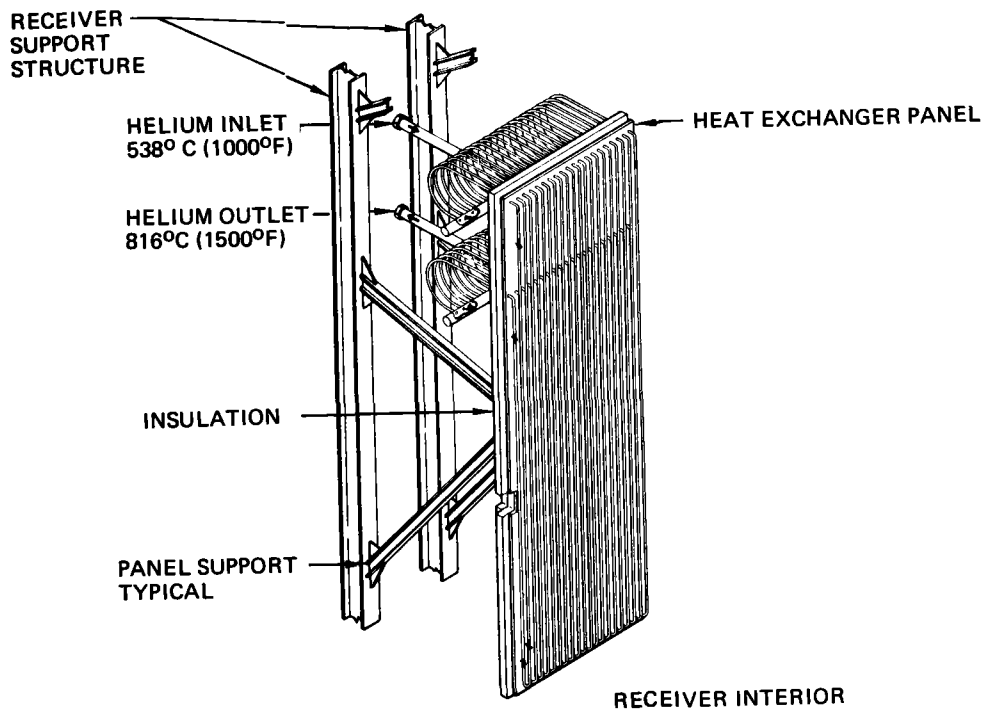


Figure 3-4. Heat Exchanger Panel

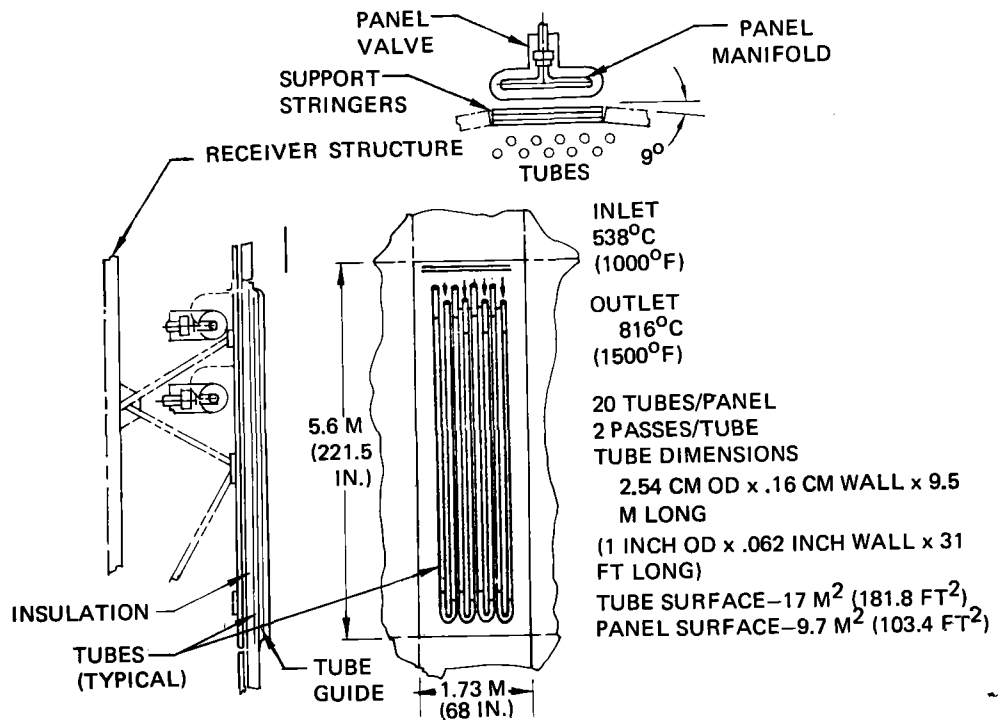


Figure 3-5. Heat Exchanger Panel Detail

3.2.3 Helium Piping Concept

The insertion of the main risers and downcomers inside the receiver supports has been described in section 3.2.1. A conceptual arrangement of the manifolding between these major supply and return lines is shown on figure 3-6.

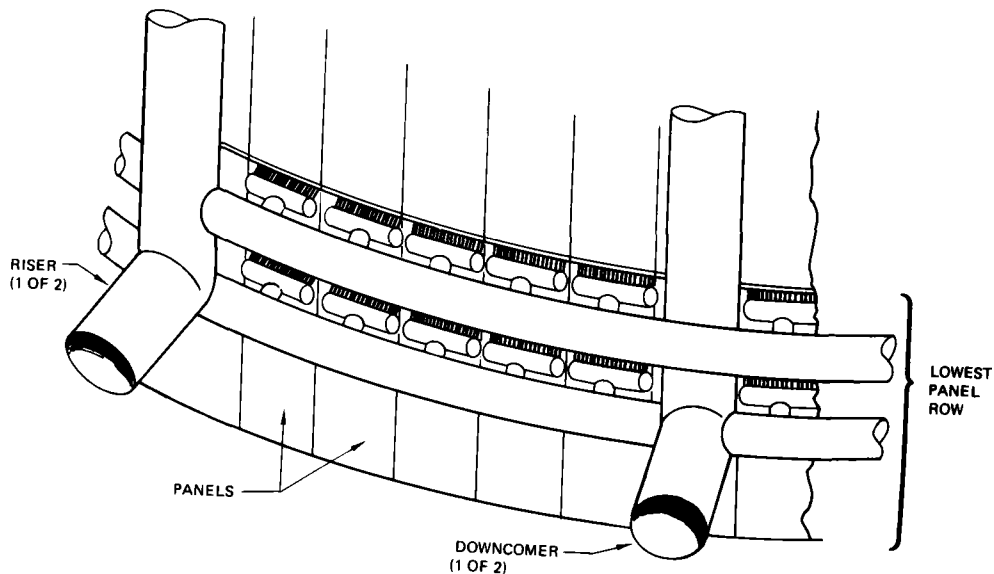


Figure 3-6. Receiver Piping Concept

If replacement of the heat exchanger panels is necessary, the piping attaching the panels to the headers can easily be disconnected. The short lines from the panel headers connect to horizontal circumferential manifolds servicing half the panels in a panel row from the major verticals. The circumferential lines are approximately 25 centimeters (10 inches) in diameter and will be insulated on the inside or the outside depending on the helium gas temperature. Four vertical lines (two for supply, two for return) service the three panel rows. These are 63 centimeters (25 inches) in diameter. Each of these four lines is connected to the proper risers and downcomers buried in the supports between the receiver and the tower top. The expansion and contraction of pipe lengths due to temperature changes will be handled by bellows.

Major valving for mass flow control and instrumentation for temperature and pressure sensing will be located at the exits from the circumferential lines to the vertical downcomers.

The two downcomers from the receiver join at the tower top into a single downcomer of 1.22 meters (4 feet) inside diameter, which traverses the 230 meters (750 feet) down the tower to the turbine inlet. Similarly, a single riser of the same internal diameter and length traverses up the tower to the two risers that go from the tower top to the receiver. Again, these heavier pipes are designed to avoid use of the more expensive superalloys.

3.2.4 Receiver Weight

Estimated receiver weights are tabulated below:

	<u>Kilograms</u>	<u>Pounds</u>
Support Ring	595,000	1,310,000
Support Columns	270,000	600,000
Heat Exchanger Panels	255,000	560,000
Superstructure	230,000	500,000
Manifolds, Risers, Valves, Downcomers & Insulation	160,000	350,000
Total	1,510,000	3,320,000

3.2.5 Receiver Performance

The receiver, as designed, collects the heat required for immediate electric power production and that to be stored for deferred power production in each 50-MW_e-rated stand-alone plant module. Two modules, thus requiring two receivers, constitute the 100-MW_e intermediate plant. The same design would collect the heat required for a 100-MW_e-rated hybrid plant, which uses only one plant module.

The performance of the receiver is dependent on the daily insolation conditions as shown by the thermal balance below for noontime conditions on June 21 and December 21.

THERMAL MEGAWATTS

	<u>Summer</u>	<u>Winter</u>
Solar input to receiver	315.0	259.0
Receiver losses:		
● Reflection out aperture	11.9	9.7
● Reradiation out aperture	33.1	29.5
● Convection to air	2.5	2.4
● Conduction through walls	6.0	5.7
Total Losses	53.5	47.3
Heat removed by helium	261.5	211.7

Receiver efficiency in delivering input heat to the helium working fluid is thus 82%-83%. The largest loss at both conditions shown is reradiation of energy back out through the aperture. This is an unavoidable circumstance for any high-temperature receiver cavity. Reflection losses through the aperture have been minimized in this design by the particular shape. Convection and conduction losses are small.

The 261.5 MW_{th} available to the turbine for the summer-noon condition exceeds the amount required for producing 100 MW_e in a hybrid plant. The winter-noon condition of 212 MW_{th} produces slightly less than 100 MW_e (93 MW_e).

The noon receiver inputs for summer and winter days have been shown as 315 and 259 MW_{th}, respectively. The complete daily receiver inputs for 4 days are displayed in figure 3-7. These curves result from applying the proper field efficiency factors to the Inyokern, California, profiles of figure 3-1.

The maximum heat supply rate to the helium in the receiver was used to determine the design and performance of the receiver heat exchangers. The final design has 210 panels, as shown in figures 3-4 and 3-5. An earlier design with all U-shaped tubes parallel to the wall required 280 panels. An analysis showed excessive temperatures at the exit of tubes located in the lowest panel row in the receiver. Consequently, the tubes on each of the panels were rerouted with all cooler inlet tubes away from the panel and returning near the panel as in figure 3-4. This design allowed better absorption by the cooler tubes and reduced maximum tubing temperatures.

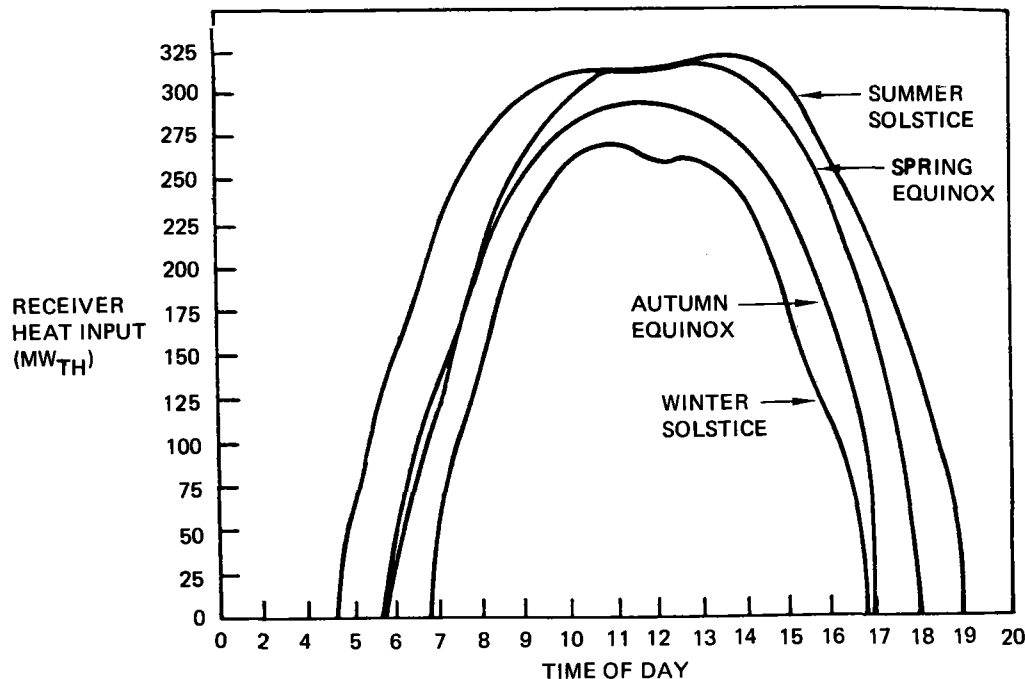


Figure 3-7. Receiver Heat Input

Detailed thermal analyses were performed on the preferred receiver to determine maximum operating temperatures at key locations and to ensure that design materials had the capability to sustain these temperatures. Figure 3-8 shows a composite of temperatures at various receiver locations. For the receiver interior, if the circled numbers are followed sequentially from the roof center down the receiver walls, it is noted that the roof insulation and the insulation behind the heat exchangers (numbers 2 and 3) have temperatures of 920°C ($1,690^{\circ}\text{F}$) or below. The temperature-reducing effect of the heat exchanger tubing, shown as an average, is evident. The high temperature of $1,100^{\circ}\text{C}$ ($2,000^{\circ}\text{F}$) occurs at the insulation surface on the hemispherical wall where the incoming solar flux is maximum. The temperature on the hemispherical wall drops to 900°C ($1,650^{\circ}\text{F}$) near the aperture.

Outside the receiver, the temperature on the heat shield extending out from the aperture is about $1,090^{\circ}\text{C}$ ($1,975^{\circ}\text{F}$). The maximum temperature on the receiver support structure crossing the field radiation is 815°C ($1,500^{\circ}\text{F}$).

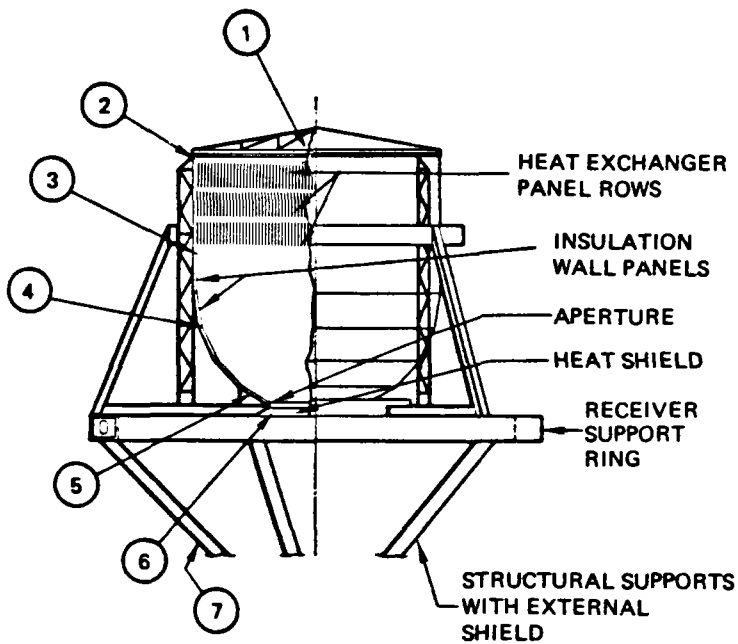
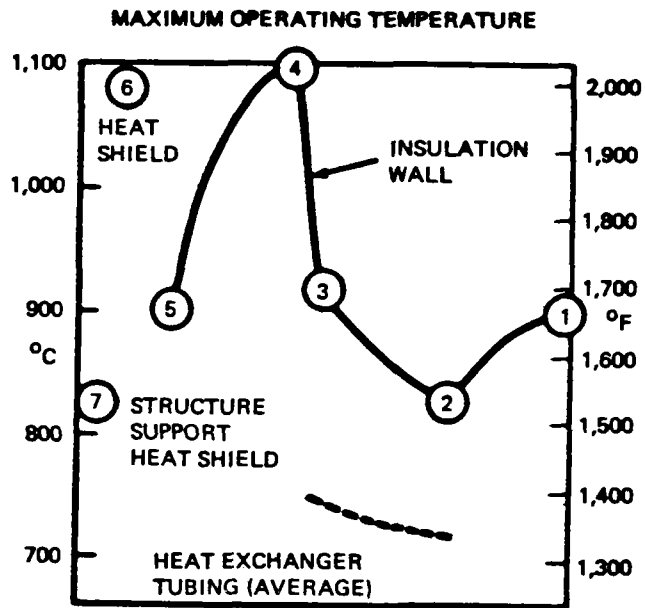


Figure 3-8. Representative Receiver Temperatures

Insulation panels entirely line the interior of the selected receiver configuration. The graph on the lefthand side of figure 3-9 shows wall heat losses for various inside face temperatures and insulation thicknesses. Referring back to figure 3-8, the highest conductive heat loss comes from the receiver hemispherical surface whose bare (without heat exchanger tubes) insulation panels have an average hot-face temperature of 980°C (1,800°F), resulting from the concentrated incident radiant flux. The design point indicated on the graph of 0.15-meter (6-inch) insulation thickness is a compromise to keep both wall conduction losses and insulation weight reasonably small. The heat loss for the chosen thickness is about 950 watts/meter² (300 Btu/hour-foot²). The insulation concept of three successive layers of material is shown and dimensioned on the right-hand side of figure 3-9. The same insulation concept is used on the heat exchanger panels behind the tubes. Face temperature for these panels is below 870°C (1,600°F). The total conduction loss through the insulation of the receiver is about 6 megawatts, or slightly over 2% of the solar input into the receiver.

The performance of the panel heat exchanger tubes was examined in detail for thermal and pressure characteristics at the various panel locations. A tre-

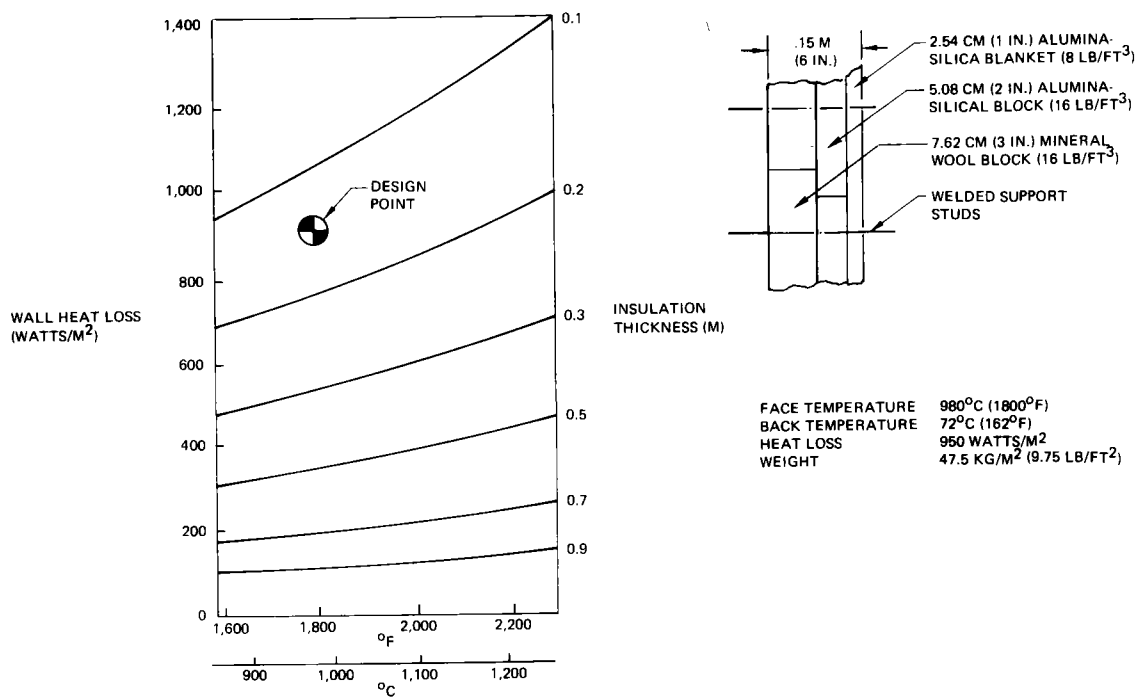


Figure 3-9. Insulation Concept

mendous advantage was obtained by the switch to three panel rows from the four panel rows extensively analyzed in the early portion of the study. The fourth or bottom row in the previous configuration had been subjected to some directly impinging radiant flux, raising its heat removal rate, average temperature, and helium mass flow and pressure drop requirements over that for the upper rows. Rather than retain these problems with the three panel-row configuration by shortening the receiver, the decision was to drop the bottom row and retain the original receiver dimensions. All three panel rows are now out of the direct incident flux and subjected to a more uniform diffused heat source. Heat removal rates per tube are nearly constant, which establishes the situation of constant mass flow and pressure drop per tube and eliminates the particularized valving and controls to handle special panel requirements. The performance characteristics for the tubes, when controlled to inlet and outlet helium temperatures of 538⁰C (1,000⁰F) and 816⁰C (1,500⁰F), are summarized below. Turbulent flow is maintained within all tubes without difficulty.

Number of tubes	4,200
Heat removal per tube)(ave)	65 kW (222,000 Btu/hour)
Helium flow per tube	0.045 kg/sec (0.1 pound/second)
Tube maximum temperature	852 ⁰ C (1,565 ⁰ F) or less
Tube average temperature	732 ⁰ C (1,350 ⁰ F)
Tube pressure drop	0.035-0.048 MN/m ² (5-7 psi)

3.3 RECEIVER TECHNOLOGY REQUIREMENTS

The selected receiver and its components are within the existing technology and design practice. No long-lead-time items exist in the receiver for development or procurement. However, life tests of superalloy materials at sustained temperatures above 760⁰C (1,400⁰F) should be initiated as soon as possible to accrue additional creep rupture test data for Haynes 188 and Inconel 617 at operational temperature limits.

3.4 RECEIVER COST

Receiver costs are based on the use of Inconel 617 for heat exchanger panel tubing and headers. All manifolds and downcomers, that operate at 816⁰C (1,500⁰F) are insulated on the inside so carbon-steel or mild-steel pipe material may be used. The 538⁰C (1,000⁰F) lines are of externally insulated stainless steel. Thus, the use of the more expensive superalloy Inconel 617 is avoided in the

large, long-flow-run tubing. The receiver costs are itemized below.

<u>ACCOUNT</u>	<u>COST (10⁶\$)</u>
Heat Exchanger Panel Assemblies (210)	1.80
Insulation Panel Assemblies and Insulation Buy for Heat Exchanger Panels	.40
Downcomers to Tower Top (2) and Exit Manifolds in Receiver	1.24
Risers from Tower Top (2) to Receiver and Inlet Manifolds in Receiver	.51
Shields, Insulation Protection on Supports and Aperture Lip	.35
Support Structure and Receiver Top	2.00
Flow Control Valves	.04
Erection, Fitting, and Welding	1.50
Total	7.84

For the 100-MW_e stand-alone plant, which requires two receivers, the total cost of receivers and their heat exchangers is about \$15.7 million, or \$157/kW. Excluded from this account are the riser and downcomer costs to traverse the 230 meters (755 feet) from tower top to bottom in each tower. For the 100-MW_e stand-alone plant, the \$2.4 million cost for tower distribution lines inclusion adds \$24/kW to plant costs. The same concept of internally insulating the downcomers (high-temperature lines) and externally insulating the risers was used. The costs were added to the account for "miscellaneous plant equipment" in the plant account shown on figure 2-6 and in section 8.4.

Section 4.0

CENTRAL RECEIVER ANALYSES AND TRADES

The baseline central receiver concept has been presented in section 3.0. This section reports the background analyses and trade studies that contributed to the receiver concept selection.

4.1 CONFIGURATION TRADES

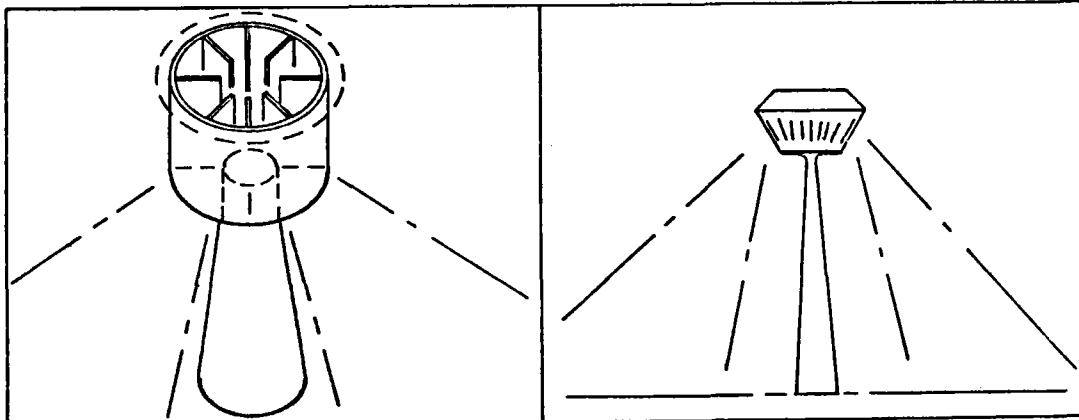
4.1.1 Preliminary Configuration Selection

A significant number of central receiver configurations were considered during the initial phase of the study. Cavity-type configurations were chosen rather than external tubing configurations (such as used with water boiler concepts) because of the requirement to restrict incident flux due to the higher operating temperatures required. Figure 4-1 shows some of the major cavity-type candidates. The preliminary evaluation was based on the following factors: site preparation requirements, turbomachinery location, overall construction complexity, access and maintenance requirements, solar heating of structural components, heat removal capability of helium, temperatures on heat exchanger surfaces, and heat losses from the receiver. Thermal storage and location of storage equipment were not initial study factors so the location of turbomachinery in the tower was optional.

These early evaluations resulted in the preliminary selection of a downward-viewing cylindrical receiver with a circular aperture. This "baseline" receiver is depicted at the lower right on figure 4-1.

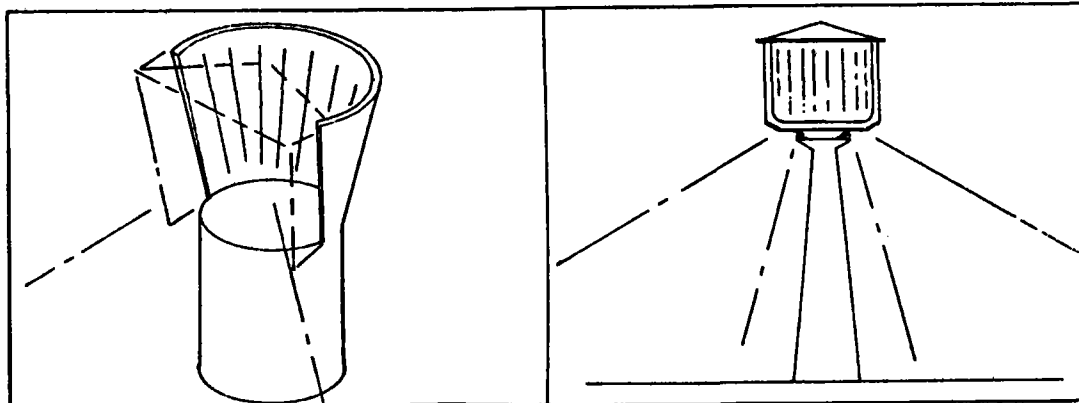
4.1.2 External Support Configuration

Selection of a receiver concept with a circular aperture at the bottom required a configuration where the receiver supports, helium risers, and downcomers must necessarily traverse the concentrated solar flux from the collector field. Various support structure candidates were examined ranging from a central column to outboard support struts. Figure 4-2 shows three configurations with the selected outboard support configuration at the extreme right.



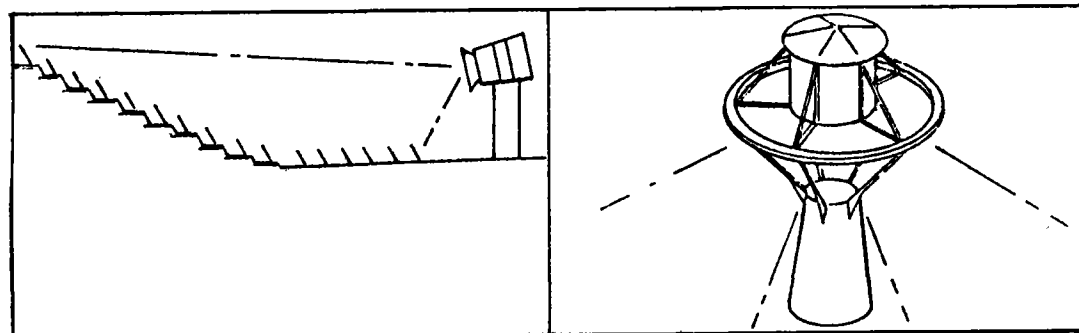
BAFFLED CAVITY—MULTIPLE
DOWNWARD FACING APERTURES—CIRCULAR
HELIOSTAT FIELD

EXTERNAL HEAT RECEIVER—CIRCULAR
HELIOSTAT FIELD



INTERNAL CRESCENT—SIDE VIEWING—
NORTH HELIOSTAT FIELD

CAVITY CIRCULAR SLIT
APERTURE— CIRCULAR HELIOSTAT FIELD



CAVITY—SIDE VIEWING
APERTURE—NORTH HELIOSTAT FIELD

CAVITY—DOWNWARD VIEWING
CIRCULAR APERTURE— CIRCULAR HELIOSTAT FIELD

Figure 4-1: Typical Central Receiver Configuration

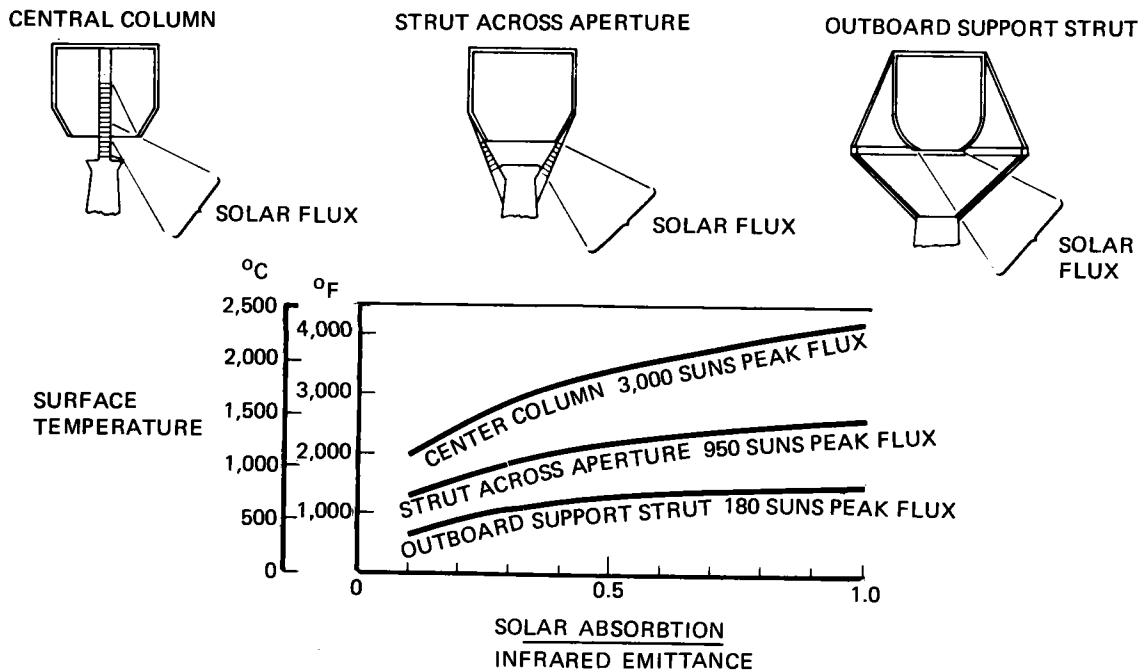


Figure 4-2. Receiver Support Structure Candidates

The rationale for the selection is shown on the flux and temperature graph. Quite clearly, the flux exposure of the outboard supports is significantly less with surface temperatures in a range where only passive protection is required. This support system is also advantageous because it presents a single large aperture to the entire field. This allows larger collector units in the field while maintaining a favorable flux-capture ratio.

The very localized heating on the outboard strut is indicated on figure 4-3. The 180-suns peak flux of figure 4-2 is confined to a few meters with a rapid dropoff on either side.

4.1.3 Baseline and Alternative Receivers

Initial task definition required selection of a baseline receiver and a best alternative configuration. Spherical, conical, cylindrical, and hemispherical receiver geometries were originally selected for study. Analyses made early in the program showed minor variations in receiver efficiency as a function of geometry. However, these results were based on erroneous receiver interior-to-aperture view factors reported in the literature, which showed a geometry dependence that

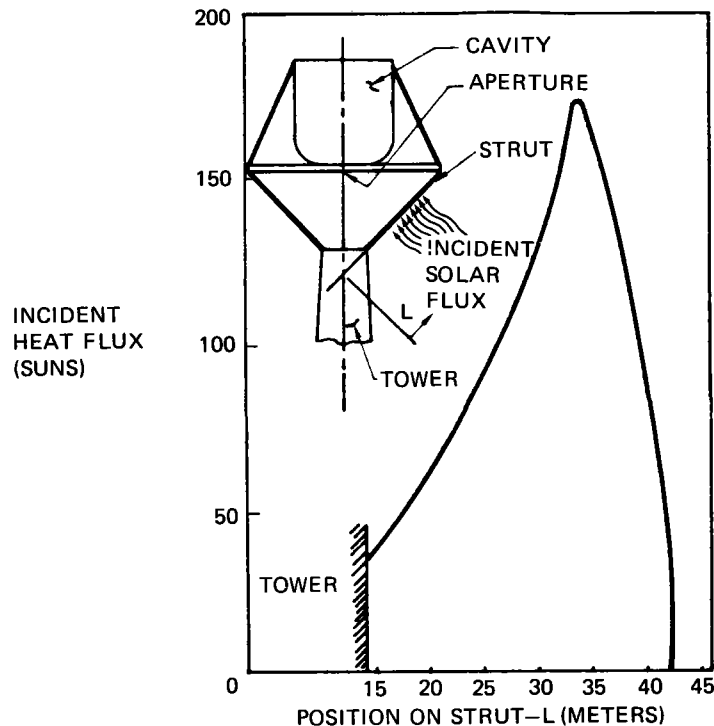
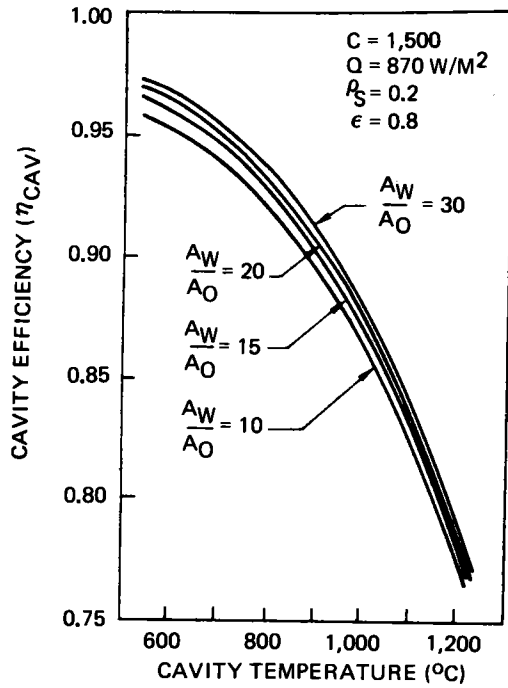


Figure 4-3. Solar Heat Flux on Outboard Support Strut

does not exist. The view factor from the aperture to the receiver cavity is one. The law of reciprocity ($\text{area}_1 \times \text{view factor}_{1-2} = \text{area}_2 \times \text{view factor}_{2-1}$) then requires the receiver cavity-to-aperture view factor to be equal to the aperture-to-wall area ratio. This result was used to calculate the cavity reflection and radiation losses and cavity efficiency. Figure 4-4 shows a representative graph of receiver efficiency and the equation that gives the efficiency. In addition to assuming diffuse surfaces, these results assume a uniform wall temperature and diffuse solar flux entering the aperture. Because of the symmetry in a spherical receiver, the last two assumptions are not required.

The solar flux entering the central receiver cavity aperture is very directional as opposed to the diffuse (Lambertian) flux assumption incorporated in figure 4-4. The solar flux distribution, at the cavity aperture centerline, resulting from a typical collector field, is shown on figure 4-5 along with the Lambertian distribution. Determination of flux distributions was accomplished by a Boeing field program, the Heliostat Array Computer Simulation Model (HACSM). The model takes the input description of the field, the field collectors, and the receiver and calculates the performance of strategically located representative heliostats.



$$\eta_{\text{CAV}} = 1 - \frac{\rho_S}{\frac{A_W}{A_O} - \rho_S \left(\frac{A_W}{A_O} - 1 \right) \left[\frac{A_W}{A_O} - (1-\epsilon) \left(\frac{A_W}{A_O} - 1 \right) \right]} \frac{A_W/A_O \epsilon \sigma T^4}{CQ}$$

- A_W/A_O = CAVITY WALL TO APERTURE AREA RATIO
- ρ_S = SOLAR REFLECTIVITY OF WALL
- ϵ = EMISSIVITY OF WALL
- σ = STEFAN-BOLTZMANN CONSTANT
- T = CAVITY TEMPERATURE
- C = CONCENTRATION RATIO, APERTURE FLUX TO AMBIENT FLUX
- Q = AMBIENT FLUX

- ASSUMPTION*
1. UNIFORM WALL TEMPERATURE
 2. DIFFUSE SOLAR FLUX AT APERTURE

*ASSUMPTIONS NOT REQUIRED FOR A SPHERICAL CAVITY

Figure 4-4. Cavity Efficiency

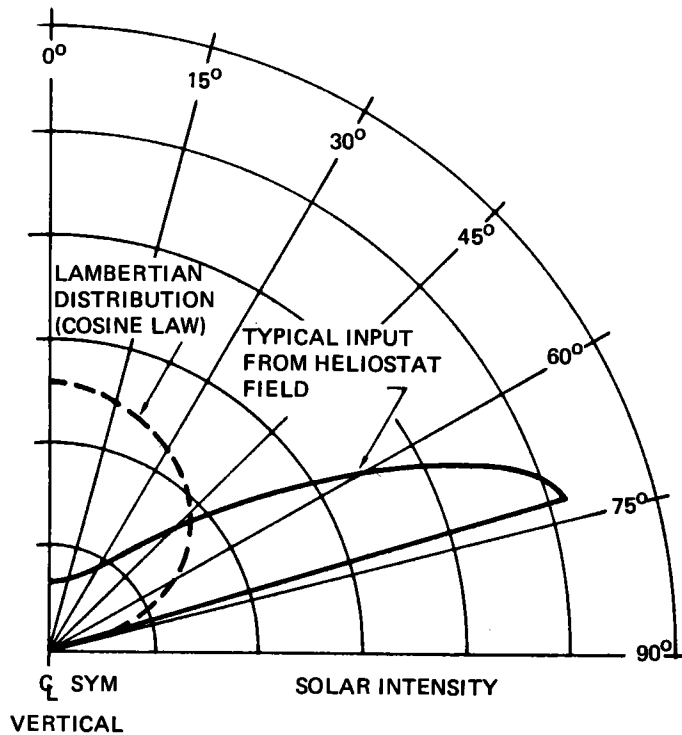


Figure 4-5. Distribution of Solar Flux in Cavity Receiver

Included are considerations of mirror aspect angle, receiver capture efficiency, shadowing and blocking, and mirror optical properties. Combining these efficiencies with the insolation levels allows the computation of the flux distributions.

The solar flux from the heliostat field is concentrated on the lower portion of the receiver cavity wall. As noted earlier, this distribution of solar flux will not affect the efficiency of a spherical receiver, but it will decrease the efficiency for the other receiver shapes. A possible exception is a cylindrical receiver with a large diameter-to-height ratio, which is impractical for other reasons.

The solar-flux distribution effects were examined in detail for the baseline and alternative receivers. A cylindrical cavity was used as the initial baseline since it results in minimum structural complexity for wall sections, plumbing, and support structure, and allows vertical tubing runs without gravity side loads. A spherical receiver cavity was chosen for the alternative receiver since it should provide the maximum cavity efficiency. Both receivers had a wall-to-aperture area ratio of 22 and an aperture diameter of 14.6 meters (48 feet). The cylindrical receiver had a height-to-diameter ratio of about 2.

The solar-flux distribution effects were determined using the Boeing Monte-Carlo ray-tracing code (AS2814). The collector-field flux distribution defined by the field computer code (HACSM) was characterized by a large number of individual rays and input to the ray-tracing code along with the receiver geometry and radiative properties. The ray-tracing code determined the disposition of the input rays over the cavity walls and back out through the aperture. Two cases were calculated for the baseline and alternative receivers. The first case, run with bare insulation on the walls, was used to define the wall regions where the intensity was low enough to install heat exchanger panels. The second case, run with heat exchanger panels installed, was used to determine the net reflective loss from the receivers.

Figure 4-6 shows the absorbed heat-flux profiles for the baseline (cylindrical) and alternative (spherical) receivers with alumina-silica insulation walls. Since the solar absorptance of the insulation is 0.3 (see section 4.2.2), the incident solar flux is about 3.3 times the absorbed flux shown in figure 4-6.

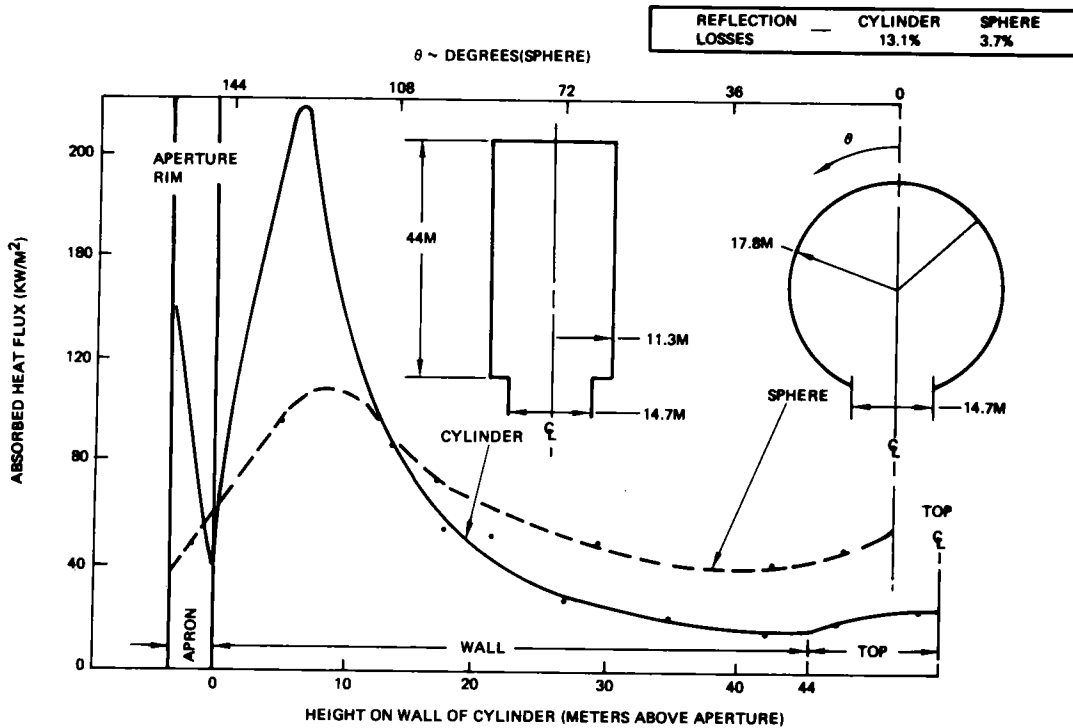


Figure 4-6. Heat Flux to Receiver Walls

The solar flux reaches a maximum near the aperture for both receivers; however, the spherical receiver has a much lower peak flux than the cylindrical receiver. At the maximum flux locations, the insulation temperature was about 1,200°C (2,200°F) for the spherical receiver and about 1,430°C (2,600°F) for the cylindrical receiver. The solar flux in the lower half of both receivers exceeds the heat exchanger tube bundle allowable incident flux of about 220,000 watts/meter² (70,000 Btu/hour-foot²). However, heat exchanger panels could be installed in the upper half of either receiver interior despite the geometric complexity of the spherical shape at that location. The reflective losses for the bare insulation case are 15.7% for the cylindrical and 3.7% for the spherical receiver. This case had the upper half of the receivers covered with heat exchanger panels that absorb 70% of the incident solar flux.

4.1.4 Receiver Selection

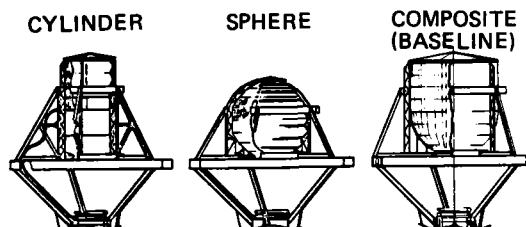
Most of the thermal and structural analyses were performed for the cylindrical receiver first selected as a baseline. Use of a cylindrical receiver simplified the design because of the vertical walls. Even though analyses show no

geometric effects on efficiency for a diffuse solar input, the cylindrical receiver reflective losses are significantly greater (about 9%) than those for a spherical receiver when the highly directional solar input from a collector field is taken into account. Thus, the size of a cylindrical receiver would have to be proportionately larger to produce the same power as a spherical receiver.

The selected receiver shape was a result of a compromise between maximum performance, achieved with the spherical geometry, and minimum cost, achieved with a cylinder. The baseline receiver design combines a cylindrical upper portion, for mounting heat exchanger panels, with a hemispherical lower portion having insulated walls. This receiver reduces the reflection losses while maintaining the design simplicity of a cylindrical receiver. It has been displayed as figures 2-1 and 3-2. It is shown again on the right side of figure 4-7, with the initial baseline and alternative configurations of which it is a composite. The table below the illustrations summarizes the selection rationale.

BASIS

EQUAL APERTURE SIZE
 EQUAL HEAT PRODUCTION FOR POWER
 SAME HEAT EXCHANGER MODULE
 MAXIMUM SOLAR POWER INPUT



CONSIDERATIONS FOR SELECTION	RATING		
	POOR	BEST	GOOD
HEAT DISTRIBUTION			
REFLECTION LOSSES (%)	13.1	3.7	3.8
OVERALL THERMAL EFFICIENCY (%)	74	87	83
ESTIMATED COST RATIO	1.0	2.0	1.5

Figure 4-7. Cavity Receiver Evaluation

The interior dimensions of the selected receiver are 39 meters (128 feet) cylinder diameter and 39 meters high. Aperture diameter was increased from 16 meters (52.5 feet) to 19 meters (62.5 feet) to accommodate the collector field characteristics supplied by EPRI and to add a flux delta for additional heat in heat storage situations.

4.1.5 Receiver/Solar-Plant Integration

Before proceeding to the more detailed thermal and structural analyses used to define receiver interior equipment and arrangements, the general adaptation of the selected configuration to the solar plant will be discussed. Section 4.1.2, for example, discussed the outboard supports where the impact of traversing the collector field flux was of dominant importance. Other areas with significant configuration implications to the receiver and/or to the solar plant are the major helium supply and return lines (risers and downcomers), adaptation to storage, and the location of turbomachinery.

Risers and Downcomers. With the receiver and tower separated to allow the field flux to enter the receiver aperture, the risers supplying helium to the receiver and the downcomers returning helium to the tower must also traverse this standoff distance. The initial concept had a riser-downcomer pair partly sheltered behind each of the five support legs to the receiver, or five sets in all. The concept is shown on the left side of figure 4-8. The concept was unsatisfactory due to the multiplicity of plumbing connections and to the amount of insulation and shields required to protect the risers and downcomers from the cavity heat and

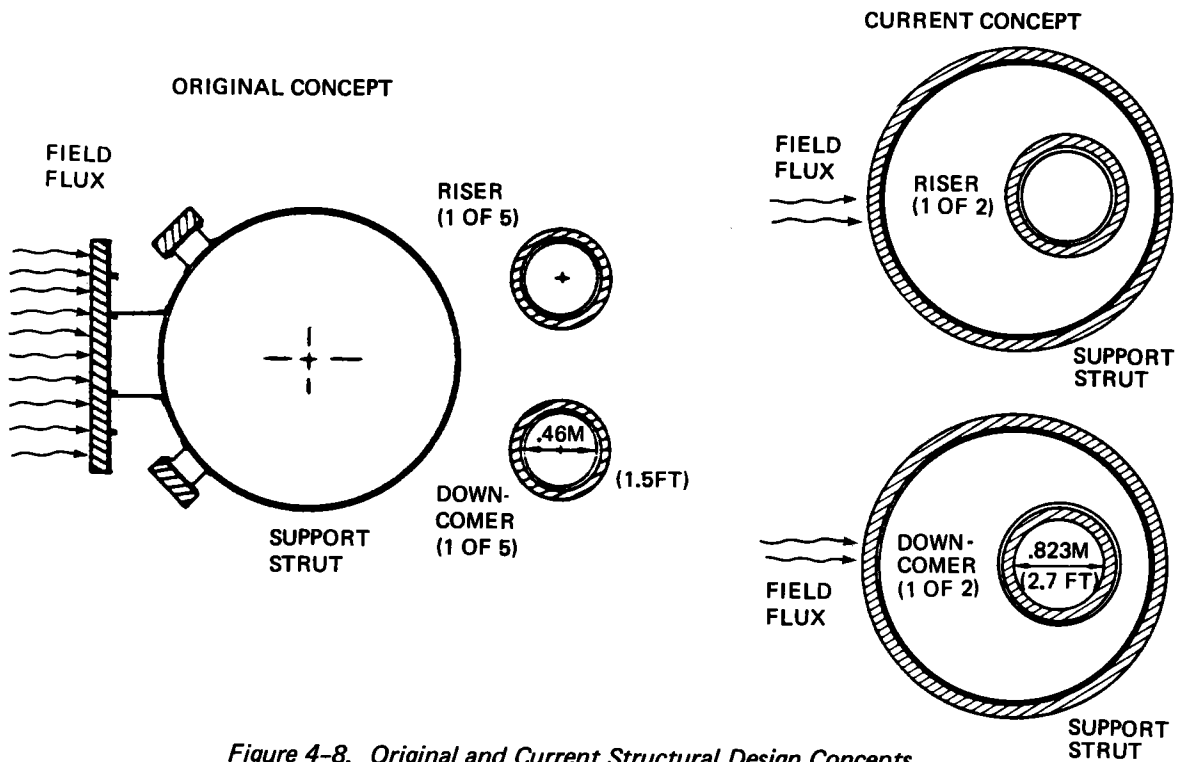
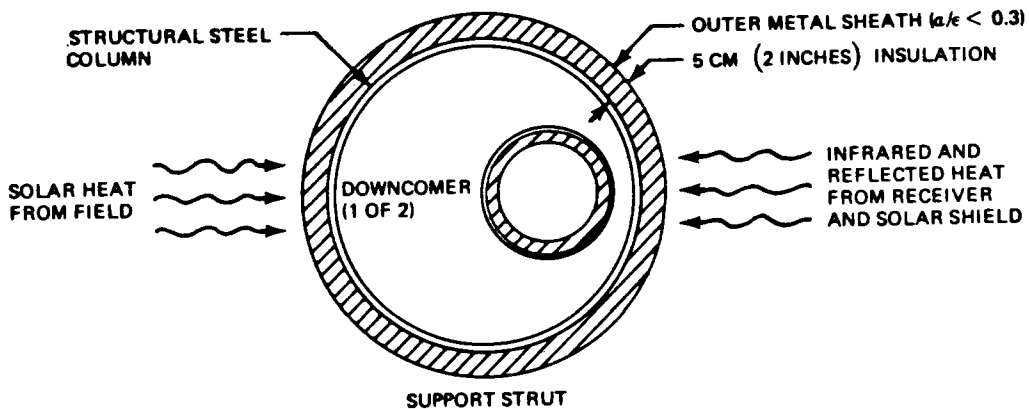


Figure 4-8. Original and Current Structural Design Concepts

the unblocked field heat. To alleviate these problems and the associated costs, the number of risers and downcomers was reduced to two each of a larger size and each pipe was placed within a separate support leg. These concepts are shown on the right side of figure 4-8. The choice of external and internal insulation for the risers and downcomers, respectively, depends on the helium temperature. This is discussed in more detail below with cost implications covered in section 4.4.

The receiver support struts located below the receiver aperture plane are heated by the external field and also by the radiated and reflected heat flux from the receiver back out through the aperture. Figure 4-9 illustrates the heating situation and the selected strut design. The structural steel column is protected by 5 centimeters (2 inches) of insulation covered by an outer metal sheath with a lower absorptance-to-emittance ratio. The local maximum temperatures on either side of the support strut are presented in the tabel on figure 4-9.



LOCAL MAXIMUM TEMPERATURES	SOLAR HEATED SIDE	CAVITY HEATED SIDE
OUTER SHEATH	816°C (1500°F)	610°C (1130°F)
STEEL COLUMN WALL	370°C (700°F)	195°C (384°F)

NOTE: STRUT INTERIOR COOLED BY NATURAL AIR DRAFT

Figure 4-9. Receiver Support Structure Design/Temperatures

A typical downcomer is shown within the support strut on figure 4-9. The design concept is to insulate the pipe containing 816⁰C (1,500⁰F) helium on the interior so that a carbon-steel pipe may be used instead of the more expensive Inconel 617. The risers with 518⁰C (1,000⁰F) helium will be externally insulated, and use of Inconel 617 is again unnecessary. The vertical height of the support structure columns has been utilized to produce natural draft cooling of the interior structure. The heat dissipated by risers and downcomer pipes and the heat leak through the structure heat shield combine to produce internal air temperatures 30⁰ to 60⁰ C above ambient. With adequate venting, the warmed buoyant air circulates upward, drawing in ambient air at the bottom.

Energy Storage. The primary adaptation made in the receiver concept for thermal energy storage inclusion in the solar plant was to ensure that the maximum amount of heat available was collected by the receiver to pass to the helium. This requirement, coupled with the EPRI redefinition of the collector field, necessitated a change in the design of the aperture radius. As a result, the aperture radius was increased from 8 meters (26 feet) to 9.5 meters (31 feet). A plot of the heat flux distribution with radial position of the aperture is shown on figure 4-10. The aperture radius was determined to be optimum when more heat would be lost by reradiation from the receiver than could be gained from the field by increased aperture size.

Part-Load Receiver Performance. Detailed thermal analysis results have been used to define a thermal performance analog model of the preferred receiver configuration. This is used in the thermal energy storage and powerplant implementation studies in sections 6.0 and 8.0. The receiver thermal efficiency at part-load solar input is shown on figure 4-11.

Turbomachinery Location. Although the reduced size of the turbomachinery required for closed-cycle helium made location at the tower top a very attractive option, factors other than size and short plumbing runs to the receiver dictated a ground-level location. The rationale for the decision is discussed in section 4.3.3.

4.2 THERMAL ANALYSIS

Figure 4-12 shows the interaction of thermal analysis activity within the high-temperature solar receiver study. The rectangular blocks represent the two types of contributions provided by the heat transfer disciplines.

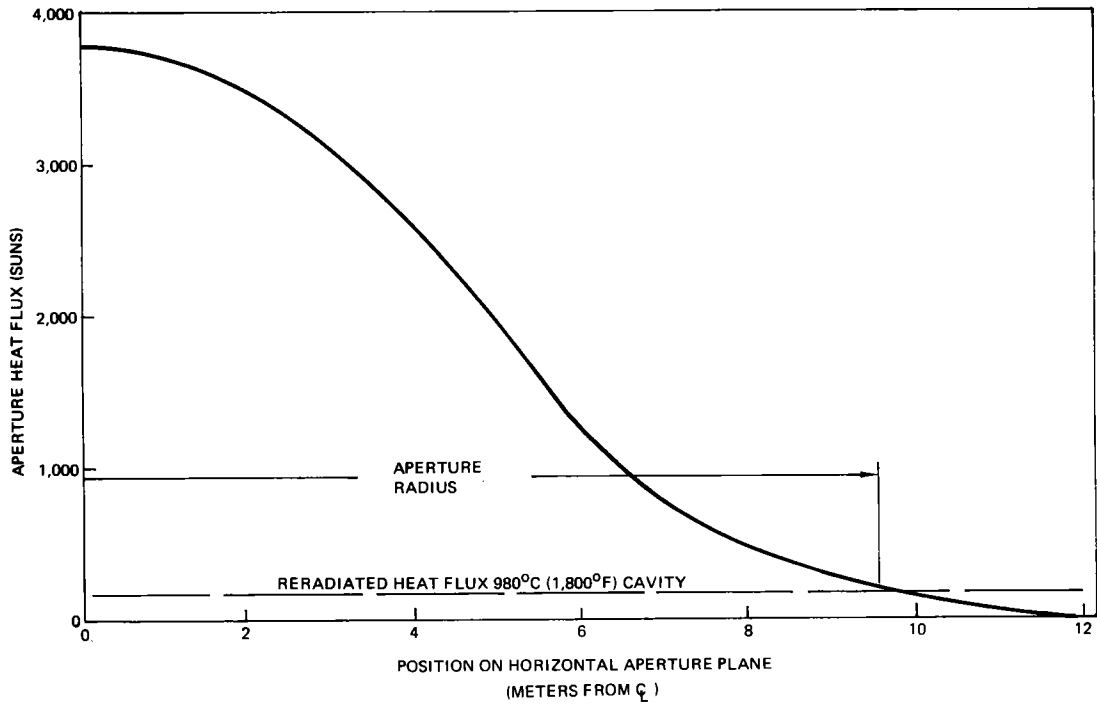


Figure 4-10. Heat Flux Distribution - Horizontal Circular Aperture

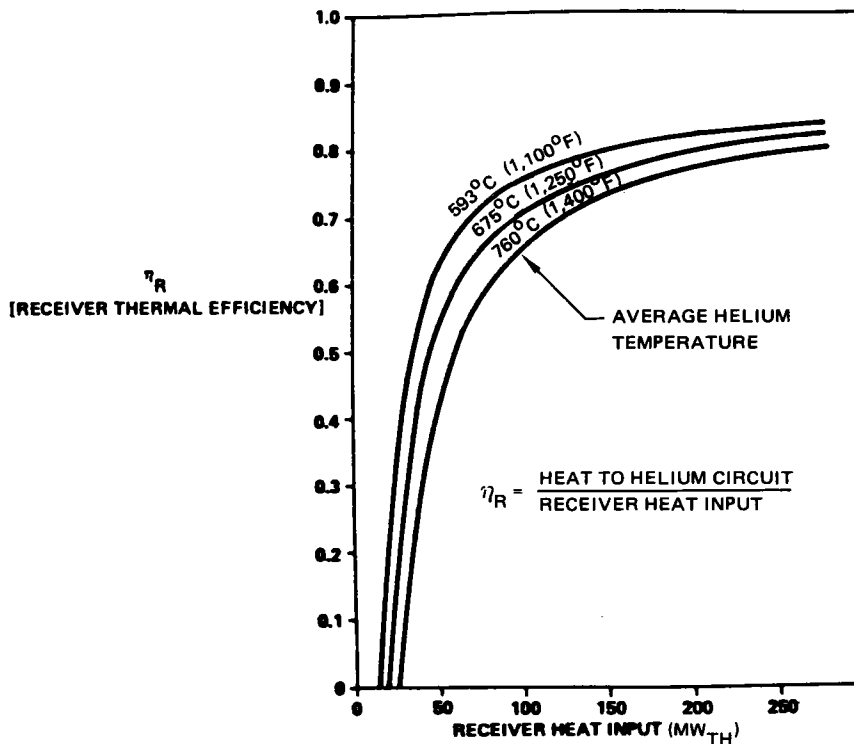


Figure 4-11. Receiver Thermal Efficiency at Part-Load Conditions

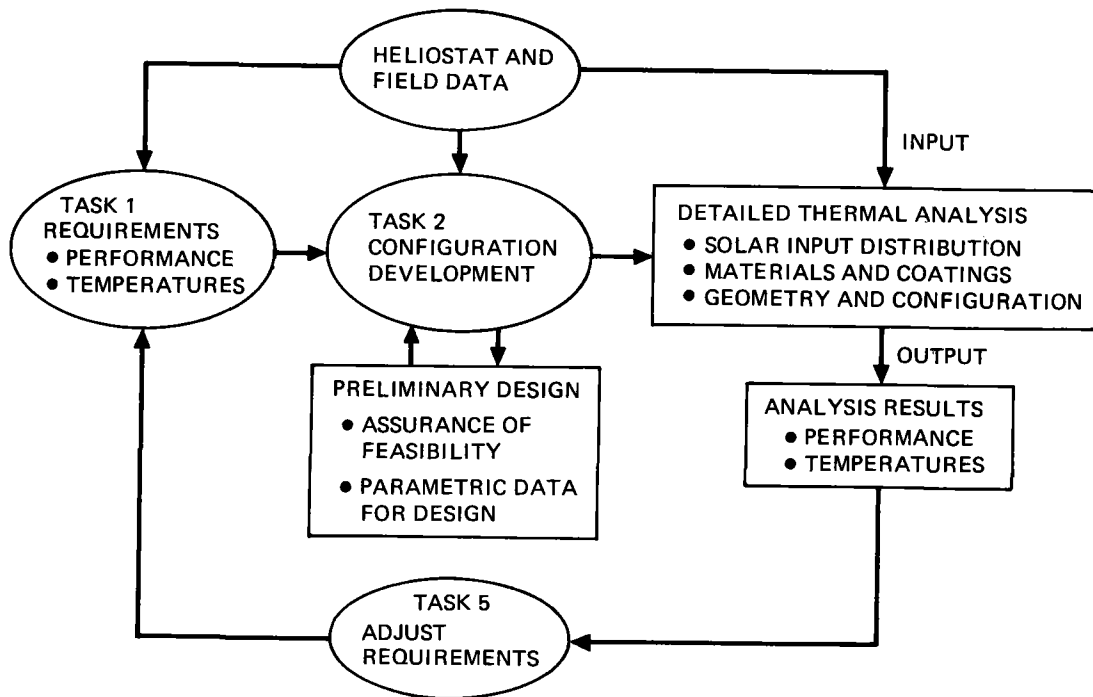


Figure 4-12. Thermal Design and Analysis Activity

Thermal analysis for preliminary design furnished qualitative and quantitative data upon which the configuration decisions were based. All of the configuration trades and results in the previous section 4.1 involved thermal analysis data. Other data developed are summarized in section 4.2.1. The configuration development activity results in the definition of the final receiver concept.

State-of-the-art thermal analysis methods were used to provide a sophisticated assessment of receiver operating temperatures and effectiveness in transporting incident solar heat into the circulating helium. A very detailed model was developed and exercised for a few thermally critical receiver conditions.

Results of this activity are presented in section 4.2.2.

4.2.1 Preliminary Thermal Design

The receiver cavity is lined with banks of heat exchanger tubes. Helium, the Brayton-cycle working fluid, is heated while circulating through these tubes. One preliminary design study defined the ranges of tubing dimensions, flow rates,

and "effective" receiver temperatures that result in acceptable pressure loss in the helium circuit. Typical parametric results are shown on figure 4-13. Heat exchanger panel locations for an earlier panel design with four panel rows in the upper receiver interior are shown. Detailed panel design is discussed in section 4.2.2.

The results of other preliminary heat exchanger design studies are:

- Heat exchanger weight constitutes a significant fraction of the total cavity weight. Moreover, the helium-in-tube heat exchanger weight increases rapidly with lower receiver operating temperature and with increases in tube size. The smallest feasible tube size provides minimum weight.
- Parallel helium flow through several thousand tubes of approximately 2.54 centimeters (1 inch) in diameter and lengths to 12.2 meters (40 feet) provides adequate heat transport and a receiver pressure loss of up to 0.1 MW/m² (15 psi). This is an acceptable pressure loss for the thermal engine.

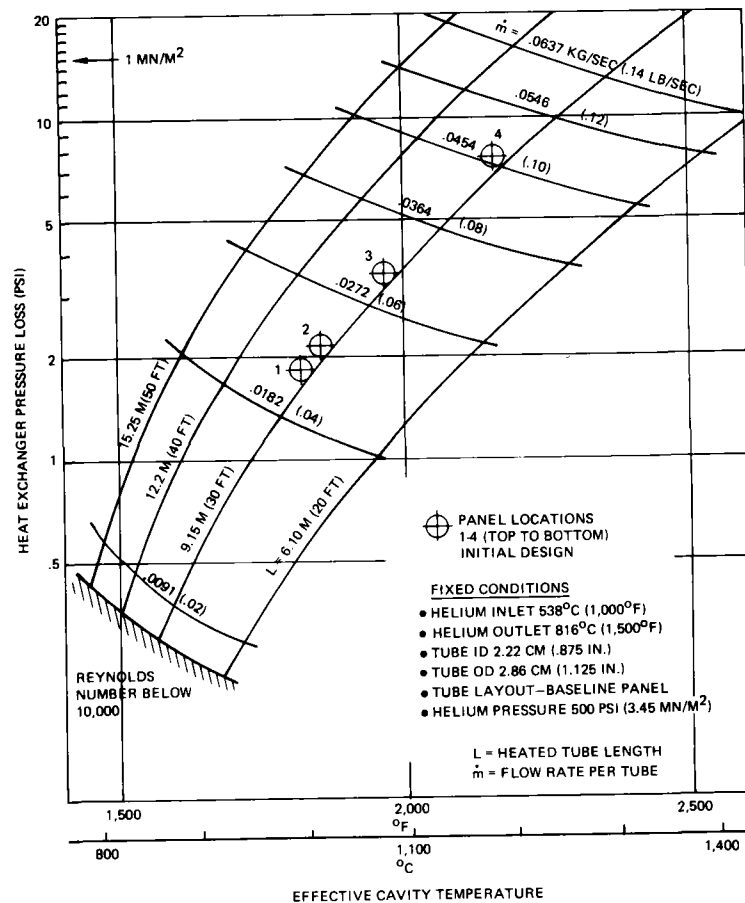


Figure 4-13. Heat Exchanger Tube Performance

- In order to maintain turbulent flow in the heat exchanger, while throttling to 20% or 30% of design flow rate, helium tubing sizes should be greater than about 1.9 centimeters (0.75 inch). Otherwise, longer tubes will be required, with higher flow rates and pressure losses significantly greater than 0.1 MW/m^2 (15 psi).
- Increased solar heat on panels at some locations within the cavity will result in higher heat-transport requirements by these panels because of the parallel flow concept. This can be accommodated by increasing the local helium-flow rate or by allowing the helium outlet temperature to rise above 816°C ($1,500^\circ\text{F}$).
- Because of the heat transfer characteristics of the receiver cavity and heat exchanger system, the tubing temperatures will be dominated by local helium temperature. Significant benefit can be achieved by mass flow alteration so that helium outlet temperature does not significantly exceed 816°C ($1,500^\circ\text{F}$). Then, due to domination by the helium, only about one-fourth of the local cavity temperature rise above nominal will be felt by the tubing.

This preliminary information and the detailed thermal design analyses of section 4.2.2 were used to select the standard heat exchanger panel and configuration shown in section 3.2.

Other preliminary thermal analyses provided insight into the receiver insulation requirements. The major conclusions are:

- Insulation walls designed to preclude heat losses greater than 1% to 2% of the solar heat conversion require thicknesses of high-temperature fibrous insulation, as shown on figure 3-9.
- One change of internal cavity air per hour results in loss of a few percent of the solar heat conversion. An airtight barrier must be incorporated in the cavity walls to prevent the escape of buoyant heated air.
- Conditions of overnight cooldown were evaluated for typical receiver cavities with varied wall insulation thicknesses. Incorporation of insulated doors, closing at night, was considered as a design option. The temperature at dawn for the range of configurations evaluated ranged from just above ambient with no doors to 538°C ($1,000^\circ\text{F}$), with the 538°C ($1,000^\circ\text{F}$) case having doors and a wall insulation thickness of 0.8 meter (2.65 feet). These parametric studies are illustrated by figures 4-14 and 4-15. Receiver doors were deleted due to tubing material properties. The thermal inertial of other components in the system must be likewise determined to be able to predict operational performance, especially the ability to handle system transients such as startup, cooldown, cloud passage, and short-term mechanical failure. These considerations are reported in section 8.0.

4.2.2 Thermal Modeling of Receiver

Figure 4-16 is a functional block diagram of the receiver thermal model. It simulates all the pertinent heat transfer mechanisms that influence cavity temperature and thermal performance. The heat exchanger panel model (upper center, figure 4-16) uses heat exchanger node temperatures from the cavity thermal model, and helium inlet and outlet temperature from the control system analog, and determines the required helium flow rate and resulting heat transfer.

Thermal modeling performance results have been presented in section 3.2.5. The following paragraphs describe the development and use of the receiver thermal model.

The central element is the cavity thermal-analyzer model, a lumped parameter model of the receiver. Insulation walls are represented by a total of 222 isothermal zones. Interconnecting conduction paths are included along with radiant-heat transfer paths across the cavity interior, from inside walls, through the aperture, and from outside walls to the ground and sky. Convection heat transfer from cavity exterior surfaces to the surrounding air is also included. The helium-in-tube heat exchangers are simulated by a total of 16 isothermal regions. By radiation, these are coupled to one another, to the cavity interior walls, and to ambient ground as viewed through the aperture.

Conduction and convection paths are readily computed by hand. The wall insulation thermal conductivity is shown on figure 4-17. A standard wall insulation layup was adopted consisting of an alumina-silica blanket on the inner one-sixth thickness, an alumina-silica block for the next one-third thickness, and mineral-wool block for the outer one-half thickness.

Radiant-heat transfer paths inside the cavity are complicated by the presence of free-standing heat exchanger tubes on the cylindrical wall section. The radiant-view factors were determined by use of the ray-tracing computer code (AS2814). This program simulates radiant exchange by random diffuse emission of rays from the node of interest and traces ray paths throughout the enclosure until absorption. Absorptions are tallied at receiving surfaces for statistically large numbers of these simulated radiant heat flux rays, the results are reduced to view factor values, and then are incorporated in the thermal analyzer model. Table 4-1 described the radiant surface properties used in the radiant-heat transfer

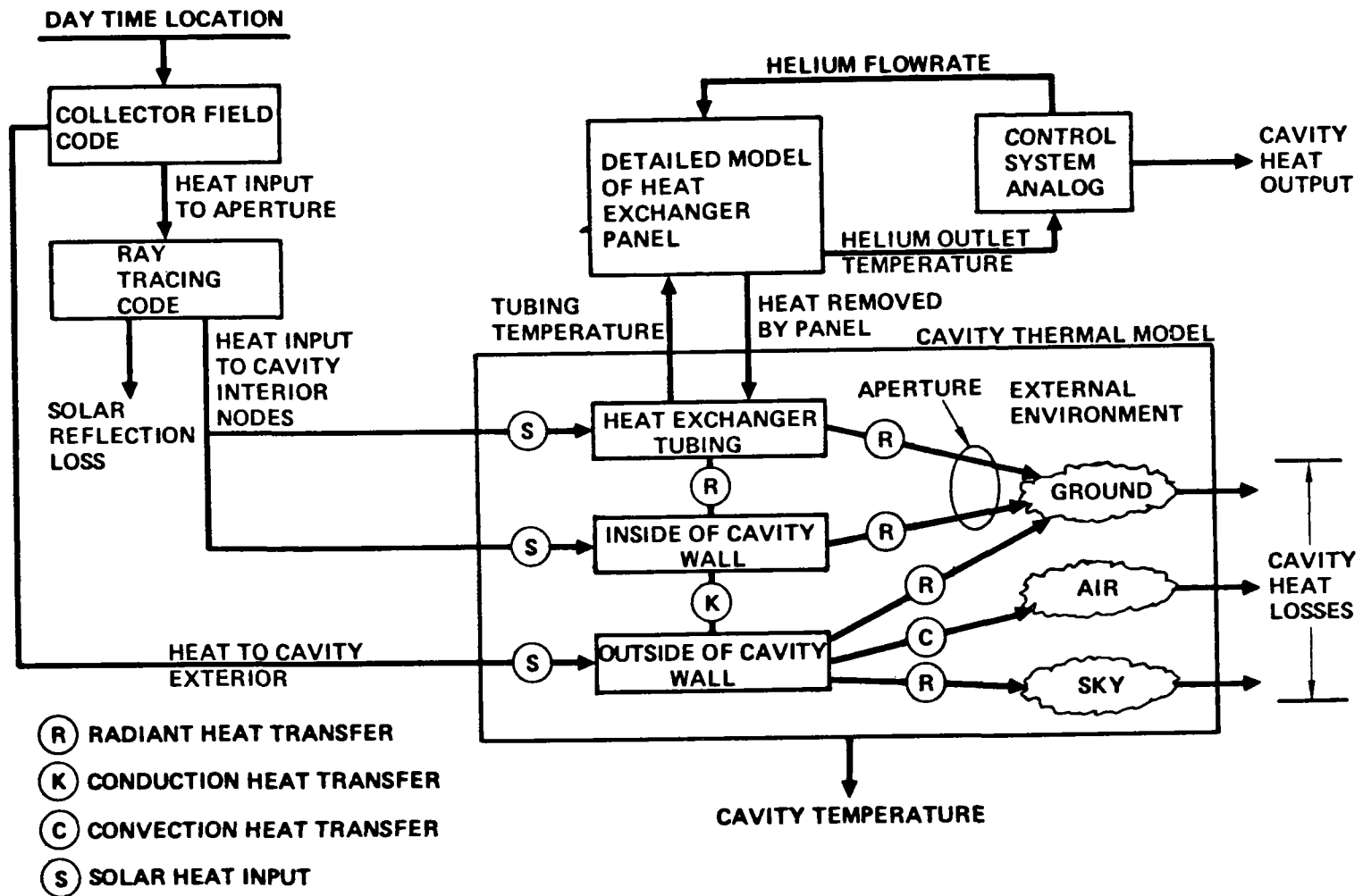


Figure 4-16. Receiver Thermal Model

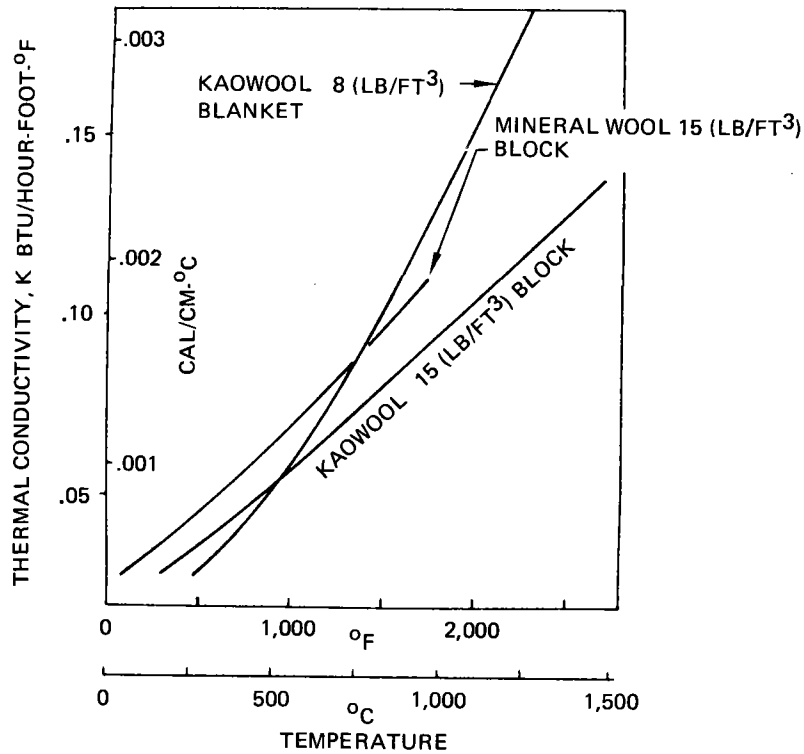


Figure 4-17. Thermal Conductivity of Kaowool (Alumina-Silica) and Mineral Wool Products

Table 4-1. Radiant Surface Properties for Receiver Thermal Model

	Solar			Infrared	
	Diffuse reflectance	Absorptance	Transmittance	Emittance and absorptance	Transmittance
Kaowool wall insulation	0.7	0.3	0	0.8	0
Oxidized surface for heat exchanger tubing	0.12	0.88	0	0.88	0
Composite properties of heat exchanger tubing bundle	0.044	0.504	0.452	0.504	0.452

model. The tube bank was subjected to a separate analysis to determine its net transmittance, absorptance, and reflectance resulting from the selected tube spacing of three diameters center-to-center. These data are also shown on table 4-1. The selection of 0.7 solar reflectance for Kaowool* wall insulation is substantiated by reflectance measurements on mixed silica-alumina samples. The kaolin fiber consists of 47% Al_2O_3 and 53% SiO_2 . Normal spectral reflectance of a 50-50 powder mixture of these materials is shown on figure 4-18. The assumed 0.7 reflectance value is conservatively low. The lower value was selected to account for darkening of the wall insulation with time. All reflected flux was assumed to be diffuse. This was verified by measurement of the bi-directional reflectance of a sample of silica fiber blanket at 0.628-micron wavelength. The reflected flux was very uniform in intensity, showing only about a 50% increase at the specular reflection angle.

The wall insulation was assumed to exhibit a gray-body emittance of 0.8. This is substantiated by the measured infrared properties of Al_2O_3 and SiO_2 powders shown on figure 4-19. The selected value is conservatively low. This again allows for maximum temperature conditions that may result with long-term aging or contamination of the wall insulation.

Three types of solar heat inputs (shown by the circled S, figure 4-16) were incorporated in the thermal analyzer model. Values were computed using the heliostat field code (HACSM) to determine the spatial distribution of solar heat at the vicinity of the receiver and the flux entering the aperture. The Monte Carlo ray-tracing code (AS2814) was used to determine the distribution of solar flux absorbed on cavity walls and heat exchanger nodes.

Calculations with the field code (HACSM) determined the performance of 101 heliostats at selected locations in the heliostat field. The effects of blocking, shadowing, and reflected beam spreading to overlap the cavity aperture were accounted for in detail. Then the computed values were increased to account for the full heliostat field. The result is a set of 101 cavity solar inputs each with a characteristic direction and magnitude. The sum equals the total solar heat input.

The detailed field heat input to the receiver aperture is used as input for the ray-tracing computer code. A total of 50,000 directed rays has been used to

*Registered trademark of Babcock and Wilcox

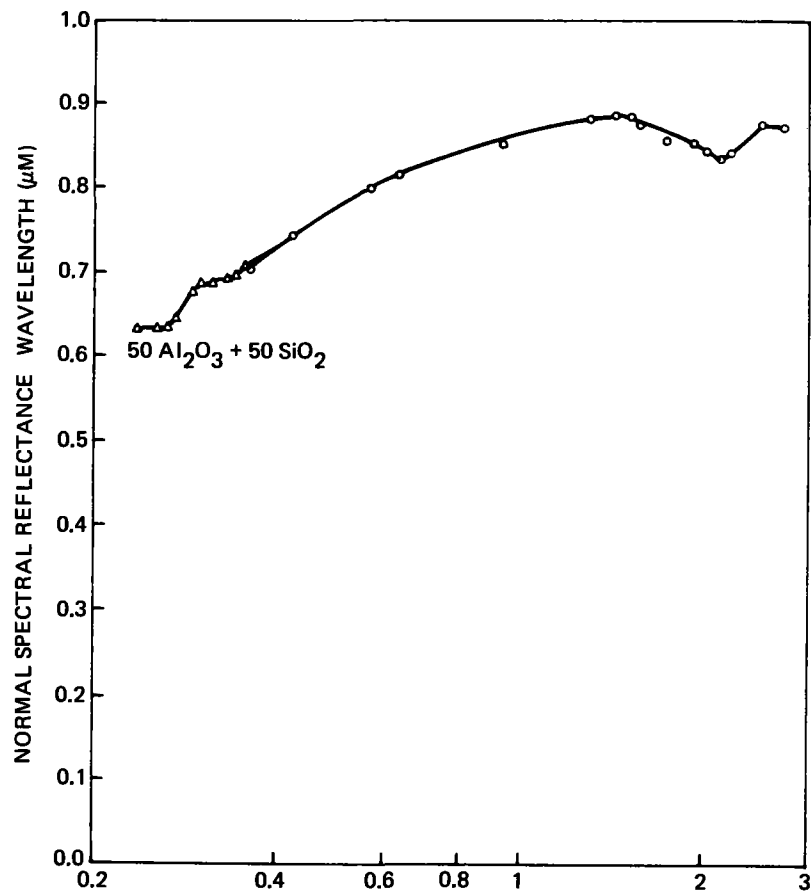


Figure 4-18. Normal Spectral Reflectance of [Al₂O₃ + SiO₂] Powders

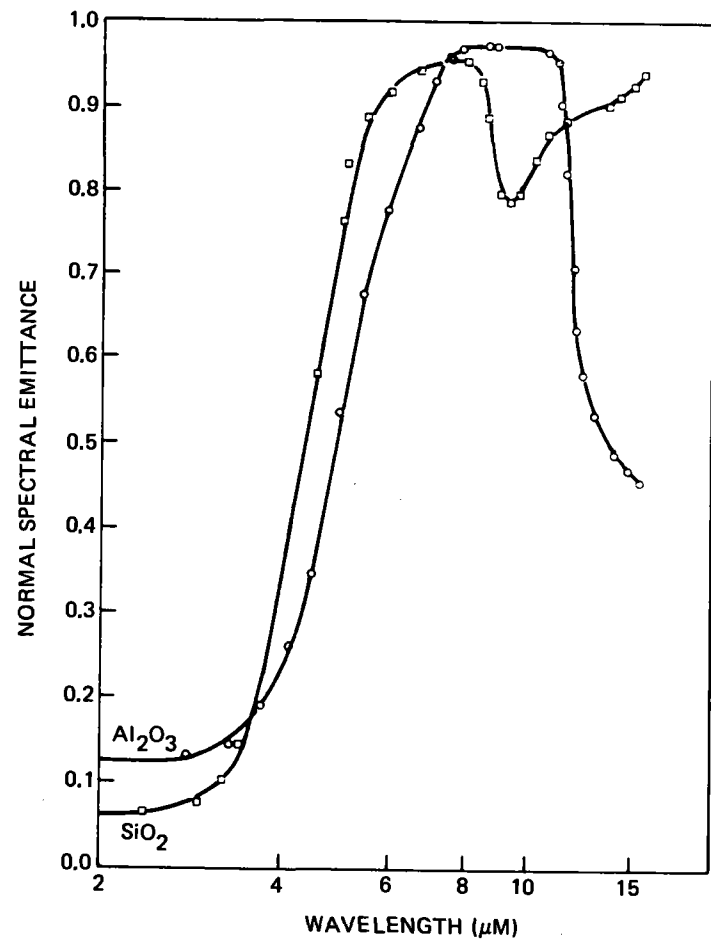


Figure 4-19. Normal Spectral Emittance of [Al₂O₃ + SiO₂] Powders

simulate the spatial solar-flux distribution. These rays, traced to their terminal absorption point (or until lost out the aperture), provide the description of solar heat input to the receiver interior surfaces. Table 4-1 describes the radiant surface properties used in the study.

The solar flux on exterior receiver surfaces near the aperture was determined from beam-spreading and aperture-overlap computations internal to the heliostat field program. It assumed normal steering of heliostats with the target being the center of the aperture.

Each of the 16 heat exchanger nodes in the thermal analyzer is furnished with a heat removal rate simulating the cooling effect of circulating helium. A separate calculation routine was needed because of the very fine division and large numbers of thermal nodes needed to model the multiple-tube heat exchanger accurately. In operation, the receiver thermal model computed thermal interface conditions for the heat exchanger panel. This information was combined with other data such as helium flow rate and temperature to define the rate of heat transport to helium. This heat removal is imposed on the heat exchanger node in the thermal analyzer. The process was repeated for each heat exchanger node at each iterative time step of the receiver model.

Another thermal analyzer model was developed to define the heat exchanger performance. This is the "heat exchanger thermal model." It is described in the following paragraphs.

Figure 4-20 describes the detailed model used to characterize the initial heat exchanger panel concept. The major factors considered in selecting this particular form of model are:

- Development of a baseline U-tube panel configuration that accommodates structural and other system requirements
- Examination of the heat transport mechanisms, which revealed major dependence of performance on the radiant heating mechanism at the tube outside diameter
- Added interest in determining detailed tube material temperatures and gradients for evaluation of thermal stresses

The model utilizes fixed temperature (Dirichlet) boundary conditions throughout. Two U-shaped tubes are coded with simulation of the boundary conditions for an infinitely wide double row. At each of three cross sections evaluated, the four

tubes are simulated by 48 isothermal nodes. Interconnections, all in the section plane, include 72 conduction paths, 24 helium convection paths, and a total of 174 radiant-heat transfer paths. Axial heat flow in the tube all is neglected.

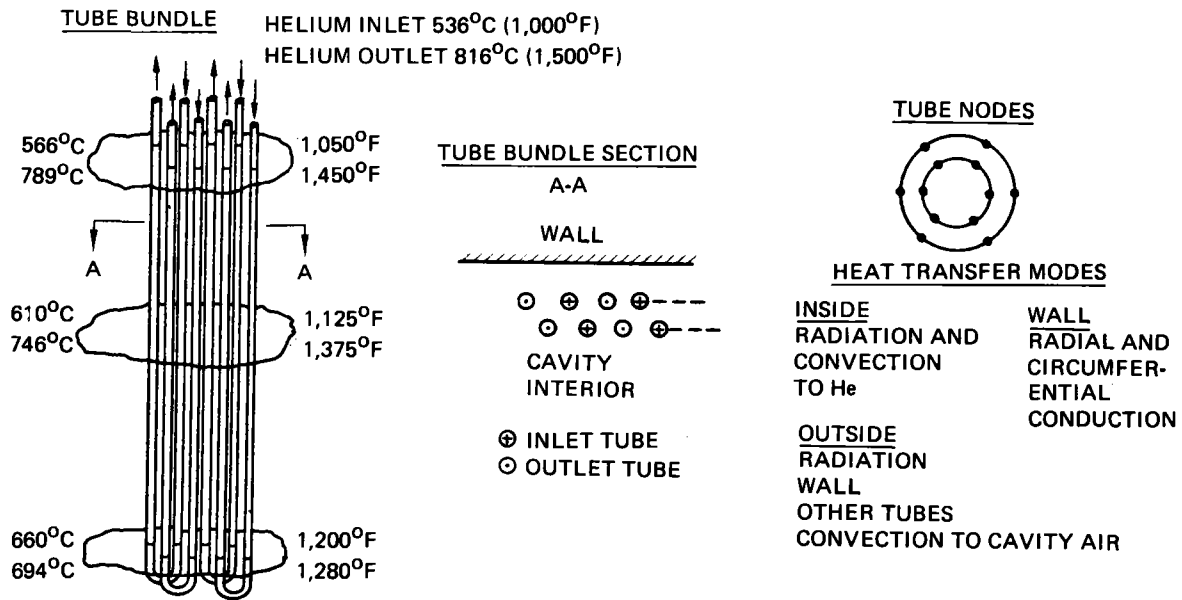


Figure 4-20. Heat Exchanger Thermal Model for Initial Studies

In operation, the temperatures of helium and the cavity environment are first specified in the model, then the equilibrium temperatures of all points in the model are derived by numerical analysis. A final output consists of definition of the rate of heat flow into each of six characteristic tubing sections per unit length. The model can also be exercised using receiver cavity heat input from both sides of the tube bank. Alternatively, the program input can be adjusted to simulate one row of alternate inlet and return flow tubes.

Figure 4-21 shows temperatures at the upper cross section of the heat exchanger panel model described by figure 4-20. The conditions are typical of those experienced by the original heat exchanger design inside the receiver. Temperatures for lower and center cross sections were obtained similarly. The six conditions evaluated, two per cross section, were used to define heat transfer performance, as shown on figure 4-22.

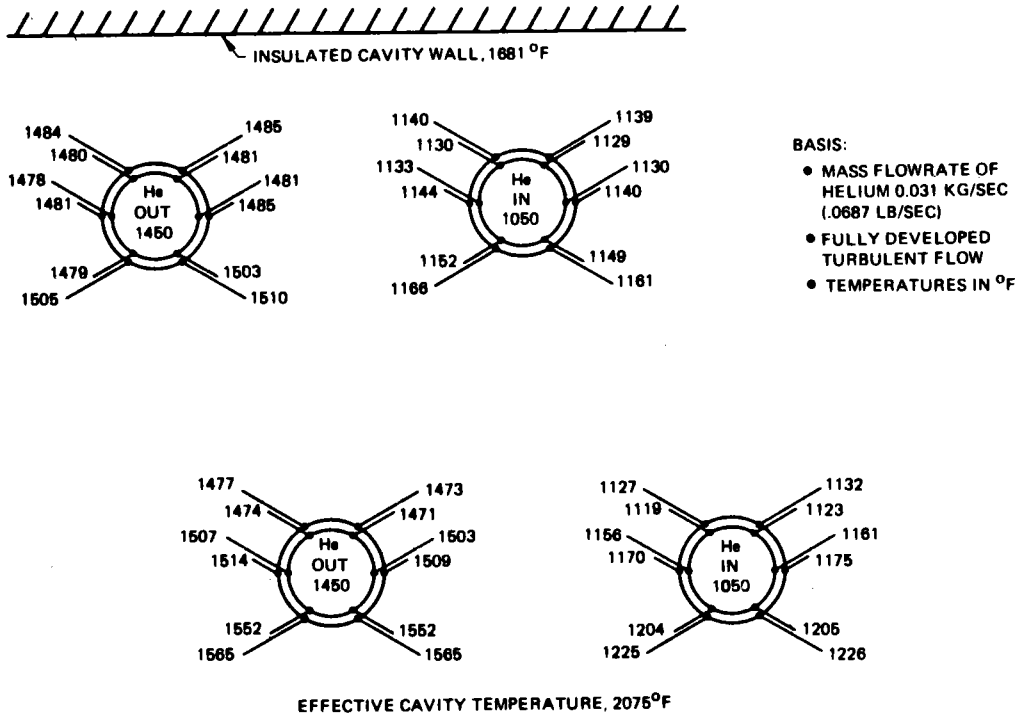


Figure 4-21. Temperature Data—Heat Exchanger Thermal Model

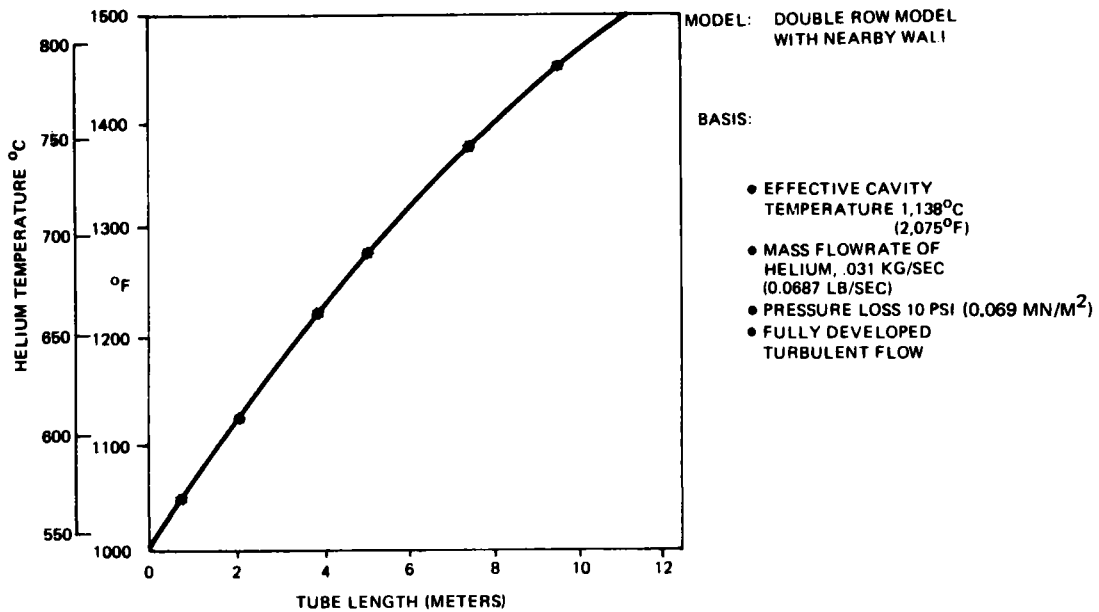


Figure 4-22. Performance Data—Heat Exchanger Thermal Model

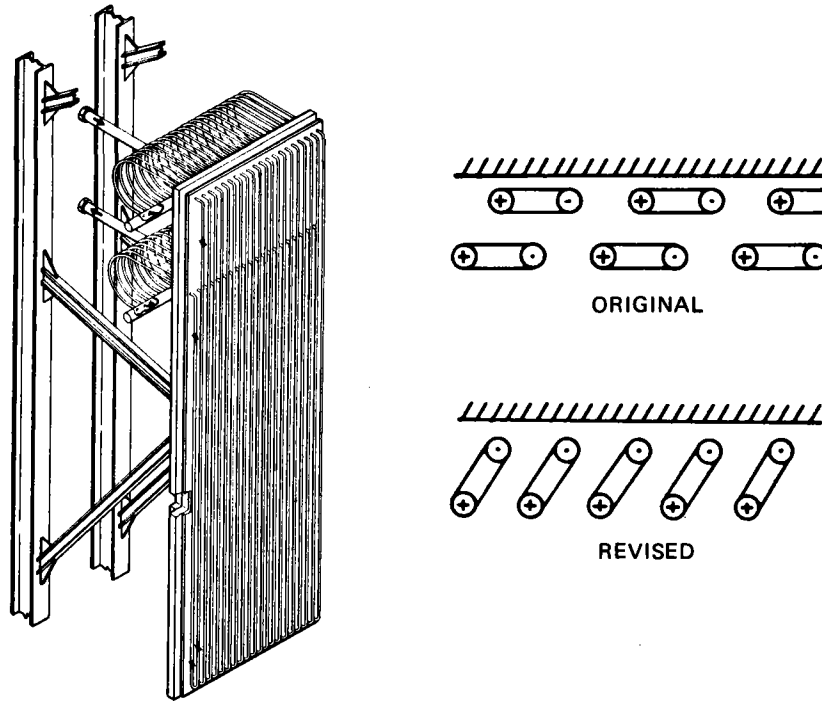


Figure 4-23. Revision of Standard Heat Exchanger Panel.

This original heat exchanger model was used for most of the early study activities. Additional thermal performance data, derived by use of the model, are reported in the Interim Technical Report for Project RP377-1.

A new heat exchanger model has been developed that incorporates recent changes in the heat exchanger panel design. The major change is in the routing of heat transfer tubing. Figure 4-23 describes the original and revised configurations.

The original configuration was preferred because of the freedom on U-shaped tubes to respond to the differential expansion of hot and cold legs by moving in a direction parallel to the receiver wall, precluding interference with the wall. However, with the tubing bend parallel to the receiver wall (as depicted for the original configuration on figure 4-23), the inner and outer rows of tubes exhibit quite different thermal response. The tube row against the wall is partially shadowed by the other tubes. As a result, when the inner row of tubes (away from the wall) reaches its maximum operating temperature and heat transfer performance the partly shaded row is operational well below maximum capacity.

A study of mechanical interactions of the heated tubes showed that deflection with differential expansion could be maintained parallel to the wall, even

with the tube bends oriented as shown for the revised configuration on figure 4-23. This is accomplished by allowing the horizontal tube sections which pass through the receiver wall to rotate. The approximate six degree rotation needed to accommodate differential expansion of the U-tube is provided by torsional wind-up of the pass-through tubing sections.

The new model is similar to the early heat exchanger analysis model shown on figure 4-20. However, rather than sectioning the tube in 6 longitudinal zones it has been divided into 14 segments. Eight are used to define the inlet portion of tube from inlet through the wall down to the U-bend, and six for the shorter portion returning upward along the wall to the outlet through the wall. Each of these is divided into 16 circumferential segments having inner and outer tube wall nodes. This results in a tubing model that consists of a total of 224 isothermal zones. Radiative, convective, and conduction heat transfer are modeled just as in the original tubing model.

A total of 89 steady-state conditions has been evaluated to characterize the heat exchanger performance as a function of inlet and outlet gas temperature, helium flow rate, and cavity environment temperature. These analytical data have been reduced to a set of two definitive figures. These are shown on figures 4-24 and 4-25.

The independent variables on figures 4-24 and 4-25 are helium temperature rise and helium flow rate. With these values specified there occurs a unique set of values for the dependent variables, which are: heat transfer per tube, which results directly for selected values of flow and temperature rise; effective cavity temperature, which is required to produce the heat transfer per tube; pressure drop in the helium circuit, which must be overcome to achieve the required mass flow; and peak tubing temperature, which exists as a result of prevailing heat transfer resistances and heat fluxes. The peak temperature is an important variable because of the strong dependence of service life of the heat transfer tubing on operating temperature.

The new tube routing design provides a significant improvement in heat exchanger performance. In addition to correcting the previous mismatch of heat loads on the two rows of tubes, the new design locates the cooler inlet leg of each U-tube toward the cavity interior. The outlet high-temperature legs located against the wall are partly shaded by the inlet tubes. As a result, the new design can

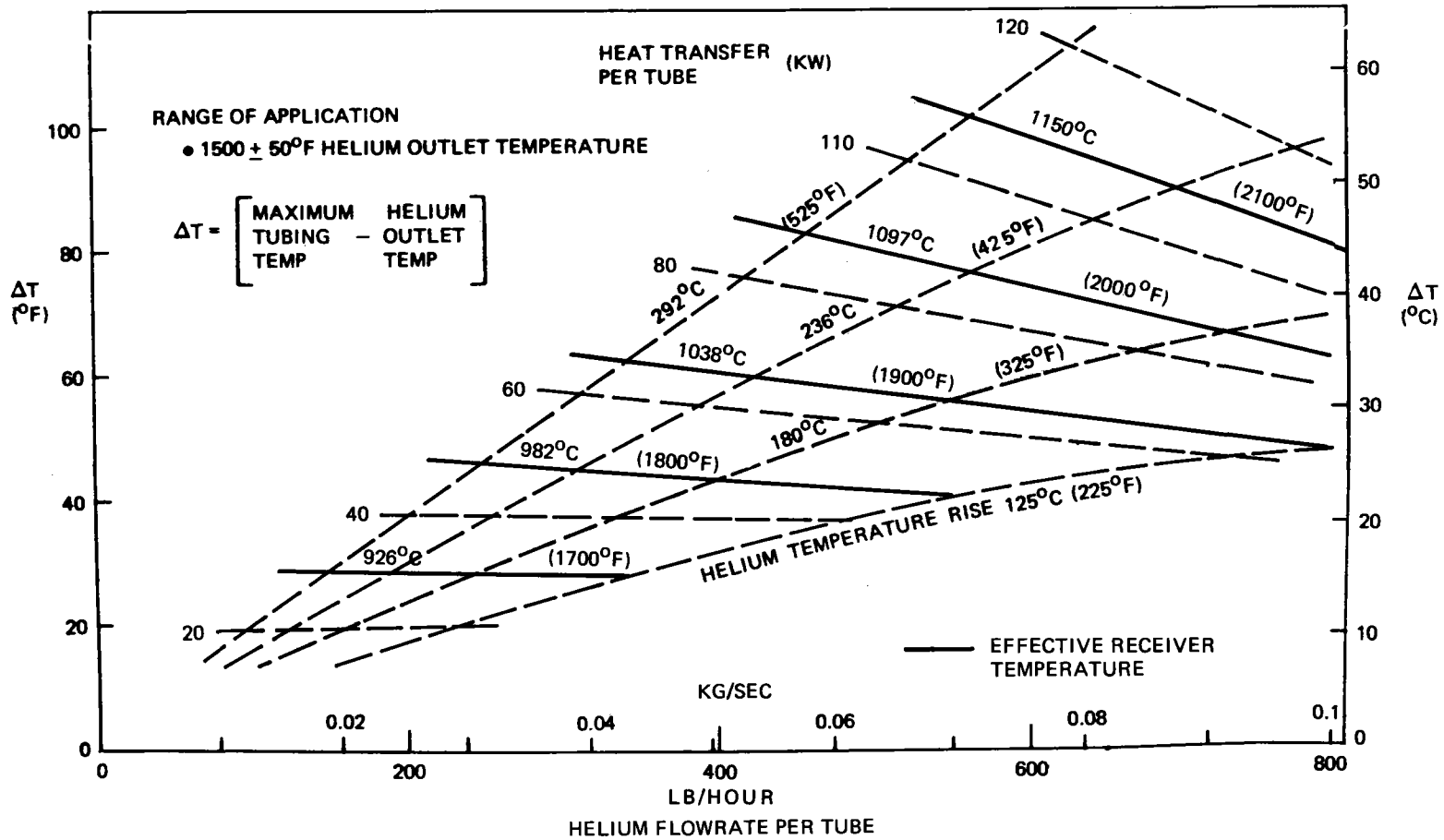


Figure 4-25. Receiver Temperature Required to Achieve Heat Transfer

be operated at higher incident flux levels without overheating the tube at its outlet end.

The heat transfer per tube is compared for the two configurations on figure 4-26. In addition to improved external view factors, the new configuration operates at higher internal mass flow for equal incident flux. This improves internal convective heat transfer, resulting in nearly twice the net heat transfer for equal incident flux.

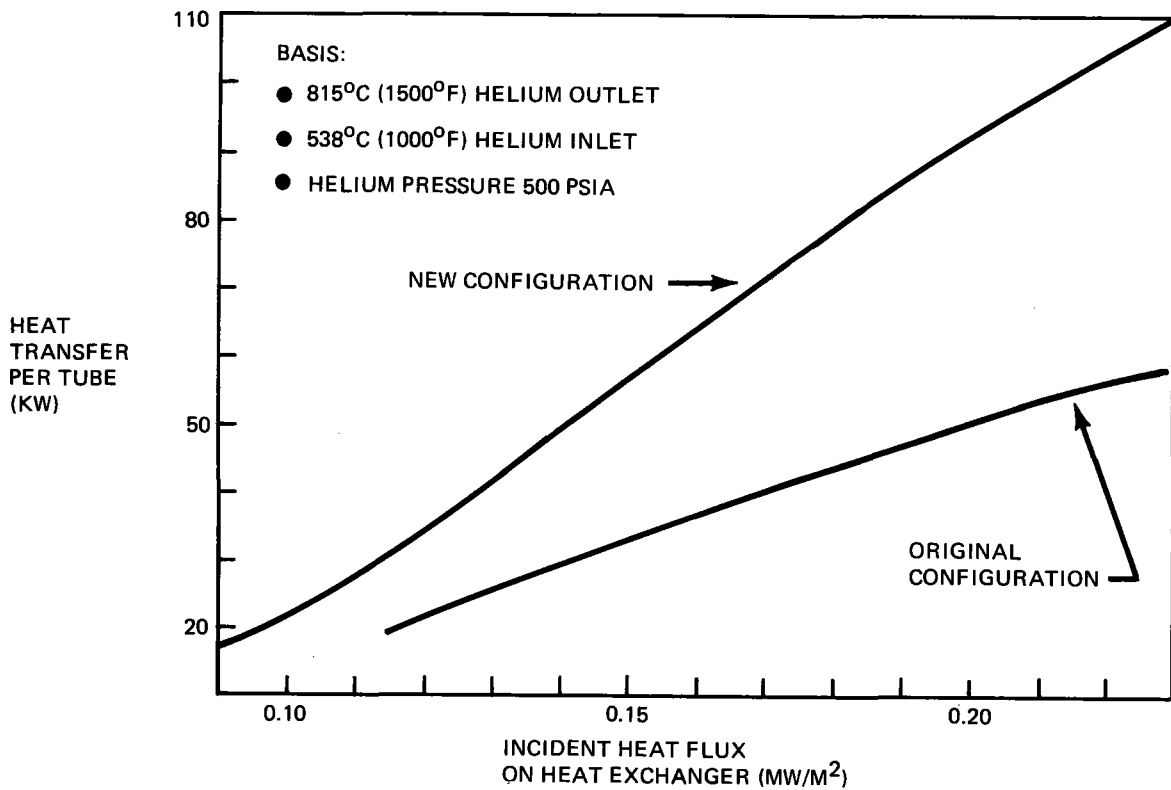


Figure 4-26 . Performance Comparison—Heat Transfer per Tube

A comparison has also been made for the two heat exchanger configurations operated at equal peak tubing temperatures. This is shown on figure 4-27. The previously discussed shadowing of the hot outlet portion of the U-tubes accounts for part of the improvement at equal incident flux. Added benefit is again provided by the increased mass flow and improved internal convective heat transfer.

The new heat exchanger has been incorporated in the most recent receiver design efforts. Improved performance results in a receiver design having 210 rather than 280 of the standard heat exchanger panels. Their maximum operating temperature, at a receiver heat load of 273 MW_{th} , is only about 850°C ($1,565^{\circ}\text{F}$) rather than the 900°C ($1,660^{\circ}\text{F}$) experienced by the original heat exchanger design. The trade between maximum heat exchanger tubing temperature and the heat exchanger surface area (number of standard panels provided in the receiver) is described on figure 4-28.

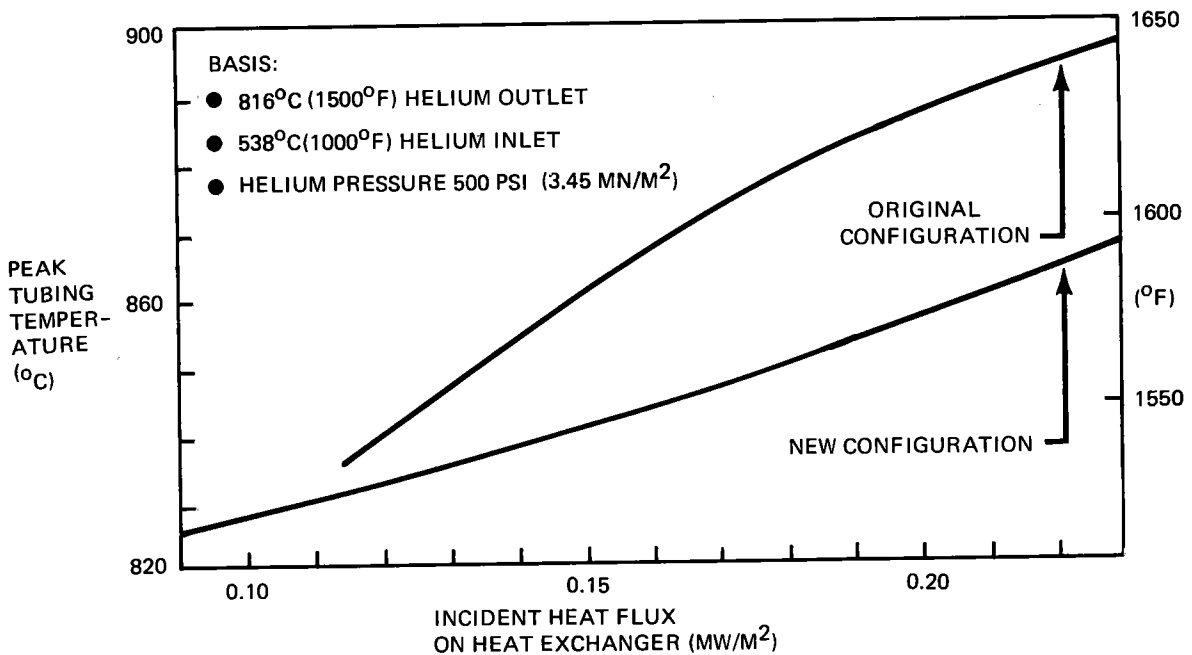


Figure 4-27. Performance Comparison—Peak Tubing Temperature

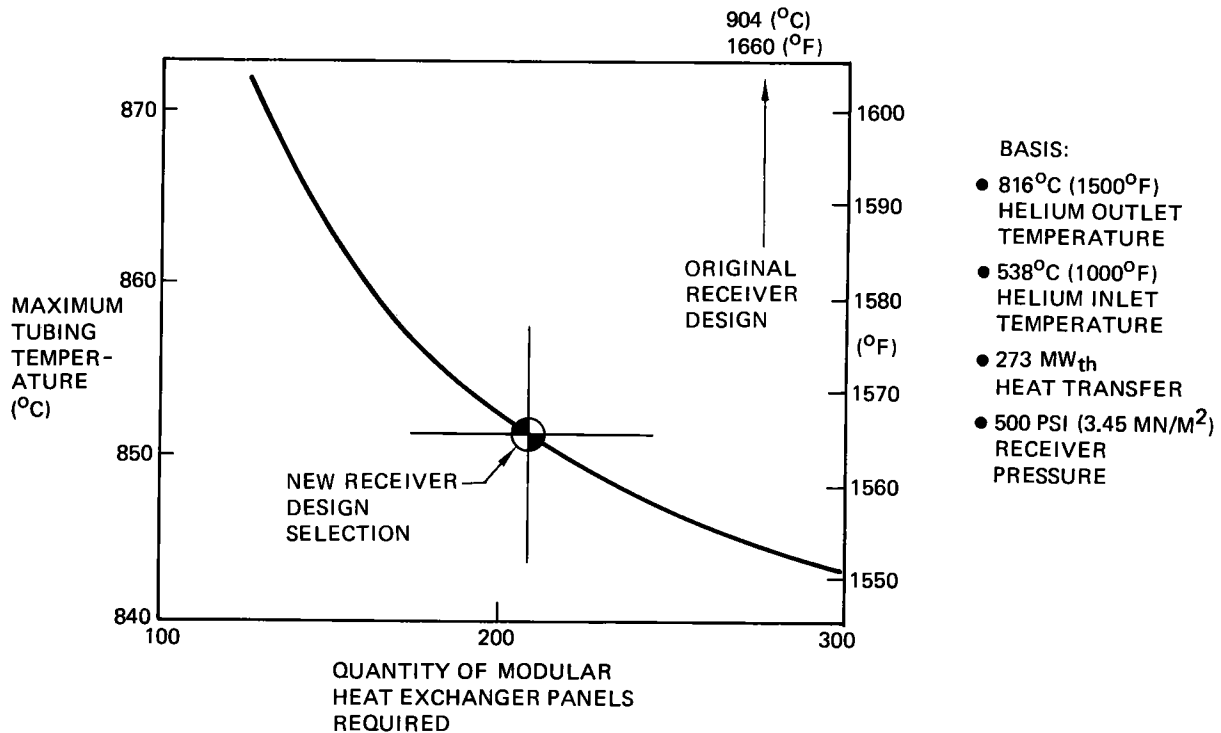


Figure 4-28. Heat Exchanger Panel Requirements Using New Configuration

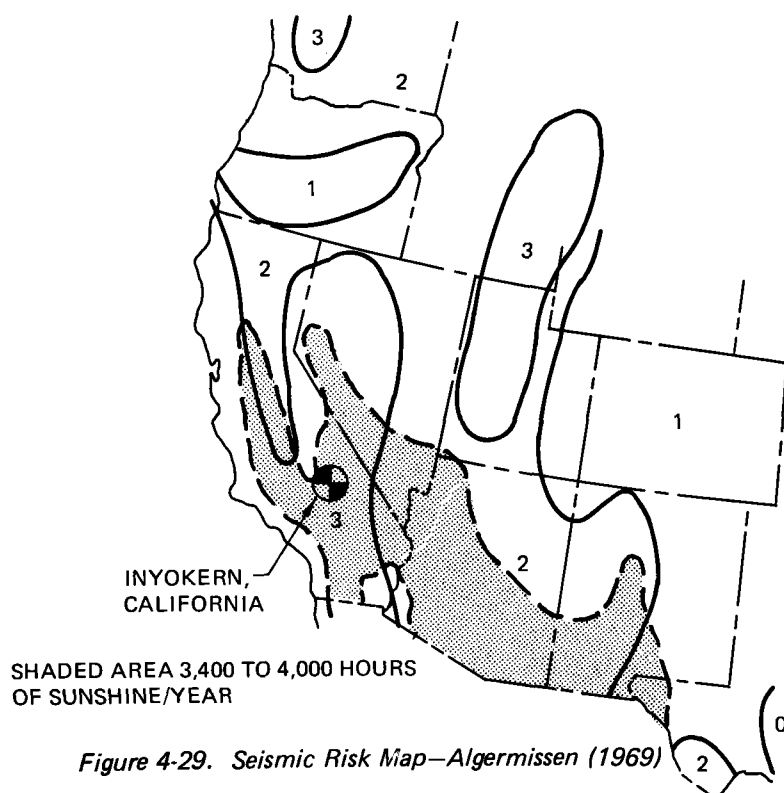
4.3 STRUCTURAL CONSIDERATIONS

Structural analysis efforts supported the determination of a baseline receiver conceptual design and an implementing solar plant concept. Some of the major configuration work has been reported in section 4.1. The study effort was concentrated on the receiver and its components and not on the tower design. Exception to this will be found in section 4.3.3, which discusses turbomachinery location in the tower and reports the results of receiver/tower dynamic analysis to seismic conditions.

4.3.1 Environmental Impacts and Constraints

The principal environmental concerns affecting receiver/solar plant design are earthquakes, winds (and associated dust), rain, and cloud cover. Probable site locations must be concerned with all of these environmental factors.

Earthquakes. The Inyokern, California, location is in the highest risk zone, Zone 3, as shown by the solid lines of figure 4-29.



The primary impact on design (and cost) in seismic risk Zone 3 is on the receiver tower requiring (1) a foundation that will accept the high base shear and (2) a tower capable of withstanding the dynamic load factors with minimal deflection. The dynamic analysis results are reported in section 4.3.3.

Winds. High winds up to a maximum of 53.6 meters per second (120 miles per hour) have two areas of impact. Tower design must provide sufficient stiffness to permit normal operation in winds up to 40 miles per hour. Additionally, there should exist no undamped vibrations initiated by vortex shedding up to the maximum of 53.6 meters per second (120 miles per hour). The receiver aperture altitude of approximately 260 meters (855 feet) is sufficient to reduce or eliminate concerns for direct dust erosion of any exposed elements; however, dust-laden thermal updrafts may be of concern. The second area of impact is the dynamic pressure loading on the receiver tower. For seismic risk Zone 3, wind loading is less severe than the seismic loads. Although outside the scope of this study, heliostat design requirements for wind and seismic conditions are similar to those on the receiver tower.

Rain. Rain probability imposes the requirement for a roof on the receiver and erosion protection for the insulation. In addition, it is mandatory that adequate venting of the insulation be provided to prevent steam damage from accumulated moisture.

Cloud Cover. Occasional cloud cover, if sharp edged, primarily affects the quantity of energy into the receiver aperture and the directionality of that energy within the receiver. Operational and control procedures are required to ensure continuous output and a constant level of electrical power production. Discussions of such conditions, which involve thermal buffering, heat storage, or transients, are provided in sections 5.4 and 8.0.

4.3.2 Receiver Configuration

Three receiver configurations, as identified in sections 4.1.2 and 4.1.3 were analyzed and led to preliminary structural designs. The cylindrical receiver was analyzed first; then the spherical receiver; and, finally, a hemispherical-cylindrical-shaped receiver. The basic design approach for all three receivers was to use mild-steel construction wherever temperatures were low enough to be within the material capability and insulated stainless-steel helium return lines for high-temperature applications.

Support structure for the three receivers was identical in basic concept, with only minor differences to accommodate configuration size and shape. Five legs project up and out from the top of the tower to a rectangular tension ring set sufficiently distant from the aperture to provide a maximum clear view of the aperture from the collector field. This design also minimizes heating by direct radiation from the field and reduces field blockage. From this main ring, five radials extend inward and upward to the receiver stringer support rings. Structural arrangements for the three receivers are illustrated in figure 4-30.

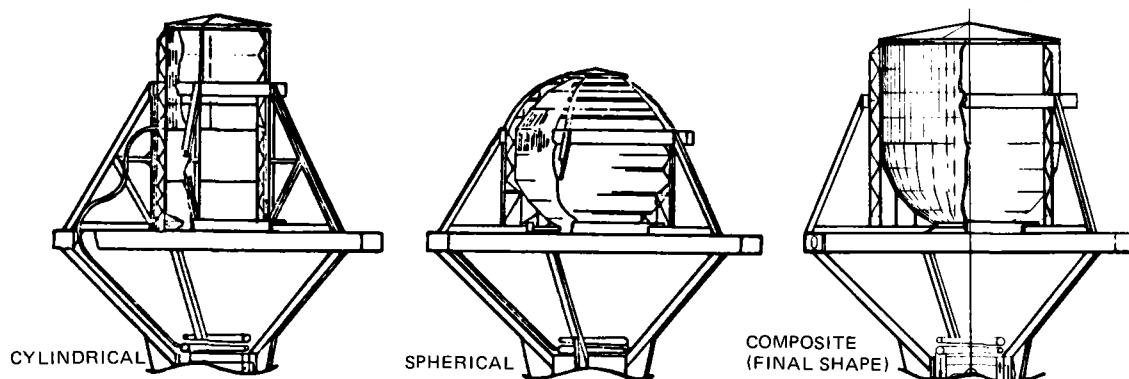


Figure 4-30. Alternate Shapes—Structural Arrangements

Vertical stringers support the roof section, heat exchanger panel supports, and the panel manifolds for the cylindrical and the final receiver. Truss beams bridge the tops of those receivers and support the top receiver panels and roofing panels. For the spherical receiver, five curved truss members extend upward and inward to the roof cap to support upper hemisphere closure. Various trade studies on cost, heat exchanger panel size, and thermal performance were used to select a final configuration that utilizes the best features of the spherical and cylindrical receivers. These have been reported in section 4.1.3. The final receiver arrangement has helium risers and downcomers that are individually supported and guided within the main verticals down to the collectors at the tower top. The configuration trade dictating this arrangement is discussed in section 4.1.5. Areas on the receiver where resultant temperatures are in excess of base-metal capability are protected by insulation and shields. As reported in section 4.1.2, support structure temperatures in regions of field-flux intercept exceed the capability of mild steel. Shielded insulation will keep support temperatures within allowable limits. Another location of heating concern near the aperture lip where the field radiation overflow is most concentrated is protected by a heat shield, as depicted on figure 3-9.

4.3.3 Receiver/Tower Integration

Two possible locations for thermal energy storage (TES) and turbomachinery were evaluated for impact on central receiver tower design. The candidate locations were the tower base and the top of the slip cast concrete structure. The tower top location was favored to take advantage of the helium turbomachinery size and the proximity to the receiver with the resultant short helium runs.

TES for the 6-hour requirements indicated a storage media mass of from 4-13 million kilograms (9-30 million pounds). The estimated receiver weight to be supported by the tower is 1.5 million kilograms (3.3 million pounds). A tower to support the additional weight of the TES was considered impractical; therefore, ground level storage was dictated.

A seismic- and wind-loading analysis was conducted to determine the effect on turbomachinery located at the tower top and to assess the impact on tower design. The tower model used in the analysis is shown in figure 4-31. It was found that turbomachinery weight had a negligible effect on tower loads; however, the tower

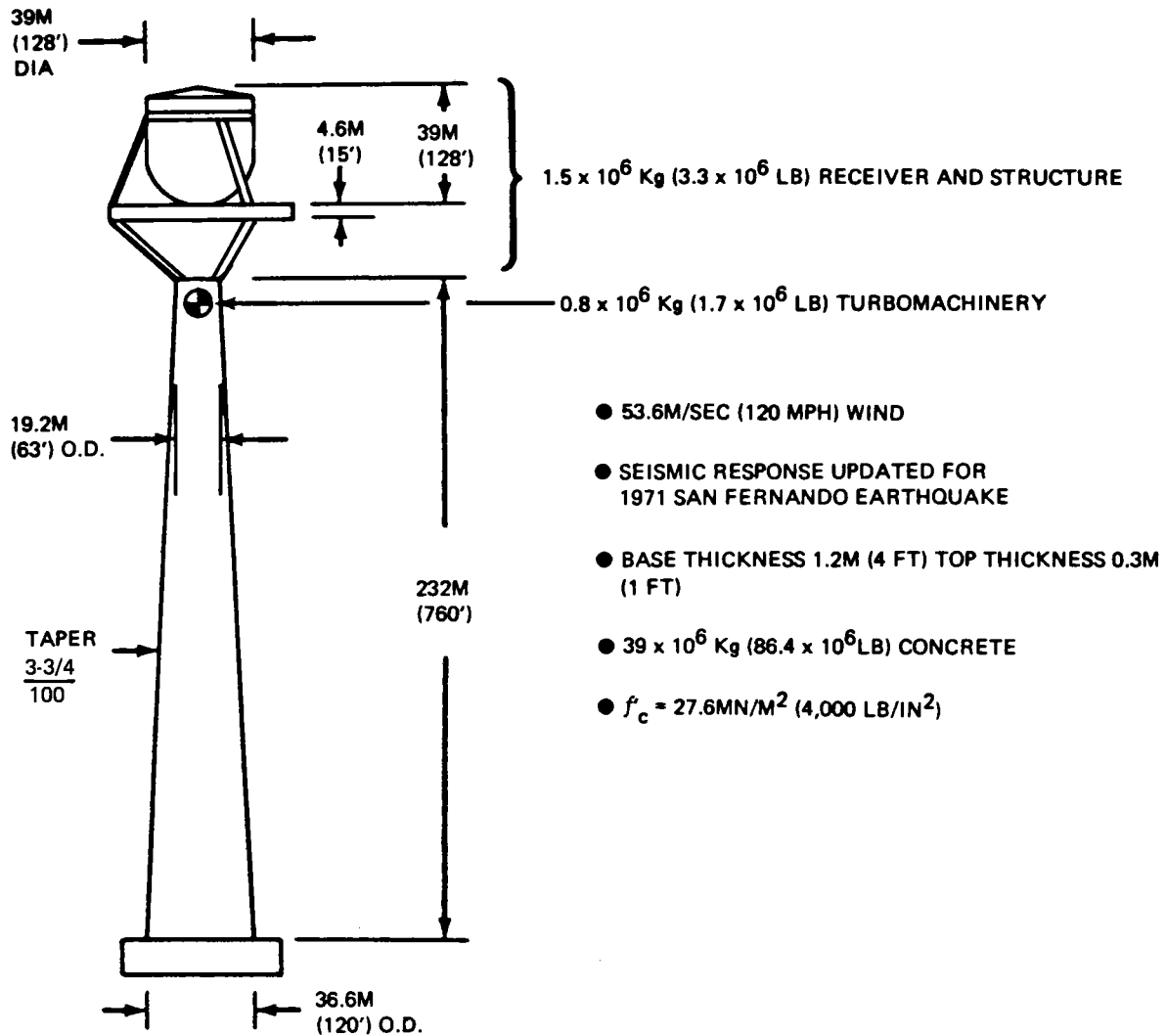


Figure 4-31. Tower Configuration

top location exposed the turbomachinery to a 1-g lateral acceleration in seismic Zone 3 as shown in figure 4-32. This loading was considered abnormal for the equipment and indicated a tower base location as shown in figure 4-33. The choice of ground-level TES necessitated long helium runs the length of the tower; therefore, locating the turbomachinery at ground level did not further penalize the system.

Figure 4-32 also shows moments, shear, and deflection of the tower due to seismic loads. Seismic and wind loads were found to be equally critical in seismic Zone 2. At Inyokern, California, and other Zone 3 sites, earthquake loading governs

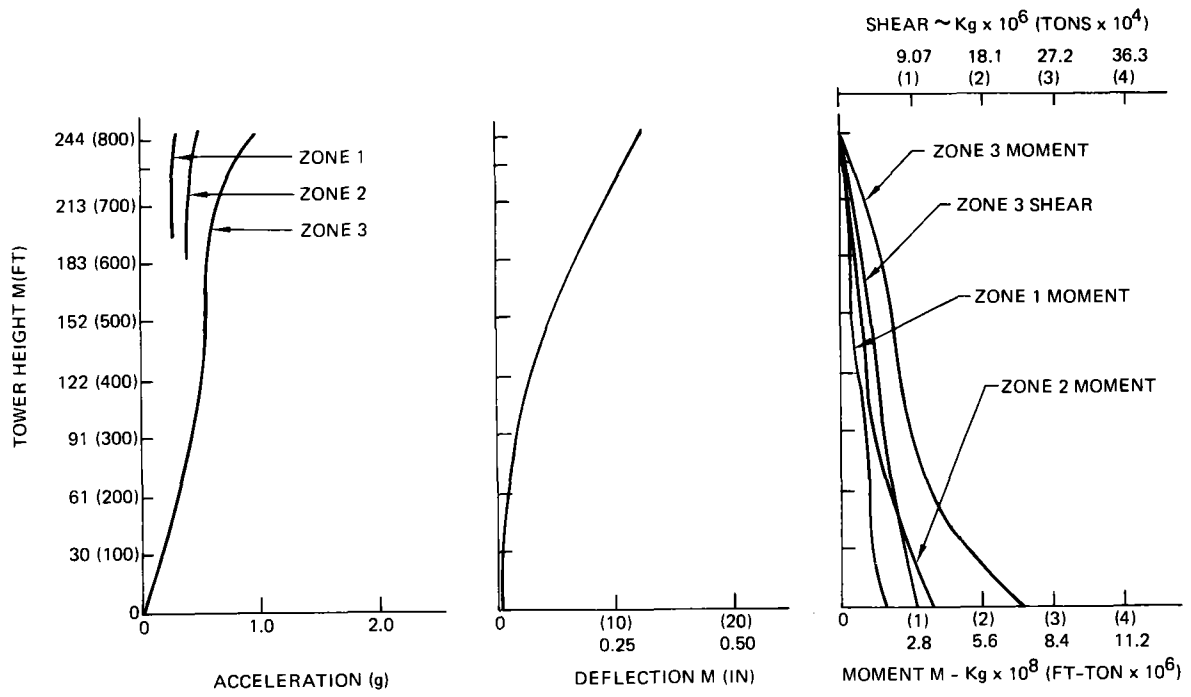


Figure 4-32. Tower Seismic Analysis Results

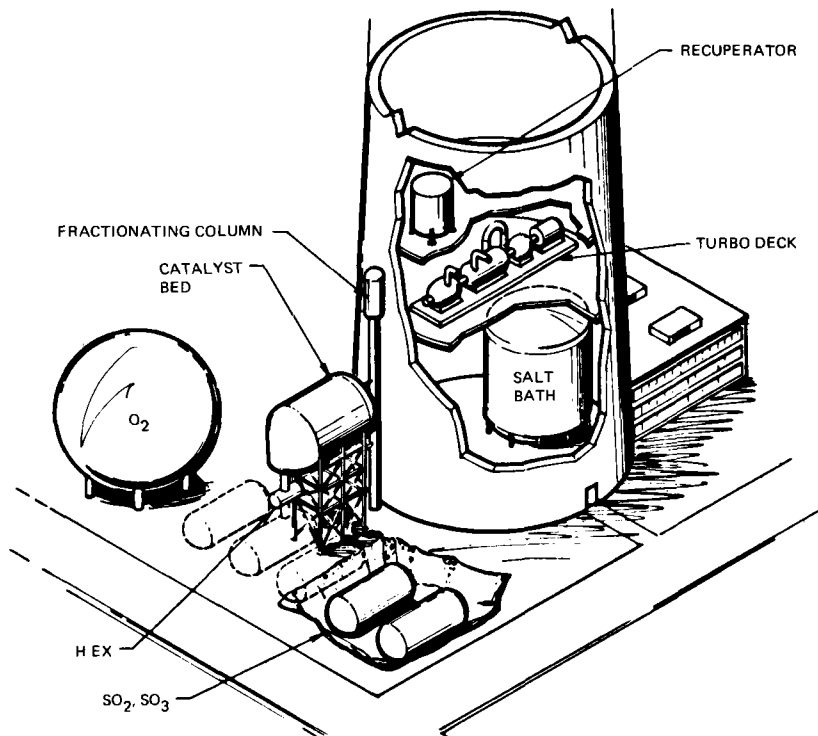


Figure 4-33. Equipment at Lower Tower Location

tower design; in Zone 1, wind loading is critical, A more complete discussion of the analysis is contained in the appendix.

4.3.4 Heat Exchanger Panel Configuration

Analysis of the receiver heat exchanger design possibilities indicated the desirability of using a standard module approach. Modularized heat exchanger panels have the following advantages:

- Modules can be assembled at ground level as a unit and lifted into place. The installation location at about 280 meters (920 feet) dictates the minimization of man-hours for erection and fitting.
- All hot-element fittings, joints, and connections can be welded on the ground in a tooled production facility. This allows for machine welding (for high quality, low cost, and consistency) and for performing the helium leak tests and preliminary functional tests prior to erection.
- Subsequent maintenance, as required, can be performed on a "remove and replace" basis, eliminating extended costly shut-down cycles.

The utilization of the upper section of any receiver for heat exchanger surfaces was dictated by thermal analysis to prevent direct impingement of solar energy through the aperture onto the heat exchanger tubes. The spherical receiver, as shown on figure 4-30, would have required a variety of modular panel shapes to accommodate the complex curvature of the upper hemispherical section. The straight cylindrical section easily accommodates a standard heat exchanger panel size. This size was determined by iteration of structural and thermal analyses.

Figures 3-4 and 3-5 of section 3.0 illustrate and dimension the standard heat exchanger panel. The standard panel consists of the helium tubing, insulation, backing, support structure, and manifolds to function as a complete unit. Weight is approximately 1,200 kilograms (2,650 pounds).

4.3.5 Heat Exchanger Panel Tubing

The primary considerations made for the high-temperature tubing for the heat exchanger panels, external manifolds, and pipes were (1) materials and properties, (2) tubing size, and (3) panel tubing arrangement. These are discussed in the subsequent paragraphs.

Materials and Properties. Materials specialists selected Haynes 188 and Inconel 617 alloys as primary material candidates for the high-temperature receiver applications. Both materials proved excellent choices by test (reported in section 7.0). Confidence has been gained for the structural use of either material in heat exchanger panel tubing, manifolds, and high-temperature piping runs.

The characteristics of the Haynes 188, Inconel 617, and other similar alloys contribute additional complexity for the heat exchanger tube configuration design. First, the materials have nonuniform thermal coefficients of expansion increasing linearly over the temperature range of interest. Additionally, large creep is evident at a 30-year lifetime. For Haynes 188, for example, this is approximately 2.4% at 816°C (1,500°F) and 38.4 MN/m² (5,600 psi) internal stress. The latter effect mitigates against effective preloading to reduce the high-temperature stress. Creep, creep rupture stress, and cyclic stress for Haynes 188 are shown on figure 4-34.

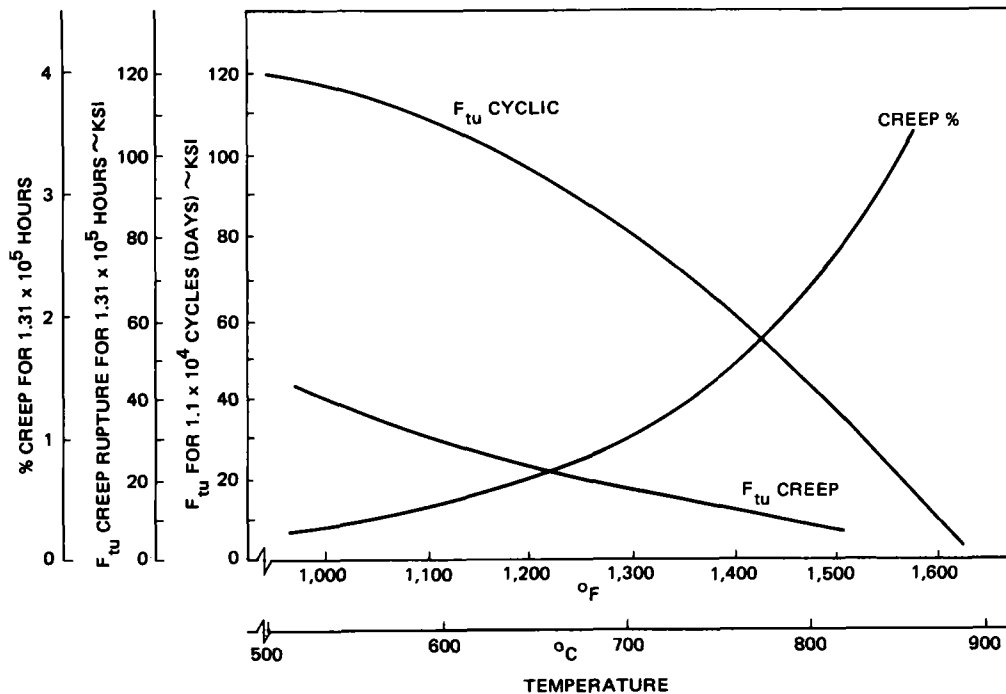


Figure 4-34. Haynes 188 Material Characteristics

The allowable creep rupture stress at 816°C ($1,500^{\circ}\text{F}$) for 30 years of operational life is about 15% of that for allowable cyclic stress. Furthermore, the allowable creep rupture stress at 554°C ($1,030^{\circ}\text{F}$), the approximate helium inlet temperature, is just equal to the allowable cyclic stress at 816°C ($1,500^{\circ}\text{F}$). Percentage of creep rises sharply past 760°C ($1,400^{\circ}\text{F}$).

The properties just discussed (on figure 4-34) have profound effects on receiver and heat exchanger tubing design philosophy. The original material concerns were for the large number of thermal cycles to be experienced in 30 years of operational life and the large thermal swing of each daily cycle from near ambient to 816°C ($1,500^{\circ}\text{F}$). To accommodate these factors, the original concept had included receiver aperture doors to close at night and a "keep warm" circuit to reduce the magnitude of the daily thermal cycle. Data on candidate materials, such as that reported on creep vs. cyclic stress, were not the only design constraints. The time at temperature, particularly time at temperatures in excess of 760°C ($1,400^{\circ}\text{F}$), could be critical due to material creep properties. Therefore, doors and "keep warm" circuits were not only unnecessary, but actually undesirable. These deletions simplified the receiver and helium tubing circuit design considerably.

Tubing Size. The heat exchanger tubing internal radius was set at a nominal 1.27 centimeters (0.5 inch) based upon thermal and fluid analyses, which considered internal heat transfer to helium and the resultant pressure drop 3.45 MW/m^2 (500 psi). The spacing between tubes and the number of tubes on a standard heat exchanger panel were determined by required surface area for heat transfer and the incident flux on the panel. A major remaining structural consideration was for a tube wall thickness to withstand the internal stress created by high pressure and temperature. Figure 4-35 shows the tube-wall-thickness to outer-tube-radius ratio (t/R_o) for the thermal and pressure stress to be experienced.

The combined stress curve on figure 4-35 for Haynes 188 shows the tubes will experience minimum stress levels at t/R_o ratios between 0.12 and 0.21. These levels are less than the maximum allowable for 30 years of life at 816°C ($1,500^{\circ}\text{F}$) of 55 MN/m^2 (8,000 ksi). Before a t/R_o ratio could be picked, consideration had to be given to the possibility of metal removal through high-temperature oxidation. Subsequent testing of Inconel 617 and Haynes 188 showed this effect to be negligible. These results are reported in section 7.0.

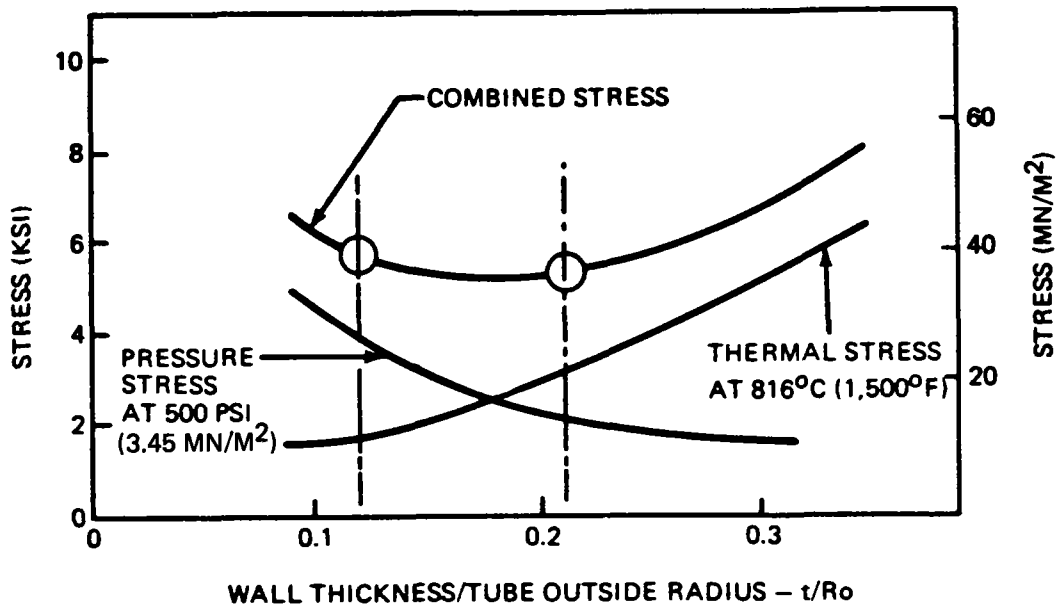


Figure 4-35. Tube Wall Thickness Selection

Panel Tubing Arrangement. Exposed tubing length for each panel tube inside the cavity was determined to be 9.5 meters (31 feet). If a tube with fixed ends utilized free flexing to accommodate thermal distortion, the simple bending stresses are over 138 MN/m^2 (20,000 psi). This is not only an intolerable level, but (short of failure) would result in configuration distortions for all the tubes on a panel, which would upset the heat transfer capability of a regular arrangement.

The solution selected was a U-shaped configuration such as is shown on the right side of figure 4-36. The expansion due to the higher thermal coefficient of the "C" high-temperature leg is balanced by the additional length of the lower temperature "A + B" leg, and creep is accommodated by rotation of the attaching tubes. The tubes have been shown on figure 3-4. The loops on the tubes after they pass through the insulation and into the header perform the same expansion accommodation function. This allows the configuration to be stable through and in front of the panel.

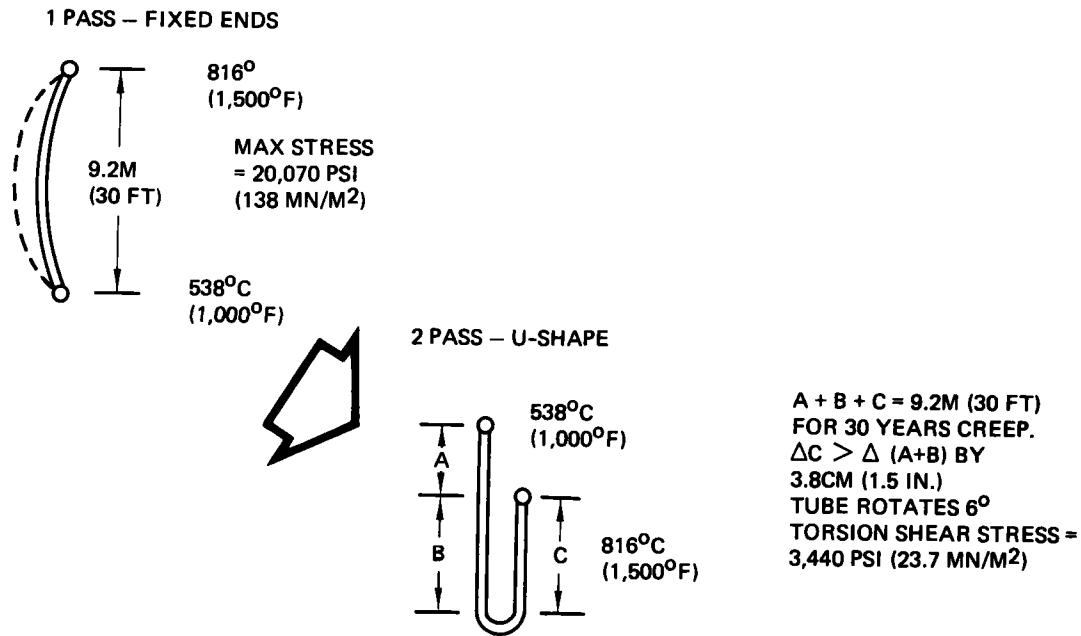


Figure 4-36. Tube Configuration Selection

4.4 RECEIVER COST TRADES

The \$7.84 million cost estimate itemized in section 3.4 for the baseline receiver concept was arrived at after extensive redesign and cost-reduction efforts, meanwhile maintaining a creditable design. The receiver concept described earlier in the interim technical and summary reports to this same EPRI contract (RP377-1) had an unreleased estimate that was more than twice as high. After the strawman plant costs were received from EPRI, receiver costs had to be made more competitive with the steam boiler costs in the strawman account.

Two major cost drivers in the earlier estimate were corrected by design changes in the final estimate. First, Haynes 188 had been the only material tested at the initial report date and it was costed as the construction material for all high-temperature applications at 538°C (1,000°F) and above. After the Inconel 617 had been tested with equally fine test performance, this less expensive material was costed, but only for the high-temperature receiver heat exchangers and the 816°C (1,500°F) panel headers. All other helium piping was carbon or stainless steel, but internally insulated for the 816°C (1,500°F) helium temperatures in the downcomers and externally insulated for the 538°C (1,000°F) supply

risers. The second factor corrected was the large number of risers and downcomers (five each) between the tower top and the receiver. These were partly shielded by the receiver structural supports but they nevertheless required additional supports and protection to traverse the field flux. These pipes, now of less expensive steels, were reduced to two risers and downcomers of larger size, located within the supports (one in each of four supports).

Another cost economy resulted as a configuration change in the heat exchanger panel tubing to achieve better tube performance. As a result, 210 panels were required rather than the earlier 280 panels. This has been described in sections 3.2.5 and 4.2.2. In another associated tubing economy, structural analysis described in section 4.3.5 showed that tubing under combined temperature and pressure stress had minimum stress sizing wall thickness-to-radius (t/R_o) ratios of 0.12 to 0.21. The thicker wall number had been used earlier when it was assumed there could be all thickness loss over 30 years of lifetime. When testing (reported in section 7.0) showed this effect to be negligible the 0.12 t/R_o value was used with a proportionate cost reduction.

The various receiver cost economies are indicated on figure 4-37.

<u>Item</u>	<u>Cost economy</u>	<u>Savings (millions)</u>	<u>Technology</u>
HEAT EXCHANGER PANELS (280)	● Reduce panel number to 210	0.6	Available
	● Use Inconel 617 instead of Haynes 188	1.0	Available
DOWN-COMERS (5)	● Reduce number to two	3.4	Internal insulation (HTGR technology)
	● Bury in supports		
	● Insulate internally		
RISERS (5)	● Use stainless steel tubes		Available
	● Reduce number to two	3.2	
	● Bury in supports		
CONSTRUCTION	● Use stainless steel tubes		Available
	● Reduced size	0.5	
OTHER	● Reduced weldments		Available
	INSULATION PANELS, EXTERNAL PROTECTION	0.3	
		<u>9.0</u>	

Figure 4-37. Receiver Cost Economies

Section 5.0

TURBOMACHINERY/CYCLE ANALYSIS

Cycle analysis has been an important inclusion in the closed-cycle solar plant study because of the direct effect cycle efficiency has on the costs of the collector field and the receiver. Collector costs are 60% of plant costs in the "strawman" plant definition from EPRI (see figure 2-6), and receiver costs for the cavity concept are projected to be higher than the "strawman" receiver. Reduction of either account and of the total plant cost, by making efficient use of the capabilities inherent in the helium cycle, was the object of the cycle analysis. The baseline helium system gives a relatively small-sized, high-efficiency system. The results of optimizing the helium cycle for the intended plant usage and for minimum plant cost are reported in section 5.1.

Availability of helium turbomachinery of 50- to 100-MWe rating is an important consideration in the feasibility of a closed-cycle helium plant. The results obtained on prospective helium turbomachinery availability to date have been encouraging. The survey was also extended to closed-cycle air systems where even more operational experience exists. The subject of helium turbomachinery availability is discussed in section 5.2.

Comparative analyses of performance and cost have been made between the baseline helium system and the open and closed air-cycle alternatives. Section 5.3 contains these quantitative comparisons and concludes with a qualitative assessment where the steam Rankine cycle is included.

Finally, section 5.4 contains the study results of applying the helium cycle in plant operation.

5.1 SYSTEM BASELINE (CLOSED-CYCLE HELIUM)

The baseline cycle considered is a closed Brayton cycle using helium (see figure 2-4). For this study, the Brayton cycle is assumed to consist of the turbo-

machinery, the recuperator, and the precooler. The other major component in the cycle, the receiver, is accounted for but not as a variable.

The procedure used for the cycle analysis was to vary the compressor inlet temperature and recuperator effectiveness, keeping the turbine inlet temperature constant. The system requirement was a fixed electrical output. A cycle pressure ratio was required before cycle performance (efficiency) and size (mass flow) could be determined. The cycle pressure ratio was set equal to the value at which the thermodynamic cycle efficiency was maximum. This defined the size of the system in terms of mass flow, which sized the precooler and recuperator in terms of heat exchanger surface area. The combination of mass flow and cycle pressure ratio defined the size of the turbomachinery.

The decision to define system size at the point where cycle efficiency is maximum is important because of the effect this decision has on the size of the Brayton-cycle equipment and the "energy source" (receiver and collectors). Two separate cycle performance parameters define the size of these major system components. Cycle efficiency defines the required size of the energy source while work per unit mass flow is the major factor in defining the size of the Brayton-cycle equipment. Cycle pressure ratio defines the length of turbomachinery as well as having a small effect on the precooler and recuperator. These two parameters are shown on figures 5-1 and 5-2 for a hypothetical helium system. As can be noted, they do not have maximums at the same pressure ratio. The cycle pressure ratio giving maximum efficiency was selected for this study because of the projected high relative costs of the energy source (primarily, the collector field). However, in examining the data on figures 5-1 and 5-2, it is possible to increase the work per unit mass flow 20% above the maximum efficiency value at the expense of 5% in cycle efficiency. Selecting this pressure ratio would result in a smaller Brayton-cycle (with a longer engine), but at the expense of a larger energy source. This area warrants further study because of the trades that are possible. However, the pressure ratio giving maximum cycle efficiency was selected for these studies.

The same philosophy of trying to maximize efficiency was taken with regard to the recuperator and precooler where the gas velocities in the two heat exchangers were kept to a minimum in order to keep pressure losses low. This is necessary for high levels of recuperator effectiveness where pressure losses play a more dominant part.

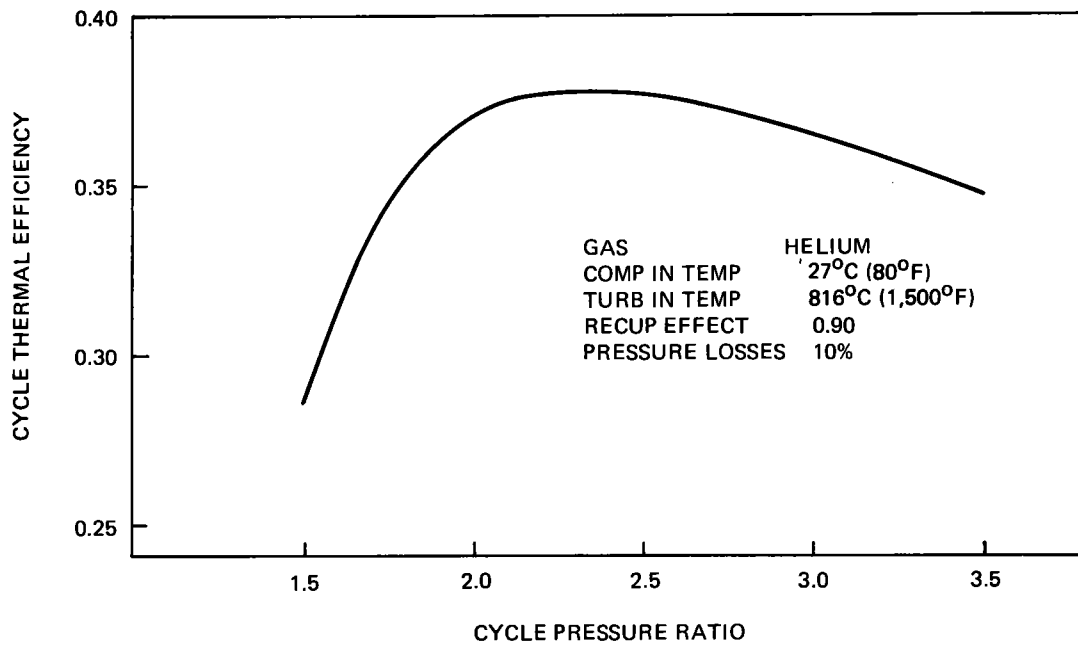


Figure 5-1. Pressure Ratio Effect on Efficiency

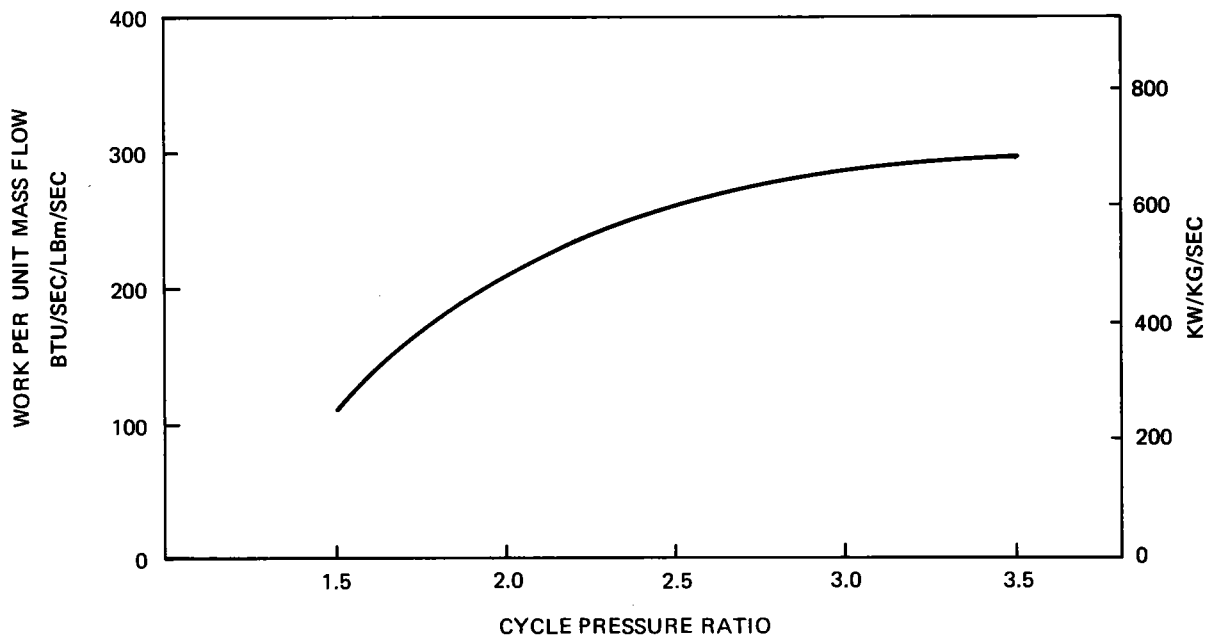


Figure 5-2. Pressure Ratio Effect on Work/Mass Flow

The assumptions with regard to the analysis of the precooler and recuperator were that they were both counterflow tube types with the precooler being a dry cooling tower as required by the study. The cycle performance to be presented has the following basis:

Turbomachinery

Compressor adiabatic efficiency	0.87
Turbine adiabatic efficiency	0.91
Turbine inlet temperature	816 ⁰ C (1500 ⁰ F)

Recuperator

Tube diameter	2.54 cm (1 inch)
Gas velocity	15 m/sec (50 ft/sec)

Precooler

Tube diameter	5 cm (2 inch)
Gas/ambient thermal ratio	0.5
Gas Velocity	12 m/sec (40 ft/sec)
Ambient velocity	3.7 m/sec (12 ft/sec)
Ambient temperature	27 ⁰ C (80 ⁰ F)

Using these as baseline values, system performance in terms of cycle thermal efficiency was calculated for various compressor inlet temperatures and levels of recuperator effectiveness, as given on figure 5-3. The surface area requirements for the precooler and recuperator are given on figures 5-4 and 5-5, respectively. In comparing figures 5-3, 5-4, and 5-5, the increase in cycle efficiency that comes with reduced compressor inlet temperature and increased recuperator effectiveness is not linear with required surface areas, the increase in surface area becoming greater as the efficiency level increases. This effect tends to create logical design points or limits. For the recuperator, effectiveness levels of 0.92-0.94 might be considered the upper limit, since in going from 0.94 to 0.96 the recuperator is approximately doubled in size and gives only a 3.5% increase in efficiency. The baseline value is 0.94 and is within the above limits. A similar argument can be made with the precooler, but the effects are not as

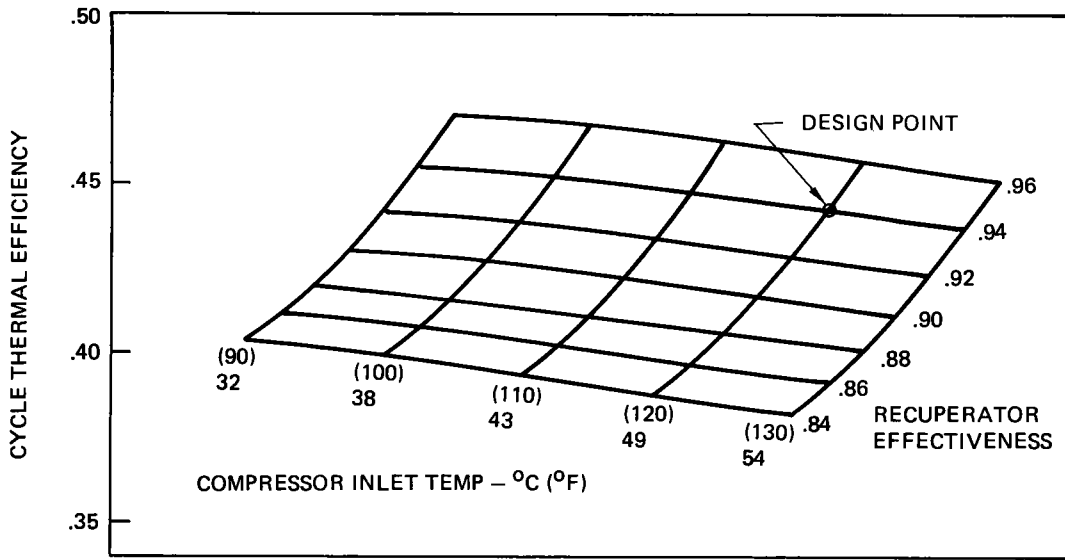


Figure 5-3. Helium Cycle Efficiency

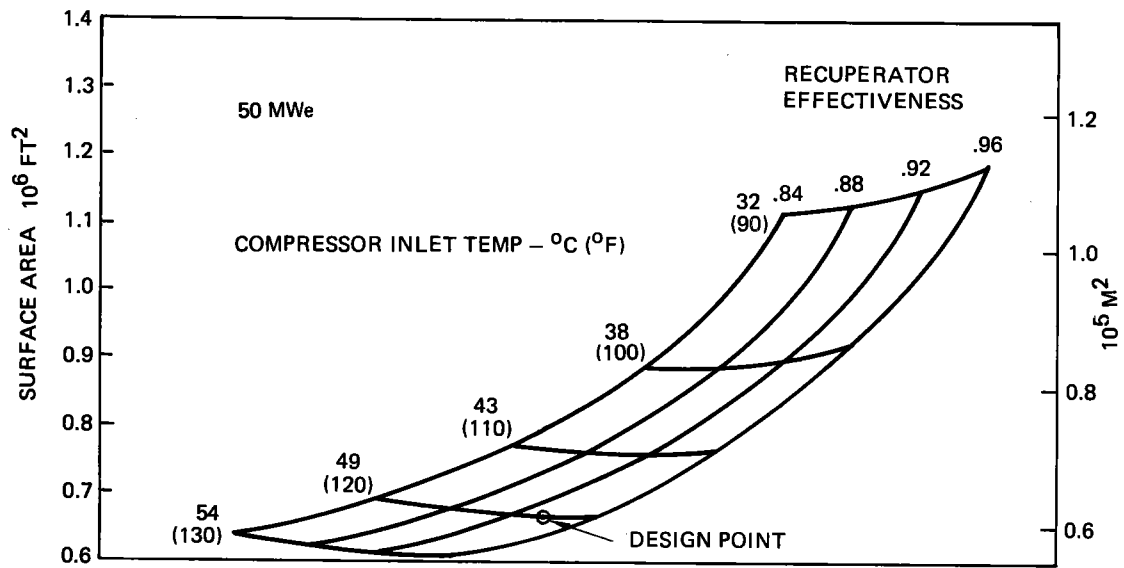


Figure 5-4. Helium Precooler Surface Area

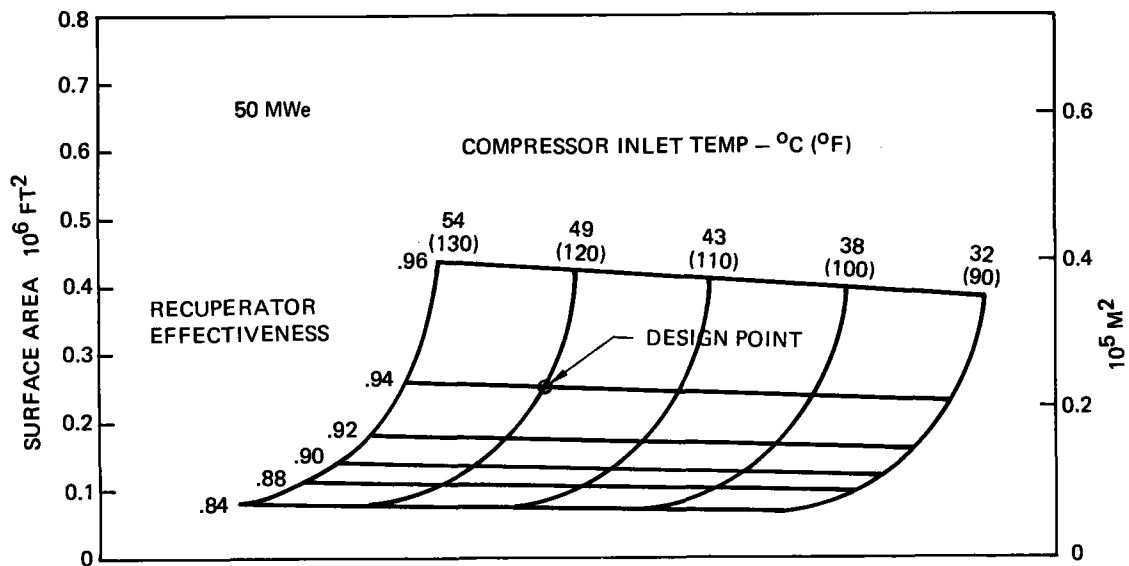


Figure 5-5. Helium Recuperator Surface Area

dramatic. In going from 54°C (130°F) to 32°C (90°F) the size is approximately doubled and gives a 17% increase in efficiency. However, the precooler will be quite large, especially from a space-required point of view. Consequently, the design limit will be more defined by space requirements and thereby be more restrictive than by actual surface area requirements with logical limits probably being in the 43°C-49°C (110°F-120°F) range. The chosen baseline value of 49°C (120°F) is again within the limits.

The effects of these changes in the precooler and recuperator cause counteracting effects with regard to the size of the turbomachinery. That is, as compressor inlet temperature increases, the mass flow (engine diameter) increases, but the cycle pressure ratio (engine length) decreases. An increase in recuperator effectiveness causes these same effects. These effects are shown on figure 5-6 and 5-7. Thus, there are no logical design points as far as engine volume goes. However, a restriction might be applied to the pressure ratio because of the large number of stages required with helium (helium has a low temperature/pressure rise per stage). This is a function of engine speed, number of compressors and turbines, and number of shafts. The scope of the study did not permit definition of these limits.

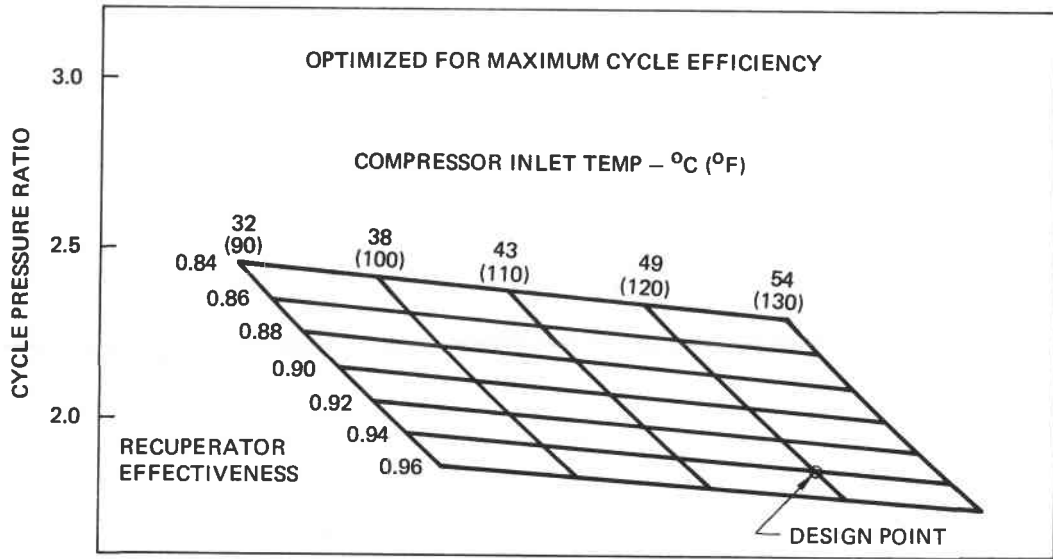


Figure 5-6. Helium Cycle Pressure Ratio

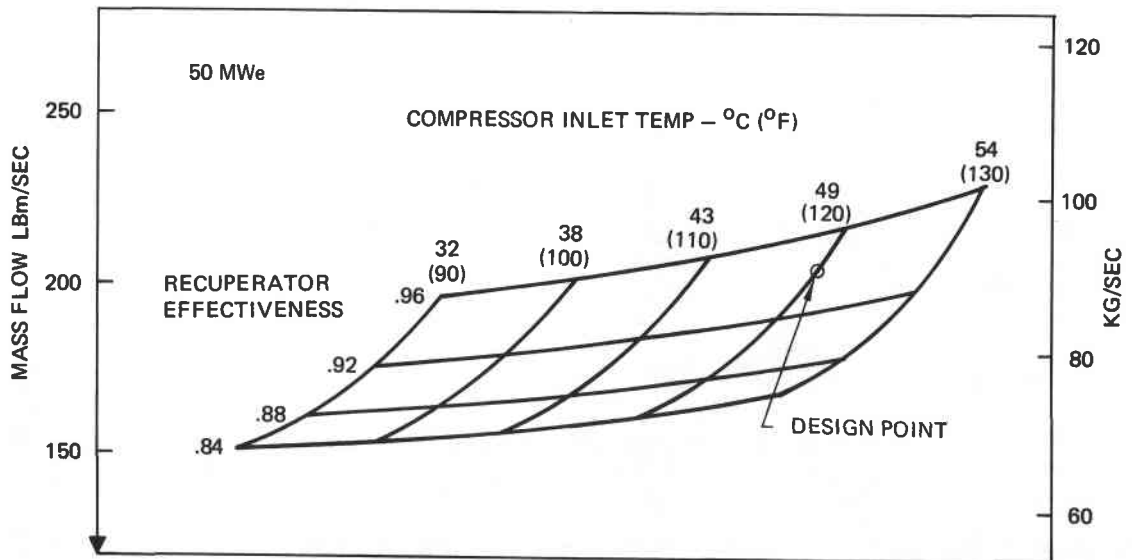


Figure 5-7. Helium Mass Flow

In summary, for a total system dedicated primarily to obtaining a high efficiency, the region of logical design points for the Brayton-cycle size is in the efficiency range of 0.428-0.447. This corresponds to a recuperator with an effectiveness of 0.92-0.94, a compressor inlet temperature of 43⁰-49⁰C (110⁰-120⁰F), and turbomachinery with a cycle pressure ratio of 1.85-2.0 and mass flow of 84-93 kilograms/second (185-204/second) for a 50-MW_e rated plant.

5.2 HELIUM TURBOMACHINERY AVAILABILITY

The primary cycle investigated utilizes helium in a pressurized closed cycle. This section deals with the availability of closed-cycle helium turbomachinery of the size required for solar powerplant application. Such turbomachinery does exist as is evidenced by the Gutehoffnungshutte (GHH) installation of a 50-MW_e turbine at Oberhausen, Germany. A photo of the installation currently in test and the helium cycle employed at Oberhausen are shown in figure 5-8.

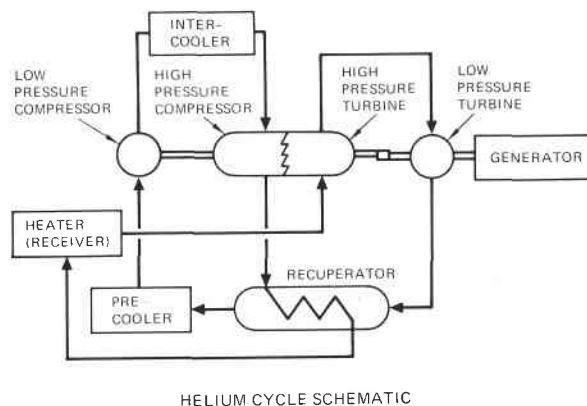
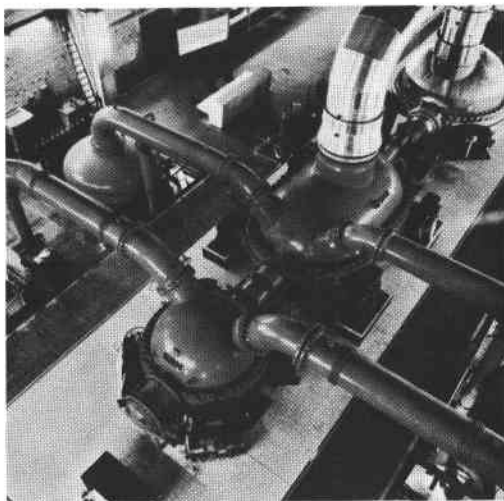


Figure 5-8. Helium Turbine Installation at Oberhausen, Germany

Another significant development in progress is the 30-MW_e helium turbine being designed for high-temperature gas reactors by Brown, Boveri and Company Ltd (BBC) of Switzerland.

In the course of the study, Boeing personnel visited the Oberhausen installation in Germany and had numerous other occasions for technical interchange with GHH,

BBC, and American suppliers. All these interchange increased confidence that the technology is available to develop closed-cycle helium turbomachinery for the use intended. The question still remained whether turbomachinery could be made available on a reasonable schedule and cost basis, considering there is no "off the shelf" turbomachinery to be used or modified.

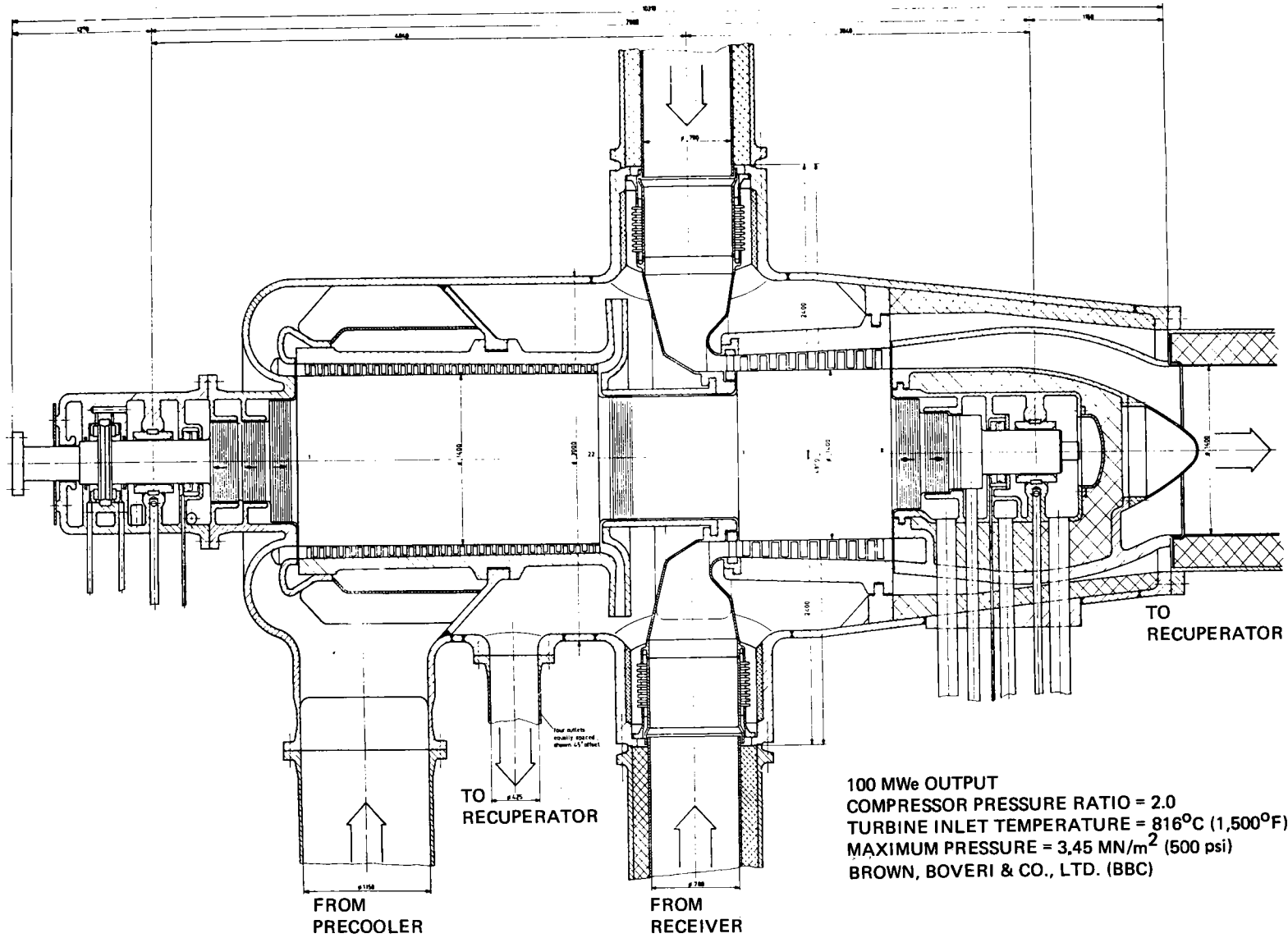
Accordingly, formal requests were sent to GHH, BBC, and United Technology asking each to do a preliminary design and ROM costing for the turbomachinery required in the design. Requests were made for both a 100-MW_e commercial plant and a 10-MW_e pilot plant.

At study conclusion, preliminary design and ROM cost data had been received from BBC for the turbomachinery required for both plants. BBC stated that either could be available in 3-4 years.

The basic cycle being proposed calls for a maximum pressure of 3.45 MN/m² (500 psia), a turbine inlet temperature of 816°C (1,500°F), and a low cycle pressure ratio of approximately 2. This gives a thermal efficiency near maximum. When these requirements are combined with a 100-MW_e output, it is possible to design a simple single shaft turbogroup running at synchronous speed (3,600 r/min). This is the preliminary design BBC is proposing, with a schematic of the design being given on figure 5-9. The BBC design takes into account mechanical and generator losses, cooling and leakage, and cycle pressure losses. The ROM cost for the turbogroup is \$6.4-6.8 x 10⁶. This does not include the generator or starting system. The size and subsequently the price could be reduced if the speed were not restricted to the synchronous speed. However, in removing the restriction, a reduction gear for the generator might be required. BBC also stated that most reduction gears are restricted to 50-80 MW_e, resulting in the requirement that two 50-MW_e turbogroups would be necessary for 100 MW_e. The units would be considerably smaller, as would be the generator, than the single 100-MW_e turbogroup/generator.

The cycle proposed by BBC for the pilot plant would be essentially the same as that for the commercial plant but with an output of 10 MW_e instead of 100 MW_e. This combination of cycle/output does not allow for a design with the turbogroup running at synchronous speed. The BBC design speed will be 8-10,000 r/min, thus requiring a reduction gear. However, the machine will be quite small (with lengths and diameters approximately 1/3 those of the 100-MW_e turbogroup). The

S-10



100 MWe OUTPUT
 COMPRESSOR PRESSURE RATIO = 2.0
 TURBINE INLET TEMPERATURE = 816°C (1,500°F)
 MAXIMUM PRESSURE = 3.45 MN/m² (500 psi)
 BROWN, BOVERI & CO., LTD. (BBC)

Figure 5-9. 100 MW He-Turbine

ROM cost for this turbogroup is $\$1.3-2.0 \times 10^6$. The generator, starting system, and reduction gear are not included in the cost.

5.3 SYSTEM DESIGN ALTERNATIVES

5.3.1 Gas-Cycle Alternatives (Open and Closed Air)

There are reasons for considering open and closed air systems as alternatives to the basic helium cycle. The open air system would be relatively simple and would not require a precooler. The closed air system might be preferred over helium because it is only slightly less efficient, and air is an easier gas to store and contain.

The analysis performed for these cycles paralleled that just described for the helium system. A maximum cycle efficiency was sought for each system. Compressor inlet temperature was varied for the closed air system, and the recuperator effectiveness was varied for both air systems as was done for helium. The result again was low gas velocities and high effectiveness levels for the closed air cycle heat exchangers. The open air cycle recuperator gas velocity ended up as a variable. At the lower recuperator effectiveness level of an open-cycle air system, pressure losses were low enough that the velocity could be changed appreciably without greatly affecting the pressure loss level while the required surface area was changed considerably.

The cycle parameters used for these two systems were:

	<u>Closed Air</u>	<u>Open Air</u>
<u>Turbomachinery</u>		
Compressor adiabatic efficiency	0.87	0.86
Turbine adiabatic efficiency	0.91	0.90
Turbine inlet temperature	816°C (1500°F)	816°C (1500°F)
<u>Recuperator</u>		
Tube diameter	2.54 cm (1 inch)	3.8 cm (1.5 inch)
Gas velocity	9m/sec (30 ft/sec)	12-21 m/sec (40-70 ft/sec)
<u>Precooler</u>		
Tube diameter	5 cm (2 inches)	-
Gas/ambient thermal ratio	0.5	-
Gas velocity	9m/sec (30 ft/sec)	-
Ambient velocity	3.7m/sec (12 ft/sec)	-
Ambient temperature	27°C (80°F)	27°C (80°F)
<u>Maximum Pressure Level</u>	3.45 MN/m ² (500 psia)	.345-.52MN/m ²

As with helium, the performance of the two systems can be represented by efficiency and heat exchanger area requirement. Figure 5-10 gives the efficiency of the closed air system for various compressor inlet temperature and recuperator effectiveness levels. The associated surface area required for the recuperator is shown on figure 5-11. For the precooler, a dry cooling tower type, the ambient air controls the heat transfer so that the surface area requirement is essentially the same as that required for closed helium, as shown on figure 5-4. As with helium, logical design points could be selected, with recuperator levels of 0.88-0.90 and the compressor inlet temperature the same as for helium, 43⁰-49⁰C (110⁰-120⁰F). The resulting efficiencies are 0.401-0.415.

For open cycle air, the only variable in this study, aside from the recuperator design parameters, was recuperator effectiveness. Efficiency and required surface areas versus recuperator effectiveness are given on figures 5-12 and 5-13, respectively. A logical design point, having the same percent change in efficiency for percent change in areas as the closed systems, would result in an effectiveness level of 0.73-0.77, giving an efficiency range of 0.355-0.365.

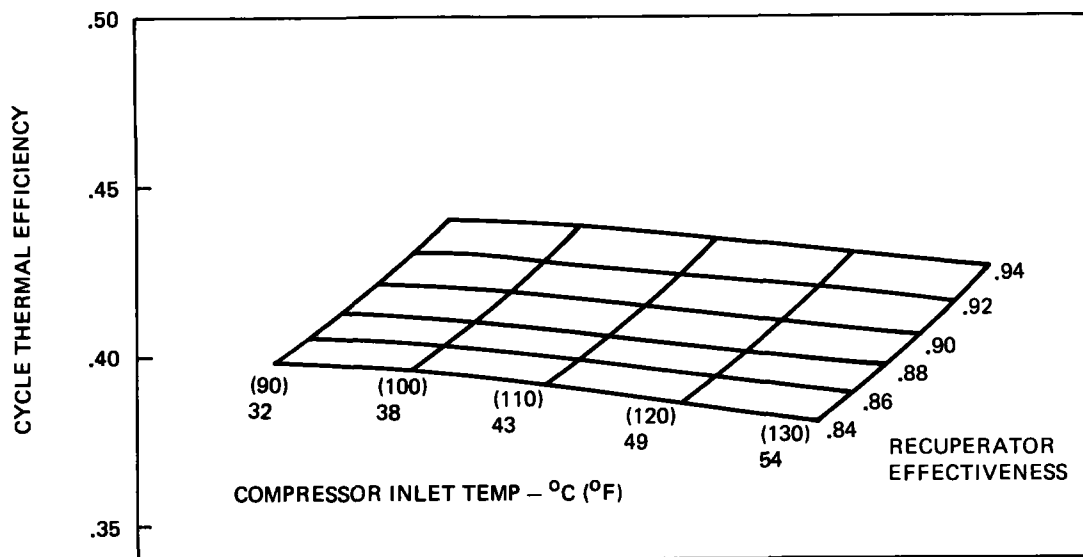


Figure 5-10. Closed Air Cycle Efficiency

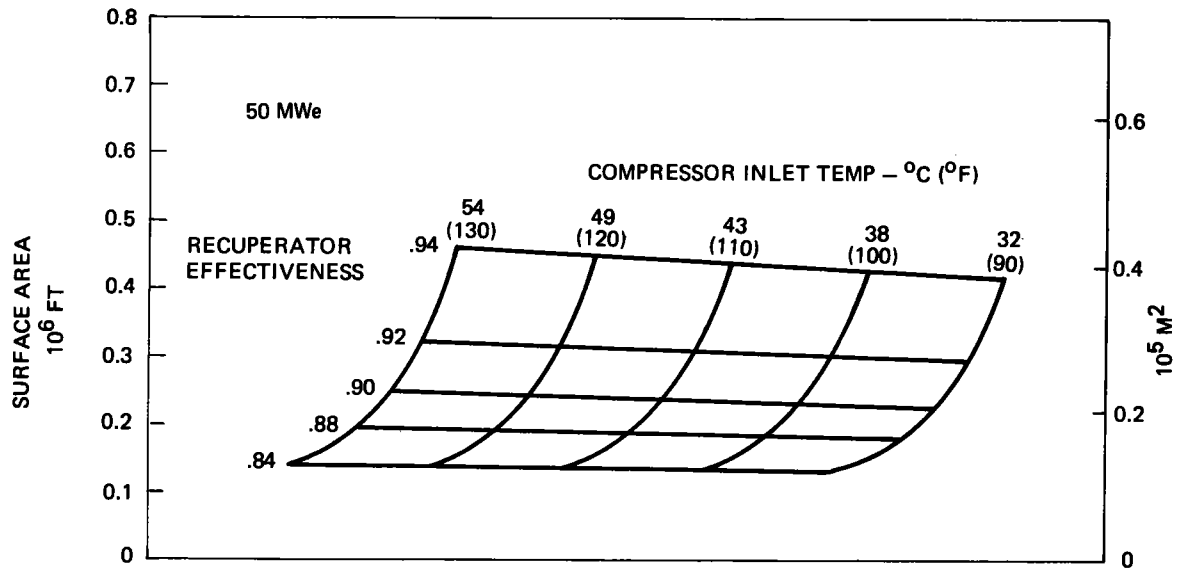


Figure 5-11. Closed Cycle Air Recuperator Surface Area

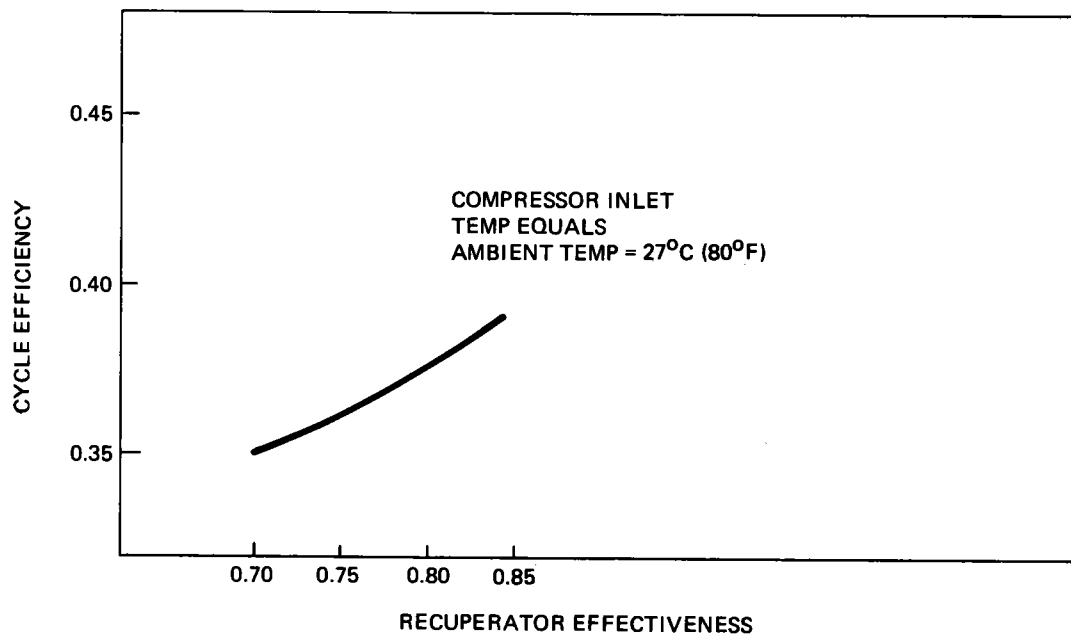


Figure 5-12. Open Air Cycle Efficiency

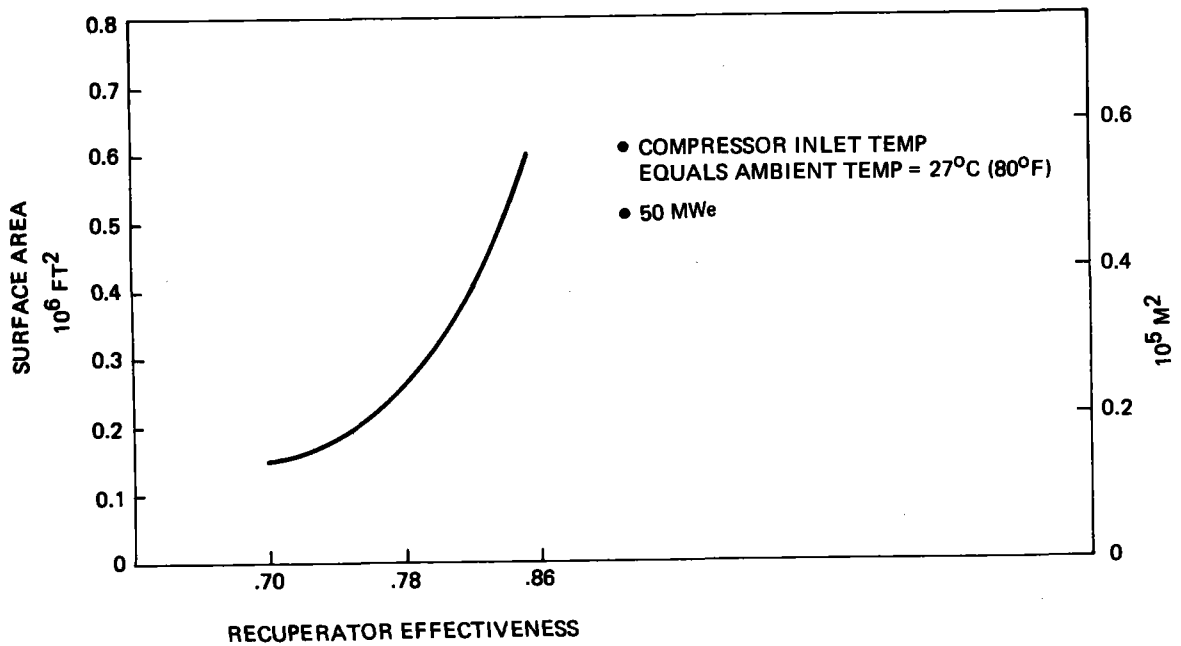


Figure 5-13. Open Cycle Air Recuperator Surface Area

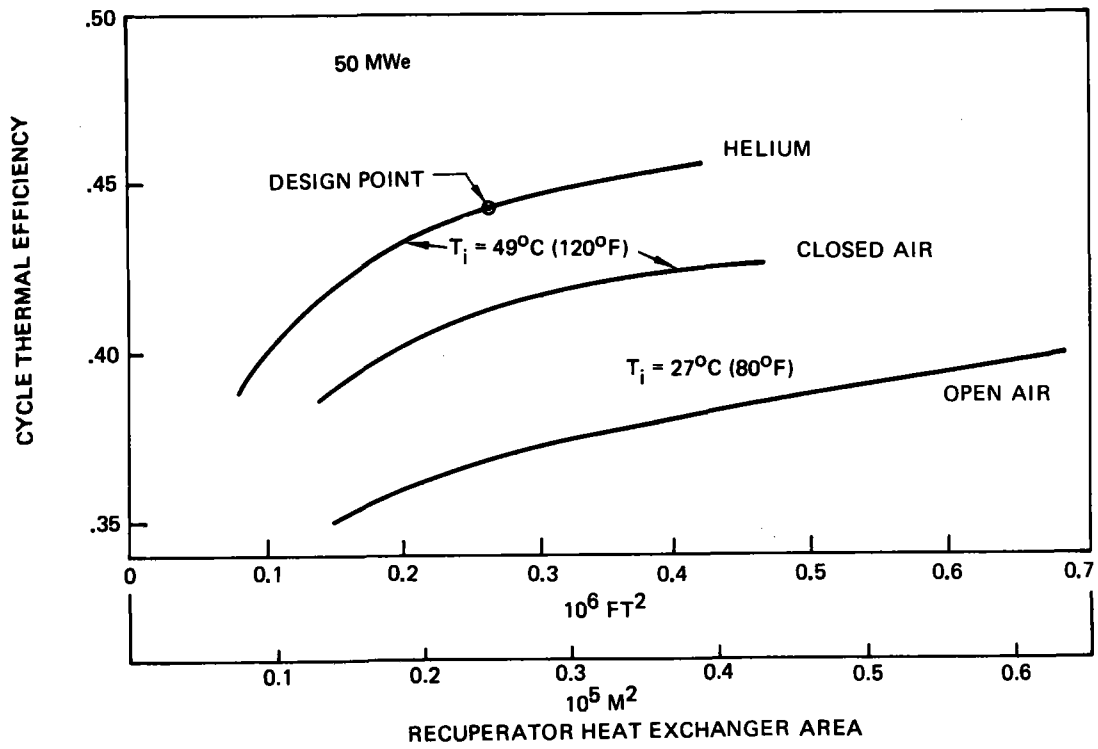


Figure 5-14. Cycle Thermal Efficiency

In summary, from a design standpoint, neither the open nor closed air systems give as high an efficiency level as helium, with open air being 0.355-0.365 and closed air being 0.401-0.415 versus helium with 0.428-0.447, as shown on figure 5-14. A compressor inlet temperature of 49°C (120°F) was selected for the closed systems. At these design points, the recuperator surface area requirements are approximately equal for the three systems.

5.3.2 Gas-Cycle Comparative Performance

Aside from the precooler pressure losses unique to the closed-cycle systems, the component accounting for the majority of the cycle efficiency differences is the recuperator. Utilization of recuperator surface area in the heat exchange process is a major factor. Figure 5-14 shows the effect of recuperator surface area on cycle efficiency and indicates that closed systems have an inherent advantage over open systems, and that closed helium has a similar advantage over closed-cycle air. The primary reason for the differences in the open and closed air systems is the increased pressure (density) level of the closed systems. The increased pressure reduces both the flow area and the heat exchange surface area requirements for equal levels of recuperator effectiveness. If the comparison is done at equal areas, the closed air system will have a higher effectiveness, and hence give a higher cycle efficiency than the open air system. The effect of pressure level on recuperator size is indicated on figure 5-15. Increased pressure level also reduces the turbomachinery size, as indicated on figure 5-16. Along with the reduced size, there is also a slight improvement in the turbomachinery efficiencies because of the increased Reynolds number.

The differences in cycle efficiency between air and helium can be explained by looking at the consequences of gas properties on recuperator size and performance. Air and helium are compared on figures 5-17 and 5-18 in terms of a volume ratio and pressure loss ratio. The two figures show that it is possible to design helium and air systems that have either equal volumes or equal pressure losses with the proper selection of gas velocities. If the two systems are designed for equal volumes, helium will have pressure losses only 10% that of air. If the two systems are designed for equal pressure loss, the helium recuperator will be 50% the size of the air recuperator. Generally, helium will require a recuperator with less surface area and have lower pressure losses than air.

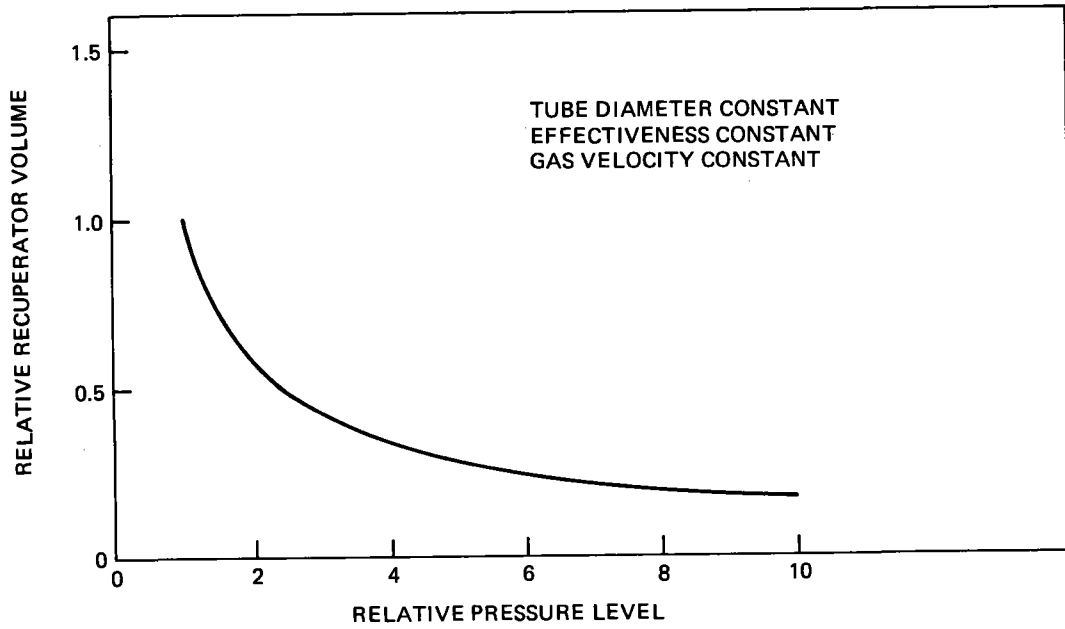


Figure 5-15. Recuperator Volume

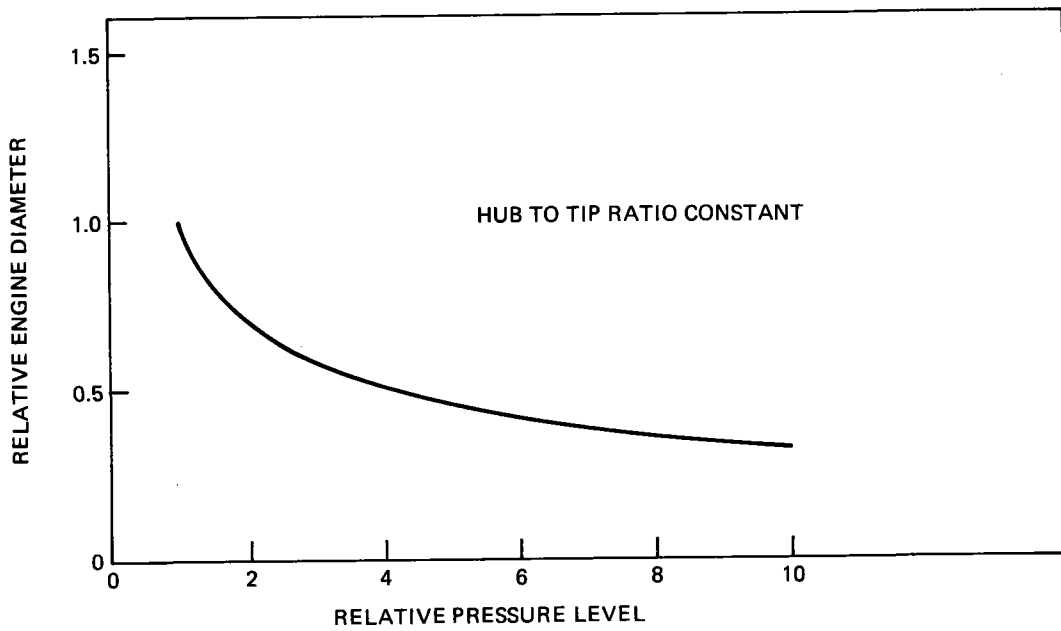


Figure 5-16. Engine Diameter

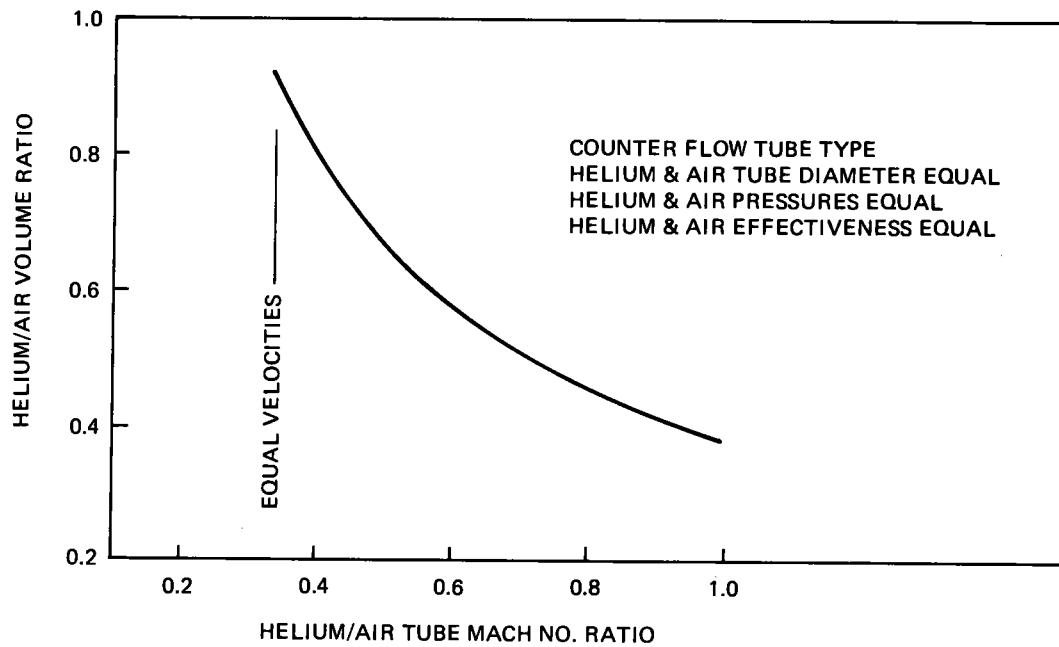


Figure 5-17. Helium versus Air-Recuperator Volume

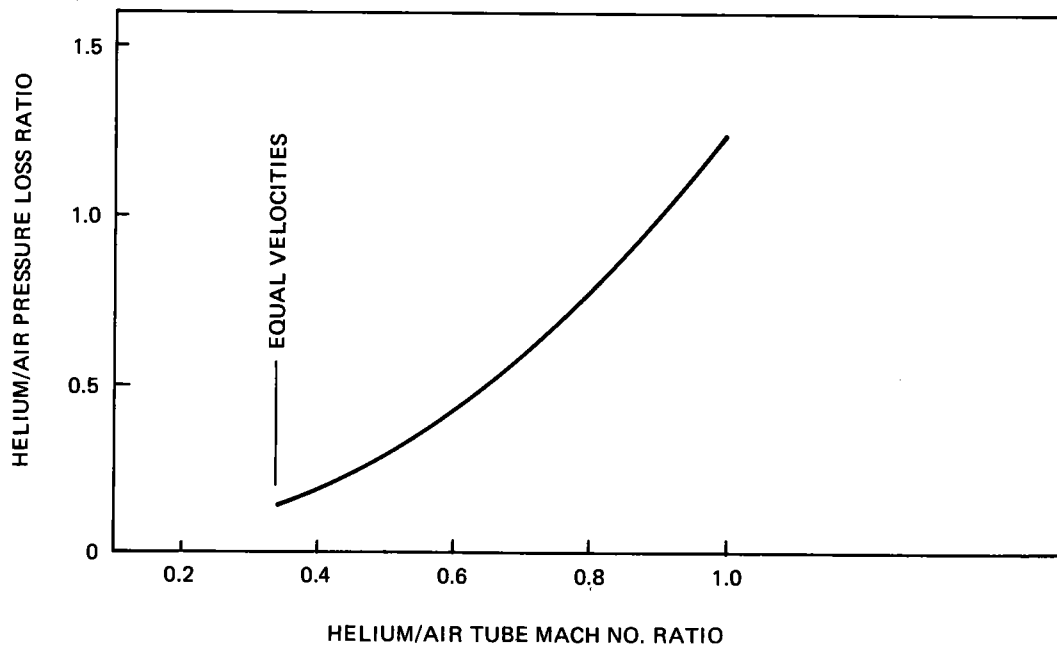


Figure 5-18. Helium versus Air-Recuperator Pressure Loss

Gas selection also has a significant effect on the turbomachinery. The same gas properties that worked to the advantage of helium in heat exchangers work to its disadvantage in the turbomachinery. For similar blading, the work per unit mass flow for the two gases would be equal. However, because the specific heat (C_p) of helium is five times that of air, the temperature rise of helium will be only one fifth that of air. Or, for an equal temperature rise, as would exist in an ideal system, helium would require approximately five times as many stages as air. However, with helium having a higher sonic velocity, the helium blades can be redesigned giving higher work per stage. This reduces the stage requirement to roughly 2.5-3.0 times as many as for air for systems with equal temperature rise.

The effects can be combined to illustrate the differences in the components of the three systems. Typical systems having equal electrical output were selected for each of the comparisons. Figure 5-19 gives the dimensions of the turbomachinery while figure 5-20 gives the dimensions of the recuperator. In comparing the open and closed air components, the size advantages discussed earlier become obvious, with the closed air components being considerably smaller. The differences in the closed air and helium components are primarily in their lengths, with the helium having a shorter recuperator but longer turbomachinery. All of these differences affect costs and these will be discussed later.

The other component in the Brayton cycle, the precooler, will also affect performance and cost, especially since the open cycle does not require one. The data of figure 5-14 include these performance differences. Even though the closed air system has this additional pressure loss when compared to the open air system, the difference is not great enough to overcome the higher recuperator effectiveness of the closed air system. In comparing the closed systems, the pressure loss through the precooler for helium will be approximately 50% of air if the two precoolers are designed to have an equal number of tubes of equal length (surface area requirements for closed air and helium are about equal).

5.3.3 Gas-Cycle Comparative Costs

A cost analysis was completed for the baseline helium system as well as for the alternative open and closed air systems. The higher cycle efficiency of 0.44 obtained and used for the helium system, while reducing the overall plant size by reducing the collector field cost, was accrued with a more expensive Brayton

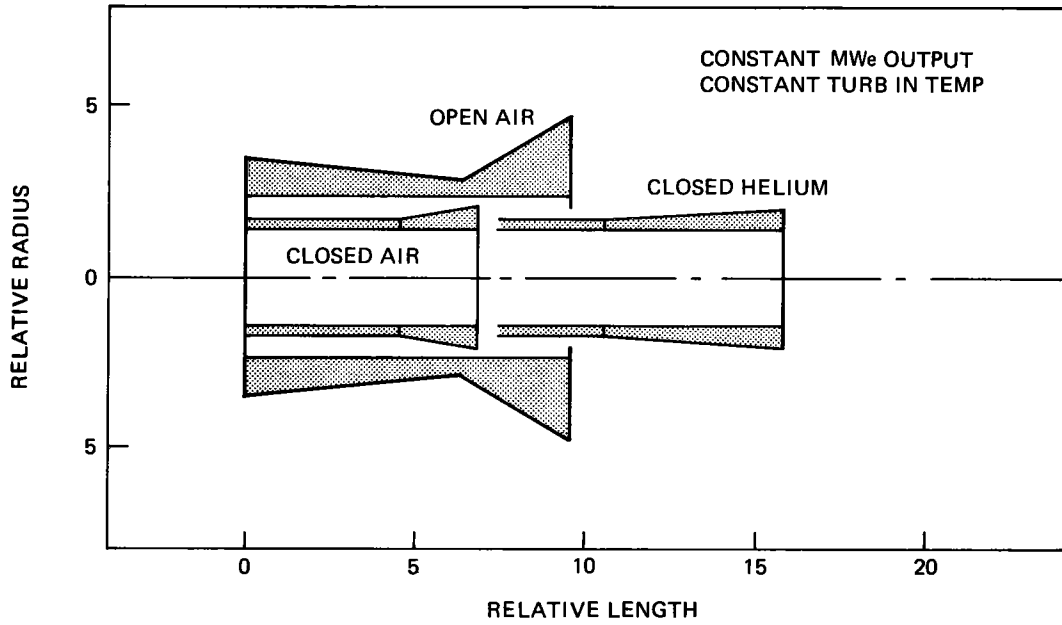


Figure 5-19. Relative Size of Turbomachinery

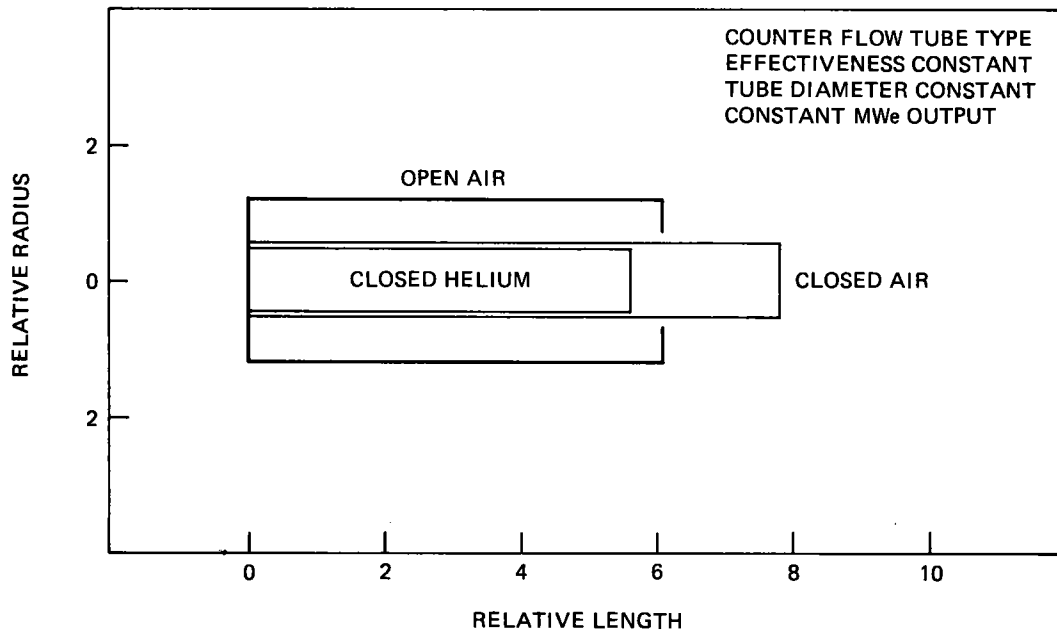


Figure 5-20. Relative Sizes of Recuperators

cycle. The two alternative open and closed air systems were likewise examined so their costs could be directly compared to the helium cycle costs, and entered into the overall plant costs.

For cost comparison purposes, the Brayton helium and air cycles include the turbomachinery, the recuperator, and the precooler. The open-cycle data for the turbomachinery and recuperator were estimated from an industrial survey of existing open-cycle equipment, most of which operates at approximately 982°C (1,800°F) turbine inlet temperature. These data were adjusted for use with the closed systems. All systems were sized and costed for 100 MW_e.

The data received from Brown, Boveri and Co. Ltd. (BBC) reported in section 5.2 substantiated the estimated costs of the helium turbomachinery made by Boeing.

The cost of the dry cooling towers for the closed systems was based upon ROM estimates from Hudson Products. These data were then parameterized to be usable with all the design points considered. Figure 5-21 displays the data in parametric form.

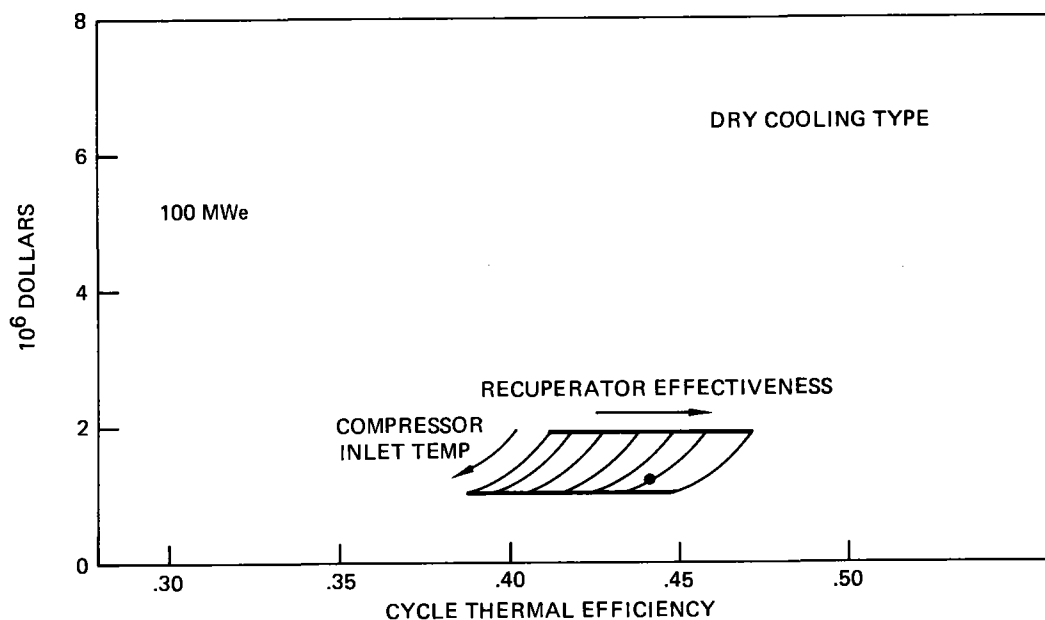


Figure 5-21. Precooler Costs

The recuperators, even though requiring considerably less surface area than the precoolers, will cost considerably more because of material requirements to use stainless steel rather than the precoolers' mild steel and because they require pressure vessels. ROM recuperator costs are given in figure 5-22 for all three systems.

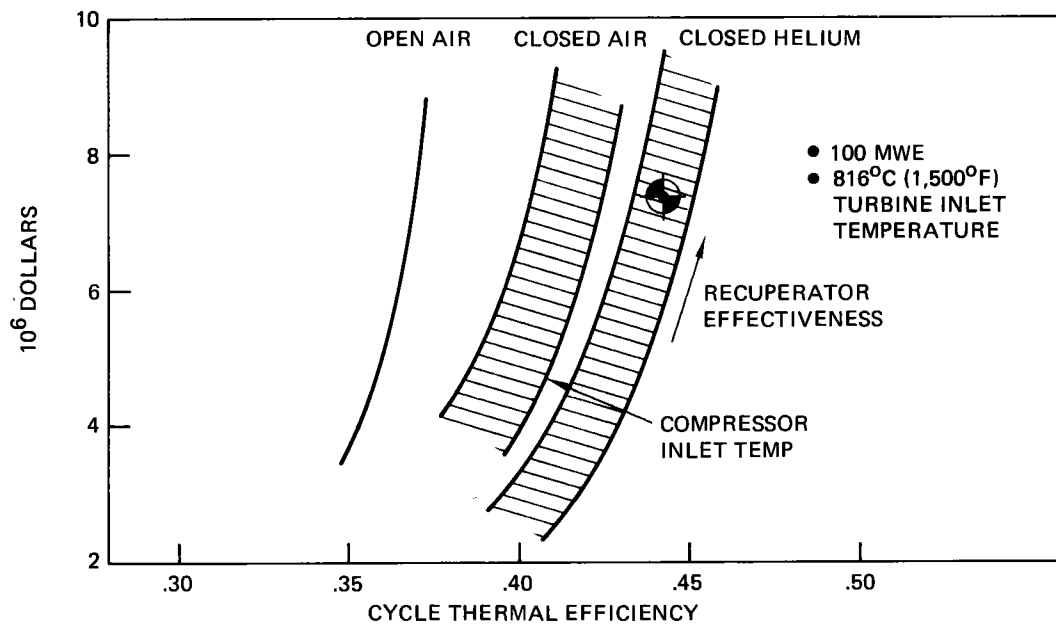


Figure 5-22. Reciprocator Costs

As expected, recuperator costs are a strong function of cycle efficiency since efficiency is a strong function of recuperator size (required heat exchanger area).

Turbomachinery costs are shown on figure 5-23 for all three systems. The ROM costs of the BBC-proposed helium turbogroup is also shown. These helium-cycle costs reflect the benefits of having a closed cycle and the penalty of using helium through the turbomachinery.

If these components costs just discussed and displayed are summarized to give overall cycle costs, one ends up with the data on figure 5-24, using 816°C (1,500°F) as a turbine inlet temperature for all gas cycles. The increasing cost with

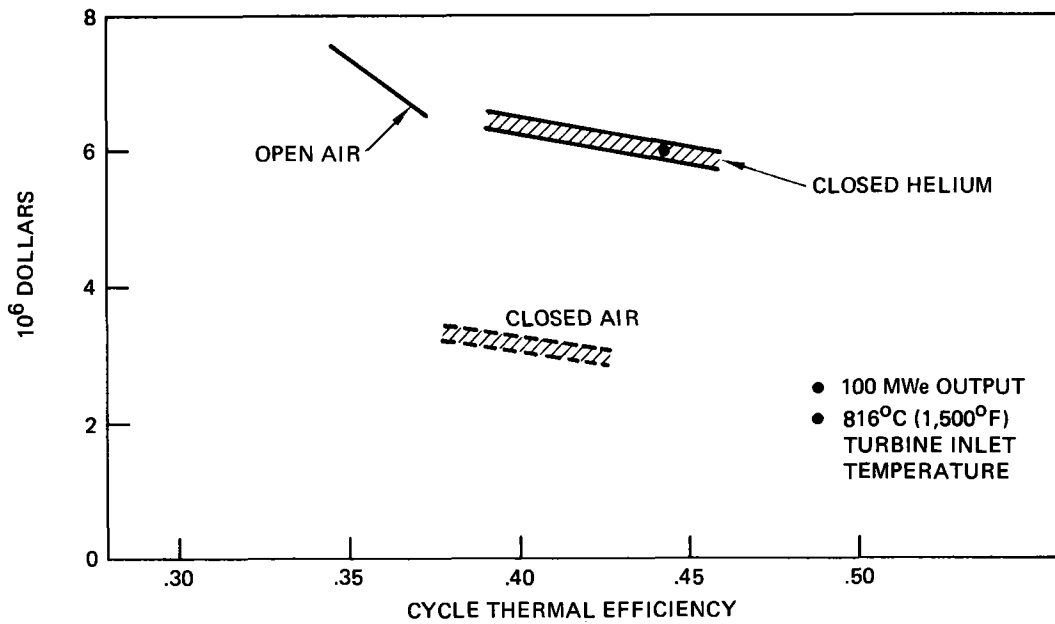


Figure 5-23. Turbomachinery Costs

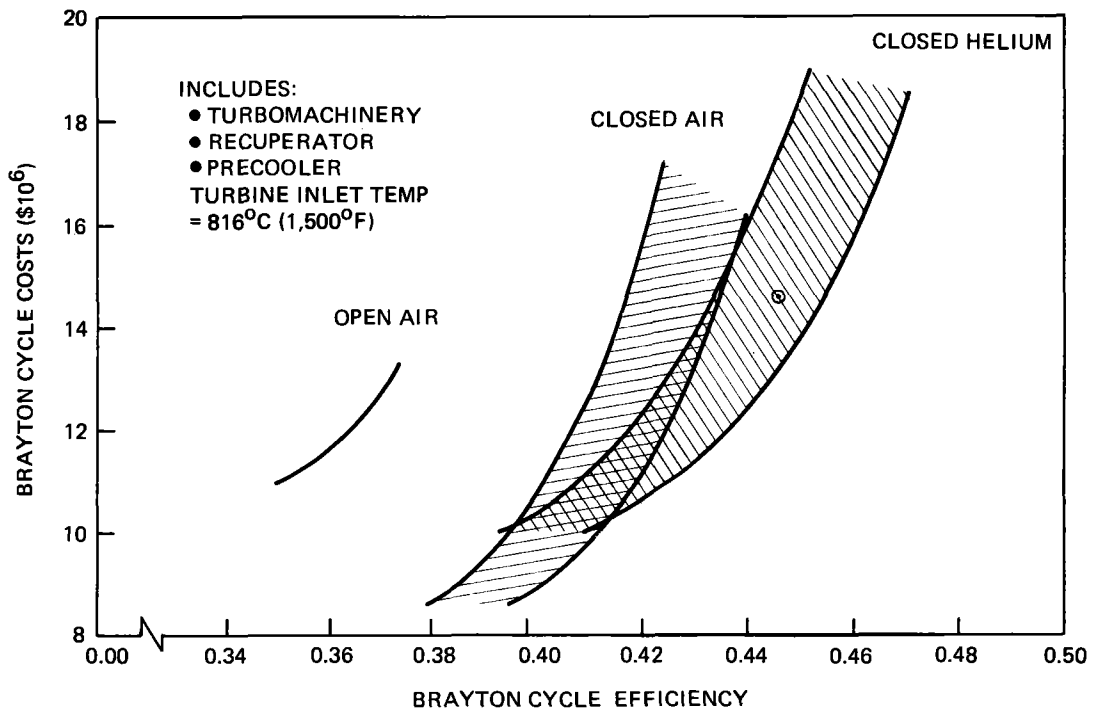


Figure 5-24. 100 MWe Brayton Cycle Costs

increasing efficiency for all three systems reflects the effect of recuperator cost and justifies the use of it as a main parameter in doing cycle comparisons. Examining the data, it is apparent that either closed system will give higher efficiencies for an equal cost. A comparison of the two closed systems indicates that there is a cross-over point for the two systems occurring at the lower efficiency levels. This is a result of the helium turbomachinery costing more than that for closed air, with the recuperator cost advantage of helium being insufficient to offset the difference. However, as efficiency increases, the recuperator sizes increase to make their costs more dominant. The smaller recuperator associated with helium more than offsets the increased turbomachinery costs. Because of these offsetting effects, Brayton-cycle gas selection is not as important at lower efficiency levels as it is for higher efficiencies. However, the selection of a closed-cycle pressurized system will give lower total system costs.

Since efficiency increases with turbine inlet temperature, a brief analysis was performed to illustrate the temperature effect on the system. Basically, for a fixed output, the increased efficiency will result in a smaller system. This is illustrated on figures 5-25 and 5-26 where recuperator and turbomachinery costs are given for open air and closed helium systems at a turbine inlet temperature of 982°C ($1,800^{\circ}\text{F}$). These ROM estimates do not include any additional money for the required technology. Total system costs for these systems are shown on figure 5-27. As before, helium gives a higher efficiency for a given cost. Also, the 982°C ($1,800^{\circ}\text{F}$) system gives a higher efficiency than the 816°C ($1,500^{\circ}\text{F}$) system for a given cost. Increased turbine inlet temperature ideally is advantageous in terms of cycle efficiency. However, this advantage has to be weighed against the cost of the technology required to operate there (both in the receiver and turbomachinery) before it can be stated that increased turbine inlet temperature is a definite system advantage.

Cycle efficiency is given as a function of turbine inlet temperature for the three systems considered. The range of efficiencies possible at each temperature is also indicated. Estimates for a 6.9-MN/m^2 (1,000-psi) steam system are also given for comparison purposes. This is shown in figure 5-28.

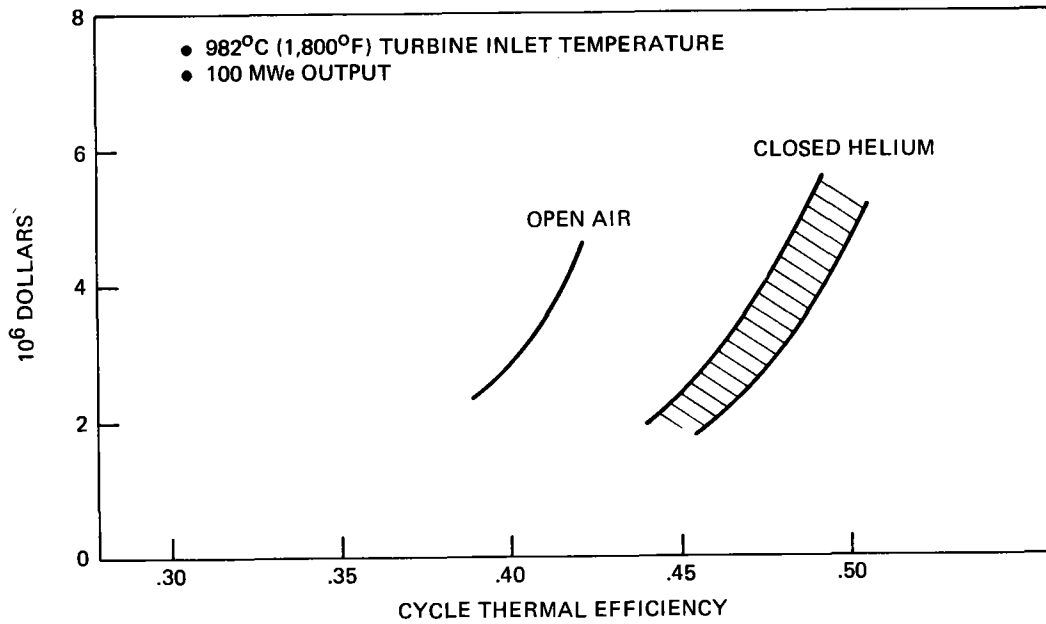


Figure 5-25. Recuperator Costs for 982°C (1,800°F) System

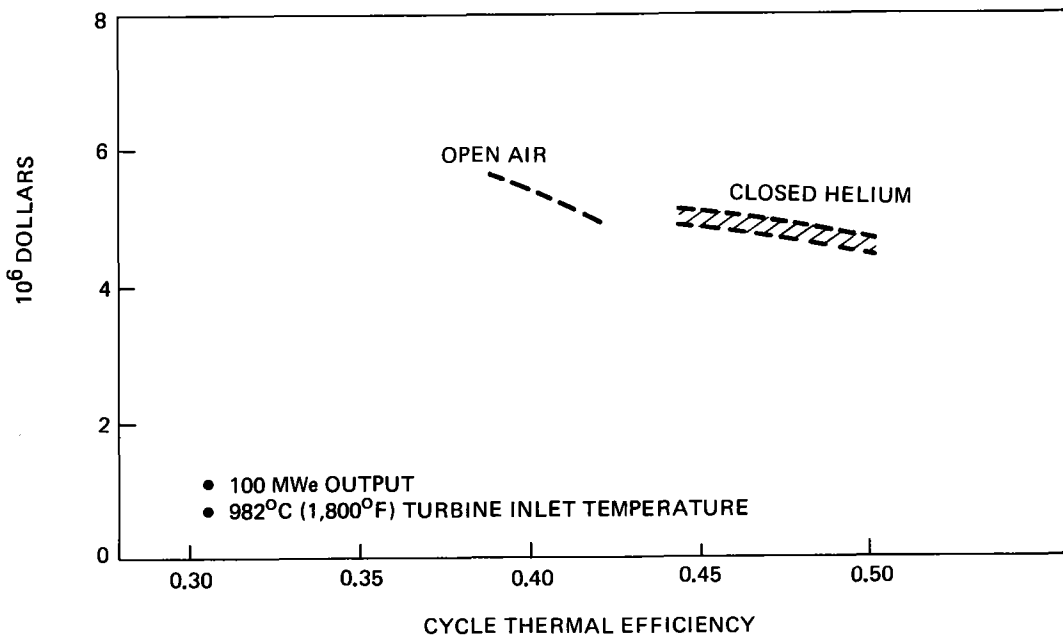


Figure 5-26. Turbomachinery Costs for 982°C (1,800°F) System

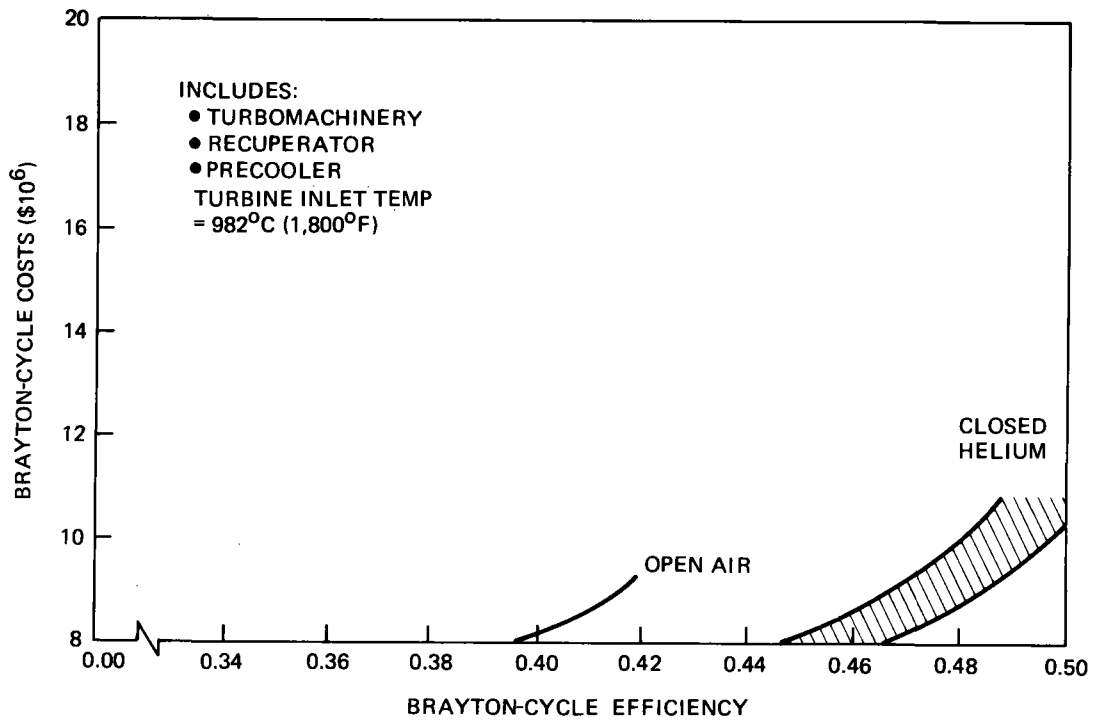


Figure 5-27. 100-MWe Brayton-Cycle Costs for 982°C (1,800°F) System

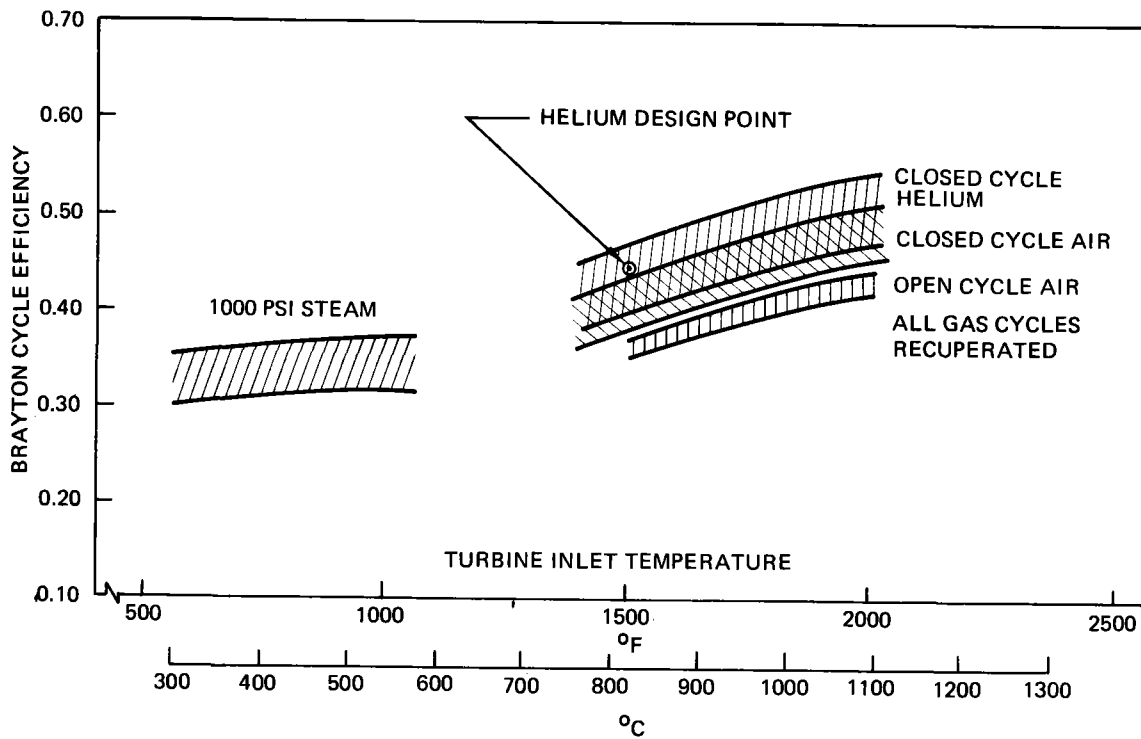


Figure 5-28 Cycle Thermal Efficiency

5.3.4 Assessment of All Major Cycles

The preceding sections have concentrated on gas cycles. The cycle given to Boeing as a strawman for comparison is a steam Rankine cycle with an efficiency rating of 0.36 in the 100-MW_e plant. This has been included in a qualitative assessment of all cycles, which is summarized in table 5-1. The closed cycles for helium and air are combined since the differences between them are less than that of the other cycles. Many of the advantages and disadvantages of the gas cycles have been covered. Items such as operating experience, operational flexibility, and complexity for the various systems are included that are either apparent or highly subjective.

Table 5-1. Qualitative Assessment of Alternate Systems

System	Advantages	Disadvantages
Closed Cycle	<ul style="list-style-type: none"> ■ High efficiency ■ Smallest turbomachinery ■ Operational flexibility ■ Good bottoming cycle potential 	<ul style="list-style-type: none"> ■ No operating experience in U.S. ■ Large precooler ■ High Brayton-cycle costs
Open Cycle	<ul style="list-style-type: none"> ■ No precooler required ■ Similar to combustion turbine design ■ System simplicity 	<ul style="list-style-type: none"> ■ Poor operational flexibility ■ Large turbomachinery ■ Large recuperator
Steam	<ul style="list-style-type: none"> ■ Proven systems available ■ Utility familiarity ■ High heat flux receiver 	<ul style="list-style-type: none"> ■ Large precooler ■ Lower efficiency ■ Complex system

QUALITATIVE CYCLE COMPARISONS

5.4 ADAPTATIONS FOR PLANT OPERATION AND CONTROL

A solar thermal conversion (STC) powerplant faces a constantly changing solar input. Normal solar variations and transients occasioned by the environment, startup, storage switchover, or shutdown make plant control a very important item.

The major control difficulty with a solar powerplant is that there is no simple throttle control, such as the fuel flow control in a fossil-fuel gas turbine. The collector field could probably be used during some transients, such as start-up, but the use of the field as a control parameter during normal operation is probably not feasible. The only other way to control a gas turbine mechanically is by use of variable vanes in the compressor and turbine, but these would be good for only small changes (on the order of 5%-10%). However, performance of a gas turbine is also a function of the pressure and temperature of the gas entering the compressor. Typically, a turbine inlet temperature and engine speed define the conditions at the compressor inlet in terms of corrected mass flow (i.e., $\frac{\dot{m}\sqrt{T}}{P}$). If, for the moment, the compressor inlet temperature is considered to be a constant, then mass flow (\dot{m}) ends up being proportional to the inlet pressure. A closed cycle has a definite advantage over an open cycle in system control because of this effect. For the open cycle the compressor inlet pressure will be equal to ambient pressure and there will be no control on the mass flow. However, some control can be exercised through bypassing recuperator mass flow. For the closed cycle, the compressor inlet pressure is a function of the amount of gas in the system. This is controllable so the mass flow also ends up being a controllable variable. The reason this is important is that both electrical output and receiver temperature are functions of mass flow (i.e., $W_{net} = \eta Q_{in}$ where $Q_{in} = \dot{m} C_p \Delta T$.)

The control possible with the closed system is a function of whether or not a storage system is used. If there is no storage system, system temperatures and cycle efficiency can be held constant by changing the pressure level (gas inventory) as the solar input changes. However, in doing so, the output also changes, basically following the solar input. There would be some margin of control on the output of this system by controlling the turbine inlet temperature, by bypassing normal mass flow through the recuperator.

If there is a storage system, output can be controlled as well as the temperature by either adding or removing the amount of heat necessary to keep the output at the desired level. This is conceptually how the baseline system will operate. System performance used in the storage analysis is given on figures 5-29 and 5-30. Various turbine inlet temperatures are displayed since operation from storage will probably be at a temperature less than the design value. The pressure level change given on figure 5-29 is for a constant output. However, it is possible to change the output at any point simply by changing the pressure level.

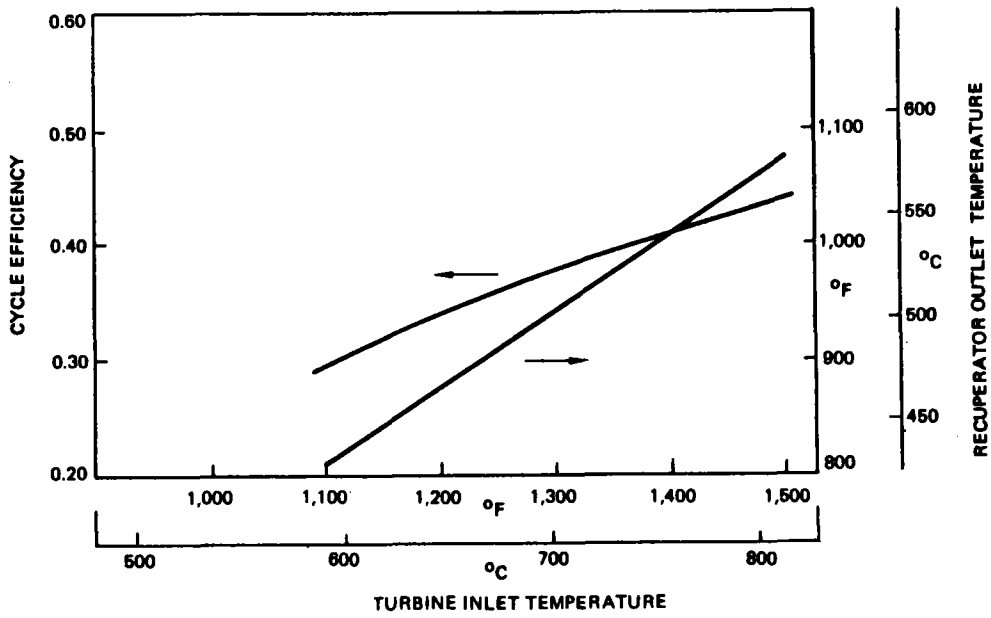


Figure 5-29. Cycle Performance

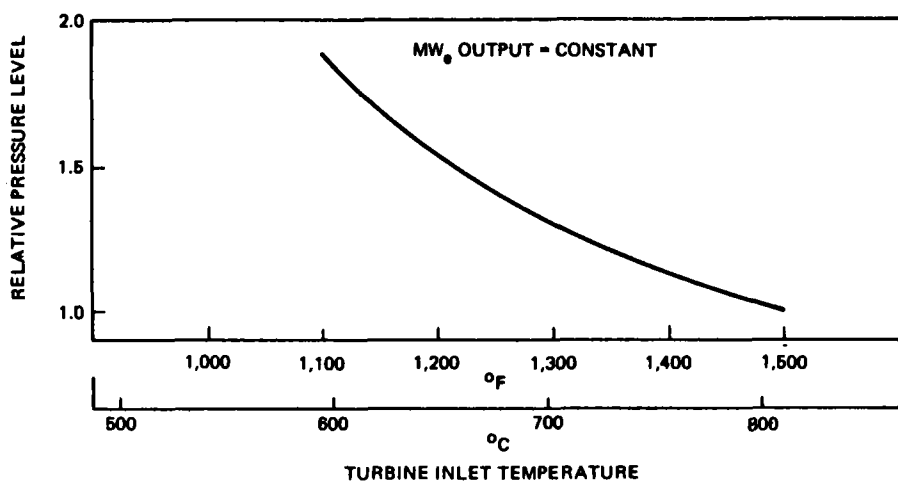


Figure 5-30. Pressure Level

Section 6.0

ENERGY STORAGE

The results of the energy storage work carried out in conjunction with the receiver and plant design work are presented in this section. The primary objectives of this work were to review and screen the energy storage system technology, to conduct conceptual design studies for candidate thermal energy storage (TES) systems, and to conduct an integration analysis of the storage device with a high-temperature solar thermal conversion (STC) power plant.

Energy storage for the STC powerplant is required for plant control (i.e., thermal buffering) and for source leveling (i.e., capacity displacement). The thermal buffering requirement is generally accepted as a $\frac{1}{2}$ hour of storage and it must be carried out by a TES device on the source side of the generator. Source leveling could be carried out on either side of the generator, and, as a result of the Aerospace Corporation "Mission Analysis" studies, is normally taken as 6 hours of storage.

A technology survey was conducted in order to establish the available energy storage concepts. The design and development status of various conventional utility storage concepts and the technology status of high-temperature TES systems was reviewed. Three high-temperature TES concepts were then carried into conceptual design and preliminary cost estimates were developed.

Math models were created to assist in the analysis of the storage system. These models were incorporated in the overall plant-operation math model. Integrated plant operation and performance studies were then accomplished.

The work presented here is scoped to meet the objectives of the receiver concept feasibility study. Considerable interest in high-temperature energy-storage-device work has been developed as a result of this work. Boeing is under contract with EPRI (RP 788-1) to continue the work and has added contractual work

for ERDA on a similar basis. The technical questions raised, as a result of the work reported here, will be addressed in the continuation efforts for EPRI and ERDA with expansion in scope and depth of the conceptual design studies.

6.1 STORAGE CONCEPTS SCREENING

A wide variety of energy storage devices are being considered for conventional utility applications. Several of the proposed devices involve current or near-term technology and are being developed for commercial application. Other devices involve longer range technology and will require a concerted R&D effort to reach commercial status.

Public Service Gas and Electric of New Jersey (PSG&E), under joint funding from ERDA and EPRI, has completed a technical and economic assessment of energy storage devices for electric utility applications. The storage concept screening work reported here is based largely on the results of the PSG&E study. Tables 6-1 and 6-2 summarize the near-term and long-term economic comparisons of the major storage devices considered by PSG&E. This information was extracted directly from the preliminary PSG&E report.

Energy storage on the load side of the STC generator is analogous to conventional utility storage; therefore, the information from PSG&E can be applied directly. Energy storage on the source side of the STC generator requires direct storage of high-temperature thermal energy. Such a device will provide the thermal inertia required to buffer rapid variation in heat source and is capable of supporting the thermal control of the powerplant. The same device also has the potential of providing the long-term storage for source leveling and would make direct utilization of the balance of plant already available in the STC powerplant.

A survey of the high-temperature thermal energy storage technology was conducted in order to identify potential device concepts for the source-side storage. Space systems, Stirling engine, underwater systems, industrial process, and nuclear powerplant applications were all included in the review. Two basic devices were identified as a result of the survey; refractory bricks and molten salts. A third device, thermochemical reactions, was also identified as a potential long-term technical solution.

Table 6-1. Energy Storage Systems Economic Data Near Term (1975-1985) Technology

Energy storage system economic characteristics	Energy storage systems		
	Hydro pumped storage	Electrochemical (battery)	Compressed air
1975 power cost (\$/kW)	90-145	70-80	120-150
1975 storage cost (\$/kWhr)	2-10	50-60	3-10
Expected life (years)	50	5-10	20-25
Efficiency (%)	70-75	60-75	—
Operation and maintenance			
a) Variable costs (mills/kWhr)	—	2.7	5.3
b) Fixed costs (\$/kW/yr)	1.6	—	—
Heat rate (btu/kWhr)	—	—	4200-5500 (58-74 mwhr (in)/ 100 mwhr (out))

Reference: Interim report Public Service Gas & Electric of New Jersey
 Technical and economic assessment of energy storage for electric utilities, RP-225

Table 6-2. Energy Storage Systems Economic Data Long Term (1990-2000 and Beyond) Technology

Energy storage system economic characteristics	Energy storage systems					
	Hydro pumped storage	Electrochemical (battery)	Compressed air	Chemical	Flywheels	Super-conducting magnetic energy storage (SMES)
1975 power cost (\$/kW)	90-145	60-70	120-130	400-500	90-120	50
1975 storage cost (\$/kWhr)	2-10	20-40	3-10	6-7	80-150	35-110
Expected life (years)	50	10-20	20-25	10-25	20-25	20-30
Efficiency (%)	70-75	70-80	—	45-55	70-85	70-85
Operation and maintenance						
a) Variable costs (mills/kWhr)	—	2.7	5.3	2.7	5.3	—
b) Fixed costs (\$/kW/yr)	1.6	—	—	—	—	1.6
Heat rate (btu/kWhr)	—	—	(3800-4300) (58-74 mwhr (in)/ 100 mwhrs (out))	—	—	—

Reference: Interim report Public Service Gas & Electric of New Jersey
 Technical and economic assessment of energy storage for electric utilities, RP-225

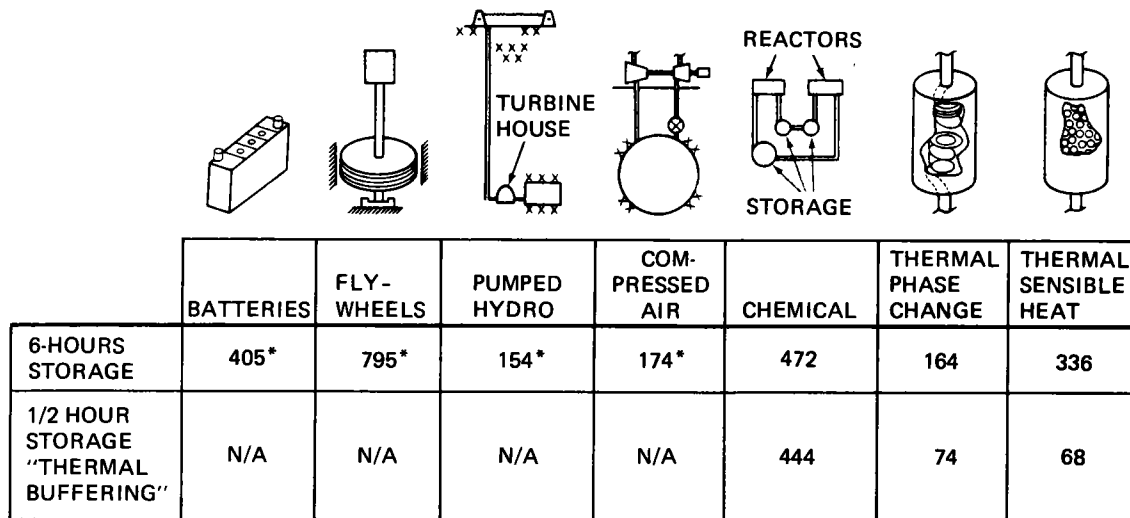
Several industrial processes store thermal energy in refractory bricks, in what are commonly referred to as "checkerworks." The technology of refractory bricks and associated thermal energy storage devices is well defined and is available for direct application to the source-side thermal energy storage.

Thermal energy storage in the latent heat of fusion of molten salts is attractive because of the very high energy storage density. Work in space systems, Stirling engines, and underwater systems uses these device concepts. Most of the associated technology is either far term or in a research and development state, although some current development work is in process at Philips, as related to Stirling engines and home heaters. R&D work is also being undertaken by NASA for space applications and the molten-salt reactor work of the last two decades is related. All of this work is based on fluoride salts in system applications at a temperature range of 600⁰ to 800⁰C (1,112⁰ to 1,472⁰F), consistent with the high-temperature STC powerplant.

A substantial amount of research work on reversible thermochemical reaction systems is also in progress. This work is related to thermal energy storage and transport and to the production of synthetic fuels. The technology status is R&D particularly as related to the reversible closed-cycle system. Thermal energy storage in reversible thermochemical reaction systems offers the highest potential in energy storage density but will require a substantial development program.

Figure 6-1 is a summary comparison of the investment costs of the major energy storage devices considered for the STC powerplant. The projected cost for the four candidate conventional utility devices shown in the figure are based on the midpoints of the cost bands in tables 6-1 and 6-2. Batteries, underground pumped hydro; and compressed air are near-term technology and flywheels are long-term.

Each of the four conventional utility devices are separate powerplants and do not provide their thermal buffering function at the solar plant. On the other hand, the three TES devices are integral with the STC powerplant, and a 6-hour device would also provide the thermal buffering function. Any one of the conventional utility-type storage devices could provide the long-term thermal storage at the STC powerplant. However, the combined cost of the conventional storage and the thermal buffering at the solar plant is, at best, marginally competitive with the all-thermal approach.



*Reference RP-225, Technical and Economic Feasibility of Energy Storage for Conventional Utility Applications, Public Service Gas & Electric of New Jersey

Figure 6-1. Energy Storage Investment Cost Comparison (\$/kW)

The projected costs of the three TES devices are ROM estimates based on the conceptual design results presented in the following section. On the basis of these cost numbers, the phase-change system has been identified as the preferred storage system. However, significant cost and performance improvements are projected for the thermochemical system, as the associated technology is developed, and the sensible-heat system is near-term technology and considered to be a competitive approach.

The cost data shown on figure 6-1 are investment cost only. Significant operating costs are associated with the compressed-air system as a result of the use of fossil fuels in the air-reheat cycle. Lifetime differences also exist among the devices. The cost comparison should actually be made on a present-worth assessment of all required future resources. The three TES devices also behave differently within the powerplant. These performance differences have been evaluated and the results of the integrated plant performance in terms of energy cost are presented in section 8.2. These results also support the selection of the fluoride salt phase-change TES device as the preferred storage system.

6.2 TES SYSTEM CONCEPTUAL DESIGN

Conceptual design studies were conducted for each of the three TES systems identified in the previous section. The objectives of these studies were to assess the technical feasibility, to develop sufficient system and subsystem design data to support preliminary cost estimates, and to identify the operational and environmental concerns for each TES concept.

6.2.1 Storage Media Constituent Selection

Several candidate thermal storage media constituents were evaluated for each of the three TES systems. In each case a preferred medium was identified and concept design studies were then undertaken. The selection rationale and supporting data are presented for each TES concept in the following paragraphs.

Preferred Sensible-Heat Storage Medium. The selection of a material for use in a sensible-heat TES device is design dependent and must be based on a careful evaluation of the factors listed in figure 6-2. Two approaches to a sensible-heat TES system seem apparent: using a liquid bath/tube arrangement or a solid porous medium pressure-vessel arrangement. The liquid bath/tube approach has the advantage of using tubes to transfer the helium flow at 3.45 MN/m^2 (500 psi) pressure. The TES container would be designed for high temperature and low internal pressure. The solid porous medium/pressure-vessel arrangement uses a solid refractory with passageways for helium flow made by laying the bricks with flow channels contained. This approach avoids the use of tubing but requires the design of a high-temperature high-internal-pressure (500 psi) vessel. Another approach to the solid medium sensible-heat TES system would be to add an intermediate heat exchanger. Energy would be transferred from the helium flow to a secondary working fluid (e.g., liquid sodium). The secondary fluid would then circulate energy through the solid medium, which, in this case, could be crushed rock. The details of such a system have not been considered in this study.

Candidate TES media are given in figure 6-2. The NaOH was found to be attractive for the bath/tube approach because NaOH has a relatively high heat capacity and low cost and because NaOH remains in the liquid state over a wide temperature range. Molten hydroxides have been proposed as moderator coolants for fused-salt nuclear reactors.^{(1)*} However, data reported in that reference indicate severe corrosion problems with molten NaOH at temperatures of 800°C ($1,472^\circ\text{F}$).

*References are listed at end of section.

Material	Melt-boil temperature °C (°F)	ρ kg/M ³ (lb/ft ³)	Cp Watt-sec 5°C (BTU/lb - °F)	k Watt/M°C (BTU/hr-ft-°F)	Cost \$/kg (\$/lb)	Stored energy per unit cost $\Delta T = 250^\circ\text{C}$ (450°F) KWH/\$ (BTU/\$)	Stored energy density $\Delta T = 250^\circ\text{C}$ (450°F) KWH/M ³ (BTU/ft. ³)
NaOH ^(a)	186-1,020 (365-1970)	1,700 (106)	2,050 (0.49)	1.2 (0.7)	0.87 (0.40)	0.163 (552)	242 (23,400)
MgO ^(b)	>> 827 (1,520)	3,000 (188)	1,260 (0.30)	10.5 (6.1)	0.26 (0.12)	0.336 (1,125)	263 (25,400)
Al ₂ O ₃ ^(c)	>> 827 (1,520)	4,000 (250)	1,260 (0.30)	6.3 (3.6)	0.53 (0.24)	0.162 (552)	350 (33,800)
Si O ₂ ^(c)	>> 827 (1,520)	2,600 (157)	1,260 (0.30)	2.3 (1.3)	0.11 (0.05)	0.795 (2,700)	228 (21,200)

● Key selection factors

- Cost
- Availability
- Chemical stability
- Phase change temperatures out of operating temperature range
- Corrosivity
- Heat capacity
- Thermal conductivity
- Density
- Vapor pressure

a) Informal communication with Dow Chemical

b) Kaiser refractories, Feb 1976 prices, f.o.b. Moss Landing, Ca

c) Informal communication with Kaiser Refractories

Figure 6-2. Candidate Sensible Heat TES

Also, the relatively low thermal conductivity of NaOH implies that a large number of He tubes would be required to meet the charge and discharge heat rate requirements. This fact alone would indicate the need of large amounts of expensive tubing material. Preliminary costing indicated the NaOH bath/tubing design was several times as expensive as the solid porous-medium approach. The potential corrosion problems and the cost impact resulted in suspending further effort on the NaOH bath/tube approach.

A comparison of various refractory materials shows that the heat capacities are about equal. MgO has superior thermal conductivity and moderate values of density and cost. These properties indicate that the MgO will provide the best performance for cost. MgO bricks also retain high strength at elevated temperatures, are resistant to spalling, and are readily available in large quantities. Mortar and construction techniques for these bricks are part of standard industry practice.

Latent Heat of Fusion Storage This TES concept involves the storage of thermal energy in the latent heat of fusion of fusible salts. Normally, the storage process takes place with small-to-moderate temperature departures from the melt temperature of the salt, resulting in a nearly isothermal storage device. Fusible salts and eutectic mixtures of those salts with substantial heat of fusion are commercially available at virtually any melt temperature between 250°C (356°F) and 1,400°C (2,550°F). Several of the salt types shown in figure 6-3 have been used in commercial molten-salt heaters and in advanced development heaters.

The selection of a salt, or salt mixture, for a particular application is design dependent and must be based on a careful evaluation of each of the technical and economic factors listed in figure 6-3. For applications with gas-turbine plants, the melt temperature range of interest is 600⁰-900⁰C (1,112⁰-1,650⁰F). Since the heat of fusion is the key to storage system economics, the fluoride salts are attractive for these high-temperature applications.

The fluoride salts are abundant, inexpensive, and chemically and thermally stable. They have been worked with and studied for thermal applications and are currently the preferred thermal energy storage media at these temperatures.

The primary source of fluoride salts is fluorspar or fluorite (CaF₂) which are mined and are available in large quantities for as little as 4 cents a pound.

Type (single salt)	Melting point range °C (°F)	Heat of fusion range cal/gm (BTU/lb)
Chlorides	246-963 (475-1765)	17-139 (31-250)
Nitrates***	260-593 (500-1100)	22-83 (40-150)
Hydroxides**	316-454 (600-850)	33-211 (59-380)
Bromides	538-760 (1000-1400)	28-56 (50-101)
Carbonates	704-1371 (1300-2500)	56-144 (101-259)
Fluorides*	816-1316 (1500-2400)	89-250 (160-450)

*High temperature salt—Phillips Labs

**Low to moderate temperature salt—Hooker Chemical,
Comstock & Wescott

***Moderate temperature salt—DuPont; Bethlehem, Black,
Sivalls and Bryson

● KEY SELECTION FACTORS:

- COST
- AVAILABILITY
- CHEMICAL STABILITY
- THERMAL CYCLE STABILITY
- CORROSIVITY
- MP TEMPERATURE
- HEAT OF FUSION
- DENSITY
- DENSITY VARIATION
- THERMAL CONDUCTIVITY
- VAPOR PRESSURE

Figure 6-3. Candidate Fusion Salts

Fluorspar is decomposed with hydrogen to produce hydrogen fluoride, which is then recombined with virtually any base-metal combination to yield a wide variety of fluoride salts. The base metal, therefore, dominates the availability and thermo-physical properties of the resultant salt. Mixtures of various salts provide a wide variation in cost, melt temperature, and heat of fusion, as shown in figure 6-4. The data base of thermophysical properties, potential safety problems, and corrosion characteristics is moderate to good.

Thermochemical Storage. The thermochemical storage concept involves the storage of thermal energy in the heat of decomposition and recombination of reversible thermochemical reactions. Candidate reactions typically considered for this kind of application are listed in figure 6-5. Generally, these reactions are well understood and are commonly derived from commercial chemical processes.

The selection of a preferred reaction is dependent on the powerplant operating characteristics, and the selection process must include a careful evaluation of all the factors listed in figure 6-5. Although the heat of reaction is a key consideration, the storability of the reaction products is of equal concern since the physical state of the reaction products will, to a large extent, establish the size of the system, the complexity of the system, and the parasitic power requirements associated with the chemical transport loops.

Melt	Salt	T _{melt} °C (°F)	H _F cal/gm (BTU/lb)	Cost* \$/kg (\$/lb)	Energy/cost Kcal/\$ (BTU/\$)
1 b, s	67 LiF/33 MgF ₂	746 (1,375)	217 (390)	4.85 (2.20)	44.75 (177)
2 f, s	65 NaF/23 CaF ₂ /12 MgF ₂	745 (1,314)	137 (246)	.90 (0.41)	152.73 (607)
3 b	5.6 KF/64.4 LiF/30 MgF ₂	713 (1,315)	226 (402)	4.70 (2.14)	48.14 (191)
4 f, b	40 NaF/60 KF	710 (1,313)	139 (250)	1.14 (0.52)	122.14 (485)
5 f, s	58 KF/35 NaF/7 MgF ₂	685 (1,264)	130 (234)	1.22 (0.56)	106.82 (424)
6 f	70 NaF/30 FeF ₂	680 (1,256)	164 (295)	1.44 (0.66)	113.89 (453)
7 b, s	60 LiF/40 NaF	652 (1,205)	130 (234)	4.07 (1.85)	31.91 (127)
8 f	67 NaF/33 ZnF ₂	635 (1,175)	143 (258)	0.97 (0.44)	147.89 (588)
9 s	46 LiF/44 NaF/10 MgF ₂	632 (1,171)	205 (370)	3.46 (1.57)	59.20 (235)
10 s	52 LiF/35 NaF/13 CaF ₂	615 (1,140)	152 (274)	3.55 (1.61)	42.77 (170)

b – Borucka Research Company, ERDA Report dated June 1975

f – Li free salts

s – Philips Labs, informal "know how" transfer, October 1975*

* – Estimate based on interim Pennwalt data FOB, Inyoken, California

Figure 6-4. Candidate Fluoride Salts

Reaction	Reaction temp °C (°F)	Approximate heat of reaction cal/g (BTU/lb)
$\text{SO}_2 + \frac{1}{2}\text{O}_2 \rightleftharpoons \text{SO}_3^*$	< 720 (1,330)	295 (531)
$\text{Ca CO}_3 \rightleftharpoons \text{CO}_2 + \text{CaO}^{**}$	< 540 (1,005)	395 (710)
$\text{Ca (OH)}_2 \rightleftharpoons \text{CaO} + \text{H}_2\text{O}$	~ 430 (807)	210 (378)
$\text{CH}_4 + \text{CO}_2 \rightleftharpoons 2 \text{CO} + 2 \text{H}_2^{***}$	~ 540 (1,005)	980 (1,770)
$\text{C}_2 + \text{CO}_2 \rightleftharpoons 2 \text{CO}$	~ 650 (1,200)	740 (1,332)
$\text{CH}_4 + \text{H}_2\text{O} \rightleftharpoons \text{CO} + 3 \text{H}_2^{***}$	~ 430 (807)	1700 (3,060)

*Sulfuric acid production

**Lime slaking

***Methane steam reforming (EVA-ADAM)

****Hyco reaction

● REACTION SELECTION FACTORS

- REVERSIBILITY OF REACTION
- REACTION ON DEMAND
- HEAT OF REACTION
- REACTION PRODUCT STORAGE
- EXOTHERMIC TEMPERATURE CONTROL
- ENDOTHERMIC TEMPERATURE CONTROL
- NONCORROSIVE, NON TOXIC, STORABILITY
- COST
- AVAILABILITY

Figure 6-5. Candidate Thermochemical Reactions

As a result of the reaction screening work, the SO_2/SO_3 reaction has been selected for the high-temperature gas-turbine application. This selection is supported by other investigators (i.e., T. A. Chubb, Analysis of Gas Dissociation Solar Thermal Power System, 1974) and is based on the following key factors:

- The SO_2/SO_3 reaction is the key reaction in the production of sulfuric acid. Consequently, its performance, maintenance requirements, reaction product storability and hazards, and supporting chemical process subsystems are well understood.
- Two of the three reaction constituents are conveniently stored as liquids and the third constituent (O_2) is commonly processed and stored as a gas, although many options are being considered, including the cryogenic storage of the O_2 constituent.
- The reaction temperature is controllable and the constituents will remain in stable equilibrium in the absence of the catalysts.

6.2.2 TES System Operating Requirements

The conceptual designs presented in the following sections are based on the following operating requirements:

- Minimum temperature* of any part of TES system is 427°C (800°F).
- Maximum temperature* of any part of TES system is 816°C ($1,500^\circ\text{F}$).
- The storage capacity is 6 hours.
- The helium pressure is 3.45 MN/m^2 (500 psi) and the pressure-drop criterion is 4%.
- The design lifetime of the system is 30 years.
- The heat loss through the TES system vessel walls and circulation lines is 2% of the thermal energy input to the system.
- Container vessel safety factors are designed with the 1974 ASME Boiler and Pressure Code, section VIII, "Rules for Construction of Pressure Vessels."
- The TES system is designed to accept hot helium for charging at the design system operating temperature and cold helium for discharging at the cold-side recuperator discharge temperature.
- The minimum helium discharge temperature at the full discharge rate and the fully discharged condition is 593°C ($1,100^\circ\text{F}$).
- The design mass flow rate, charge and discharge rates, and temperature swing of the media for the TES system conceptual design are given below:

*The difference, $816^\circ - 427^\circ\text{C}$ ($1,500^\circ - 800^\circ\text{F}$), is not the temperature swing of the TES media. The actual temperature swing experienced is a function of integration into the entire plant operation and cannot be specified as a requirement.

	Latent Heat Sensible Heat <u>TES</u>	Thermochemical <u>TES</u>
Design Mass Flow rate	200 kg/sec (400 lb/sec)	92 kg/sec (202 lb/sec)
Discharge Rate	170 MW _{th}	113 MW _{th}
Charge Rate	126 MW _{th}	102 MW _{th}
Temperature Swing	162°C (292°F)	234°C (421°F)

The latent-heat/sensible-heat TES and thermochemical TES conceptual designs are based on slightly different conditions. The latent-heat/sensible-heat TES systems are based on a varying discharge temperature, whereas the thermochemical TES system is based on an isothermal discharge temperature.

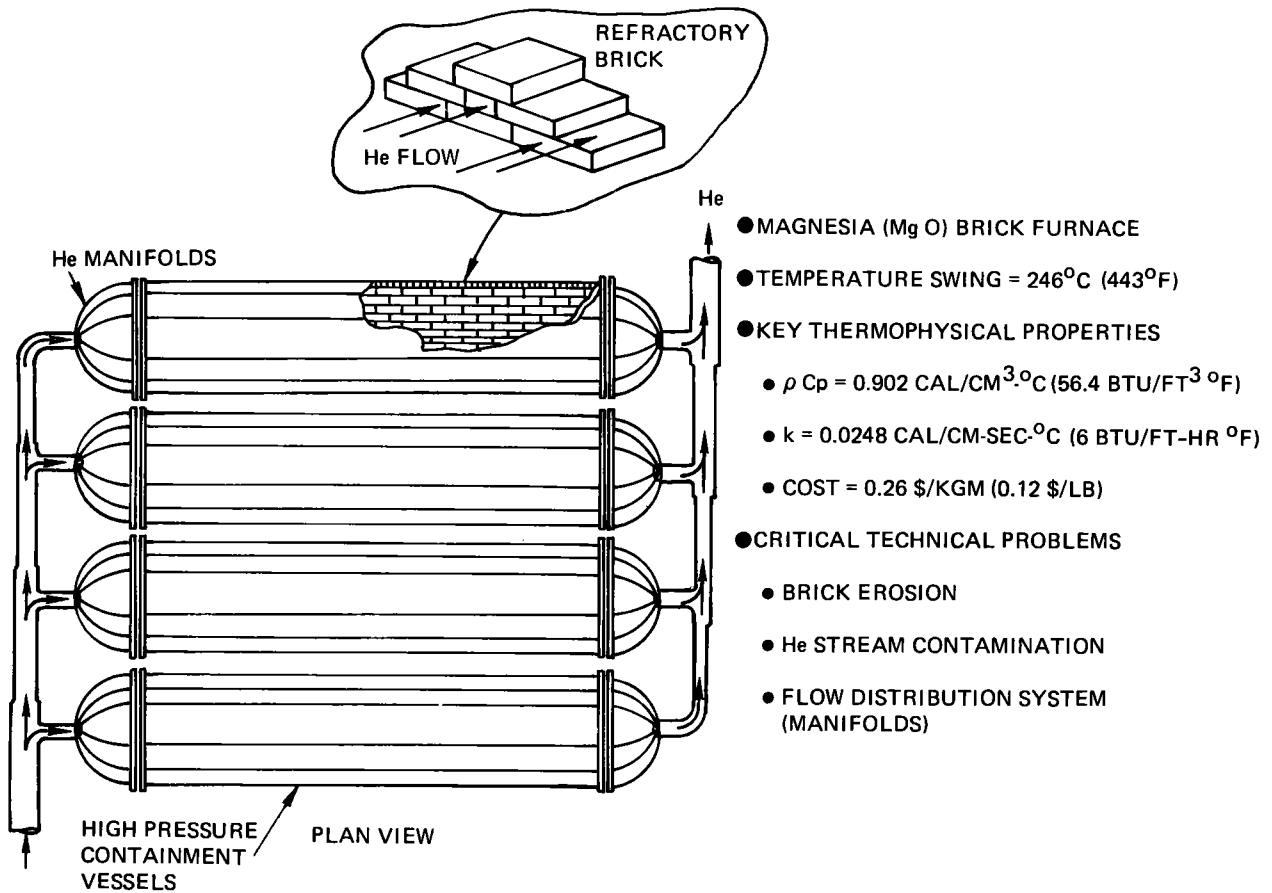
6.2.3 Sensible-Heat TES System

This section presents the conceptual design of a state-of-the-art sensible-heat thermal energy storage system. Included in this section are a design description; materials compatibility and availability; systems costs and critical technical problems; and safety, maintenance, and ecological considerations.

Design Description. The conceptual design is based on the same operating requirements listed in section 6.2.2. The sensible-heat TES system designed to meet the operating requirements is summarized in figure 6-6. The refractory brick is contained in four horizontally placed, insulated cylindrical pressure vessels (6.2-meter inside diameter x 32.0-meter length). The helium flow is distributed and collected by a piping system to each vessel.

Diffuser plates in each vessel distribute the flow evenly to channels contained in the refractory brick checkerwork. A schematic of the vessel design is given in figure 6-7. The refractory material is MgO. Thermophysical data on this refractory are given in figure 6-6. The surface of the bricks is smoothed to eliminate any loose material. The brick is surrounded with a layer of insulation. Kaowool*(R) is used on the bottom third of each tank to support the brick checkerwork. Mineral wool is used in the remaining areas where loading stresses

*Registered trademark of Babcock and Wilcox



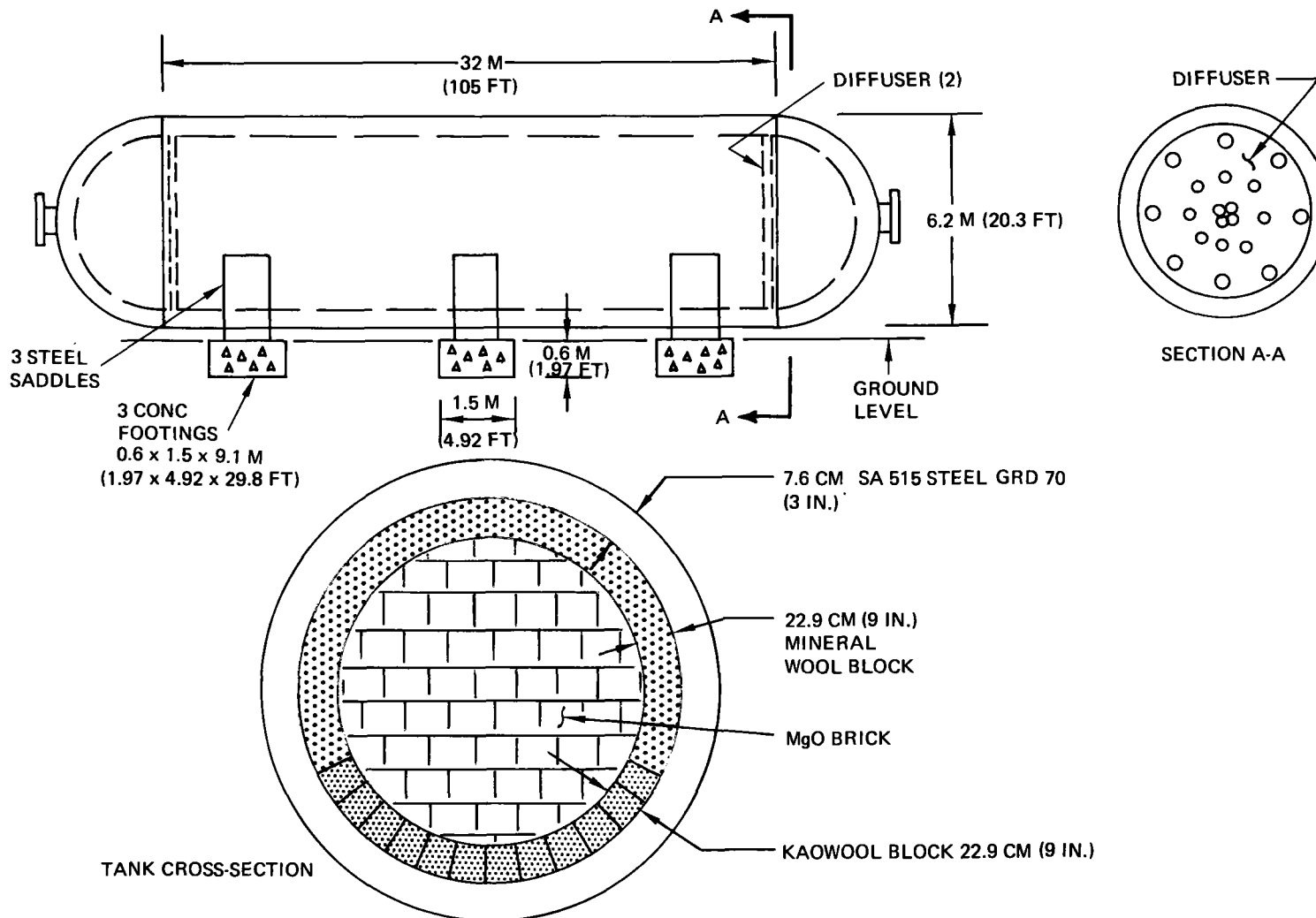
Account	Quantity	Unit Cost	Total cost (M\$)
Brick (Mg O)	8.2×10^6 kgm	0.26 \$/kgm	2.1
Storage containers (4) (6.2 m x 32 m)	1.8×10^6 kgm	6.20 \$/kgm	11.2
Insulation	4.4×10^4 kgm	11.30 \$/kgm	0.5
Heat exchanger*	1.7×10^6 bricks	0.76 \$/brick	1.3
Helium circulation system	20 MW	87,000 \$/MW	1.7
Total system			16.8

Estimated system mass: 10×10^6 kgm (22×10^6 lb)

*Brick construction cost – 145 bricks per man-day/\$110 per man-day (1976 mean cost data)

4.8 kgm/brick – 1.7×10^6 bricks @ 76¢/brick

Figure 6-6. Sensible Heat TES



6-14

Figure 6-7. Sensible Heat TES Tank Schematic

are much smaller. The insulation thickness was sized to allow a 2% maximum heat loss. The vessel wall is made of 7.6-centimeter (3-inch) carbon steel (ASTM 516). The vessel is designed in accordance with 1974 ASME Boiler and Pressure Code, Section VIII, division II. The thickness of material is consistent with on-site welding vessel fabrication practice. ⁽²⁾ The design wall thickness and vessel diameter allow the use of four vessels, each with a length-to-diameter ratio of about 5, to contain the required volume of solid thermal storage medium.

The helium circulation system consists of a compressor sized to recoup the 4% pressure drop through the TES system while maintaining the design mass flow rate. Also included in the circulation system is a filter to remove any particles that may erode from the brick.

Materials Compatibility. The main concern in the area of materials compatibility for the sensible-heat TES conceptual design is the possibility of brick erosion and the subsequent contamination of the helium stream. By careful design of the manifold, it is expected that the helium flow velocity through each channel in the refractory will be low enough to minimize any brick erosion. The relatively high resistance to spalling exhibited by the MgO bricks minimizes this materials problem. Another materials problem could be introduced by thermal cycling stresses inherent in such a TES system. Again, the high strength of the MgO brick would alleviate this problem.

Systems Costs. The systems costs are presented in figure 6-6. The refractory brick material cost is based on manufacturers' estimates (see section 6.2.1). The assembly costs of the bricks into a heat exchanger form are listed in a separate account. The costs are based on data gained from 1976 means cost data for fire-brick installation. The costs for the storage vessels are based on estimates given by Chicago Bridge and Iron for vessel dimensions of the design used. The helium-circulation system costs were estimated by scaling up existing compressor costs to the power rating required. ⁽³⁾

Critical Technical Problems. The main technical problem involved with this conceptual design centers around ensuring that the helium stream does not become contaminated with brick particles. The detailed design of the manifolds dictates a careful reduction of the inlet flow velocity to levels that will not induce brick erosion. A filter system may be necessary to ensure that particles do not enter and contaminate the compressor system.

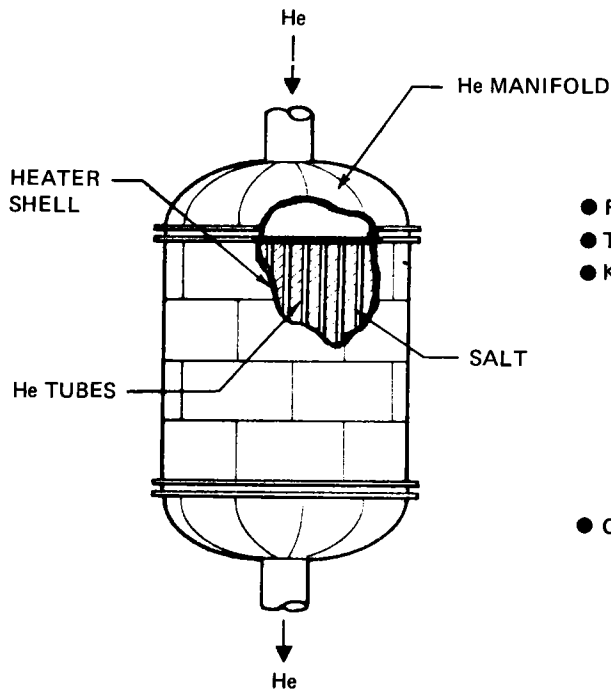
Safety, Maintenance, and Ecological Considerations. Other areas that require considerations in the sensible-heat TES conceptual design have been identified. The chief safety concern is the design of a pressure vessel for use at the expected temperature levels. By using several smaller diameter vessels and adhering to pressure vessel construction codes, it is expected that this problem can be controlled. The high temperature levels require that nonflammable materials be used in the construction and insulation of the container vessel. By using the solid medium for thermal storage, there are no ecological hazards that could be released in the event of a leak in the container vessel. However, the specifics of a particular location and a particular design must be considered before a definitive statement on the ecological impact of a sensible-heat TES system can be made.

In the area of maintenance, continuous monitoring of the system performance will be required. Also, periodic inspections for leaks or possible failures are needed. Continuous monitoring of the helium flow will allow the detection of any contaminating brick particles. The modular tank approach allows the shutdown of only a portion of the system for repair or refurbishment at selected times during the lifetime of the TES system.

6.2.4 Phase-Change TES System

This section presents the results of the conceptual design of a phase-change thermal energy storage system. Included in this section are design description; materials compatibility and availability; systems costs; critical technical problems; and safety, maintenance, and ecological considerations.

Design Description. The conceptual design is based on the operating requirements listed in section 6.2.2. The phase-change TES system designed to meet the requirements is summarized in figure 6-8. The phase-change material and heat exchanger are contained in an insulated cylindrical vessel 13.1 meters (43 feet) in diameter and 13.1 meters (43 feet) in height. The helium flow is dispersed and collected by manifolds into 11,000 tubes of 1.37-centimeter (0.54-inch) diameter with an 0.08-centimeter (0.032-inch) wall placed vertically in a square-spacing pattern. Centerline-to-centerline tube spacing is 0.113 meter (0.37 foot). The eutectic fluoride salt is contained as a bath between the helium tubes. The vertical flow arrangement, with the hot helium entering the top manifold during charging and the cold helium entering the bottom manifold during discharging, will maintain



- FUSIBLE FLUORIDE SALT BATH
- TEMPERATURE SWING 246°C (443°F)
- KEY THERMOPHYSICAL DATA
 - $T_{MELT} = 635^{\circ}\text{C}$ (1176°F)
 - $\rho C_p = 0.672 \text{ CAL/CM}^3\text{-}^{\circ}\text{C}$ (42 BTU/FT³-°F)
 - $h_f = 143 \text{ CAL/GM}$ (258 BTU/LB)
 - $k = 0.0103 \text{ CAL/SEC-CM}^{\circ}\text{C}$ (2.5 BTU/FT-HR-°F)
 - COST = 0.97 S/KGM (0.44 \$/LB)
- CRITICAL TECHNICAL PROBLEMS
MATERIAL COMPATIBILITY

<u>Account</u>	<u>Quantity</u>	<u>Unit cost</u>	<u>Total cost (M \$)</u>
Salt (fluoride eutectic)	3.2×10^6 kgm	0.97 \$/kgm	3.1
Storage container (13.1 m x 13.1 m)	14.6×10^4 kgm	13.00 \$/kgm	1.9
insulation	99 m ³	1918 \$/m ³	0.2
Heat exchanger			
(1.37 cm OD) tubes (13.1 m)	11,000 tubes	110.00 \$/tube	1.2
welds (3/tube)	33,000 welds	12.00 \$/weld	0.4
Helium circulation system	20 MW	87,000\$/MW	1.7
Total system			8.5

Estimated system weight: 4.0×10^6 kgm (8.8×10^6 lb)

Figure 6-8. Phase Change TES

the solidified salt below the liquified portion. This arrangement will ensure that the salt will remain in intimate contact with the helium tubes by avoiding the formation of voids during salt solidification. Inconel 617 is the present choice for the tubing metal. The fluoride eutectic is 67 NaF/33 ZnF. Thermo-physical data on the eutectic are given in figure 6-8. The container vessel wall has an inner layer of graphite, a middle layer of refractory brick, and an outer layer of metal or reinforced concrete. The helium circulation system consists of a compressor sized to recoup the 4% pressure drop through the TES system while maintaining the design mass flow rate. Also included in the circulation system is a filter to remove any fluoride that may enter the helium system via a leak.

Materials Compatibility and Availability. An important concern in the phase-change conceptual design is in the area of materials compatibility. The main problem is the possible corrosive action of molten-fluoride salts on tubing metal and vessel wall. Inconel 617 exhibits desirable creep rupture properties at the expected operating temperatures. The possible corrosive attack of fluorides on the chromium in the alloy has been shown to be controlled by the addition of small quantities of aluminum to the salt mixture.⁽⁴⁾ Inconel 617 is being employed in other fluoride eutectic designs.^{(5), (6)} An alternative choice for tubing metal is Hastelloy-N. This alloy is identical to INOR-8, an alloy specially developed by the Atomic Energy Commission for use with high-temperature fluoride eutectics in their molten salt reactor program.⁽⁷⁾ During corrosion tests conducted by AEC, the low-chromium alloy INOR-8 exhibited excellent corrosion resistance after lengthy exposure to molten-fluoride eutectics. Based on these data, it is expected that the tubing metal and the fluorides would be compatible. It is known that the fluorides will attack the silicates and oxides found in refractory bricks. However, using graphite as an inner layer, these problems can be avoided. Based on testing done by AEC,⁽⁸⁾ it was found that graphite and eutectic fluorides do not react with each other. Also, the molten salt will not "wet" the graphite. Therefore, by choosing the pore size of graphite carefully, the surface tension of the melt will not allow the salt to permeate the graphite. An alternative design would employ a metal liner instead of graphite.

Another area of materials compatibility is the differential thermal expansion of the salt and the tubing metal. The detailed manifold design will require allowance for thermal expansion. Also, since the salt will probably expand/contract

at a different rate from the metal, a "dead volume" will have to be allowed to accommodate the salt volume when completely molten.

The availability of the fluoride salts seems certain. Based on conversations with the Pennwalt Corporation, the constituents NaF and ZnF can be supplied in the volumes envisioned. The availability of the Inconel 617 is also not of great concern, although a certain amount of lead time will be required to produce the quantity needed. The availability of the graphite and refractory brick is also certain.

Systems Costs. The systems costs are presented in figure 6-8. The fluoride salt cost is based on estimates of 1981 fluoride prices delivered to Inyokern, California, in quantities of 725 metric tons (800 tons).⁽⁹⁾ The metal costs were based on $\$99,000/\text{meter}^2$ ($\$2,800/\text{feet}^3$) of base metal cost + $\$4.92/\text{meter}$ ($\$1.50/\text{feet}$) fabricating costs. This relationship was derived from cost estimates given by Huntington Alloys.⁽¹⁰⁾ The helium circulation system costs were estimated by scaling up existing compressor costs to the power rating required.⁽³⁾ The cost estimates for the container vessel and insulation are based on a metal inner liner, refractory middle, and cold-rolled steel outer shell. The estimate accounts for materials and construction costs. It is expected that a graphite inner liner and a concrete outer shell will lower these costs.

Critical Technical Problems. The main critical technical problem that remains is ensuring that the corrosion data now available are applicable to the particular materials used in this design. Also, the long-term resistance of graphite to cracking caused by thermal cycling stresses is an area of concern. If this problem becomes serious, the alternative design would use a metal liner. The details of the manifolds requires additional work.

Safety, Ecological, and Maintenance Considerations. Other areas that require consideration in the TES design have been identified. The chief safety concern is the containment of the molten salt. The safety problems associated with high-temperature TES systems have been reported by the Philips Labs.⁽⁶⁾ As explained in that report, the high chemical stability of the fluorides indicates that it is unlikely that reducing reactions would take place if the fluorides were released accidentally. However, because of its high temperature, a leak in the molten salt would pose a fire hazard to any flammable substance it contacts. This will require the use of nonflammable insulation materials.

For aboveground construction, a catch basin may become necessary to contain any molten-salt release. However, a salt leak is "self-healing"; that is, the leaking salt will solidify and tend to plug the hole. Release of large quantities of salt will require a massive structural failure. Again, because of the chemical stability of fluoride salts, it is unlikely that a release of the salts will pose a hazard to the environment. A number of fluoride salts occur naturally in the environment, for example, NaF (villiaumite), CaF_2 (fluorite), MgF_2 (sellate), Na_3AlF_6 (cryolite), NaMgF_6 (neighborite), and $\text{Ca}_5(\text{PO}_4)_3\text{F}$ (fluorapatite). However, the specifics of a particular location and a particular system design must be considered before a definitive statement on the ecological impact of a phase-change TES system can be made.

In the area of maintenance, continuous monitoring of the system performance will be required. Also, periodic inspection for leaks or possible failures is needed. A means of sampling the salt at various levels will allow determination of any corrosion or sedimentation occurring. The helium stream must be constantly monitored to ensure that leaks into the helium flow will not foul the helium circulation system. A filter used in conjunction with the compressor should allow the helium flow to remain uncontaminated. A drain/fill system for removing/filling the molten salt will allow inspection and/or repair of the system at various times during the lifetime of the plant. It should be noted that the TES system materials are recoverable, except possibly for the tubing metal. This means that the salt eutectic is not expended and can be reprocessed and purified if necessary. The graphite and refractory brick can be repaired and/or replaced. This would allow a given TES installation to be refurbished and placed back in service at a fraction of the cost of building a replacement.

6.2.5 Thermochemical TES System

This section presents the results of detailed analysis of the chemical energy storage (CES) system integrated with the STC powerplant. This work was performed by Rocket Research Corporation as a subcontractor to Boeing. Their results are presented in detail elsewhere.⁽¹¹⁾ A summary of the major technical issues and conceptual design results is presented here.

A large number of chemical reactions were scanned for their use as chemical energy storage reactions. Several of these are summarized in section 6.2.1. Most of these involve solid or entirely gaseous constituents that are difficult to

manipulate and to store. The selection criteria for CES systems are also summarized in section 6.2.1. As yet, no purely liquid CES system with high-temperature capabilities has been identified. The best compromise in terms of energy storage density and high-temperature capability to date is the sulfur dioxide/oxygen system, even though one of the reactants has to be stored as a gas.

The sulfur dioxide/oxygen system is readily reversible and was first proposed by T. A. Chubb.⁽¹²⁾ A complete system study of the sulfur dioxide/oxygen CES system has never been published. As far as is known, the study presented here is the first systematic attempt to evaluate the SO_2/O_2 reaction on a system level and to determine the storage efficiency. Several areas are still under investigation, and additional results will be obtained during separate contracts with EPRI and ERDA.

A summary of the system design characteristics and the corresponding cost estimates are shown in figure 6-9. The following paragraphs describe the operation of the CES system and summarize the critical technical issues.

System Chemistry. The chemical energy storage system is based on the reversibility of the dissociation of sulfur trioxide:



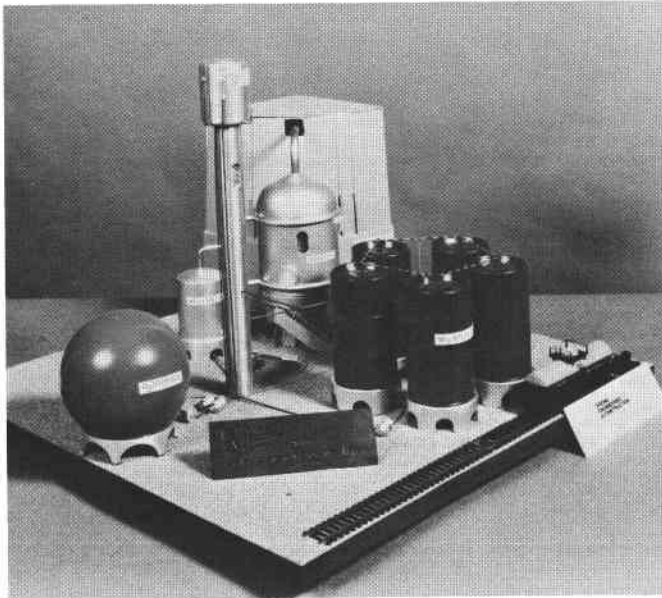
In the reactant generating mode, sulfur trioxide is decomposed to sulfur dioxide and oxygen:



This process is endothermic and consumes energy at the rate of 295.3 cal/g SO_3 (531.5 Btu/lb SO_3). Conversely, the same amount of energy is released when SO_2 and O_2 recombine in the heat generation mode to form SO_3 :



The theoretical evaluation of the thermodynamic conversion efficiency is the basis of the system chemistry. In addition, kinetic calculations determine if the reaction will proceed to completion within reasonable time. Both thermodynamic and kinetic results determine the conversion efficiency achieved in a



- REACTION

$$\text{SO}_3 + \text{H}_r \rightleftharpoons \text{SO}_2 + \frac{1}{2}\text{O}_2$$
- HELIUM TEMPERATURE SWING 221°C (400°F)
- KEY PROCESS DATA
 - ENDOTHERMIC REACTION
 - $P = 0.102 \text{ MN/m}^2$ (14.7 PSI)
 - $\eta_{\text{CON}} = 64\%$
 - $H_r = 295 \text{ CAL/GM}$ (531 BTU/LB)
 - EXOTHERMIC REACTION
 - $P = 0.102 \text{ MN/m}^2$ (14.7 PSI)
 - $\eta_{\text{CON}} = 90\%$
 - $H_r = 295 \text{ CAL/GM}$ (531 BTU/LB)
- CRITICAL TECHNICAL PROBLEMS
 - DISSOCIATION REACTOR DESIGN
 - MATERIAL COMPATIBILITY

<u>Account</u>	<u>Quantity</u>	<u>Unit cost</u>	<u>Total cost (M \$)</u>
Sulfur trioxide	$2.3 \times 10^6 \text{ kgm}$	0.44 \$/kgm	1.0
Storage containers			
Oxygen	10 (5.32 m ³)	29,000 \$/tank	0.3
SO ₂ /SO ₃ (1 MN/m ²)	6 (227 m ³)	32,000 \$/tank	0.2
Reactor			
Heat exchanger			
(1.37 cm OD) tubes (15.2 m)	11,000 tubes	125.00 \$/tube	1.4
welds (3/tube)	33,000 welds	12.00 \$/weld	0.4
Vessels (1 MN/m ²)	$35.2 \times 10^4 \text{ kgm}$	23.59 \$/kgm	8.3
(15.2 m x 15.2 m)			
Insulation	147 m ³	1836 \$/m ³	0.3
Catalyst	$0.9 \times 10^5 \text{ kgm}$	2.20 \$/kgm	0.2
Miscellaneous plant equipment			
O ₂ compressor	1 (10 MW)	2.5×10^6 \$/unit	2.5
SO ₂ /SO ₃ /O ₂ compressor	2 (15 MW)	3.7×10^6 \$/unit	7.4
Other			0.4
Helium circulation system	10 MW	115,000 \$/MW	1.2
Total system			23.6
Estimated system weight: $3.6 \times 10^6 \text{ kgm}$ ($7.92 \times 10^6 \text{ lb}$)			

Figure 6-9. Thermochemical Energy Storage System

given piece of hardware, which in turn determines the round-trip storage efficiency of the overall system.

An existing thermochemical equilibrium computer program, CEC 72, developed by the NASA Lewis Research Center in Cleveland, Ohio, was used to calculate dissociation as well as synthesis equilibria under a wide range of conditions. Dissociation data were calculated for temperatures and pressures in intervals of 111°C between 427° and $1,093^{\circ}\text{C}$ (800° and $2,000^{\circ}\text{F}$) and in intervals of 0.02 MN/m^2 between 0.1 and 0.2 MN/m^2 (14.7 to 29.4 psia).

The data show that doubling the dissociation reactor pressure will reduce the dissociation efficiency at 760°C ($1,400^{\circ}\text{F}$) by 14%. The pressure in the dissociation reactor should therefore be kept as low as possible, particularly at the high exit temperature.

Basically, the same thermodynamics that govern the sulfur trioxide dissociation will also determine the yield of sulfur trioxide and the sulfur dioxide conversion fraction. In addition to the composition calculations that were performed for SO_3 dissociation, a series of more complicated calculations were performed for the synthesis reaction. These include the effect of pressure and the effect of elevated feed-gas temperature.

An increase of pressure will shift the sulfur oxide equilibrium in the direction of smaller molar volume (i.e., in the direction of sulfur trioxide). At the same time, the adiabatic flame temperature will also increase. The desired helium temperature of 816°C ($1,500^{\circ}\text{F}$) can theoretically be achieved with a reactor pressure of 1.27 MN/m^2 (184 psia). In practice, however, a reactant temperature above 816°C ($1,500^{\circ}\text{F}$) will be required to overcome the thermal resistance at the exit of the reactor/helium heat exchanger. A temperature differential of 55°C (100°F) would be desirable to achieve high rates of heat transfer. This higher temperature can be achieved by either increasing the reactor pressure beyond 1.27 MN/m^2 or increasing the feed-gas temperature. The data developed to date indicate that a leveling at higher pressures and the benefit to be derived by that means may be marginal.

After an initial steep increase of conversion with pressure, the data levels off at 2.07 MN/m^2 (300 psia). Little improvement in conversion can be achieved by increasing the pressure further. For the conceptual design, a reactor pressure of 1.01 MN/m^2 (147 psia) has been chosen. The other method of increasing the

reactant temperature by preheating the feed gas is discussed in the following paragraphs.

In the CES system, the feed gas will enter the reactor at higher than ambient temperature because it will have exchanged heat with the hot reaction products leaving the reactor. The temperature to which the reactor feed gas is preheated will depend on the reactor pressure and the feed-gas inlet temperature at the heat exchanger inlet. For the calculations performed here, a wide range of inlet temperatures has been assumed that will most likely include actual operating data.

The data developed on the CEC 72 program show that the objective of a flame temperature of 871°C ($1,600^{\circ}\text{F}$) cannot quite be achieved at ambient pressure and a feed-gas temperature below 500°C ($1,932^{\circ}\text{F}$). For the currently selected reactor pressure of 1.01 MN/m^2 (147 psia), this temperature goal can be achieved by preheating the feed gases to at least 337°C (639°F). The products will leave the reactor at a temperature slightly above the helium inlet temperature of 495°C (922°F). The reactants can most certainly be preheated to above 337°C (639°F) with this available heat. Based on these calculations, it is possible to achieve a reactor temperature of 871°C ($1,600^{\circ}\text{F}$) and a helium temperature of 816°C ($1,500^{\circ}\text{F}$). The higher feed-gas temperature will result in lower conversion, at least in the inlet portion of the reactor. However, the overall conversion that can be achieved in the reactor is determined more by the helium inlet temperature than by the reactant feed-gas temperature.

The kinetics of the sulfur trioxide dissociation and formation reactions are an important selection criterion in the design of a CES system. As outlined in the introduction, it is important to select a reaction that can be turned on and off by contact with a catalyst. If this were not possible and the equilibrium could not be stabilized at the high-temperature condition, the dissociation reaction would revert itself while the dissociation products are cooling off.

Kinetic rates are required for both the catalyzed and the uncatalyzed reaction. A preliminary literature search has provided some literature references on SO_2/SO_3 kinetics, but additional work is required, especially on the dissociation of sulfur trioxide, which is not a useful industrial process. Consequently, little work has been done on sulfur trioxide dissociation.

The kinetics of sulfur dioxide oxidation have been extensively studied because this reaction constitutes an important industrial process in the production of sulfuric acid. Even though sulfur monoxide and atomic oxygen do not show up as reaction products in the equilibrium calculations, they may play an important role in the kinetics and may be involved in rate-determining steps of the reaction.

The results of these initial investigations confirm the results of T. A. Chubb.⁽²⁾

- The purely gas-phase decomposition time is longer than the residence time of the gas in a practical size reaction chamber.
- Hence, surface reactions must be employed to achieve chemical equilibrium.
- Purely gas-phase recombination rates are too slow to cause significant heat evolution in the heat exchange.

These are precisely the results needed for practical application of a reversible thermochemical reaction in a controlled closed-loop CES system.

Storage System Description. The basic requirements for the storage system operation and interface with the STC power plant are presented in section 6.2.2. The single characteristic unique to the CES system is that through proper design of the chemical process system, helium outlet temperature can be controlled in both the charge and discharge mode of operation.

Operation for 6 hours at the design discharge rate of $113 \text{ MW}_{\text{th}}$ requires approximately 2×10^6 kilograms (4.4×10^6 pounds) of reactants to be stored. These reactants consist of 80% by weight SO_2 and 20% by weight O_2 . After being converted to the vapor phase and mixed, the reactor feed gas consists of 66.7% by volume SO_2 and 33.3% by volume O_2 .

The total reactant storage plus the holdup allowance consist of 1.7×10^6 kilograms (3.7×10^6 pounds) sulfur dioxide and 0.43×10^6 kilograms (0.9×10^6 pounds) oxygen. This adds up to 2.13×10^6 kilograms (4.6×10^6 pounds). The liquid density of sulfur dioxide is 1.34 grams/centimeter³ at 38°C (11.16 pounds/gallon at 100°F). The storage volume is 1,250 meters³ (3.31×10^5 gallons).

Sulfur dioxide is commonly shipped in 35,000-gallon tank cars, and stationary storage tanks can hold up to 151 meters³ (40,000 gallons) of sulfur dioxide. Mild steel can be used in the construction of sulfur dioxide storage tanks as long as the liquid is kept dry. Dry sulfur dioxide will not corrode steel, but

traces of moisture, in particular in the presence of sulfur trioxide, will make the liquid more corrosive. At an ambient temperature of 25°C (77°F), the vapor pressure in a liquid sulfur dioxide tank is 0.38 MN/m² (55 psia). Liquid storage of both sulfur dioxide and sulfur trioxide is preferred over gaseous storage because the storage volume is smaller and no heat is required to prevent condensation.

Sulfur dioxide storage poses no problem and is existing technology. However, compressed oxygen storage of the dimensions proposed here has never been attempted. Oxygen storage has to comply with strict safety authority requirements with regard to system cleanliness and quantity-distance relationships. The formation of hot spots during high flow rates through curved tubing or discharge orifices must be avoided because it may lead to ignition of the metal.

If compressed oxygen is stored in heavy-walled compressed gas cylinders, a large number of these will have to be manifolded together to form a storage bank. This technique is currently used for storage of small amounts of oxygen for industrial purposes. During the past decades, many oxygen storage installations have been converted from compressed gas to cryogenic liquid-oxygen storage. A tradeoff study will be conducted in the follow-on work to determine if more economical oxygen storage methods are available or if the system can be operated with an open oxygen system or air loop as opposed to the closed-loop oxygen system now envisioned.

The sizing of the reactor in the exothermic mode depends on the thermal-to-electric conversion efficiency. With the 816°C (1,500°F) turbine inlet temperature, the conversion efficiency is 0.442. Thus, to provide 500 MW_e, the reactor has to deliver 113 MW_{th}. The mass flow requirements would be 91 kilograms/second (201 pounds/second). However, the conversion of SO₂ and O₂ to SO₃ is not 100% efficient. As discussed in the preceding paragraph, a maximum theoretical conversion efficiency of 96.2% by weight would be achieved at 495°C (922°F) and 1.01 MW/m² (147 psia). Higher conversion efficiencies could be achieved at higher reactor operating pressures. However, the conversion efficiency is also limited by kinetic rates and mass transfer to and from the catalyst surface, and 96.2% by weight efficiency could only be achieved with a long reactor. A long reactor would have a high pressure drop and heat loss. The tradeoff dictates a shorter reactor and a less-than-theoretical conversion efficiency. A conversion efficiency of 90% by weight for a single pass through the reactor has been assumed for the following calculations. This increases the mass flow

rate to 101.7 kilograms/second (223 pounds/second). This consists of 81.4 kilograms/second SO_2 and 20.3 kilograms/second O_2 .

For the reactant generation cycle, the key specification is the charge-to-discharge power ratio. In the final analysis the charge-to-discharge ratio is set by the integrated operation of the STC powerplant and storage system, the results of which are presented in section 8.2.

For the purpose of the initial conceptual design charge-to-discharge ratios (C_r) of 1.4 and 0.9 were investigated. The design results presented in figure 6-9 and discussed in this section are based on the lower C_r ratio of 0.9.

The results at the higher C_r ratios of 1.4 indicate that the reactor sizes for the charge and discharge modes would be very dissimilar, implying a requirement for two reactors. Since reactor cost is almost 50% of the total system cost, this leads to the conclusion that practical limits in charge-to-discharge ratios will be encountered in system design and that the limit is approximately $C_r = 1.0$. The results given in section 8.2 are well within this practical limit.

For the $C_r = 0.9$ design condition, the system would have a charging load of 102 MW_{th} . With this much thermal energy available, 83 kilograms/second (182 pounds/second) of SO_3 can be dissociated. However, dissociation efficiency at ambient pressure and 816°C ($1,500^\circ\text{F}$) is poor, 29% by weight remaining undecomposed as shown in the preceding system chemistry discussion. The SO_3 will therefore have to be separated from the dissociation products and recycled repeatedly to achieve complete dissociation of all SO_3 in storage. The nominal theoretical minimum mass flow through the reactor is therefore higher by a factor (100:71) than the 83 kilograms/second (182 pound/second) that can be dissociated, increasing the mass flow to 116 kilograms/second (256 pounds/second). The theoretical maximum dissociation probably cannot be achieved in a real reactor of finite length. An actual SO_3 decomposition of only 90% of the theoretical 71% (or 0.64) has therefore been assumed in sizing the system. This increases the flow rate by a ratio of 100:64 over the mass flow of SO_3 that can be dissociated, resulting in an SO_3 feed rate of 129 kilograms/second (284 pounds/second) to the reactor.

Oxygen is commonly stored at 15.2 MN/m^2 (2,200 psi) pressure. At this pressure, storage density is 0.206 gram/centimeter (12.9 pounds/cubic foot) at 27°C (81°F).

The net usable storage volume of compressed oxygen would be 2.06×10^3 meters³ (7.25×10^4 feet³). The above calculation assumed that the oxygen storage cylinders would be emptied to below atmospheric pressure. However, the lowest useful pressure in the storage tanks is slightly over the reactor pressure. This leaves 6.7% of the oxygen in the storage tank unused, which is well within the holdup allowance of 10% initially assumed.

For the reactant generation mode, SO₃ storage requirements are comparatively easy. A maximum of 2.13×10^6 kilograms (4.6×10^6 pounds) SO₃ will have to be stored when the system is in the completely depleted condition. This will most likely be the startup condition after the system has been filled with chemicals for the first time. The same filling level will never again be achieved during later operation because of SO₂ and O₂ holdup in the system. As a matter of fact, one could size the SO₃ storage requirements at 90% of the above number and assume that SO₃ will be replenished after the first run to compensate for holdup in the system.

The liquid density of SO₃ at 100°F is 1.843 grams/centimeter³ (115 pounds/cubic foot). The storage volume is 1,150 meters³ (3.02×10^5 gallons = 4.04×10^4 feet³). In a joint SO₂/SO₃ storage system, the total volume required would be dictated by the more bulky sulfur dioxide, 1,250 meters³ (331,000 gallons).

A significant simplification and weight saving of the overall system is possible by using joint storage tanks for sulfur trioxide and sulfur dioxide. In the fully charged or discharged condition, only one or the other has to be stored. SO₂ and SO₃ are completely miscible over the entire range of compositions. Inevitably, some contamination will occur if liquid SO₃ is filled into a tank that has previously contained SO₂ and vice versa. However, the ingredients in the CES system are not expected to remain in the chemically pure state, and the fractionation column will not be designed to achieve 100% separation. A small amount of SO₂ in SO₃ may actually be beneficial in lowering its melting point, widening the liquid range, and preventing accidental freezing. The sulfur trioxide tanks have to be kept above 38°C (100°F) all the time to prevent solidification of the tank contents.

Based on information obtained from Stauffer Chemicals, all materials selected for storage system components proved to be compatible with sulfur trioxide (the more

aggressive of the two oxides) and can also be used for sulfur dioxide service. The tanks have to be designed for the higher vapor pressure of sulfur dioxide.

System Schematic. The system operating schematics for both operational modes are presented on figures 6-10 and 6-11. The lines that are operational in a particular mode of operation are drawn in bold lines. Partial flow is designated by dashed lines, and the light lines show inoperational paths in the particular mode of operation.

As shown in figures 6-10 and 6-11, the central receiver and the CES reactor are arranged in series. An alternative arrangement would be to operate them in parallel with a split helium flow for partial flow conditions. At present, calculations have only been conducted for full-load conditions with the helium heated and the turbine driven by either this receiver or the CES reactor. The CES reactor and the downstream components would work less efficiently if the reactor were fed with preheated helium from the receiver with helium inlet temperatures above 495°C (922°F).

Major Chemical Process Systems. The CES system requires two major chemical process systems that must be designed and developed for this specific application. The conceptual design and technical considerations for these two systems, the reactor and the fractionation column, are presented in the following paragraphs.

As discussed in the preceding paragraphs, the charge-to-discharge power ratio is nearly unity, allowing the use of a single reactor for both the endothermic and exothermic reactions. The dimensions of the reactor will be determined by the rate of sulfur trioxide dissociation that can be achieved in the endothermic mode. Although sulphur trioxide synthesis is common, there are no dissociation reactors after which the endothermic reactor could be patterned. The dimensions of the endothermic reactor will depend on the operating pressure selected, the desired degree of conversion, and the catalyst size. In particular, the diameter of the reactor is determined by the pressure drop and the space required for the helium tubing, whereas the length is determined by the bed loading, the kinetic rates, and the rate of heat transfer.

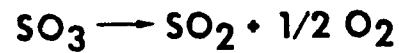
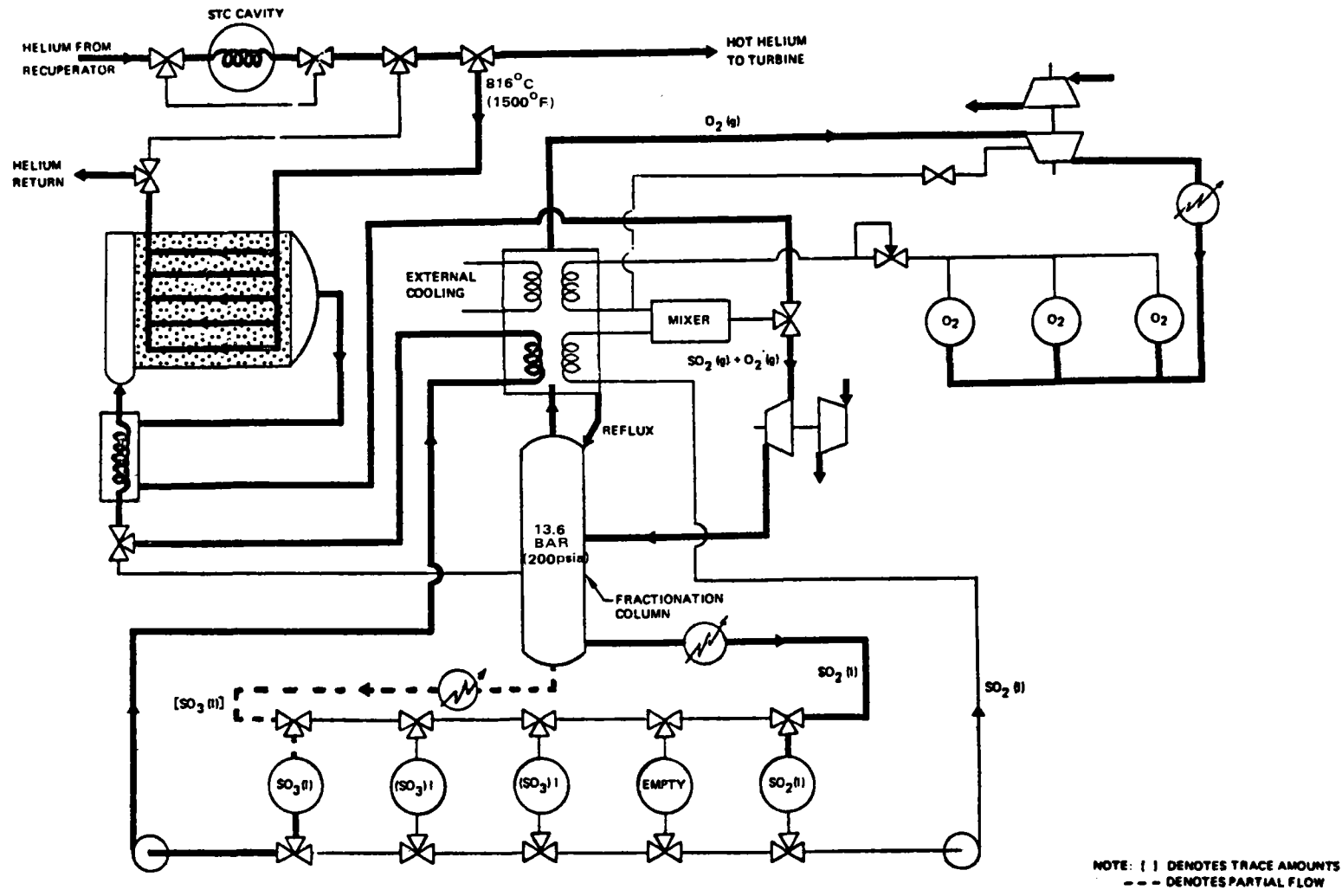


Figure 6-10. Chemical Energy Storage System—Reactant Generation Cycle

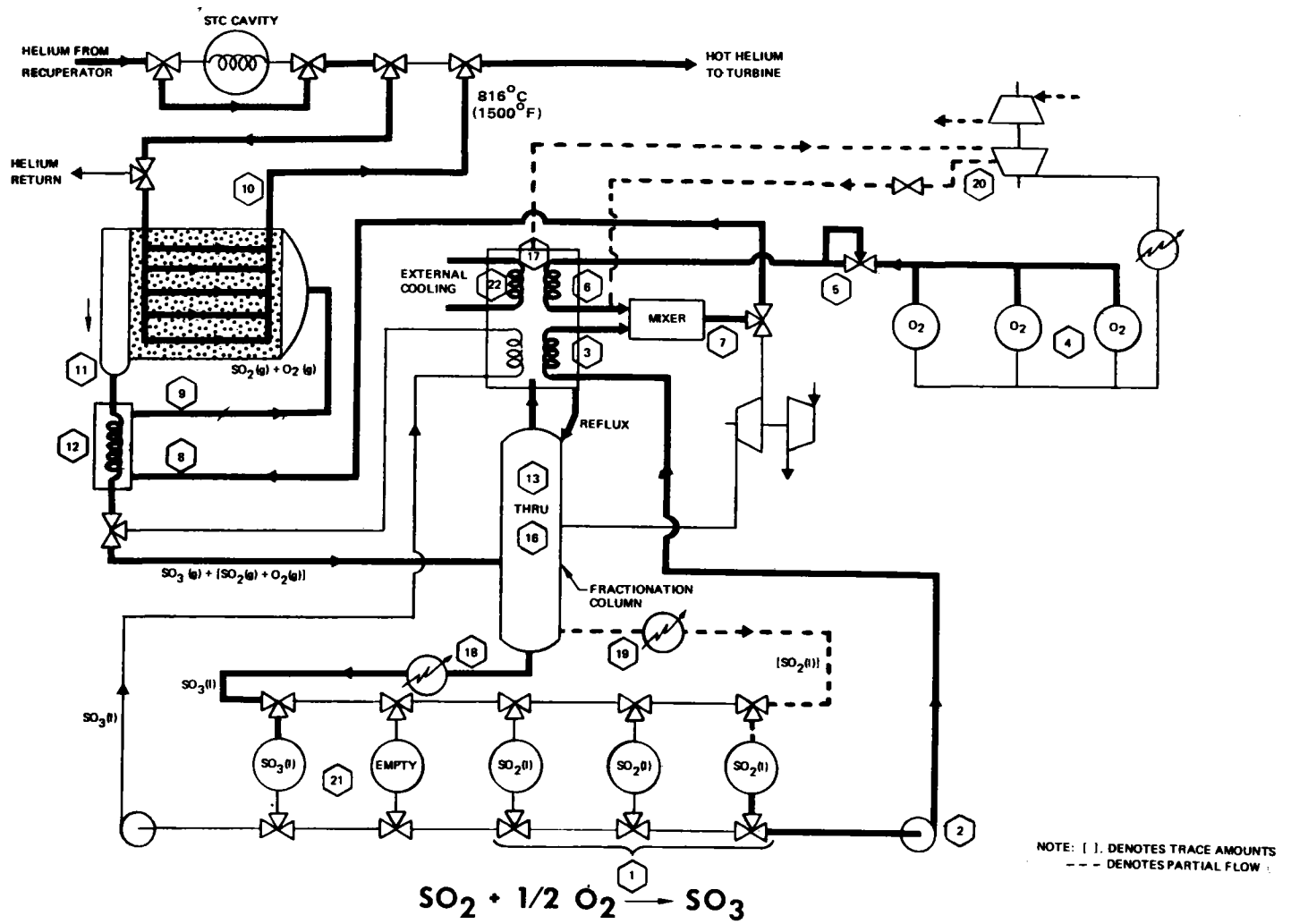


Figure 6-11.. Chemical Energy Storage System – Heat Generation Cycle

The number of helium tubes and the diameter of helium tubes is determined by the pressure drop on the helium side (4.0% of operational pressure) and by the surface area required to achieve effective heat transfer. The heat transfer in turn is determined by the temperature differential across the wall of the tubes; helium and reactant flow conditions; and, to a lesser extent, the wall thickness of the tubes.

A cutaway sketch of the reactor is shown in figure 6-12. The illustration shows a pelletized catalyst bed. The risk of using existing or improved catalysts is considered a critical technical problem and is discussed in that context in a later paragraph. With 3/8-inch catalyst pellets and an L/D of 1.0, a pressure drop below 0.069 MN/m^2 (10 psi) could be achieved with a reactor size 15 meters (50 feet) in diameter.

The conceptual reactor construction includes a ceramic-lined superalloy shell covered by external insulation. The heat losses from the reactor are minimized by applying the high-temperature insulation both inside and outside the reactor shell. The inside coating could be flame-sprayed alumina or zirconia (Rockide-A or -Z). The coating has a low thermal conductivity and will also protect the

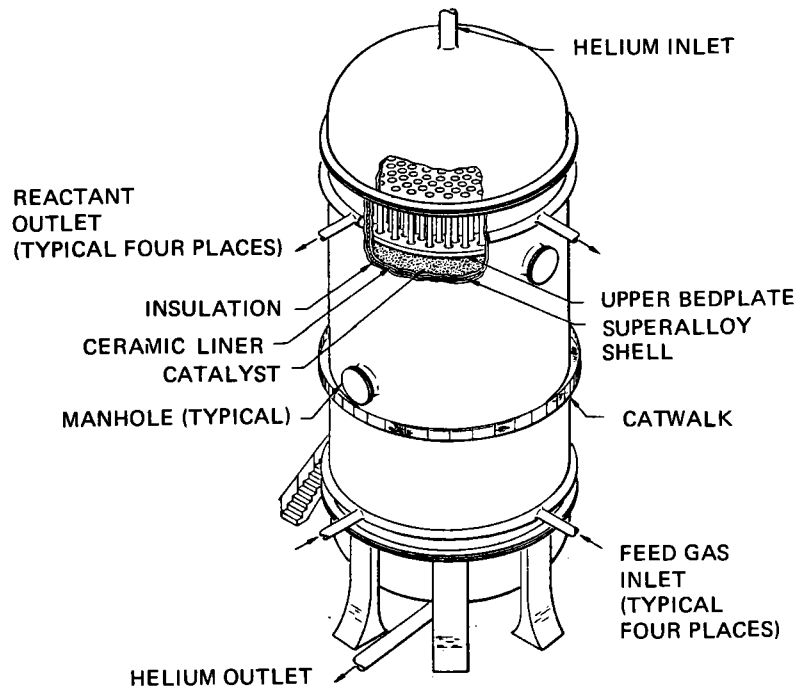
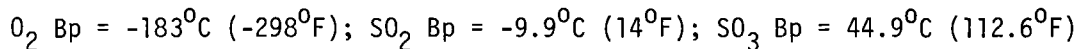


Figure 6-12. Cutaway View of Catalytic Reactor

metal from corrosion. Even though the coefficient of thermal expansion of the coating is similar to that of the base metal, the wide temperature fluctuations and the rapid temperature rise upon startup cause a design problem. The coating may have to be subdivided in numerous panels with expansion joints. On the outside of the reactor, an asbestos insulation can be applied to minimize heat loss. John Mansville, Inc., offers various types of industrial insulation materials for this purpose. The amount of insulation will determine the cooling rate when the reactor is turned off. Restart will be significantly simpler if the reactor remains hot during idle periods.

The fractionation column separates the dissociation or reaction products so that the undissociated or unreacted species can be returned to the reactor. The fractionation column operates both in the reactant generation and in the heat-generation cycle. Fractionation columns are commonly employed in chemical industry to separate liquid mixtures with different boiling points. The fractionating efficiency depends on the difference of boiling points of the compounds to be separated. Fortunately, in the case of the CES system, the boiling points (Bp) are spread far enough apart to allow complete separation of the constituents:



The amount of sulfur oxide contamination in the oxygen leaving the top of the column depends on the temperature of the coldest cooling coil available and the operating pressure of the system. It is desirable to keep the sulfur contamination in the oxygen as low as possible in order to eliminate corrosion in the oxygen compressor and high-pressure storage.

The sulfur dioxide will be withdrawn in the upper half of the column, whereas sulfur trioxide accumulates in the "bottoms." Only part of the condensed SO_2 is withdrawn, and a large portion of the condensate is returned to the column as reflux. The reflux ratio can be varied depending on the degree of separation of SO_2/SO_3 required.

Many different designs of fractionating columns are in use. The objective of all designs is to achieve intimate interaction of the rising vapors and the counter-current condensing liquid. This is achieved by filling the column with large-surface-area geometrical shapes (Raschig rings, Berl saddles) of glass, ceramic, or steel or by bubbling the vapor through a stack of trays. A typical example of a fractionation column is shown in figure 6-13.

The product to be separated is generally fed to a position approximately halfway up the column. Within a fractionation column there exists a temperature gradient from the hot bottom to the colder top. The column does not have to be perfectly insulated and some heat loss can be tolerated or may even be desirable.

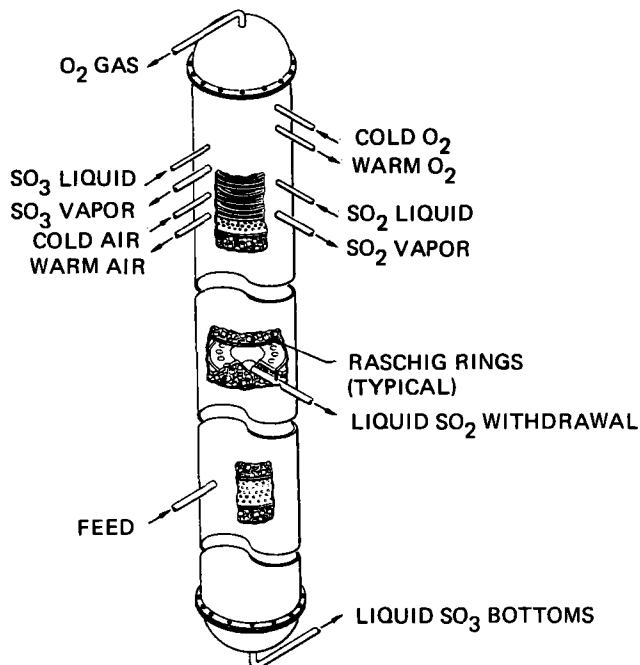


Figure 6-13. Cutaway Sketch of Fractionation Column

The top of the column has a condenser with a cooling coil. The cooling fluid has to be cold enough to allow condensation of the components to be separated (except oxygen, which passes through as a gas).

The fractionation column has been sized using first-order approximations for both the endothermic and exothermic mode of operation. The following assumptions were made in calculating the column dimensions:

- Ideal gas behavior for all vapors
- Ideal solutions
- Oxygen is insoluble in liquids.
- Feed enters column at bubble point of lowest boiling constituent.
- Tower packing factor = 17
- Allowable pressure drop
- 2% by weight sulfur dioxide allowed in sulfur trioxide bottoms and vice versa

Under these conditions and in order to limit the vapor velocity to 0.65 meter/second (2.14 feet/second), the column has to have a diameter of 3.4 meters (11.2 feet) and a packing height of 13.3 meters (43.8 feet). The packing includes several spacers and flow equalizers that have to be inserted between each 3-meter (10-foot) unit (approximately) of column packing. This increases the column height by approximately 1.7 meters (6.2 feet). The condenser section on top of this will be at least 4.5 meters (15 feet) in diameter and 6 meters (20 feet) tall. The total height of the condenser is approximately 21 meters (70 feet).

Materials and Components Selection. The high-temperature environment in the reactor and the corrosive action of sulfur oxides makes material selection for the CES system a difficult task. From a standpoint of creep rupture resistance and desired 30-year service life, Haynes 188 and Inconel 617 have been identified as candidate materials for the STC receiver and other parts of the system. Inquiries have been sent to Cabot Corp/Stellite Division and to Huntington Alloys inquiring on the high-temperature compatibility of these metals with $O_2/SO_2/SO_3$. However, no compatibility data could be obtained for this system at $816^{\circ}C$ ($1,500^{\circ}F$). Most data in the literature are for flue gases, which contain only small amounts of SO_2 or SO_3 . Materials compatibility evaluation in flowing $O_2/SO_2/SO_3$ at $816^{\circ}C$ ($1,500^{\circ}F$) will be required. Weight change, tensile strength, microhardness, and metallurgical investigation of cross sections under the microscope will be required to document the compatibility data.

For the storage tanks, pumps, vaporizers, and fractionation column, there are sufficient data from the chemical processing industry to allow the selection of materials with long-life capability. Close coordination with SO_2 - and SO_3 - producing companies will be required in this phase of the program.

Sulfur dioxide and sulfur trioxide are common chemicals and are readily available, inexpensive, and easily transported. The only other material question unique to the CES system is in the area of catalysts, which is discussed separately as a critical technical problem.

Pumps, valves, regulators, pressure gauges, thermocouples, mass flowmeters, and fill-level indicators for SO_2/SO_3 service are standard items and can be selected from the stock of various equipment manufacturers. As the program progresses to the hardware stage, a more detailed list of suppliers, specifications, and prices will be compiled.

System Costs. A preliminary system cost statement is presented in figure 6-9. As much cost data as possible were assembled on the various components (i.e., valves, filters, pumps, compressors, air coolers, heat exchangers, distillation columns, and storage vessels) that constitute much of the system. The results are summarized on figure 6-9.

The reactor costs are based on the design detail listed in figure 6-9 and discussed in the preceding paragraphs. These cost data include materials and allowances for construction. All cost data are based on 1975 dollars.

Safety Considerations. Sulfur dioxide and in particular sulfur trioxide are hazardous chemicals. However, these chemicals are routinely handled in large quantities in the industry and sufficient experience has been accumulated to allow safe handling. In the CES system, the chemicals would be hermetically sealed most of the time and the chemicals have to be handled only during initial loading of the system and eventual repair work.

Direct contact with either SO_2 or SO_3 represents extreme personnel hazards. Safety and treatment procedures will have to be adopted and readily available throughout the plant.

In order to minimize the problems that can develop when liquid sulfur trioxide is spilled, every plant using or storing liquid sulfur trioxide should develop a predetermined plan to contain possible minor and major spills. Should a small leak or spill occur, the best procedure is to absorb the liquid with dry sand or dirt, expanded clay, diatomaceous earth, or another nonreactive absorbent material until repairs can be made. It can then be removed from the area and neutralized with water or a solution of soda ash, lime, or any caustic material. A large or uncontrolled spill of liquid sulfur trioxide will produce dense clouds of "smoke." The "smoke" obscures the source of the liquid sulfur trioxide and makes it extremely difficult to determine the cause of the spill. "Smoke" from such a spill should be controlled with water or a mechanical foam system. Use of water fog or mechanical foam to control the "smoke" generates sulfuric acid mist that is formed by the reaction of the water with the sulfur trioxide. Liquid sulfur trioxide confined within an open reservoir or sump can be sealed over with an inert immiscible fluorocarbon oil mixed with glass bubbles. The seal prevents reaction of the moisture vapor in the air with the sulfur trioxide and the

resultant production of "smoke." All plants should be equipped with either an in-place slurry seal system, or with a manifold installed to dispense slurry seal over the spilled liquid sulfur trioxide surface within the hot room.

Environmental Effects. The operation of a CES system in a normal operating mode is not expected to result in any significant environmental effects. Any SO_2 or SO_3 that escapes through small leaks is readily absorbed by rain and soil. A minimum sulfur (sulfate) content of soil has to be maintained if optimum crop yields are expected from agricultural land. Neither SO_2 nor SO_3 are persistent contaminants such as polychlorinated biphenyl heat transfer fluids or other halocarbons. SO_2 and SO_3 are naturally occurring in volcano vents and fumaroles, and the SO_2/SO_3 content of the Earth's atmosphere was most likely much higher during geological periods of high volcanic activity.

Maintenance. The design attempts to minimize the number of pieces of equipment with moving parts, such as pumps, compressors, or valves. Potential problem areas that require frequent maintenance, if not properly designed, are the feed-throughs where pump shafts or valve stems are exposed to sulfur oxides on one end and to humid air on the other end. Fortunately, the STC powerplant will be located in a dry climate and the low relative humidity should make maintenance easier. Automated leak detectors would locate a leaking gasket before significant corrosion damage can occur.

Chemical processing industry maintenance experience with similar sulfuric acid plants indicates that the annual maintenance materials cost is approximately 2% of capital investment and maintenance labor equals the operating labor.

A critical maintenance cost item is the catalyst. Typical catalyst life in sulfuric acid plants is 10 years. If the CES system would operate at the same temperature as the air oxidation temperature of SO_3 , the expected catalyst life would be in excess of 10 years because the chances of poisoning the catalyst are significantly lower in a closed system than they are in an open system where the feed gas contains phosphorous, selenium, and arsenic as contaminants. On the other hand, the higher operating temperature may more than offset the benefit of the pure feed gas in a closed-cycle system. No life data are available for catalyst operating with stoichiometric sulfur-dioxide/oxygen feed gas. The reactor will be designed such that the spent catalyst can be poured out with a minimum

of effort, and reproducible packing density can be obtained after replacing the catalyst. The downtime during catalyst replacement can be kept to a minimum if a sintering of the catalyst can be prevented.

System Startup Operations. A short response time is essential to the mission of the CES system within the STC powerplant. Temperatures in both the receiver and the helium flow to the turbine drop rapidly after sun loss. The system has to respond rapidly to the demand for hot helium to keep the turbine operating.

Reactor sizing is based on pressure drop, mass flow, and approximate space velocity considerations only. Response consideration may pose additional constraints on the size of the reactor.

Initial startup after the CES system has been assembled can be achieved either in the endothermic or in the exothermic mode. Because it is easier to transport liquid SO_3 than to transport liquid SO_2 and compressed O_2 , it is suggested to start the plant from an SO_3 -filled condition in the endothermic mode. Prior to loading the chemicals, the entire system should be thoroughly cleaned from all welding spatter, metal chips, turnings, etc., and must be thoroughly dried by heating under vacuum or in a purge of dry air. The system is then backfilled with gaseous oxygen and the tanks are loaded with liquid SO_3 .

If the CES system is called upon immediately after operating in the endothermic mode, the reactor is hot enough to continue in the exothermic mode and a minimum of delay. The initial flow rate in the exothermic mode would be identical with the nominal flow rate, because the reactor does not have to be heated up.

Depending on the insulation and the rate of heat loss of the reactor after termination of the endothermic mode, the reactor will remain in a restartable condition and can be started without external heat provided until the temperature drops below 400°C (752°F). If the temperature drops below this threshold, the reaction rate $\text{SO}_2 + \frac{1}{2}\text{O}_2 \longrightarrow \text{SO}_3$ is too slow to start the reactor and become self-sustaining. Some catalysts can be started at temperatures below 400°C (752°F), thus widening the cooldown temperature range.

In calculating the startup time when starting the reactor from ambient temperature, the following assumptions were made: (1) the heat loss to the outside is negligible because the initial temperature is low and the reactor is well

insulated; (2) the convective thermal resistance between the catalyst and the gas is very low; (3) the catalyst mass and heat capacity are large in comparison to the mass and heat capacity of the heat exchanger tubes; and (4) no helium is flowing during startup.

The calculation was performed for two different flow rates: the nominal exothermic flow rate of 110 kilograms/second (242 pounds/second) and a startup flow rate of 227 kilograms/second (500 pounds/second) which is higher than the endothermic flow rate that the reactor is capable of handling for a C_p of 0.9. The transient analysis produces the results illustrated in figure 6-14 for two different flow rates. At the nominal flow rate, it takes 4.7 minutes to reach 90% of the steady-state temperature and 10.4 minutes to reach 99% of the steady-state temperature. If the flow rate is doubled during the startup, these times decrease to 2.3 and 5.0 minutes, respectively. In reality, the response times from the beginning of the reactant flow will be shorter because the reactor will have to

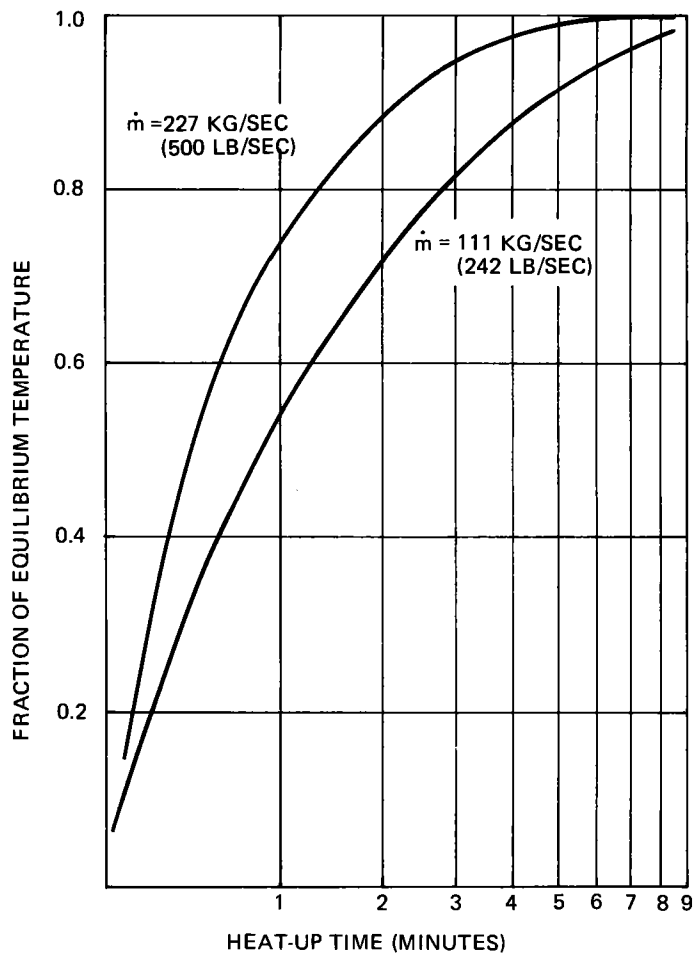


Figure 6-14. Exothermic Reactor Startup Transient

be pre-heated by an external source to a threshold temperature of 482°C (900°F) beyond which the $\text{SO}_2 + \text{O}_2$ reaction becomes self-sustaining. Preliminary calculations for the baseline reactor indicate that the cooldown rates with no helium flow are small and that several successive days of cooldown would be required to bring the reactor temperature down below 482°C (900°F).

Critical Technical Problems. Several areas of the CES design concept are beyond established technology, and additional development work and small-scale testing will be required before the full-sized plant can be designed with confidence. A large amount of experience of $\text{SO}_2 \longrightarrow \text{SO}_3$ conversion exists with sulfuric acid and sulfur trioxide producers. However, all these reactors operate at lower temperatures and ambient pressure. The CES reactor constitutes a significant step beyond current state of the art.

A major unknown is the lifetime of existing vanadium or platinum catalysts under CES reactor conditions. Most catalysts lose activity when heated to temperatures above their nominal operating conditions. This loss of activity is caused by all or several of the following reasons:

- Loss of active surface area by sintering
- Loss of active material by evaporation
- Poisoning of active sites by contaminants

In addition to supported catalysts envisioned for the CES reactor skeleton, catalysts of the Raney-vanadium type should be evaluated. These catalysts could possibly be flame-sprayed directly onto or into the reactor heat exchanger tubes and would result in maximum possible heat transfer rates. A similar catalyst is currently being tested by the ERDA Pittsburgh Energy Research Center in methanation reactors.

According to Matthey-Bishop, Inc., at one time platinum gauze, similar to that used for nitric acid production by combustion of ammonia, has also been used for the oxidation of SO_2 with air. However, this technology has been totally superseded by the vanadium pentoxide catalysts, and data sheets on platinum gauze for SO_2/SO_3 conversion are no longer available. The contact time in a pack of platinum gauze is short, of the order of 10^{-4} to 10^{-3} seconds, and the space velocity is high, GHSV = 10^6 /hr. A thin layer of platinum gauze wrapped around the helium heat exchanger tubes would be another possible catalyst configuration. However, the cost of platinum catalyst (except as a starter bed in the reactor inlet) may be prohibitive.

Expert observations have been made that during sulfur dioxide oxidation, vanadium-pentoxide/alkali-pyrosulfate catalysts consist of a highly viscous melt that covers the carrier with a film. This is of significance in the development of alternative catalysts with high-temperature capability. It appears that a high surface area support (e.g., gamma alumina) is not a prerequisite for sulfur trioxide catalysts. As soon as the active material melts, the catalyst pores would become plugged. It was also shown that a liquid melt consisting of a solution of vanadium pentoxide in fused alkali pyrosulfate constituted an active catalyst system for the oxidation of sulfur dioxide to sulfur trioxide. Recent work reported by Westinghouse relative to their sulfur-cycle thermochemical decomposition of water indicates that they have found a practical catalyst for operating conditions not unlike those considered here.

The area of maximum heat flux in the reactor constitutes a high-risk area. Little is known about compatibility of Haynes 188 or Inconel 617 with sulfur oxides at such high temperatures. Sulfur compounds are inherently corrosive and traces of sulfur (mostly sulfide) are sometimes sufficient to drastically alter mechanical properties of structural alloys, frequently resulting in material failures. Another potential problem area is associated with the bearings and vanes in compressors being exposed to sulfur oxides. As a general rule in engineering practice, the sulfur content in fuels for gas turbines and similar equipment is kept as low as possible. Special alloys may have to be developed to satisfy service requirements in such a corrosive environment. The reactor shell can be protected by a ceramic liner. This liner would reduce heat loss and protect the shell from corrosion, even though it will be difficult to design a seamless liner. The area of ceramic liners requires additional evaluation.

6.3 STORAGE AND POWERPLANT INTEGRATION

Thermal energy storage system and powerplant integration studies were undertaken in order to determine the impact of storage on receiver design and plant performance. The studies also lead to a consistent set of storage-system design and performance requirements for use in establishing the relative merit of the various TES system alternatives. Each of the three TES systems behaves differently, and thermal performance math models for each system were developed for inclusion in the overall plant operation model. This section includes a discussion of the TES system performance, a description of thermal behavior of each TES system, and a brief technical presentation of the corresponding math models. The approach used to integrate the TES system into the overall thermodynamic loops of the powerplant is also presented.

6.3.1 Storage System Performance

Energy storage device performance is normally described in terms of round-trip efficiency (i.e., energy output from storage per unit energy input to storage). For conventional utility storage, the storage input* and output are both in terms of electrical energy, and round-trip efficiency becomes an excellent parameter to characterize losses. The TES device performance can be characterized on the same basis by simply including the effects of input and output thermal energy quality differences.

As shown in figure 6-15, the round-trip efficiency of the TES system is represented by three component efficiencies. The primary loss in the storage cycle is associated with the input power conditioning. The thermodynamic cycle seen by the helium in the storage charging cycle is shown schematically in figure 6-15 in the form of a temperature/entropy diagram. The heat added by the

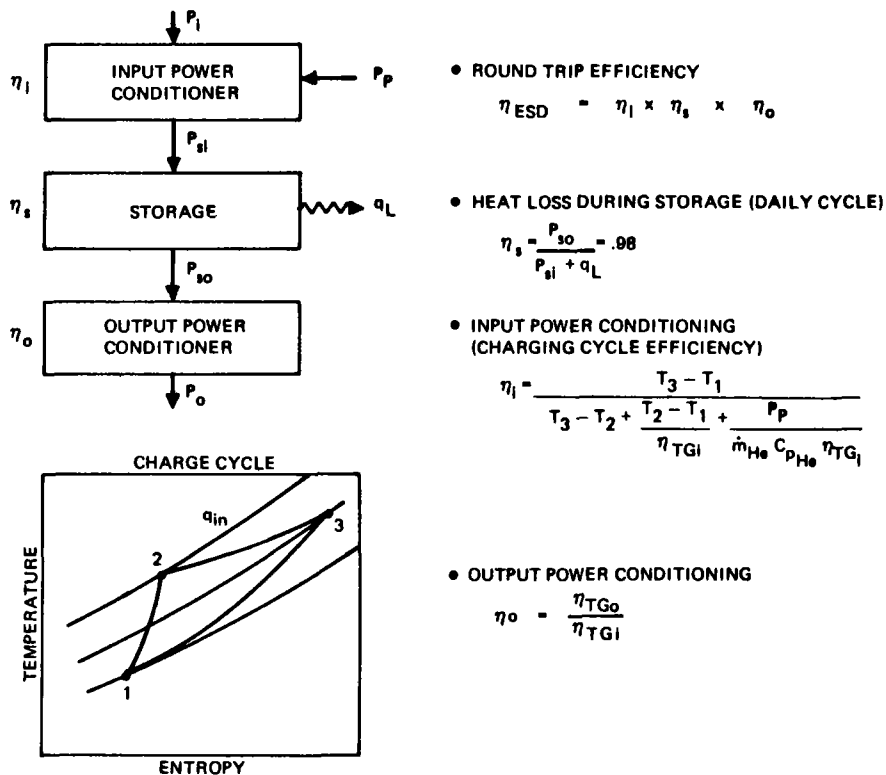


Figure 6-15. Thermal Energy Storage System Performance

*An exception is compressed air storage which is commonly designed with fossil fuel supplement for the air reheat prior to output power generation.

receiver (q_{in}) between state points 2 and 3 is given up to the storage system from state points 3 to 1 and the pressure losses are recouped with irreversible losses between 1 and 2. An additional term has been added to the charge-cycle efficiency expression shown in figure 6-15 to account for parasitic pumping requirements within the storage device that do not effect the thermodynamic state of the helium (i.e., chemical pumping requirements in the thermochemical storage device).

The remaining components of the overall round-trip efficiency are heat lost during the daily cycle and output-power conditioning losses, which account for the quality difference in the output heat versus the input heat used to charge the device. This quality difference is simply represented as the ratio of the turbine conversion efficiency at the two helium temperatures, as shown in figure 6-15.

The efficiency of the charge cycle (input-power conditioner) is dependent on the charge rate ($\dot{m}_{He} C_{p_{He}}$) and the thermal performance of the storage device ($T_3 - T_1$), both of which vary dramatically throughout the daily cycle. The output helium temperature of the storage device is also time and rate dependent. Consequently, the round-trip efficiency cannot be represented by a single value. A time integral of the various power quantities will produce an analogous efficiency on an energy basis rather than on an instantaneous power basis. The resultant energy conversion efficiency of the TES device over a daily or yearly cycle gives a more complete picture of the storage device performance.

However, it is interesting to look at representative power-based round-trip efficiency estimates. For example, the latent-heat TES device performance is strongly dependent on the fusion temperatures of the selected phase-change material (i.e., "candidate melts"). Ideally, the latent-heat device charges and discharges to a constant source and sink temperature (i.e., the fusion temperature). The degree to which the helium conforms to this temperature is dependent on the heat exchanger effectiveness (i.e., the thermal size of the heat exchanger). For latent- and sensible-heat systems, there are no parasitic pumping requirements other than those associated with the helium circulation.

In this case, the round-trip efficiency can be related to the charge-cycle pressure losses, the pump or compressor efficiency, the storage system heat exchanger effectiveness ratio, and the fusion temperature. Figure 6-16 shows the results of such an analysis for some representative pressure losses and compressor

efficiencies as a function of salt melt temperature for a fixed-charge temperature of 816°C (1,500°F). High-melt temperature reduces the charge-cycle efficiency while the low-melt temperatures reduce the output-power conditioning efficiency producing the combined effects shown in figure 6-16. These data led in part to the selection of "candidate melt" 8 (see figure 6-4) as the preferred melt.

For comparison purposes, a data point from the results of a full-integrated-plant-operation component run is also shown in figure 6-16. This data point is based on the same requirements and heat exchanger performance used to develop the idealized data described above. It is clear that the transient thermal behavior and other time-variant system performance parameters must be considered in the total plant performance predictions.

Math models to describe the basic thermal behavior and the parasitic pumping requirements for each TES device have been developed and included in the plant operation model described in section 8.2. A brief technical description of each of these models is presented in the following paragraphs.

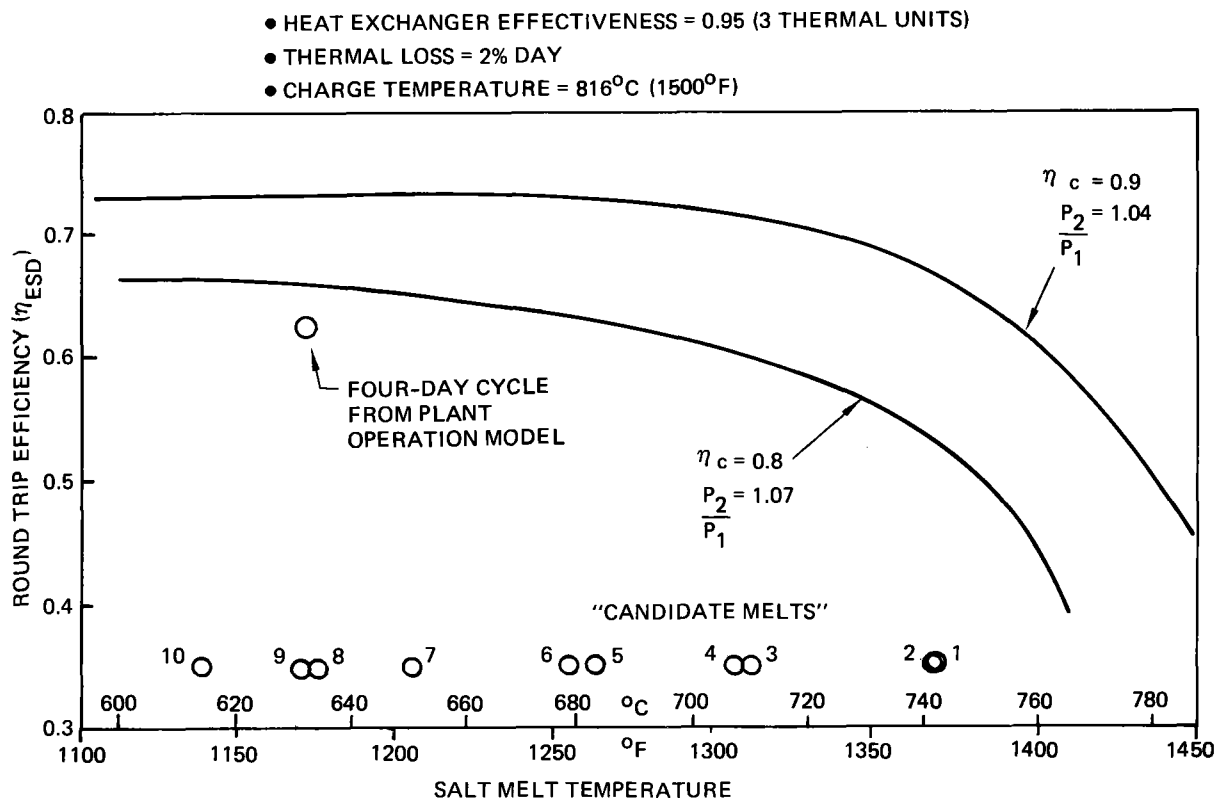
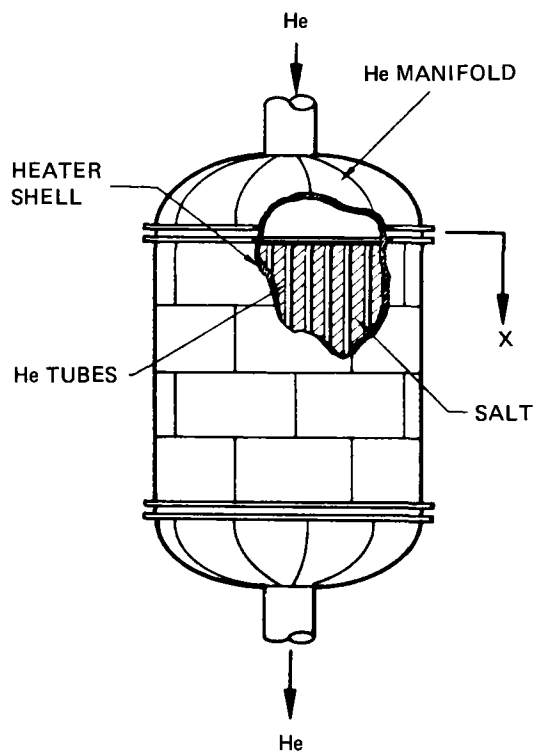


Figure 6-16. Latent Heat TES Roundtrip Efficiency

Sensible-Heat and Phase-Change TES Math Model. The transient thermal math model for these two TES devices is based on a finite-difference (nodal) solution to the one-dimensional transient partial-differential equations shown in figure 6-17. These equations assume that the heat transfer is dominated by the gas-in-tube convective heat transfer and that the heat flow into the storage media can be approximated through the unit conductance on the basis of a single node.

For both storage devices, the storage media is stationary and the helium flow direction is reversed in order to maintain the natural thermocline developed within the media. For the latent heat system, a simple tube-in-bath approach has been taken with the tubes arranged vertically. The hot end of the heater is at the top in order to prevent the formation of voids during the heating and cooling cycle.

The first assumption in the math-model equations of figure 6-17 neglects the axial conduction effect which has been shown to be negligible during the charge



● ENERGY BALANCE

$$\frac{\partial T_f}{\partial X} = \frac{UA/\Delta X}{\dot{m} C_{p_f}} (T_s - T_f)$$

$$\frac{\partial T_s}{\partial \tau} = \frac{UA}{m_s C_{p_s}} (T_f - T_s)$$

● TECHNICAL APPROACH

- NO AXIAL CONDUCTION
- SINGLE NODE LATERAL HEAT FLOW
- REVERSE FLOW DIRECTION FOR CHARGE AND DISCHARGE
- LUMPED HEAT LOSS THROUGH HEATER SHELL

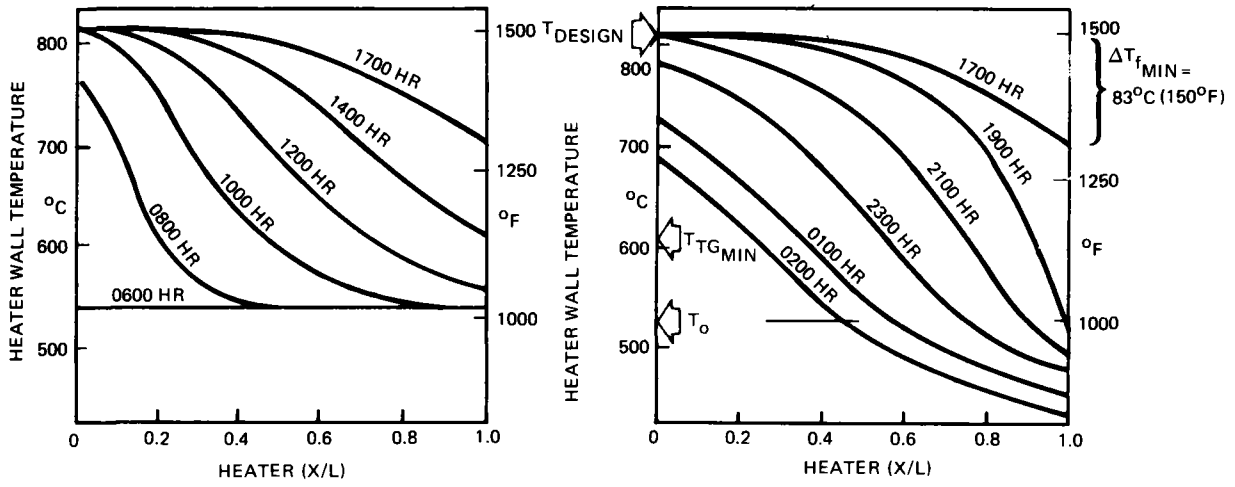
Figure 6-17. TES Performance Model

and discharge cycle. Idle periods will, of course, require the consideration of this effect to appropriately model the overnight (idle operation) diffusion of the natural thermoclines developed in the storage media.

The accuracy of the second simplification has been investigated by comparison with the appropriate exact solution. T_S is taken as the bulk temperature of the media and the unit-conductance model is the sum of the three resistances in the conduction path (i.e., (1) convective film coefficient, (2) metal tube wall resistance, and (3) storage media thermal resistance). The path length associated with the storage-media conduction is taken as half the distance to the adiabatic plane of symmetry between the tubes. With these assumptions, the comparison of heat rates with the exact solution is good. Biot and Fourier numbers were varied over two orders of magnitude with representative storage media thermal properties, and the maximum heat rate error encountered for the all solid or all liquid media was about 15%. During periods of phase change of a given node, the storage-media conduction-path length must be modified to account for the location of the melt face relative to the tube wall. However, the average heat flow rate over the zone of the heater undergoing phase change is adequately represented by the simple half-length conduction path described above.

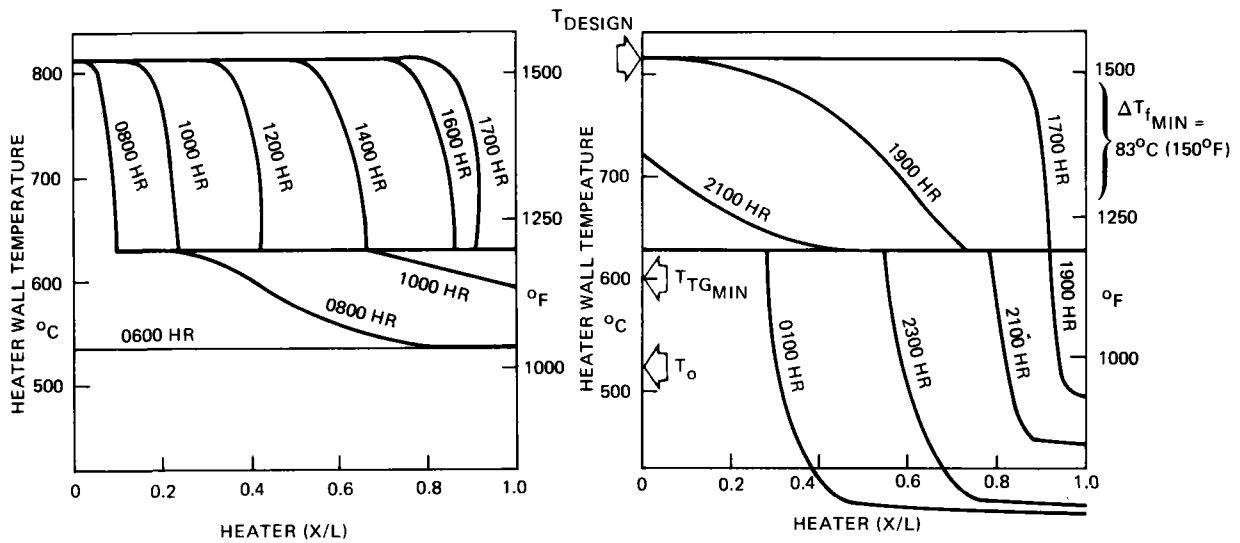
In the latent heat device, energy is transferred to or from a media that can be entirely solid, entirely molten, or a combination. At any one time the rate that energy can be transferred to or from the media is dependent upon the thermodynamic state of the media. During a phase change, each portion of the media (node) must receive or release a quantity of energy equal to its latent heat of fusion. An energy-exchange accounting system is used to simulate the melt-face propagation axially through the molten-salt heater. Each node is surveyed to see if it is at or undergoing a phase change. If the node is undergoing a phase change, the accounting system corrects the enthalpy of the node and maintains the nodal latent heat of fusion.

Temperature profiles in the storage media during a typical day's operation of the solar powerplant are shown in the following two figures (6-18 for sensible-heat storage and 6-19 for latent-heat storage). The data shown here are taken from the output of the complete powerplant operation model and include the effects of all systems operating. The model simulates the environment by using the summer-day insolation data for Inyokern, California. In both cases the initial conditions are taken as a neutral thermocline at an energy level consistent with



- SUMMER INSOLATION
- INYOKERN, CALIFORNIA
- CLOSED CYCLE HELIUM SYSTEM

Figure 6-18. TES Temperature Profile (Sensible Heat)



- SUMMER INSOLATION
- INYOKERN, CALIFORNIA
- CLOSED CYCLE HELIUM SYSTEM

Figure 6-19. TES Temperature Profile (Phase Change)

the minimum turbine operating temperature (i.e., the end state of the previous day's operation less overnight energy losses due to 2% conduction out of the storage device walls). The thermal mass of both systems is based on a 246°C (443°F) temperature swing. The charge limit is set by the pinch-point temperature limit of 83°C (181°F), consistent with a pumping load of approximately 20 MW_e; the overall conductance of the heat exchanger is sized for consistency with the charge rates, discharge rates, pinch-point temperature limit, and turbine-temperature swing at minimum operating temperature. These data are representative of the thermal behavior of the two TES devices as incorporated in the 50-MW_e modules of the STC powerplant.

During the follow-on energy storage contracts, this math model will be improved and expanded. The transient thermal analysis for the latent-heat device will be expanded to handle the melt-face propagation in the fused salt. This expansion will ensure that the transient heat rate calculations during charge and discharge of the phase-change heater are reliable and accurately model the actual physical processes. Because of the impact of the heat transfer rates on the phase-change heater performance, this work is a key task in support of the plant operation analysis.

An additional area of concern that could significantly affect the melt-face propagation is the possibility of increased heat transfer within the salt due to the partial transparency of the salt to its own thermal radiation. Figure 6-20 shows the transmission of several fluoride salts at room temperature as well as the blackbody thermal spectrum associated with a temperature of 871°C (1,600°F).

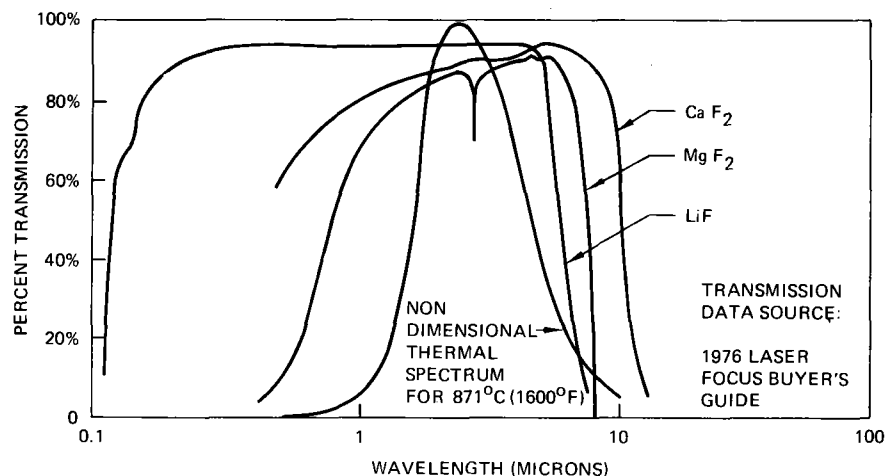
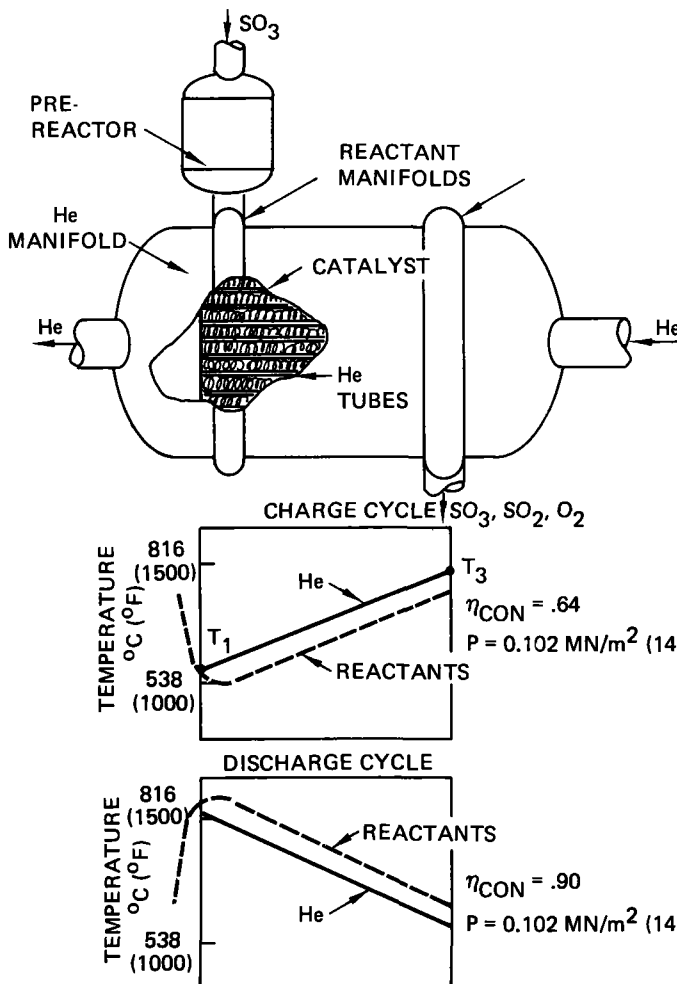


Figure 6-20. Transmission of Fluoride Salts

As a result of this effect, the salt will transmit considerable quantities of energy by radiation in addition to the regular conduction. This will tend to smooth out salt temperature profiles between tubes and in effect increase the rate of melt-face propagation through the salt.

CES Storage System Performance Model. The only thermal interface between the helium flow and the CES system is in the integral reactor heat exchanger. The reactor is designed and controlled to maintain a specific helium-temperature distribution from reactor input to reactor output, as shown schematically in figure 6-21. The prereactor functions to condition the reactants prior to direct contact with the integral helium heat exchanger. This approach is one



- REACTOR DESIGNED FOR COMPLETE HELIUM TEMPERATURE SWING

- REACTANT REQUIREMENTS

$$\dot{m}_{SO_3} = \frac{m_{He} C_{p_{He}} (T_3 - T_1)}{H_R \eta_{CON}}$$

$$H_R = 296 \text{ CAL/GM}_{SO_3} \text{ (531 BTU/LB)}$$

- PARASITIC POWER REQUIREMENTS – CHARGE (PROPORTIONAL TO m_{SO_3})

- REACTANT COMPRESSOR
- OXYGEN COMPRESSOR

- PARASITIC POWER REQUIREMENTS DURING DISCHARGE VERY SMALL

Figure 6-21. Thermochemical Energy Storage Requirements and Performance

of two alternatives suggested in the reactor design discussion in section 6.2.5. The CES performance model reduces to a simple computation of the parasitic power losses as a function of charge and discharge heat ratio. Table 6-3 summarizes the parasitic power requirements within the CES system equipment complex for the charge and discharge cycle. It is apparent from the data that the dissociation product compressor and the oxygen compressor are the major power consumers.

Each of the parasitic power requirements listed in table 6-3 apply to the design charge- and discharge-rate conditions. In each category, the parasitic power required is proportional to the mass flow rate of the associated reaction constituent. The simplified math model developed for the CES performance analysis determines constituent mass flow rate on the basis of charge- and discharge-heat rates $(\dot{m}_{He} \dot{C}_{p_{He}} (T_3 - T_1))$, heat of reaction, and reaction conversion fraction. The design parasitic power requirements are then scaled by these flow rates to determine the instantaneous parasitic powerplant requirements. The above requirements are based on the initial design studies summarized in section 6.2.5 and are strongly dependent on the system design approach selected for those initial studies. A number of design alternatives will be investigated during the follow-on studies. Parasitic power requirements are a major concern not only in the CES system performance but also in plant performance since this power is supplied directly by the primary gas turbine in the plant.

Table 6-3. CES Parasitic Power Requirements

	MW _T	MW _E
Endothermic mode		
SO ₃ storage heater	TBD	
SO ₃ pump		.052
Dissociation product compressor		21.3
Oxygen compressor		6.5
Net cooling load	≈ 28	
Exothermic mode		
SO ₂ pump		.03
Oxygen compressor		.093
Net cooling load	≈ 38	

Storage System Fluid Circulation System Power Requirements. A separate fluid circuit provides charging energy for the thermal energy storage system. This circulation system includes a pump or compressor that must recoup the pressure losses throughout the storage charging fluid circuit. The power required to make up this pressure is determined by the overall pressure losses in the circuit, the instantaneous helium mass flow rate in the charging-flow circuit, the discharge temperature from the storage device, and the efficiency of the circulating pump. The temperature and pressure changes in the helium stream across the pump are determined as a part of each of the storage system performance models. The corresponding pumping power, which is provided directly by the primary gas turbine, is then simply determined by the temperature rise across the pump and the corresponding gas flow rate.

6.3.2 Storage/Plant System Operation

Figure 6-22 shows schematically the approach to be used to integrate the thermal energy storage system into the thermodynamic loop of the STC powerplant. This particular approach is used in view of the thermal behavior of the proposed TES device and was selected on the basis of overall plant performance. During periods of high insolation, energy input to the helium stream in excess of that required to drive the turbine is used to charge storage, as shown on the left-hand side of figure 6-22. The high-temperature gas flow from the receiver is transported in part to the turbine to meet the plant demand output and in part to a separate fluid circuit, which includes the storage device and a high-temperature pump. The pump provides the input energy required to circulate the helium and must be sized to meet the flow requirements encountered as the storage device reached its fully charged condition.

During periods of reduced or no insolation, thermal energy is withdrawn from storage to supplement the receiver input or to replace the receiver as a heat source. The integration and operation of the storage/plant as a system in this mode is shown schematically as the right-hand side of figure 6-22. During periods of no insolation, the storage device is used directly as the heat source in the helium turbine cycle. In this mode, there is no helium flow into the receiver circuit and the high-temperature pump is bypassed on the inlet side of the storage unit.

During periods of partial insolation, the helium from the recuperator first passes through the receiver and then through the storage device. In this mode,

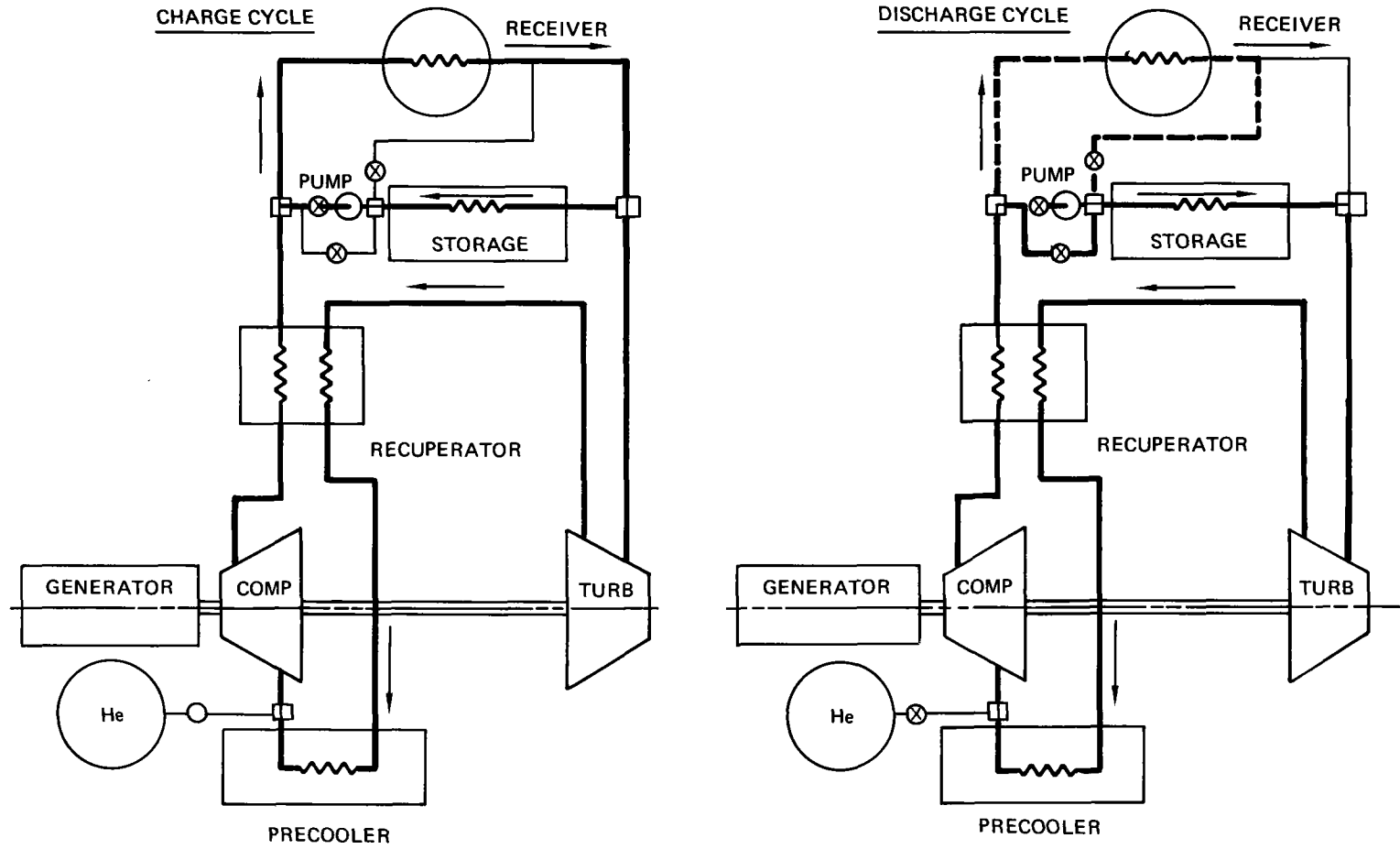


Figure 6-22. Storage/Plant Schematic

the receiver and storage device act in series as the heat source for the helium turbine, with the receiver providing the low-temperature heat increment and the storage providing the high-temperature increment. This approach keeps the high-temperature end of the storage unit nearest the turbine inlet and gives the highest conversion efficiency in the receiver.

6.4 REFERENCES

- 6-1 Reactor Handbook, Vol. 2, Engineering, Section 6, "Fused-Salt Systems," May 1955, pp. 799-850
- 6-2 Private communication with Chicago Bridge and Iron
- 6-3 Boeing Coordination Sheet, "Turbomachinery Costs," K-6161-GLV-079
- 6-4 Philips Labs, informal "know-how" transfer, October 1975
- 6-5 Davison, J. E., Evaluation of Eutectic Fluoride Thermal Energy Storage Unit Compatibility, Interim Technical Report, AFAPL-TR-75-92-Part I, Air Force Aero-Propulsion Lab, Wright-Patterson AFB, OH, October 1975
- 6-6 Boser, O., Study of Safety Aspects of High-Temperature Thermal Energy Storage Systems, Interim Technical Report, Philips Labs, Briarcliff Manor, NY, January 1976
- 6-7 Fluid Fuel Reactors, Part II, "Molten-Salt Reactors," edited by J. L. Lane, Addison-Wesley Publ. Co., Inc., Reading, MA, 1958
- 6-8 Grimes, W. R., "Molten Salts at Reactor Materials," Nuclear News, ANS, V. 7, N. 5, May 1964, pp. 3-8
- 6-9 Letter from Pennwalt Corp., King of Prussia, Pa., April 9, 1976
- 6-10 Private communication with Huntington Alloys, Huntington, W.V.
- 6-11 Rocket Research Corp., Chemical Energy Storage - Chemical Reaction Subsystem - Technical Assessment Paper, RCC-76-R-J02, January 1, 1976
- 6-12 Chubb, T. A., "Analysis of Gas Dissociation Solar Thermal Power System," Solar Energy, 17, 129-26 (1975)

Section 7.0

MATERIAL SELECTION AND TEST

7.1 MATERIAL SELECTION

A number of metal alloys were chosen as candidates for high-temperature heat exchanger tubing based on considerations of present manufacturing capability, performance capability, and economics. The high-temperature limit for such state-of-the-art materials was established as 816°C (1,500°F) to 870°C (1,600°F). Materials had to show promise of meeting the 30-year service-lifetime requirement of repeated thermal cycles and stresses due to internal gas pressure and high temperature. Major evaluation criteria (from published data, and later from test) included stress-rupture strength, creep properties, oxidation resistance, and metallurgical stability.

Preliminary screening of commercially available high-temperature alloys led to selection of four alloys for more detailed evaluation: Haynes 188, Inconel 617, Inconel 625, and Inconel 601. Nominal chemical composition and physical properties for these four alloys, as furnished by suppliers, are shown on the upper half of table 7-1. Other data furnished for elevated-temperature properties of strength and stress rupture are summarized in the lower tabulation on table 7-1. The Haynes 188 stress-rupture life plot is shown on figure 7-1. Based upon the elevated-temperature properties and the reported oxidation resistance of Haynes 188 and Inconel 617, these alloys were selected as optimum candidates.

7.2 MATERIAL TESTS

Two important test series were completed on the Haynes 188 and Inconel 617 material candidates. Each material was subjected to a thermal cycle test at high temperature. A complete description is provided in section 7.3. The materials were then subjected to elevated-temperature rupture tests to determine the effect of purposely or accidentally overheating helium-pressurized tubing in excess of the proposed service temperature of 830°C (1,525°F). This test is described in section 7.4.

Table 7-1. Heat Exchanger Material Selection

Candidate materials/properties											Physical properties		
Alloy	Nominal composition (%)										Relative thermal conductivity at 1500°F (816°C)	Relative mean coeff expansion to 1600°F (870°C)	Specific heat at 1500°F (816°C)
	Ni	Cr	Co	Fe	Mo	Cb	W	Al	La	C			
Haynes 188	22	22	Bal	3	—	—	14	—	0.1	0.15	174	9.4	0.133
Inconel 617	54	22	12.5	—	9	—	—	1	—	0.07	178	8.7	0.147
Inconel 625	Bal	22	—	5	9	4	—	0.4	—	0.10	150	8.8	—
Inconel 601	60	23	—	Bal	—	—	—	1.5	—	0.10	171	9.4	0.158

Structural properties at 1600°F (870°C)

Alloy	Stress-rupture life			Temperature strength		
	10,000 life hours	100,000 life hours	1,000,000 life hours	Tensile ultimate	Tensile yield	Elongation % in 2 inches
Haynes 188	5.4	3.5	2.3	62	40	80
Inco 617	6.0	3.8	2.5	36	31	92
Inco 625	4.1	2.7	—	40	35	110
Inco 601	2.5	1.6	—	22	18	92
Stress to failure (ksi) \triangleright				Strength (ksi)		

\triangleright 1 ksi = 6.895 meganewtons/meter²

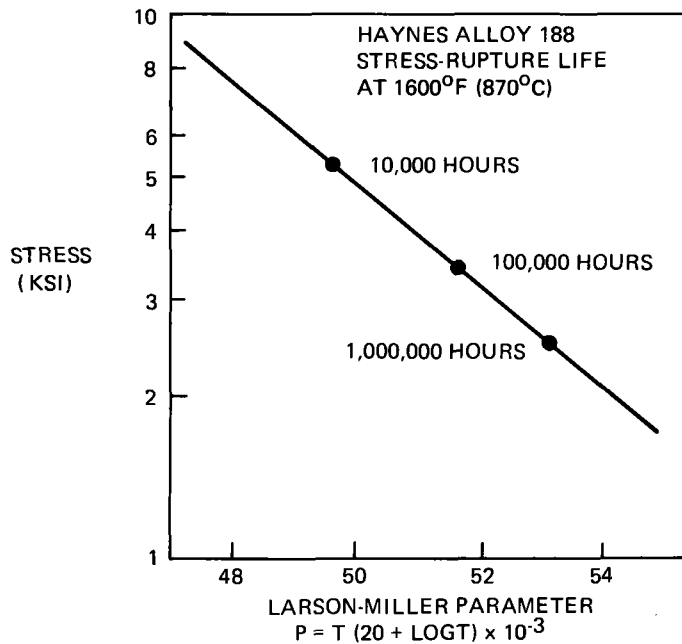


Figure 7-1 . Stress Rupture Properties at 1600°F (870°C)

7.3 THERMAL-CYCLE TESTS

Thermal-cycle tests were planned and conducted on Haynes 188 and Inconel 617 to evaluate their material characteristics and to verify their lifetime in the design concepts for the central receiver heat exchangers and the other high-temperature applications. For the 30-year tubing lifetime required, the expected number of thermal cycles under pressure is approximately 10,500, and the lifetime simulations were developed to that number.

7.3.1 Pretest Operations

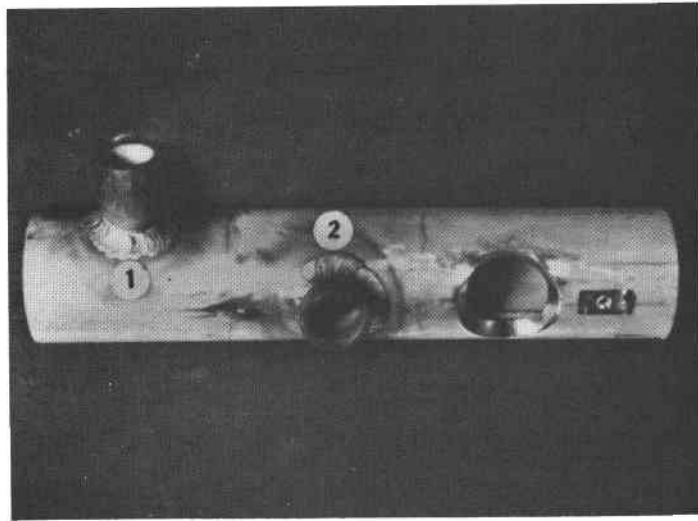
Welded tube lengths of Haynes 188 and Inconel 617 were obtained for construction of the specimen heat exchangers to be built and tested. The advantage of seamless over welded tubing for the application was recognized, but delivery dates precluded use of the seamless form of either material. Chemical composition of the supplied Haynes 188 and Inconel 617, as certified to Boeing, essentially duplicated the furnished data shown in table 7-1. Mechanical properties are summarized in section 7.3.3 Thermal-Cycle Test Results so that before-and-after test results can be directly compared.

Prior to fabricating each heat exchanger for a thermal-cycling test, a series of header/tube test joints were made to establish weld control parameters and to check the feasibility of X-ray inspection of the weldments. Header/tube joints were welded with filler material of the same composition as the tube alloys. Production X-ray facilities were found inadequate for inspection of the Haynes 188, apparently due to the radiographically-dense cobalt-base Haynes alloy, which contains 14% tungsten. As a result of this finding the outer surface of all heat exchanger welds was penetrant inspected. No defects were found. An assessment of the fabrication characteristics of both alloys is presented in table 7-2.

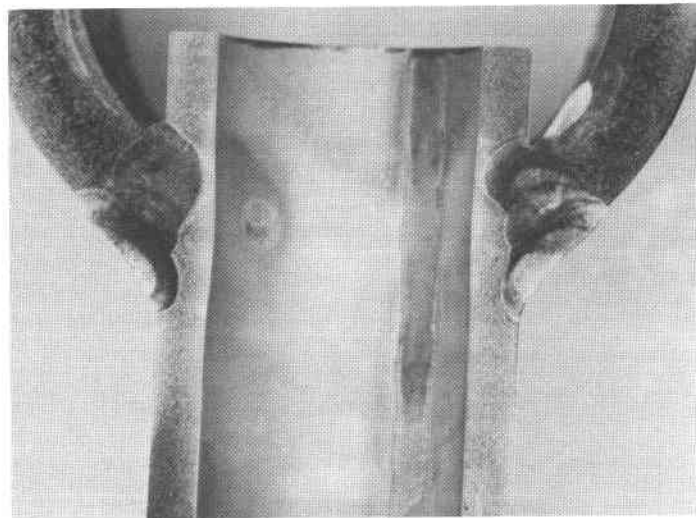
Table 7-2. Material Fabrication Characteristics

Property	Haynes 188	Inconel 617
Formability	Excellent	Excellent
Weldability	Good	Fair
X-ray inspection	Special requirement	Standard practice

Two header/tube test welds, in the as-welded condition, were sectioned and mounted for metallographic examination. These welds and a typical microsection for Haynes 188 are shown in figure 7-2. Microstructure of the weld zones is shown in figure 7-3.



TYPICAL HEADER/TUBE WELD JOINT



CROSS SECTION OF HEADER/TUBE WELD JOINT

Figure 7-2. Header/Tube Weld (Haynes 188)



WELD FUSION ZONE, HEADER/WELD



WELD METAL



HEADER BASE METAL



WELD FUSION ZONE, TUBE/WELD

Figure 7-3. Weld Joint Microstructure (Haynes 188)

Two test specimens simulating the central receiver heat exchangers were fabricated from welded tubing of Haynes 188 and Inconel 617, respectively. Figure 7-4 illustrates the test specimen configurations. Tubing sizes used in the test assembly fabrication are listed on table 7-3. Tubing sizes are different due to the ready availability of Inconel 617 in the sizes shown. The receiver concept planned and costed uses tubing runs of 2.54-centimeter (one-inch) outside diameter and of 0.157-centimeter (0.062-inch) wall thickness.

Individual small coupons of Haynes 188 and Inconel 617, due for the same exposure to the thermal cycle test conditions as the heat exchanger specimens, were carefully measured and weighed. This would be repeated after test to determine changes due to cycling and the effect of oxidation.

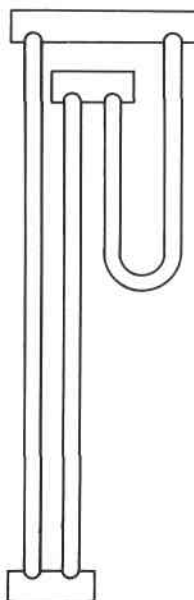


Figure 7-4. Heat Exchanger Test Specimen

Table 7-3. Test Specimen Tube Dimensions

Nominal size	Haynes 188		Inconel 617	
	Tube	Header	Tube	Header
Outside diameter (inch)	1.0	2.0	0.844	1.50
Wall thickness (inch)	0.125	0.250	0.055	0.125

7.3.2 Test Operations

A schematic of the thermal-cycle test setup is shown by figure 7-5. Heat was supplied by controllable quartz lamp heaters; the 3.45-MN/m^2 (500 psi) gas was supplied from helium bottles.

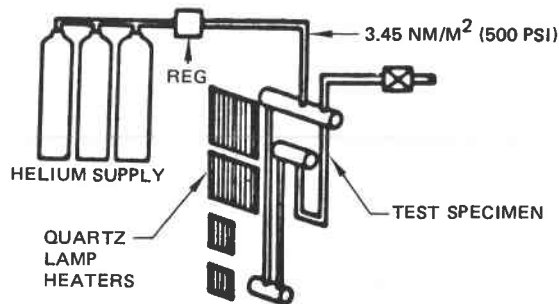


Figure 7-5. Thermal Cycle Test Schematic

There were 27 thermocouples attached to each test specimen. The heat exchanger tubing runs had 16 thermocouples at various locations, 12 on the outside surface, and 4 inside the tubing. The headers had 11 thermocouples, 9 outside and 2 inside the headers. Two of the thermocouples mounted on the tube were used for quartz lamp control of maximum and minimum temperatures. Positions for all thermocouples are indicated on figure 7-6. Pressure regulators and gages were installed to control gas pressure at 3.45 MN/m^2 (500 psi). A photograph showing the instrumented Haynes 188 test assembly is included as figure 7-7.

Each test assembly was subjected to over 10,000 thermal cycles to simulate approximately 30 years of diurnal cycles in the central-receiver-concept heat exchangers. The temperatures were cycled from 483°C (900°F) to 830°C ($1,525^{\circ}\text{F}$). The latter temperature was chosen to correspond to the maximum expected tube temperatures in the receiver and the former chosen low enough to ensure that significant effects of thermal-cycling stress could occur. Pressure was held at a constant 3.45 MN/m^2 (500 psi). The test conditions are depicted on figure 7-8.

Cycle times shown on figure 7-8 are only representative. The first 1,695 cycles on Haynes 188 were run at 9 minutes per cycle. The remaining cycles and the

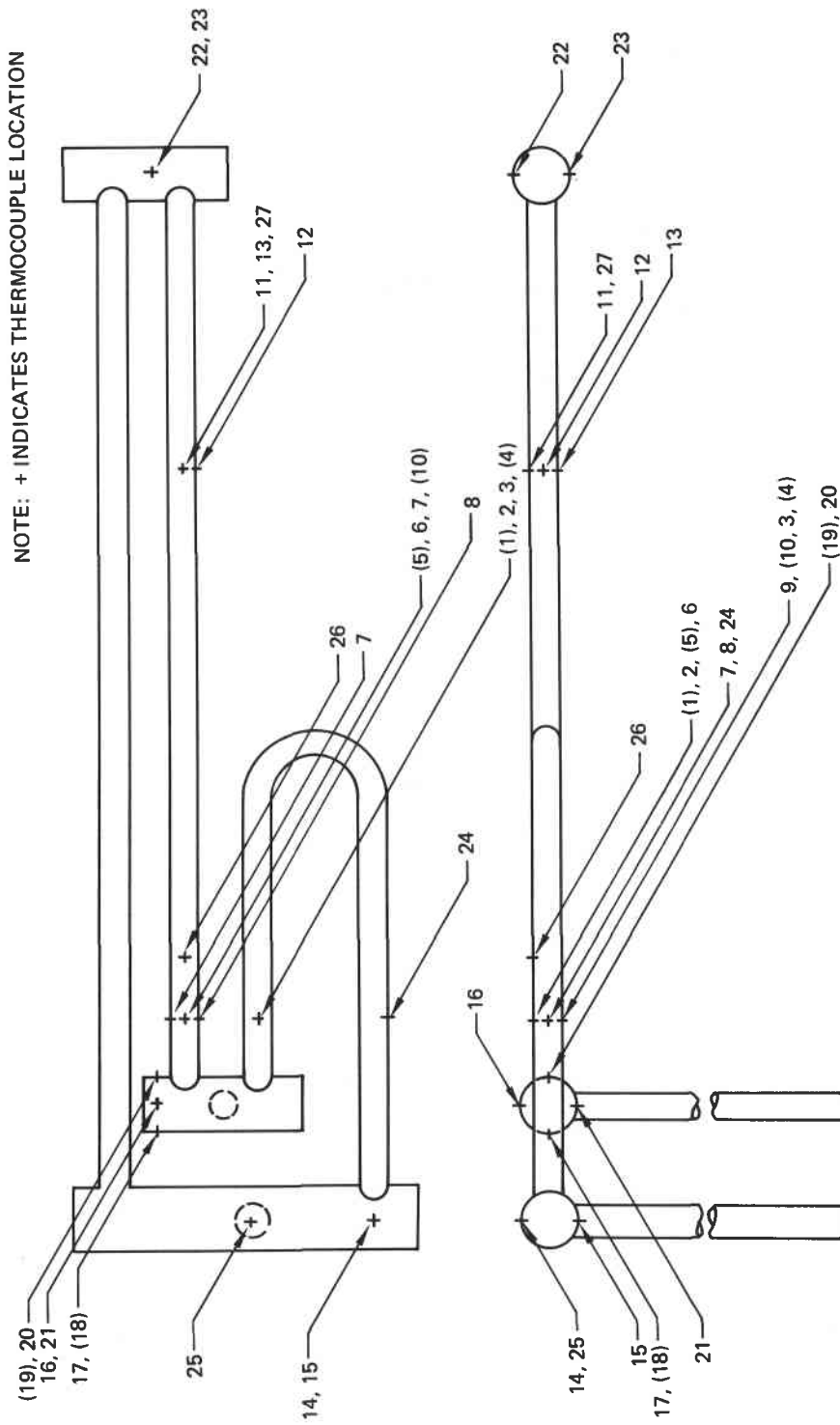


Figure 7-6. Thermocouple Locations

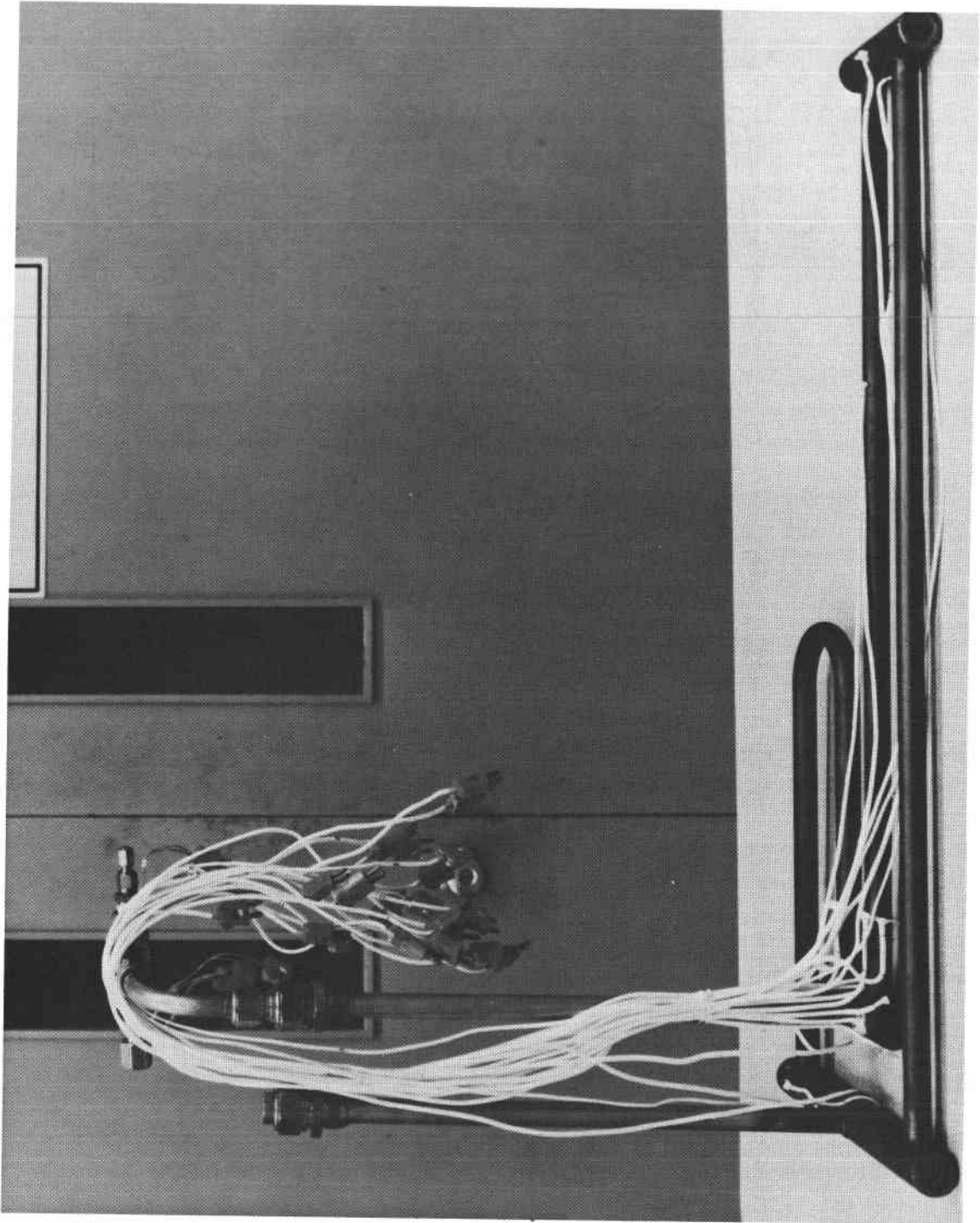


Figure 7-7. Test Specimen Assembly

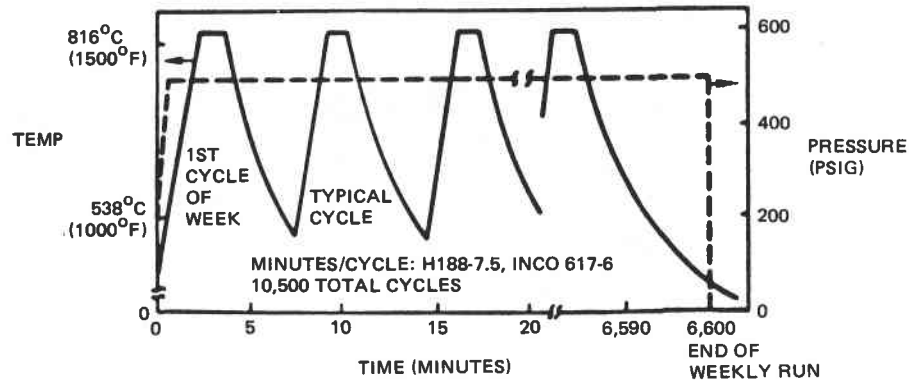


Figure 7-8. Thermal Cycle Test Conditions (Simulated 30-Year Life)

entire Inconel 617 test were run at 6 minutes per cycle. After the first 1,695 cycles were completed, the pressurized gas was changed to air and held at 3.45 MN/m^2 (500 psi) with a slight bleedoff to introduce oxygen continuously into the assembly. At the completion of 3,370 cycles, the gas was changed back to helium for the balance of the test. These gas changes provided convenient opportunities to remove or insert test coupons inside the welded assembly.

A specimen, with testing in progress, is shown in figure 7-9. The quartz lamp heaters parallel the entire length of the assembly on one side. The heaters gave a controlled rise and hold time. Cooldown was accomplished by lamp shutoff and introduction of convective cooling to the test-cell environment.

7.3.3 Thermal-Cycle Test Results

Temperatures. Two sheets typical of the extensive temperature data recorded during the tests are displayed on figures 7-10 and 7-11. These Haynes 188 data show the pertinent temperatures and temperature differences recorded for the 2.54-centimeter (1-inch) tube and the 5.08-centimeter (2-inch) headers. Thermocouple locations are identified as shown on figure 7-6. Maximum and minimum temperatures, as measured by thermocouples 2, 6, and 11, show the accuracy of control to the temperature-cycle limits on the tubing. Thermocouples 14, 16, and

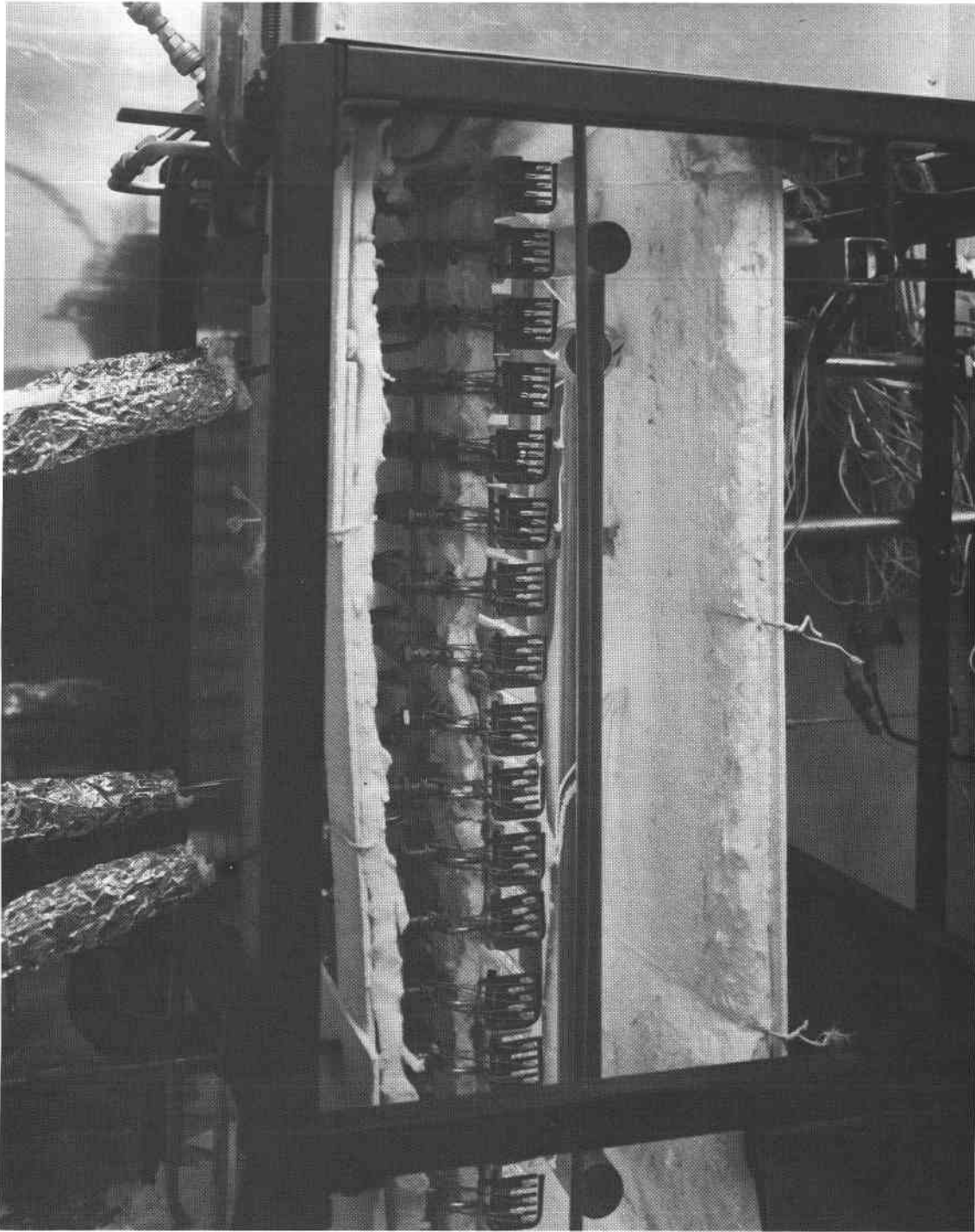


Figure 7-9. Specimen in Test

Note: GHe
 9 min/cycle
 T = temperature (°F)

Time: 1600
 Date: 5-6-75
 Test cycle: 1235

	1" tube											Manifolds											
	T			ΔT								T			ΔT								
T/C location	2	6	11	1-2	5-6	2-3	9-6	7-6	6-8	8-9	7-9	14	16	22	17-18	19-20	14-15	22-23	16-21	16-17	16-20	17-21	20-21
Max temp	1550	1480	1492	x	x	x	x	x	x	x	x	1470	1475		x	x	x	x	x	x	x	x	x
Min temp	950	925	890	x	x	x	x	x	x	x	x	1050	995	890	x	x	x	x	x	x	x	x	x
Max wall + ΔT	x	x	x	30	60	x	x	x	x	x	x	x	x	x	30	60	x	x	x	x	x	x	x
Max wall - ΔT	x	x	x	20	20	x	x	x	x	x	x	x	x	x	25	25	x	x	x	x	x	x	x
Front to rear max ΔT	x	x	x	x	x	112	105	x	x	x	x	x	x	x	x	x	220	290	230	x	x	x	x
Circumferential ΔT	x	x	x	x	x	x	x	90	45	65	11	x	x	x	x	x	x	x	x	140	115	85	110

Note: GHe
 Start of 6 min/cycle
 New lamp array
 T = temperature (°F)

Time: 1540
 Date: 5-12-75
 Test cycle: 1670

	1" tube											Manifolds											
	T			ΔT								T			ΔT								
T/C location	2	6	11	1-2	5-6	2-3	9-6	7-6	6-8	8-9	7-9	14	16	22	17-18	19-20	14-15	22-23	16-21	16-17	16-20	17-21	20-21
Max temp	1540	1485	1540	x	x	x	x	x	x	x	x	1400	1420	1445	x	x	x	x	x	x	x	x	x
Min temp	965	960	860	x	x	x	x	x	x	x	x	1000	1042	1050	x	x	x	x	x	x	x	x	x
Max wall + ΔT	x	x	x	45	25	x	x	x	x	x	x	x	x	x	15	35	x	x	x	x	x	x	x
Max wall - ΔT	x	x	x	13	25	x	x	x	x	x	x	x	x	x	25	22	x	x	x	x	x	x	x
Front to rear max ΔT	x	x	x	x	x	155	135	x	x	x	x	x	x	x	x	x	230	225	220	x	x	x	x
Circumferential ΔT	x	x	x	x	x	x	x	125	50	80	10	x	x	x	x	x	x	x	x	140	130	80	85

Figure 7-10. Test Cycle Data Sheet—Helium

Note: Air
6 min/cycle
T=temperature (°F)

Time: 1545
Date: 5-13-75
Test cycle: 1918

	1" tube											Manifolds											
	T			ΔT								T			ΔT								
T/C location	2	6	11	1-2	5-6	2-3	9-6	7-6	6-8	8-9	7-9	14	16	22	17-18	19-20	14-15	22-23	16-21	16-17	16-20	17-21	20-21
Max temp	1522	1470	1530	X	X	X	X	X	X	X	X	1385	1422	1435	X	X	X	X	X	X	X	X	X
Min temp	935	950	950	X	X	X	X	X	X	X	X	980	1030	1015	X	X	X	X	X	X	X	X	X
Max wall + ΔT	X	X	X	40	25	X	X	X	X	X	X	X	X	X	13	26	X	X	X	X	X	X	X
Max wall - ΔT	X	X	X	15	21	X	X	X	X	X	X	X	X	X	25	12	X	X	X	X	X	X	X
Front to rear max ΔT	X	X	X	X	X	145	130	X	X	X	X	X	X	X	X	X	245	210	230	X	X	X	X
Circumferential ΔT	X	X	X	X	X	X	X	125	50	80	5	X	X	X	X	X	X	X	X	145	145	80	85

Note: Air
6 min/cycle
T=temperature (°F)

Time: 1930
Date: 5-18-75
Test cycle: 3010

	1" tube											Manifolds											
	T			ΔT								T			ΔT								
T/C location	2	6	11	1-2	5-6	2-3	9-6	7-6	6-8	8-9	7-9	14	16	22	17-18	19-20	14-15	22-23	16-21	16-17	16-20	17-21	20-21
Max temp	1565	1510	1525	X	X	X	X	X	X	X	X	1420	1475	1380	X	X	X	X	X	X	X	X	X
Min temp	925	940	865	X	X	X	X	X	X	X	X	975	1035	975	X	X	X	X	X	X	X	X	X
Max wall + ΔT	X	X	X	40	30	X	X	X	X	X	X	X	X	X	15	25	X	X	X	X	X	X	X
Max wall - ΔT	X	X	X	17	22	X	X	X	X	X	X	X	X	X	25	15	X	X	X	X	X	X	X
Front to rear max ΔT	X	X	X	X	X	165	140	X	X	X	X	X	X	X	X	X	240	230	235	X	X	X	X
Circumferential ΔT	X	X	X	X	X	X	X	137	60	85	3	X	X	X	X	X	X	X	X	155	130	82	97

Figure 7-11. Test Cycle Data Sheet—Air

22 show that effect on the manifolds. Delta-temperature differences across the wall thickness are displayed by thermocouple pairs 1-2, 5-6, 17-18, and 19-20. Temperature differences from the front surface to back surface are shown by 2-3, 9-6, 14-15, 22-23, and 16-21. Circumferential temperature differences from front surface to sides are shown in the last line of each data set. The results are considered very encouraging in that temperature differences in actual application will be reduced from those shown. In summary, the test met the temperature-cycle objectives and furnished encouraging temperature results.




Figure 7-10 shows the change from the 9 minutes/cycle with which the test originated to the 6 minutes/cycle used through the remainder of the 10,560 test cycles. Figure 7-11 shows the change to air used for 1,675 cycles to test resistance to oxygen.


Test Physical Effects. External surfaces of all thermally cycled tube components were coated with a thin, tightly adherent, dark-green/black scale. Interior tube walls were coated with a thin, uniform, dark-green scale. Optical measurements made on cross sections cut perpendicular to the axis of the 2.54-centimeter (1-inch) tubing showed no significant metal loss due to the test. Before-and-after measurements of wall thicknesses agreed to four decimal places.


Table 7-4 shows weights of Haynes 188 material samples (1-4) that were sealed into the test assembly for various exposure times and environments. Weight gains were small except for sample number 1, where the gain is not understood. Sample number 5 of Inconel 617 was mounted externally to the test specimen and saw the heating cycles but no internal pressure.

Specimen dimensional changes (for the Haynes 188 specimen) are displayed on figure 7-12. There were no changes evident in tube outside diameters. There was a slight distortion of the test specimen in the plane shown by pushing outward of the tube bend and to the top by the inner manifold. In addition, there was a slight rotation upward (out of the plane) by the topmost corner of the inner manifold (0.024 inch) as shown.

TABLE 7-4: Oxidation Sample Weights

SAMPLE NUMBER	INITIAL WEIGHT (grams)	FINAL WEIGHT (grams)	WEIGHT GAINED (grams)	NUMBER OF CYCLES EXPOSED	ATMOSPHERE
1	8.4560	8.4700	0.0140	10,565	GH _e , Air, GH _e
2	7.6698	7.6701	0.0003	1,695	GH _e
3	8.4529	8.4531	0.0002	3,370	GH _e , Air
4 	8.9280	8.9282	0.0002	1,675 	Air
5 	197.2	196.0	-1.2	10,565	Air

 Installed at cycle number 1,695

 2.54 centimeter (one inch) diameter x 20.3 centimeters (8 inches) (Inconel 617 in external thermal environment)

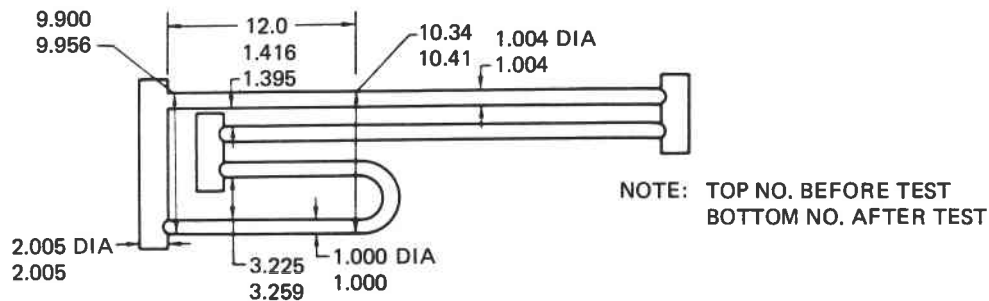





Figure 7-12. Test Results—Specimen Dimensional Changes (Inches)

Mechanical Properties. Tensile specimens were prepared from tube segments in both the as-received and after-test condition. A summary of mechanical-property testing taken with three specimens is shown on table 7-5.

Table 7-5. Material Property Summary

Condition 	Haynes 188				Inconel 617			
	FTU ksi 	FTY ksi	Elong %	Hard Rc	FTU ksi	FTY ksi	Elong %	Hard R _b
Annealed—before tube forming	139	71	49					
After tube forming	166	128	33	20	113	55	60	90
After thermal cycling	166	112	25	34	129	63	43	95

 Condition prior to test: HA-188, as rolled and welded
INCO 617, as rolled and welded + solution annealed

 1 ksi = 6.895 meganewtons/meter²

The major material effects are: (1) the constancy of the ultimate tensile strength and small reduction of yield strength in the Haynes 188 from fabrication through test; (2) the increase in these same properties for Inconel 617; (3) the larger reduction in elongation properties for both materials; and (4) clear evidence of aging in both the base metal and weld-zone properties. Available data on the two alloys support the observed behavior of an increase in mechanical properties after exposure to elevated temperatures. Additional strengthening of the Haynes 188 material occurred as a result of the cold work applied during tube forming.

Metallurgical Effects. The test specimens were sectioned after completing the thermal-cycling tests and subjected to intensive examination of material macro- and microstructure. The wall thinning effect of the 180 degree bend in the Haynes 188 specimen is evident in figure 7-13. A 10% reduction in the outer wall thickness was measured. Bending produced an oval contour in the tube section.



Figure 7-13. Wall Bending Effects

A cross section through a Haynes 188 tube/header weld joint, after test, is presented in figure 7-14. It shows the typical bead contour and the weld penetration obtained. Microscopic examination of cross sections removed from weld joints after testing revealed several sharp defects. These defects originated during welding, but did not propagate during thermal cycling.

A section of the scaled surface is shown in the lower picture of figure 7-15. No intergranular oxide penetration was noted; however, a section through the 180 degree bend in the 2.54-centimeter (1-inch) tube disclosed an apparent thin surface zone of alloy depletion. This is also shown in the upper picture of figure 7-15.

Microstructures typical of various zones of the tubing assemblies have been shown in figures 7-2, 7-14, and 7-15. Figures 7-16 and 7-17 provide similar data on tubes. A typical annealed structure is evident in all as-received material. Light carbide precipitation was noted in the as-welded heat-affected zone. The aging affect of thermal cycling is clearly evident in the microstructure of specimens taken from the assembly after exposure. Moderately heavy carbide precipitants formed in the grain boundaries are evident in both alloys. The increased tensile strength, increased hardness, and reduction in elongation noted in mechanical testing are consistent with the aged microstructure.

7.4 ELEVATED-TEMPERATURE RUPTURE TESTS

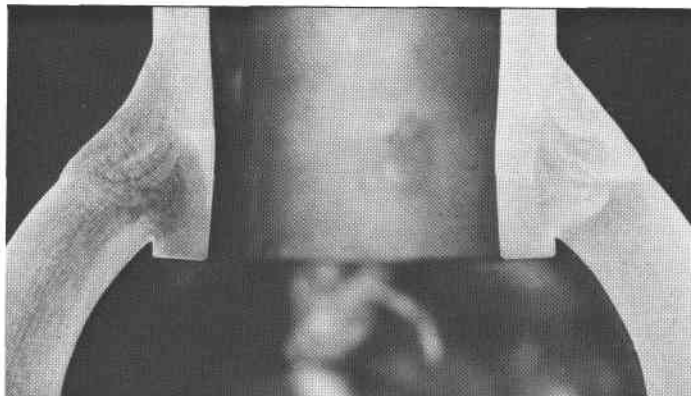
7.4.1 Test Purpose

Elevated-temperature tests-to-rupture were run on Haynes 188 and Inconel 617 tubes to determine the effects of "overheating" pressurized tubing in excess of the proposed service-temperature maximums of 830°C (1,525°F). Such overheating information was desired in terms of operational effects, potential safety hazards, and the possibility of raising the service temperature beyond 830°C (1,525°F).

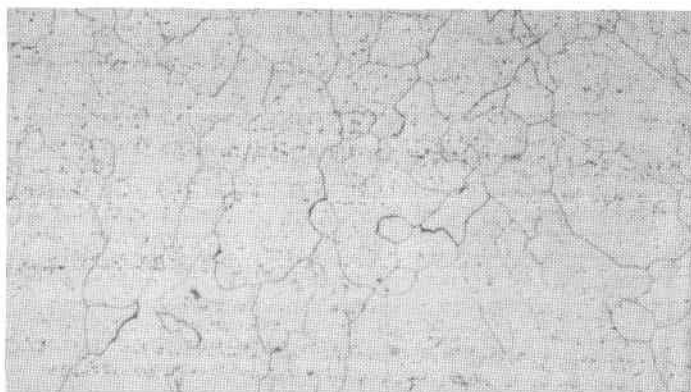
7.4.2 Test Operations

Single tubular specimens of the Haynes 188 and Inconel 617 alloys, both in the as-received and after-thermal-cycling conditions were pressurized with helium gas at 3.45 MN/m² (500 psi) and thermally cycled at successively higher temperatures until stress-rupture failure occurred. Figure 7-18 shows the test specimens, the upper two Haynes specimens being machined down prior to test to the approximate diameter and wall thickness of the Inconel tubes. A special two-furnace test bed was prepared so two test specimens could be tested simulataneously.

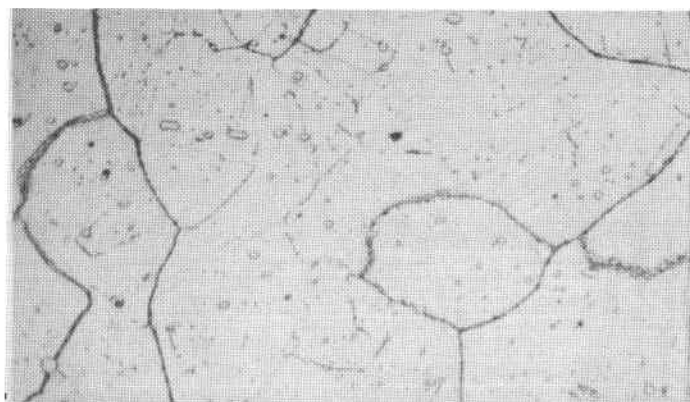
TEST ASSEMBLY WELD JOINT A



(a) HEADER-TUBE CROSS-SECTION 2X

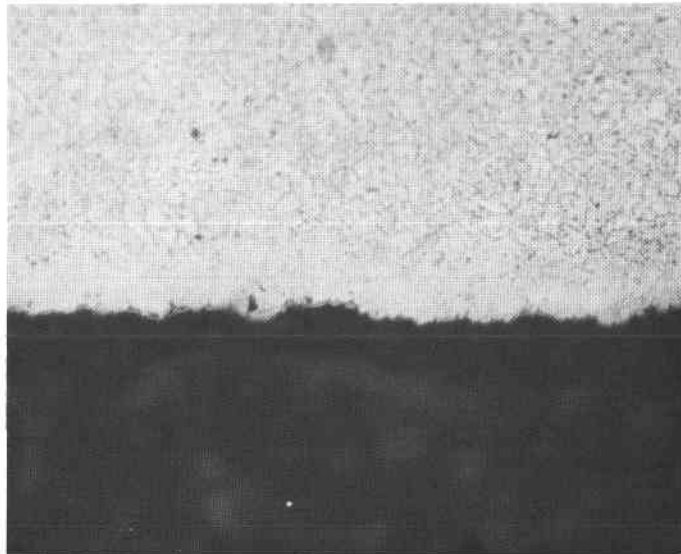


(b) HEADER BASE METAL KALLINGS ETCH 100X

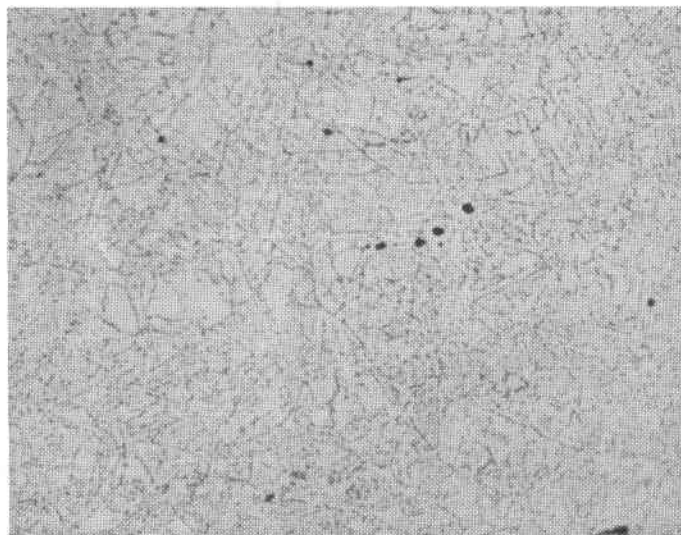


(c) HEADER BASE METAL KALLINGS ETCH 500X

Figure 7-14. Haynes 188 Tube Header Weld Joint After Test

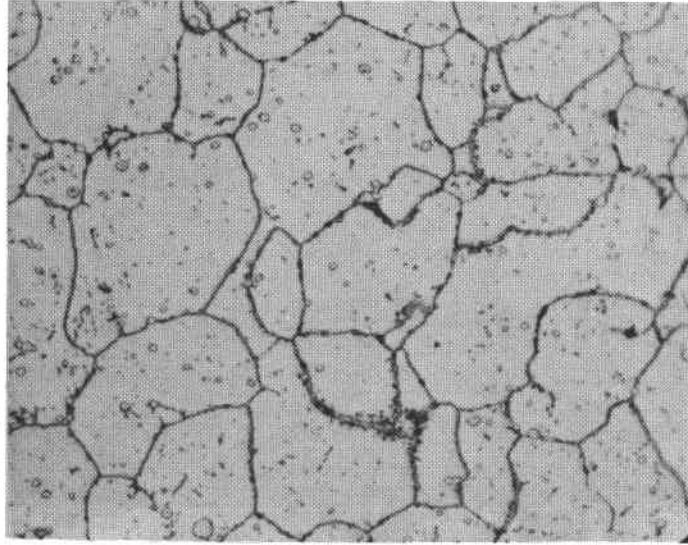


OUTER SURFACE SHOWING THIN SCALE FILM
(INTERMITTENT, LT. GRAY)

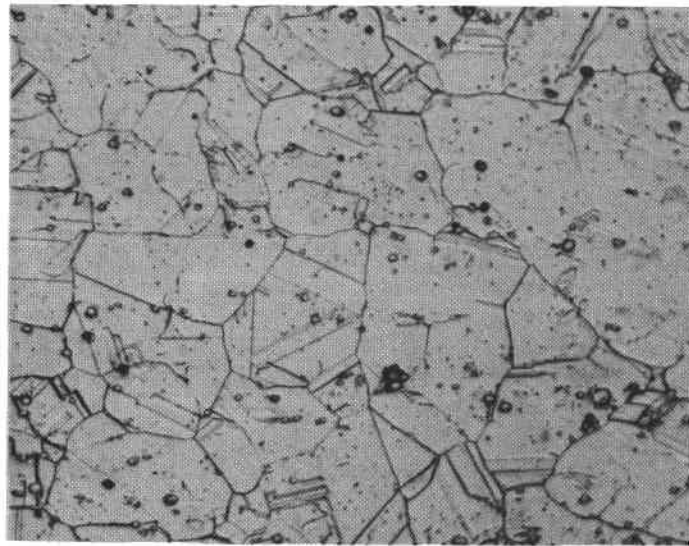


FINE GRAIN INTERIOR STRUCTURE

Figure 7-15. Outer Wall of 180° Bend Microstructure for Haynes 188 After Cycling (Kallings Etch—500 x)

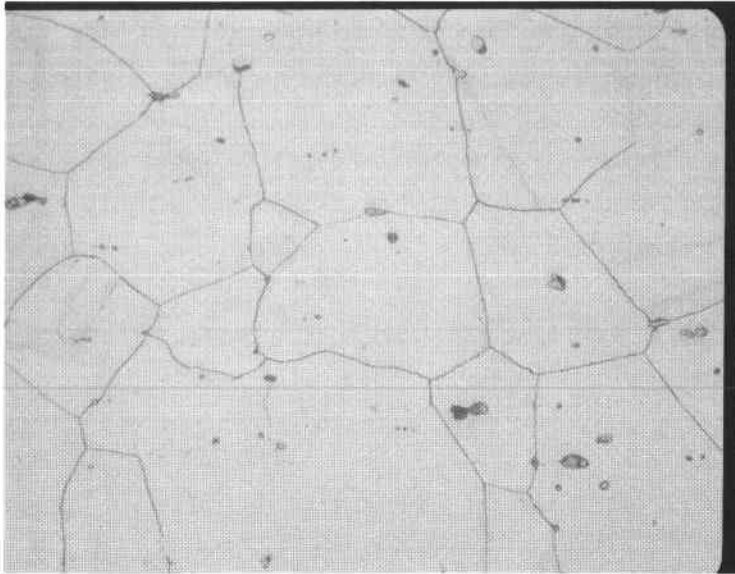


BEFORE CYCLING

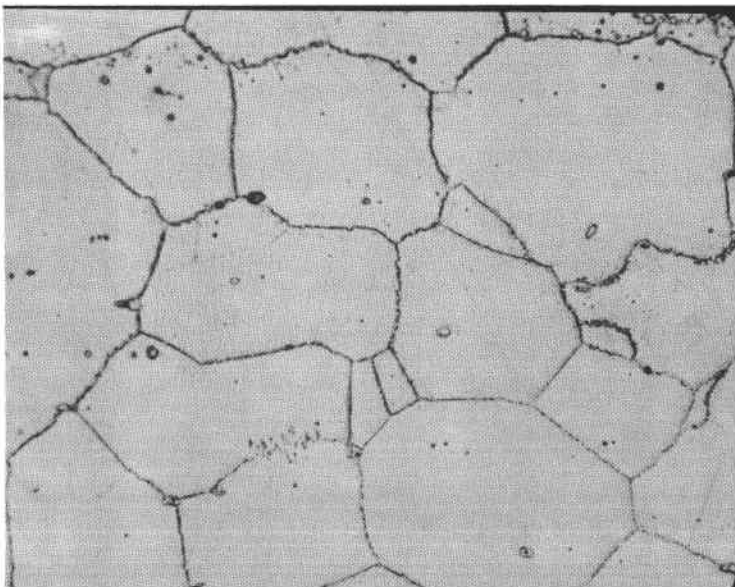


AFTER CYCLING

Figure 7-16. Haynes 188 Tubing—Microstructure, 500 x Kallings Etch



BEFORE CYCLING



AFTER CYCLING

Figure 7-17. Inconel 617 Tubing—Microstructure, 500X, Kallings Etch

Each test specimen was placed in a furnace with 10 infrared lamps irradiating the specimen. The backside of the furnace was insulated with Fiberfrax and fire brick. Figure 7-19 shows a test bed and the associated infrared lamp arrays. Figure 7-20 has a specimen in place in a test bed. Thermocouple locations are indicated on the photograph. A special excess-flow valve was used to shut off gas flow when rupture occurred. A plenum chamber was used to stabilize the pressure by allowing expanded gas to flow into it during the temperature rise.

Test temperatures were programmed to come to the desired temperature level in 2 minutes. The temperature was held for 50 minutes and then removed for 10 minutes. This test cycle was repeated 50 times at each test temperature. Test temperature levels were 871°C (1,600°F), 926°C (1,700°F), 982°C (1,800°F), 1,037°C (1,900°F), and 1,092°C (2,000°F). Between each test-cycle temperature change to the next higher level, tube diameters were measured and recorded. Figure 7-21 typifies the longitudinal gradients on the test specimens. Thermocouple locations and identifying numbers are as shown on figure 7-20.

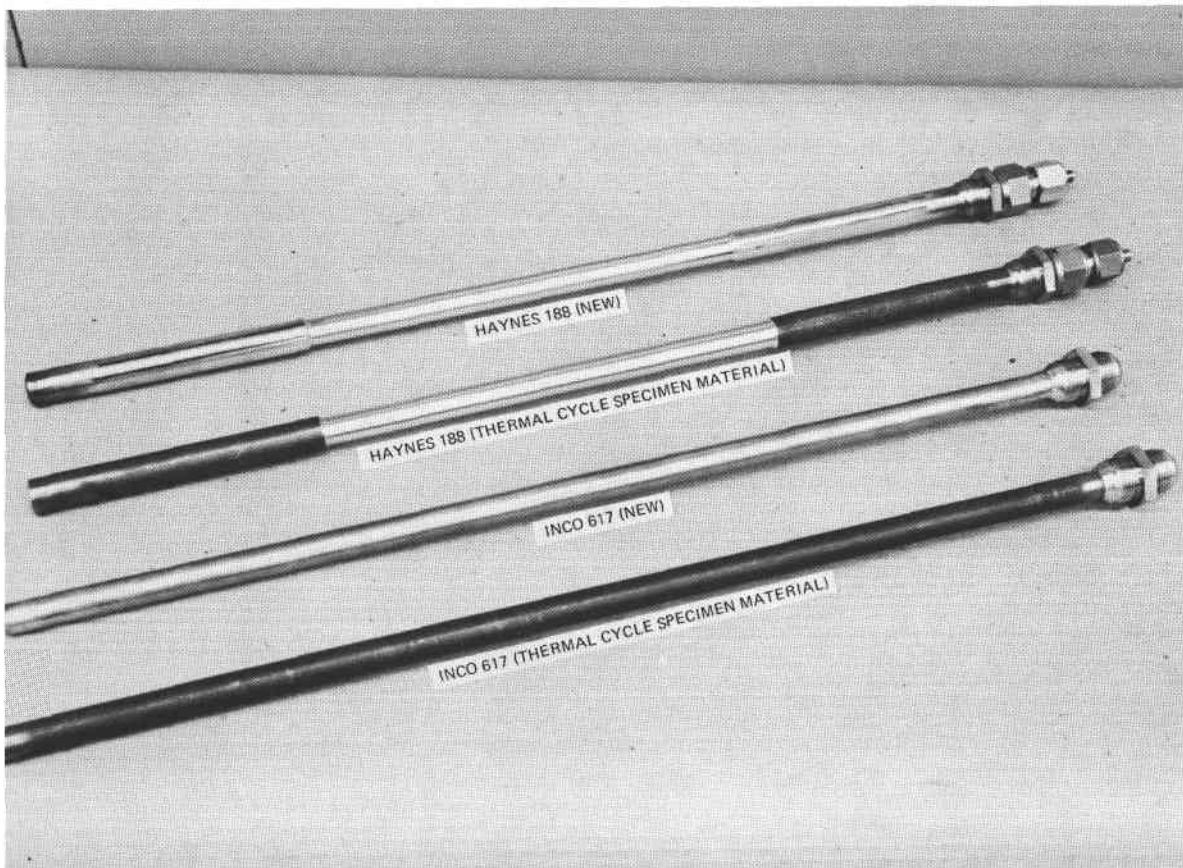


Figure 7-18. Elevated Temperature Rupture Test Specimens

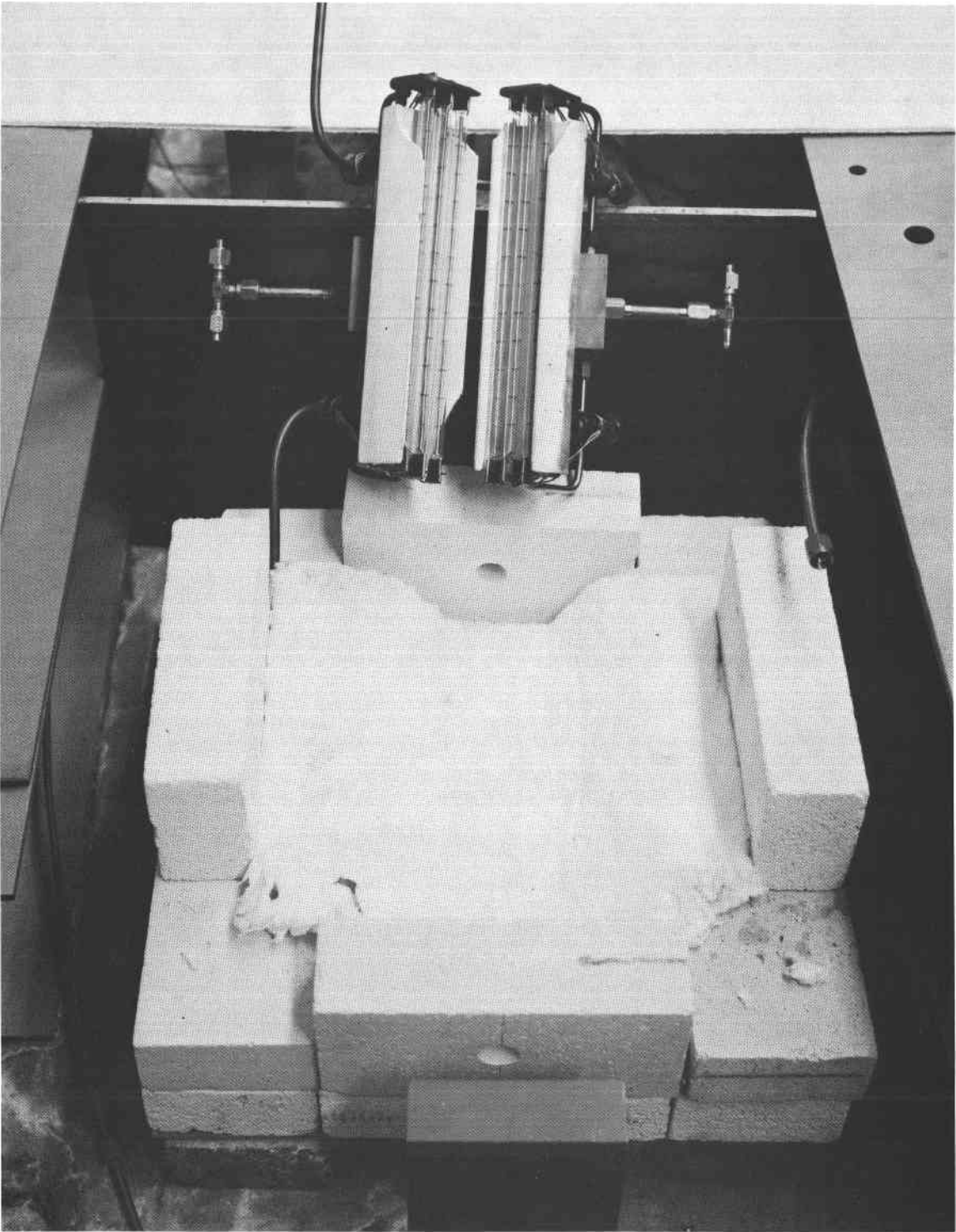


Figure 7-19. Test Bed and IR Lamp Arrays

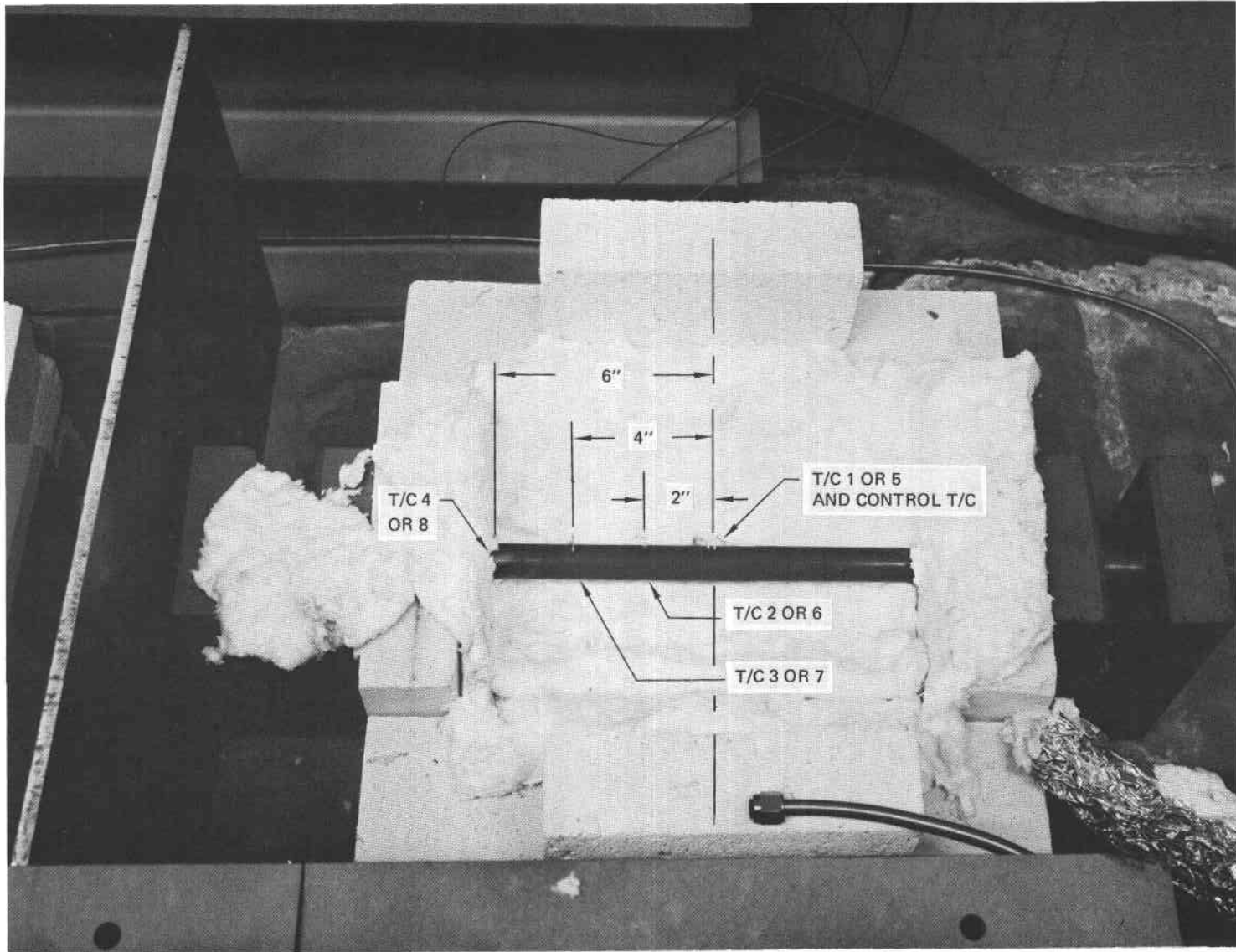


Figure 7-20. Specimen in One Test Bed (Thermocouple Locations Noted)

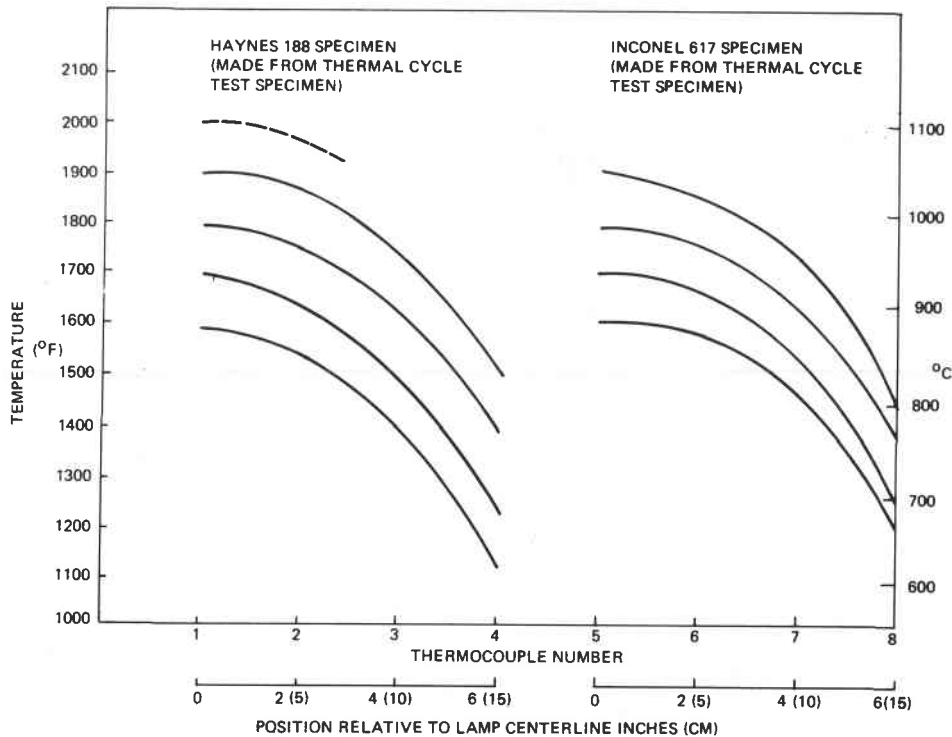


Figure 7-21. Longitudinal Temperature Gradients

7.4.3 Test Results

Prior to discussing specific test results, a few general observations should be made that have specific implications to operations and safety hazards of the receiver heat exchangers (and other high-temperature tube applications). All ruptures of the test specimens occurred in the 1,037°C (1,900°F) and 1,092°C (2,000°F) test range and all failures were noncatastrophic. Small cracks occurred and helium leakage was so slow through the fissures that the helium pressure was maintained by makeup supply when the test was on automatic (unattended operation). There were no explosions or fast crack propagation. This provides confidence that high-pressure helium can not only take periods of "overheating" without failure, but also shows that, should a failure occur, there would be no adjacent tube damage or safety hazard.

Endurance of the tubes during test is summarized in table 7-6.

Table 7-6. Cycles to Failure

Temperature °F (°C)	Haynes 188		Inconel 617	
	Exposed	As received	Exposed	As received
1600 (871)	NF	NF	NF	NF
1700 (926)	NF	NF	NF	NF
1800 (982)	NF	NF	NF	NF
1900 (1037)	NF	37	33	11
2000 (1092)	1.5	—	—	—

NF — No Failure

The Haynes tube that had been previously exposed to 10,500 cycles lasted better than the new material and reached into the 1,092°C (2,000°F) level. Previously exposed Inconel also showed itself more durable than the new, as-received material.

The tube diameters were measured at the end of each temperature level and at the end of test (after rupture). The values obtained for the Haynes 188 and Inconel 617 specimens of new material are indicated in table 7-7.

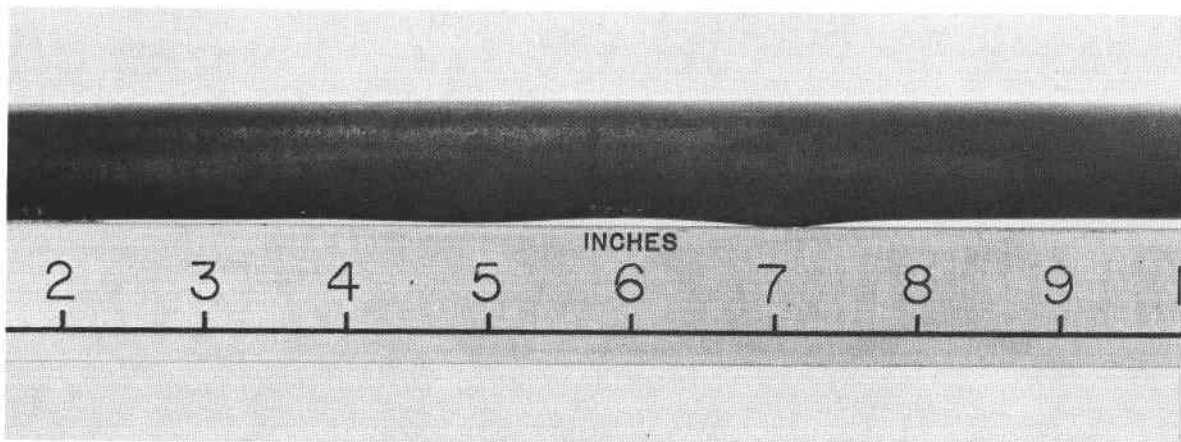
Table 7-7. New Material Specimen Diameter Data

Haynes 188			Inconel 617		
Cycle temp °F (°C)	Number of 1-hour cycles	Diameter inches (cm)	Cycle temp °F (°C)	Number of 1-hour cycles	Diameter inches (cm)
1600 (871)	0	0.849 (2.16)	1600 (871)	0	0.847 (2.15)
1600 (871)	50	0.849 (2.16)	1600 (871)	50	0.847 (2.15)
1700 (926)	50	0.849 (2.16)	1700 (926)	50	0.847 (2.15)
1700 (926)	61*	—	1800 (982)	50	0.847 (2.15)
1800 (982)	50	0.849 (2.16)	1900 (1037)	11	Tube cracked
1900 (1037)	17	0.868 (2.20)	1900 (1037)	17	0.8685 (2.21)
1900 (1037)	37	Tube cracked			
1900 (1037)	37	0.883 (2.24) (Non ruptured area)			
1900 (1037)	37	0.909 (2.31) (Ruptured area)			

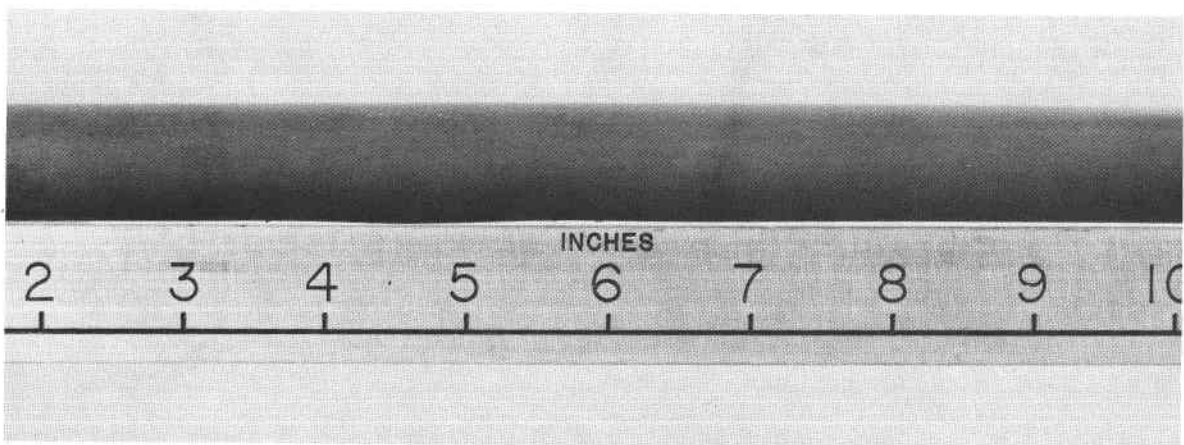
*11 cycles ran at a temperature of 1700°F (926°C) instead of 1800°F (982°C) due to a lamp failure

Figure 7-22 shows the ballooning of the new material specimens after rupture. The previously cycled specimens were similar in appearance. The rupture area of all four tubes is shown on figure 7-23.

Metallurgical specimens were removed from each tube at four locations. Typical microstructures at these locations are shown in figure 7-24 (a) through (d). Inner and outer surfaces are included in addition to a complete section of each tube wall. The locations referenced are: location 1, 1 inch from centerline; location 2, 1 inch from centerline; location 3, 2 inches from location 2; and location 4, 2 inches from location 3.



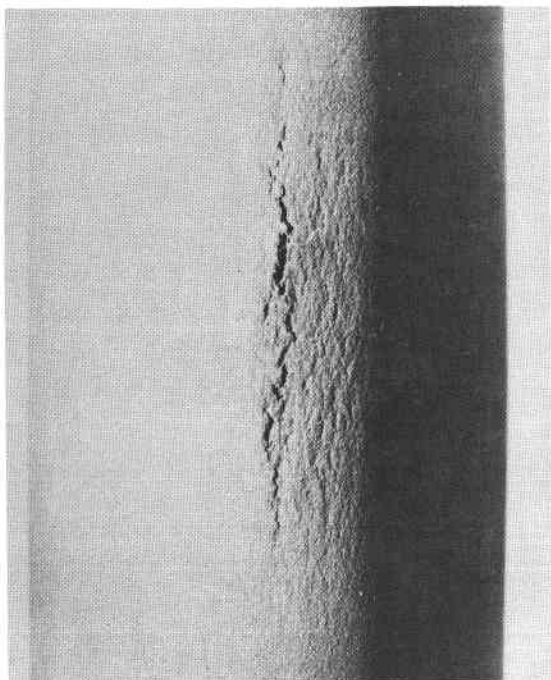
HAYNES 188 (NEW MATERIAL)



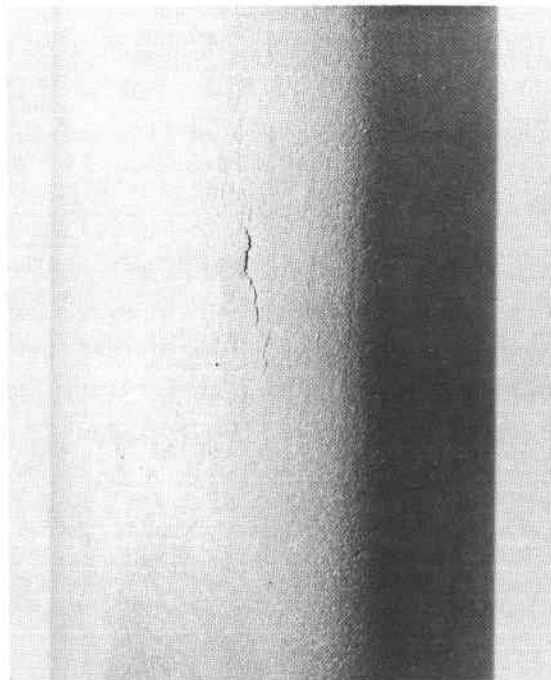
INCONCEL 617 (NEW MATERIAL)

Figure 7-22. Tube Ballooning After Rupture

NEW TUBES

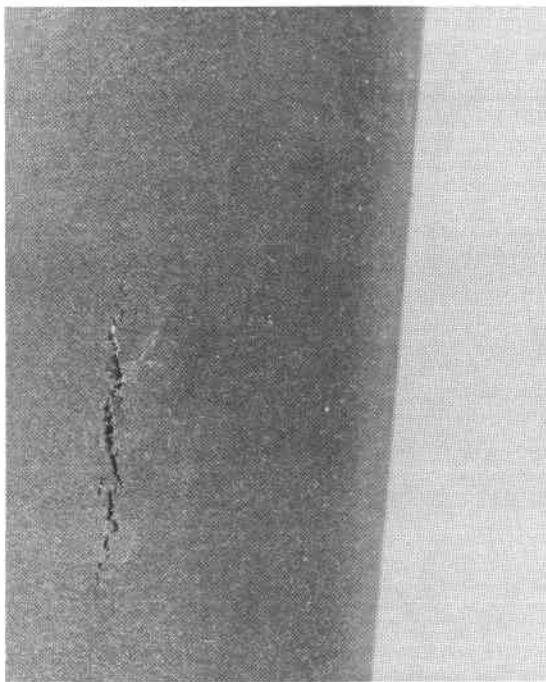


HAYNES 188

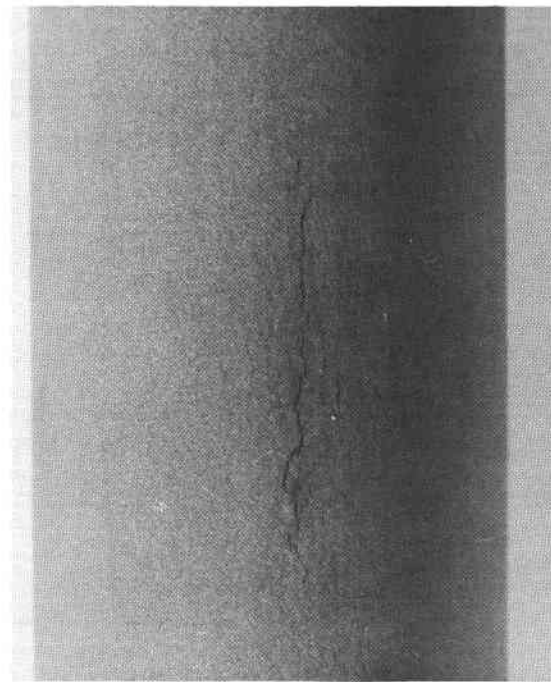


INCONEL 617

PREVIOUSLY-CYCLED TUBES



HAYNES 188



INCONEL 617

Figure 7-23. Tube Rupture Sites

LOCATION 1

LOCATION 2

LOCATION 3

LOCATION 4

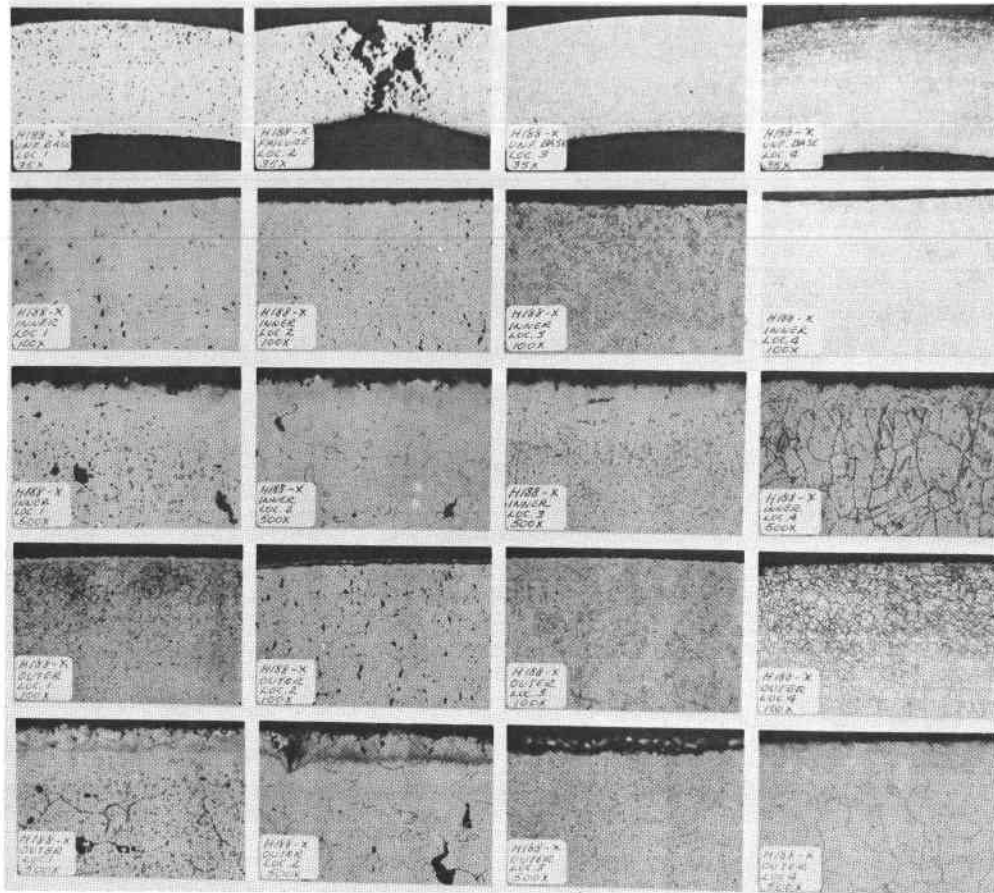


Figure 7-24 (a). Haynes 188 Microstructure (Previously Cycled Material)

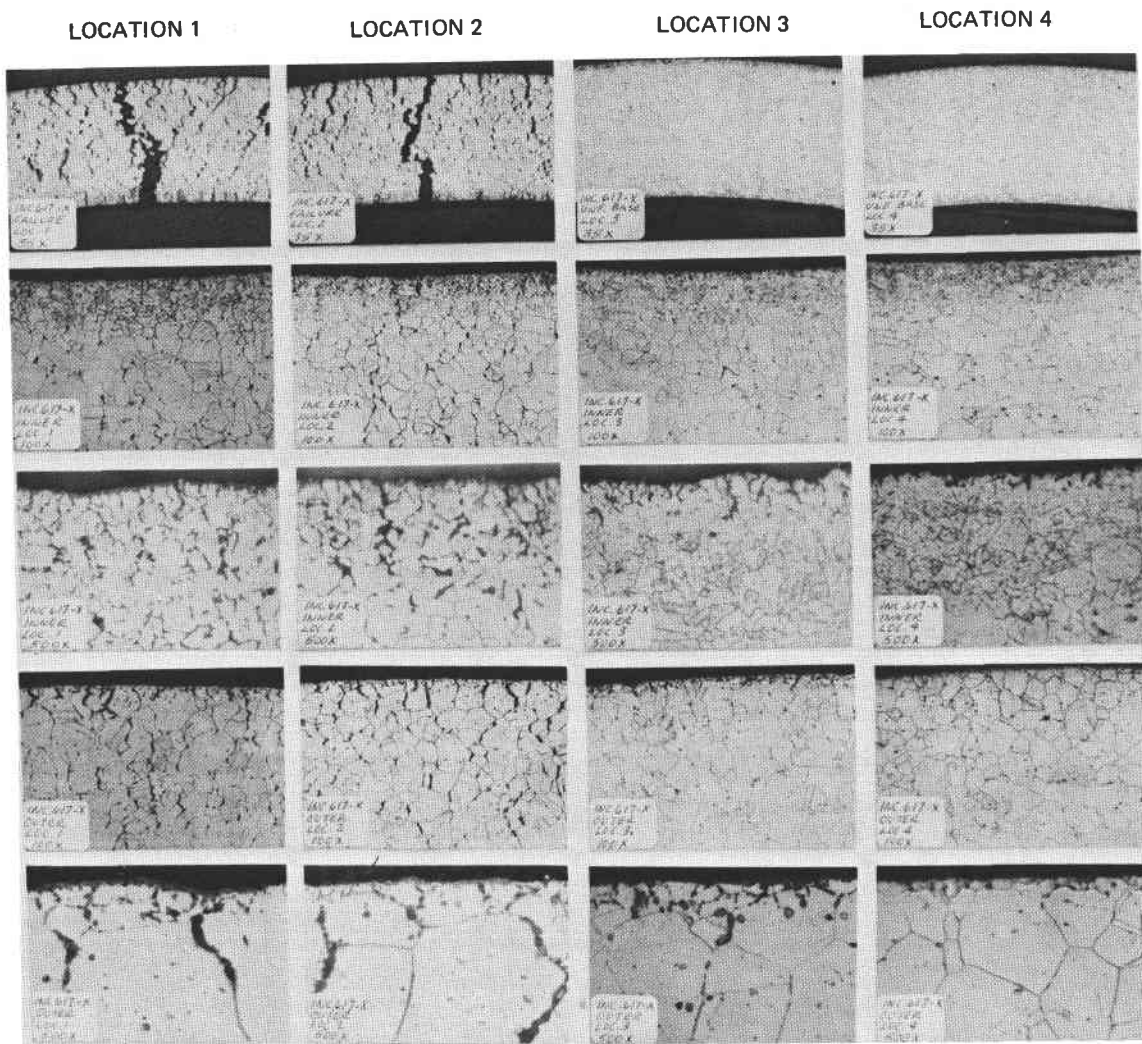


Figure 7-24 (b). Inconel 617 Microstructure (Previously Cycled Material)

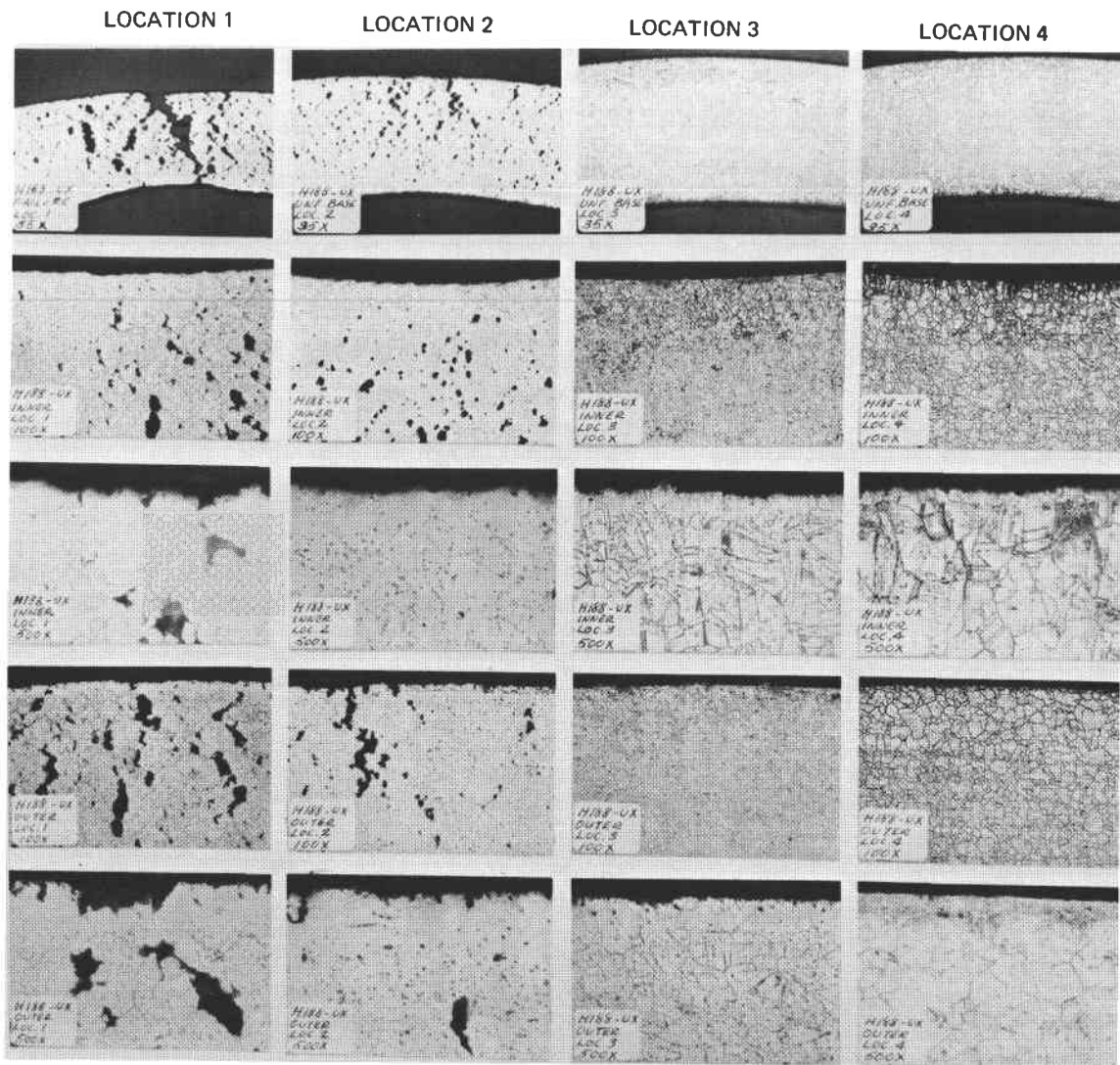


Figure 7-24 (c). Haynes 188 Microstructure (New Material)

INCONEL 617 NO PRIOR THERMAL CYCLING

LOCATION 1

LOCATION 2

LOCATION 3

LOCATION 4

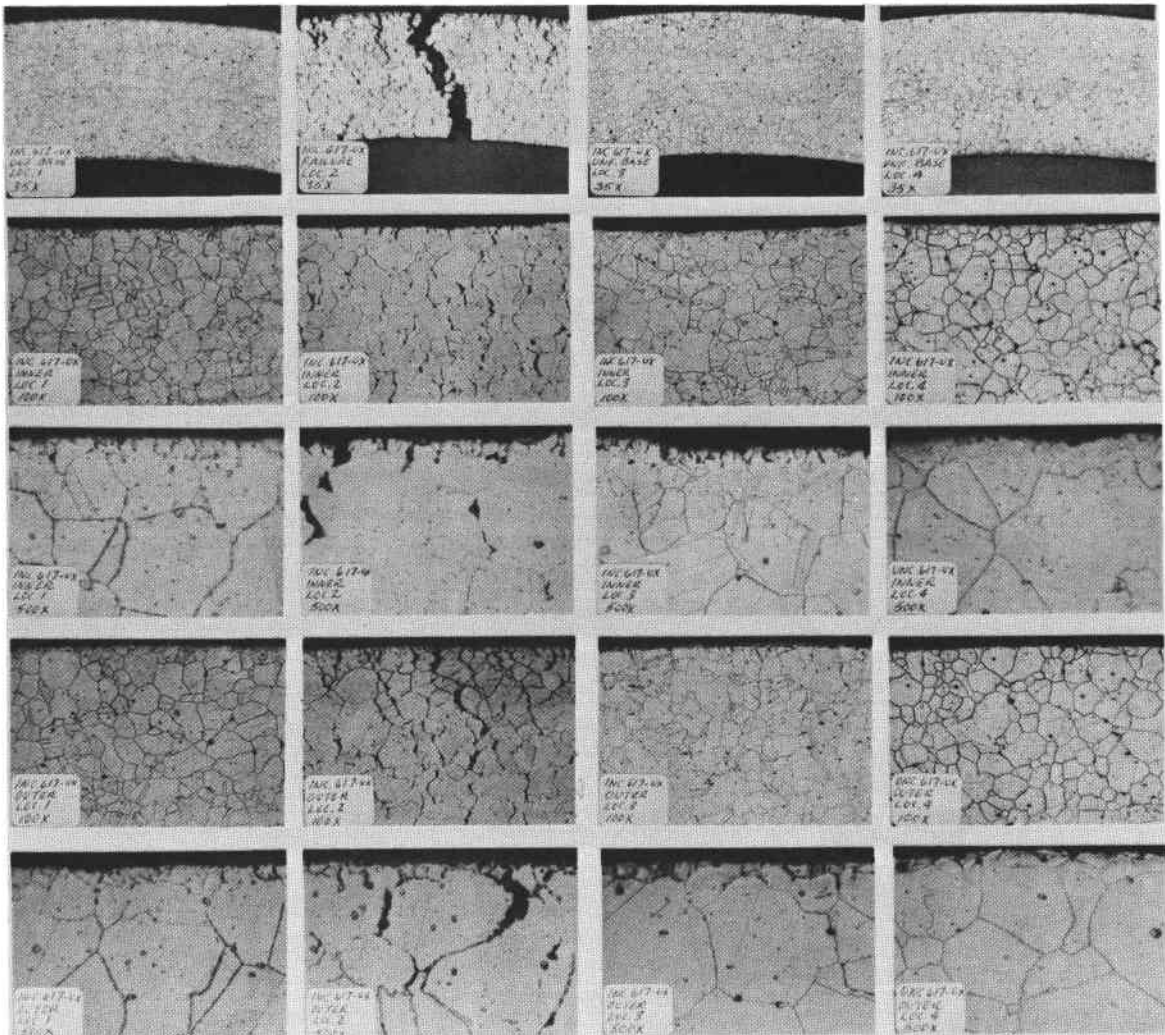


Figure 7-24 (d). Inconel 617 Microstructure (New Material)

7.5 MATERIAL TEST RESULTS

The thermal cycle tests show that:

- Haynes 188 and Inconel 617 tubing/headers in the receiver heat exchangers could survive 30 years of cycling in the environment of a solar plant.
- Temperatures and temperature differences as recorded are a sufficient simulation of expected heat exchanger conditions.
- Oxidation resistance of both materials is excellent. Scaling that occurred was tightly adherent.
- Mechanical and metallurgical properties of test materials show an aging effect. Carbide precipitation occurs that has both strengthening and embrittling effects.

In summary, the thermal cycle tests verified both Haynes 188 and Inconel 617 as excellent choices for central receiver high-temperature applications. Sufficient data have been accumulated to make a final selection between the two on the basis of performance, availability (large quantities), and economics.

The elevated-temperature rupture tests show that the materials can withstand much higher temperatures than 830⁰C (1,525⁰F) for a period of time and that the ability to withstand higher temperatures is dependent on the amount of prior operating temperature in the normal use range. All failures were noncatastrophic with relatively small fissures in the tubes. This shows the safety hazard to be small and the operational effect of a single tube failure to be isolated to itself. The Haynes 188 exhibited more ductility at the rupture than the Inconel 617.

Welded tubing, of the quality tested, would probably perform as well as seamless tubing in the receiver application. Welds were not involved in the planned stress-rupture failures, and defects in manually welded joints did not propagate during the tests.

Section 8.0

PLANT IMPLEMENTATION

The study not only considered a closed-cycle, high-temperature receiver but also included an analysis of the required commercial-size solar thermal conversion (STC) plant to implement the receiver and produce 100 megawatts of electrical power. Section 8.1 highlights the plant concept and those subsystems that, with the receiver subsystem, comprise a total powerplant.

Section 8.2 describes STC plant operation and includes the integration of subsystem elements and options. Plant performance, performance sensitivity, and costs are addressed. The transient processes in the plant and plant elements are discussed in section 8.3 and represent initial efforts to establish plant control parameters.

In Section 8.4 comparisons are made of the closed-cycle helium plant costs to that of the "strawman" plant prescribed by EPRI for that purpose.

8.1 PLANT CONCEPT

The solar plant concept with which the study began has been illustrated opposite page 1-1. A central receiver (the selected receiver reported in section 3.0) is supported by a tower in the midst of a collector field whose individual collectors track the sun and reflect available solar energy into the aperture in the receiver base. In a departure from the field depicted, the study was completed using a field of uncovered collectors prescribed by EPRI and referred to as the "strawman" field. The focused radiant energy is converted to heat in the receiver and absorbed by the transport fluid, helium. The helium then transports the heat to a turbine-generator set in the tower for the production of electrical energy. The total system concept as used in the study consists of the following subsystems: central receiver, collector field, tower, thermal transport, thermal engine, and energy storage. These are discussed in the following subsections.

8.1.1 Central Receiver Subsystem

This subsystem has been extensively described in sections 3.0 and 4.0 of this document. The subsystem function is to receive the reflected radiant energy concentration and to distribute the energy for controlled heat transport.

Specific functional requirements are to:

- Receiver reflected energy from the collector field subsystem and absorb the energy in the receiver
- Provide high-temperature heat exchanger tubes to receive the cavity heat energy and to contain the heat transport fluid
- Provide heat exchanger tube/panel distribution to maintain controlled temperatures
- Provide insulation to prevent excessive heat loss to receiver exterior

8.1.2 Collector Field Subsystem

The collector field subsystem consists of a number of collectors (reflectors) arranged about the base of the receiver tower. The subsystem performs the function of receiving the solar energy and reflecting that energy through the aperture of the receiver. The requirements for the subsystem are to:

- Provide surfaces for receiving and reflecting solar insolation
- Provide for tracking and pointing to reflect solar energy continuously to the receiver subsystem aperture plane
- Protect vulnerable components from environmental damage
- Provide reactance to contingency situations
- Accept and execute commands
- Provide for power and signal cabling, including supporting structure, clamps, and restraints

The collector field size, performance and unit costs were prescribed by EPRI for a standard plant module. Boeing had the freedom to vary all field parameters except cost if the performance of the STC plant could be improved.

8.1.3 Tower Subsystem

The primary functions of this subsystem are to support the elevated central receiver and to enclose all other major equipment. It is the major system element where the seismic risk and wind loadings discussed in section 4.3 apply to the design, particularly in volume, base size, and turbomachinery location.

The height to the receiver aperture plane is 260 meters (855 feet) as baselined by EPRI; the actual tower height is approximately 230 meters (755 feet).

8.1.4 Thermal Transport Subsystem

This subsystem consists of the heat transport fluid, helium, and its circuit. Its primary function is to collect and transport the heat required for power generation and/or energy storage. More specifically, the subsystem has the requirements to:

- Provide helium working fluid and reserve supply
- Provide pressure regulators, control valves, and temperature sensing at all critical helium circuit locations
- Deliver thermal energy to the thermal engine subsystem for immediate conversion to electrical energy and/or to the energy storage subsystem for deferred conversion

After attaining the nominal temperature rise of 278°C (500°F) in each of the central receiver's 210 heat exchanger panels, the helium goes through a main collector manifold and down one of the two downcomers to the tower top. There, a single downcomer transports the helium to the turbine(s). After passing through the recuperator (low-pressure side), the helium flows through the coolers, the high-pressure compressors, and back through the recuperator (high-pressure side). From there the helium goes up a single pipe to the tower top. The circuit is completed by helium flowing up through the risers to the manifolds and headers supplying the receiver heat exchangers. Tubing sizes were selected to keep pressure losses in the supply and return lines at a small percentage (about 5%) of the total system pressure of 3.45 MN/m^2 (500 psi). Excellent materials are available for the high-temperature tube applications in Haynes 188 and Inconel 617. Helium mass flow rate is approximately 165 to 227 kilograms/second (360 to 500 pounds/second).

8.1.5 Thermal Engine Subsystem

The normal engine cycle baselined for the study was a closed-loop recuperative Brayton cycle, using helium as a working fluid. The function of the subsystem is to provide for conversion of heat energy to electrical energy. The subsystem's specific functional requirements are to:

- Receive thermal energy from the heat transport subsystem

- Provide the necessary turbomachinery, recuperators, coolers, and associated equipment to pressurize the fluid, generate shaft power, and cool the heated fluid
- Maintain temperature and pressure at all subsystem control points
- Maintain shaft power during generating periods
- Accept and execute necessary commands

The thermal engine subsystem consists of a turbine-generator set, compressor(s), a recuperator, and a precooler. The study concentrated primarily on a helium gas turbine-generator with the capability to produce 100 megawatts of electrical power. Section 5.0 discusses the cycle, the turbomachinery, and the parametric analysis leading to subsystem definition.

8.1.6 Energy Storage Subsystem

Various thermal energy storage concepts were examined and screened for the energy storage subsystem definition. These were all source-side types rather than load side, the distinction being a location where storage can supply the turbine with stored heat. The subsystem has the primary function of supplying heat for conversion to electrical power during noninsolation periods and for temporary situations when solar power is interrupted or reduced. More specifically, the subsystem has the functional requirements to:

- Receive thermal energy from the thermal transport subsystem
- Deliver thermal energy to the thermal engine subsystem for direct conversion to electrical power
- Provide containment for thermal energy storage media
- Provide thermal and temperature control
- Provide control equipment for the storage and the retrieval of the thermal energy
- Provide sufficient thermal storage capacity to meet the performance requirements of the STC plant for short-term (buffering) protection and long-term electrical production from storage

Energy storage subsystem concepts are discussed in section 6.0 and concept integration into plant operation in section 8.3.

8.1.7 Other Subsystems

Several other subsystems could be added to the list for a complete STC plant. These areas would cover:

- Thermal protection and control
- Command and control
- Load interfacing and control
- Power distribution
- Maintenance and spares

All items but the first, which is treated in the report on subsystem-by-subsystem basis, were outside the scope of the study.

8.2 PLANT OPERATION AND INTEGRATION

The operation and control of the STC powerplant, with source-side thermal energy storage for source leveling, involves an understanding of the source profile, the load profile, and the plant operating policy. A limited amount of work has been done in this area as a part of the Aerospace "Mission Analysis" work and as a part of current STC powerplant utility impact studies. The approach used in the plant operating policy will affect the resultant energy economics and will, to some extent, affect the design decisions and operating requirements of the various plant subsystems.

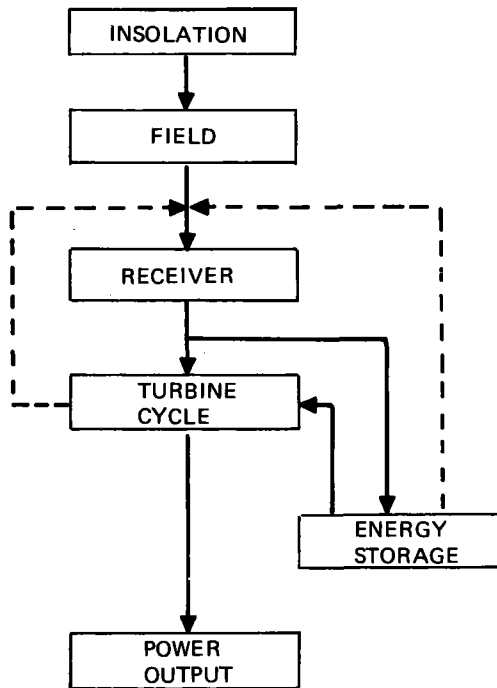
A math model of the high-temperature STC powerplant was developed as a part of the current study to support the plant design and performance analysis. The model predicts the plant performance on an hour-by-hour daily cycle basis, including the effects and performance of all of the major plant subsystems.

A technical summary of the elements of the plant-operation math model is included in this section. Representative STC powerplant operating characteristics and the sensitivity of the resultant energy costs to collector area and storage system characteristics are presented at the end of this section.

The principal objective of this work is to relate subsystem design requirements to the daily insolation cycle and the basic operating requirements of the powerplant. Consequently, it is appropriate to simplify the demand profile and plant operating policy, recognizing that the resultant plant performance estimates are limited by these simplifications. The work reported here is based on a flat demand profile that begins at 8 a.m. The plant operating policy simply provides energy for storage on an as-available basis with first priority to direct generation of electric power.

8.2.1 Plant Operation Computer Program

A simplified schematic of the plant-operation math model is shown in figure 8-1. Each of the major subsystems in the powerplant functional flow is characterized in a separate program module. The effects of the primary operation parameters for each subsystem are included in these program modules.



- Insolation and field modeled as hour by hour solar heat into the receiver aperture

- Receiver modeled by efficiency

$$\eta_R = \frac{\text{Heat to helium circuit}}{\text{Solar heat into receiver}}$$

- Turbine generator cycle efficiency, mass flow, and He temperature distribution all modeled
- Energy storage — includes parasitic losses, thermal losses and He temperature distribution
- Fixed level power output — model determines capacity in hours

Figure 8-1. Plant Operation Computer Program Schematic

The control logic for the program provides the framework for the simulation of the plant as a function of time. At each time step the current thermodynamic state points shown in figure 8-2 are combined with the insolation input to determine heat rates throughout the plant. These rates are integrated to establish new thermodynamic state data, completing the analysis cycle for the time step. The results of each complete daily cycle are analyzed to determine component efficiency, overall plant efficiencies, component energy consumption, and component energy output. Printed results include thermodynamic state data at each time point, daily analysis results, and the overall results with energy economics of several representative days analyzed as a yearly operation.

At each time point the control logic determines the plant operating mode and calls up the necessary program modules to evaluate each plant function. A brief technical description of each of the subsystem math models and the plant control logic is included in the following paragraphs.

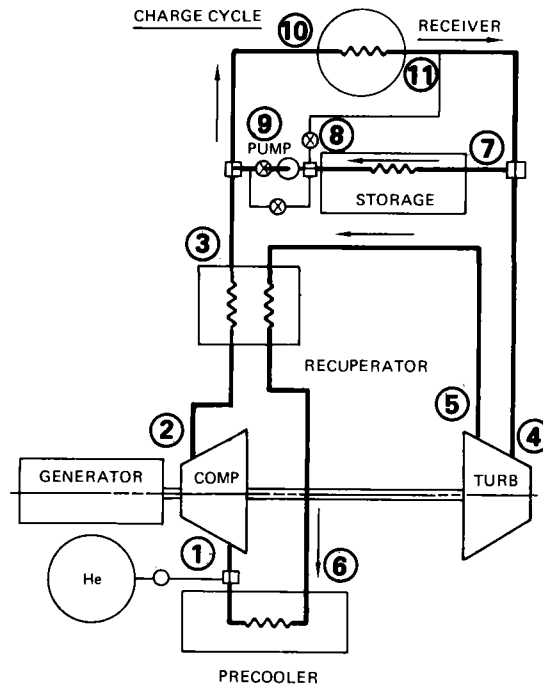


Figure 8-2. Thermodynamic State Points

Insolation and Reflector Field Model. Hourly insolation data for each day to be analyzed are the primary input variable in the program. Tables of reflector field efficiency are combined with the hourly insolation data and the collector area to produce the necessary heat input. The field efficiency tables are a function of time for each day of the year and include tracking efficiency, mirror reflectivity, and receiver intercept efficiency.

Receiver Model. The receiver performance analysis is based on a thermal scaling analysis of the baseline receiver. An iterative procedure is used to solve for the receiver power output as a function of the average helium temperature, the receiver geometry, and solar heat into the receiver. The thermal analysis, as described in section 3.2, includes the radiant heat losses through the aperture,

convective heat losses, reflective solar heat losses, and conduction losses through the receiver wall.

Turbine Performance Model: The turbine-cycle performance and operating condition analysis is based on the data presented in section 5.4. The thermal-cycle conversion efficiency and recuperator outlet temperature are modeled as tabular functions of turbine inlet temperature. These data are used over the operating range of turbine inlet temperature to compute helium mass flow requirements needed to maintain a constant electrical power output.

Plant output power would normally decrease with a decreasing turbine inlet temperature caused by reduced solar input or operation from the storage system. However, by increasing the pressure level (i.e., mass flow) of the system to compensate for the reduced thermal efficiency, the electrical output can be maintained at the desired level. The pressure level/mass flow ratio variation with turbine inlet temperature is also presented in section 5.4.

The turbine will also be operated to produce power to meet instantaneous demand. This is accomplished by maintaining a fixed turbine inlet temperature while changing pressure level and mass flow to follow the demand load. The selected modeling approach assumes that the turbogenerator thermal-cycle efficiency is a function mainly of the turbine inlet temperature, which remains constant with varying electrical output during plant operation in this mode.

Thermal Energy Storage (TES) Model. The purpose of the energy storage model is to compute the parasitic power requirements and the thermal performance of the storage device and to maintain an accounting of the energy transferred to and from storage. Each of the three basic TES devices has a different thermal behavior, as discussed in section 6.3.1, and is represented by a separate math model. These models range in complexity from finite-difference solutions of the energy balance equations to simple scaling models of parasitic power requirements. A technical description of the math models for each of the three thermal storage devices is presented in section 6.3.1.

Plant Control Logic. The following plant operation policy is the framework of the powerplant control logic.

- General output to meet demand load is always first priority.

- Insolation energy in excess of generator demand is always used to charge storage.
- Demand load profile is flat with a specified start time (normally taken as 8 a.m.).
- Early morning insolation prior to generator startup is used to charge storage.
- Insolation energy in excess of storage limit is rejected in the reflector field.
- Storage is charged in a separate flow circuit (see figure 8-3).
- Storage is discharged in a series circuit with receiver (see figure 8-3).
- Powerplant operates as a stand-alone system with the turbine providing all power requirements, including grid demand and storage parasitic power.
- Plant operation is based on a complete daily cycle; daily operation is complete when storage is nearly depleted.
- Plant begins daily operation with storage nearly depleted.

8.2.2 System Operating Characteristics

A representative daily plant operating cycle is shown in figure 8-4. The cycle shown here is typical of the transient nature of the plant operation when managed in accordance with the operating policy described in the preceding section. The minimum turbine energy consumption under full load is $113 \text{ MW}_{\text{th}}$ and the maximum heat in the helium circuit, for the case shown in figure 8-4, is over $250 \text{ MW}_{\text{th}}$. Consequently, the powerplant reaches a peak solar multiple of over 2.2 with the summer insolation.

Daily cycle data are generated by the plant operation model for each of four representative days covering the four seasonal extremes. These data are analyzed to determine the energy output on a daily basis and then used to establish the yearly energy output of the powerplant. Yearly plant operation data for the baseline receiver with all three TES devices are presented in the following paragraphs.

Insolation Data. The insolation values used in the development of plant operation parameters are based on clear-day specular insolation data taken at Inyokern, California, in 1963. Insolation profiles for four representative days were taken from the data tapes assembled by the Aerospace Corporation.

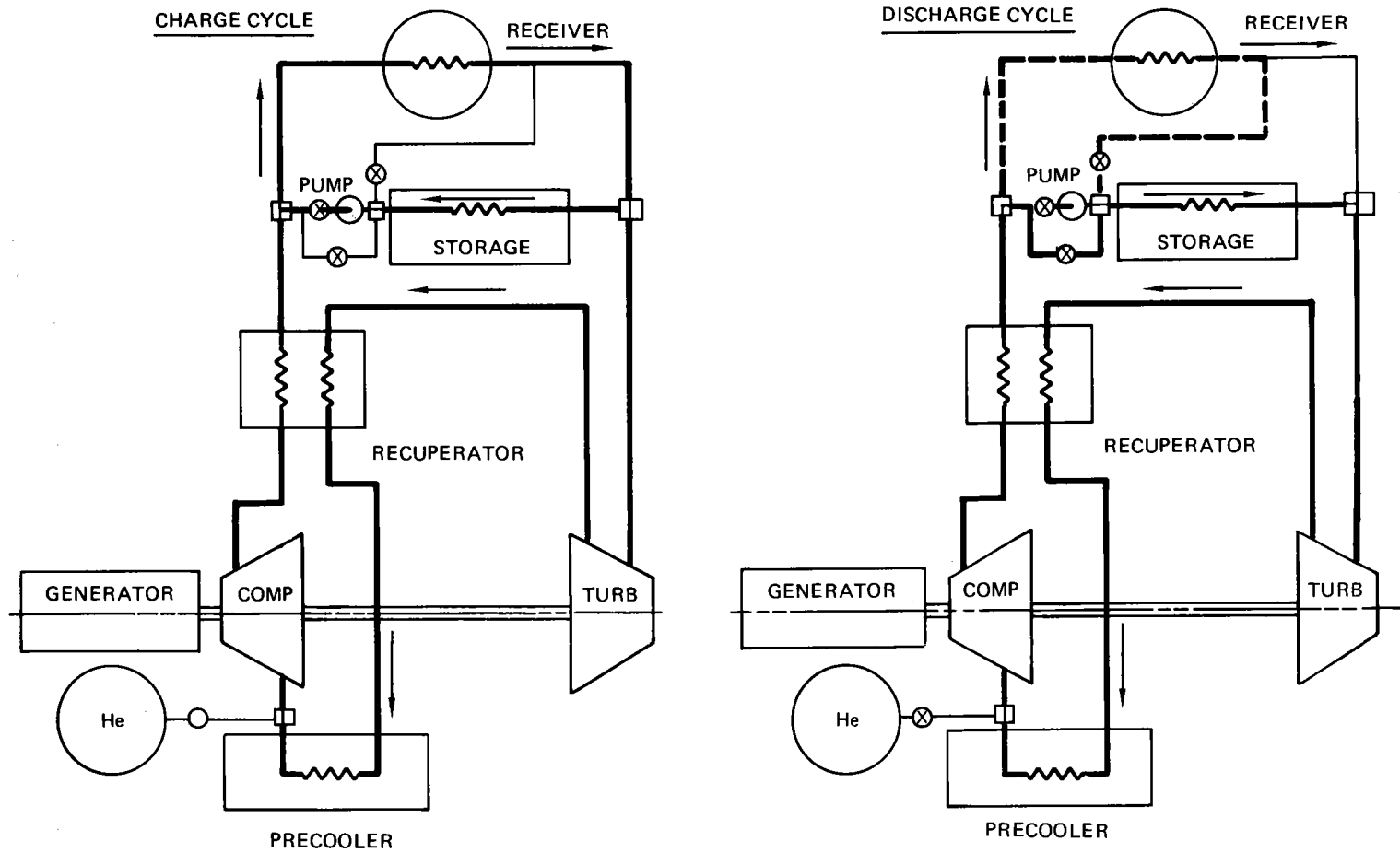


Figure 8-3. Storage/Plant Schematic

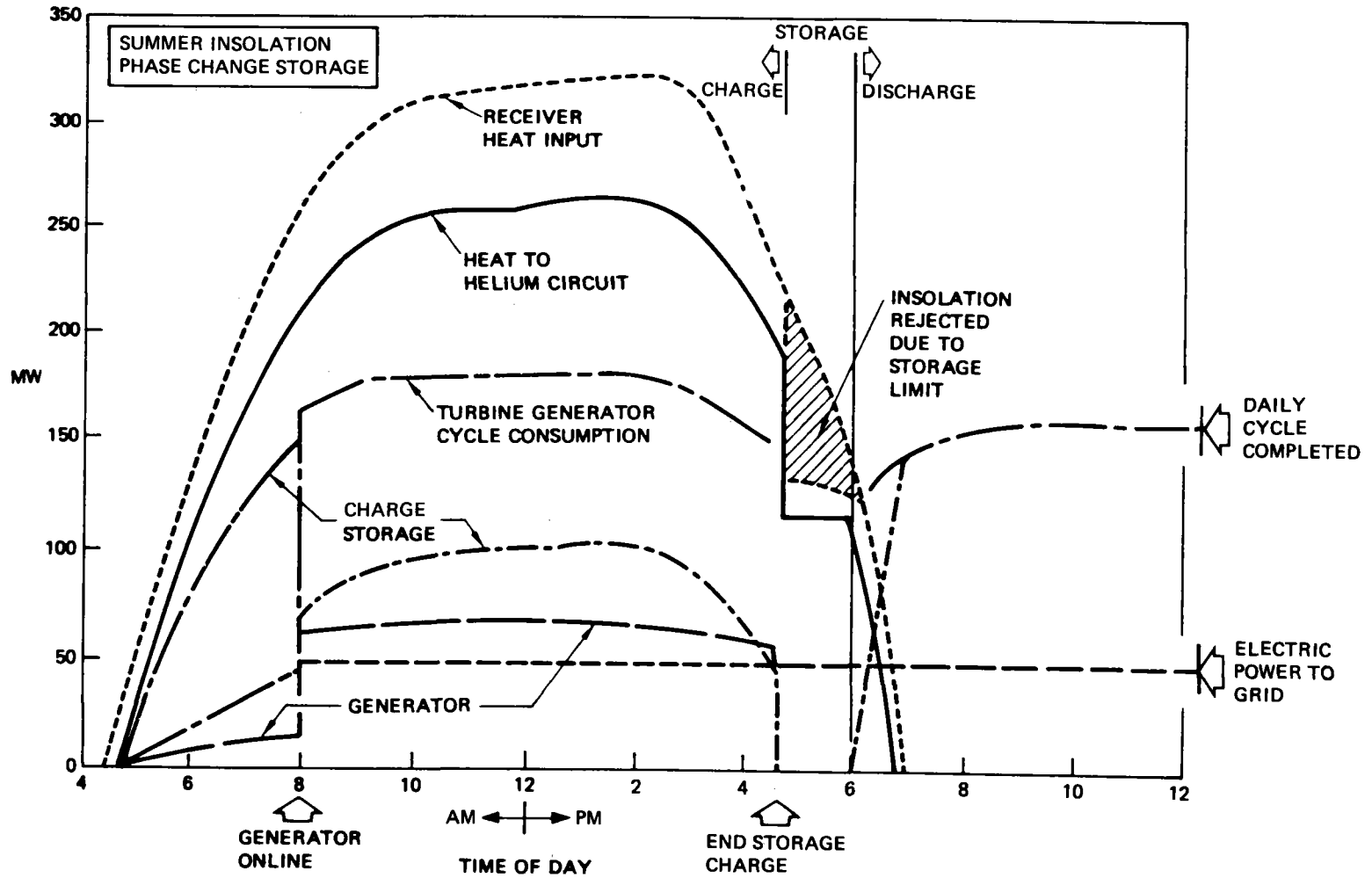


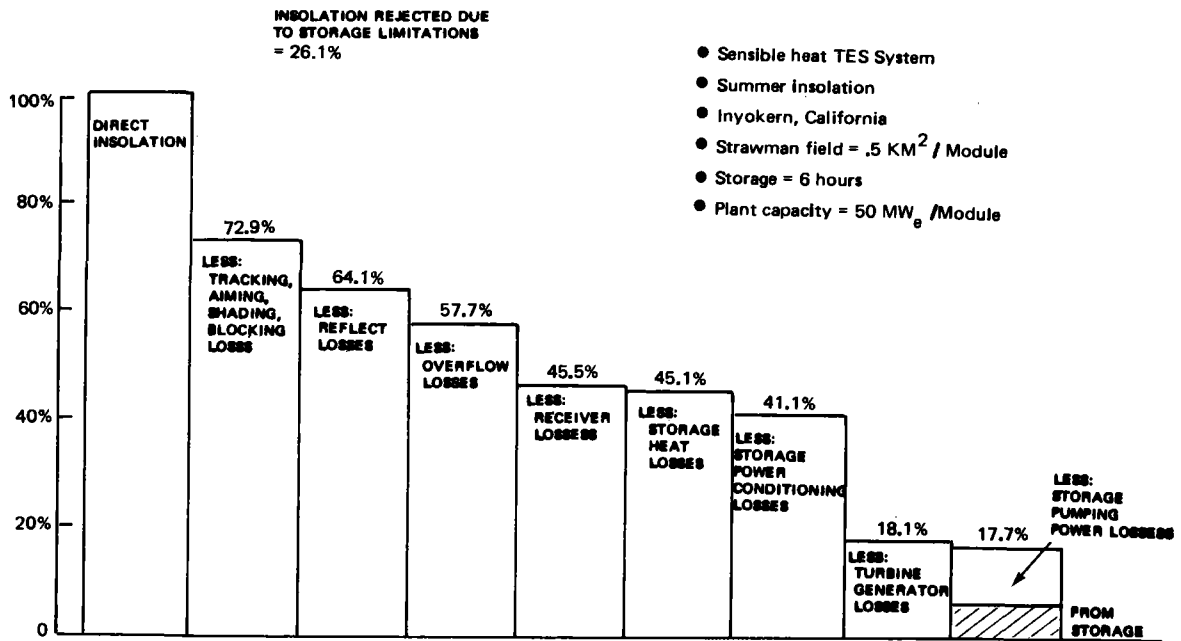
Figure 8-4. Plant Operation-Representative Daily Cycle (Power Distribution) (Latent Heat TES System)

Yearly Plant Operation Data. Yearly plant operation data for the preferred receiver and plant configuration with the three TES device alternatives are shown in figures 8-5, 8-6, and 8-7. These data are based on the 0.5 km² "strawman" module field and a plant module capacity of 50 MW_e. The bar chart at the top of each figure is an analysis of the daily cycle energy losses for the summer insolation condition. The tables at the bottom of each figure summarize the key performance parameters for each of the four insolation conditions. The analysis of the energy losses shows, as expected, that the sensible-heat storage device gives the best energy output for the powerplant. This is a direct result of the increase in round-trip efficiency of the storage device, which is reflected primarily in a reduction in storage system pumping losses. Round-trip efficiency is the ratio of total energy (electrical equivalent) out of the storage device to that used to charge and operate the device.

The baseline phase-change storage system, as described in section 6.2, is a fluoride salt with a melt temperature approximately midway through the temperature swing of the receiver at its design point operation. A simple segregation of the molten salt heater with two or three properly selected melt temperatures will significantly improve the round-trip efficiency of the latent-heat system. This approach is being considered in the storage system follow-on work.

The data on figures 8-5, 8-6, and 8-7 show that the storage concept significantly affects the performance and design requirements of the STC powerplant. There are also significant cost differences among the storage devices. Consequently, an evaluation of the total system cost per unit of throughput energy is required in the final system selection. Initial studies of this type have been carried out, and the results are presented below.

Plant costs in dollars per kilowatt are computed in the following manner, based on procedures and costing parameters outlined by EPRI in its "strawman" requirements. Total direct plant cost is computed by summing the costs associated with each of the plant subsystems. Contingency allowance and spare parts allowance, indirect costs, and interest during construction are added to this cost. The final summing of costs yields the total capital cost in dollars per kilowatt. Figure 8-8 summarizes the costing procedure and gives the subsystem costs when the "strawman" field is utilized. This situation provides the most power production, but receiver costs must be updated.



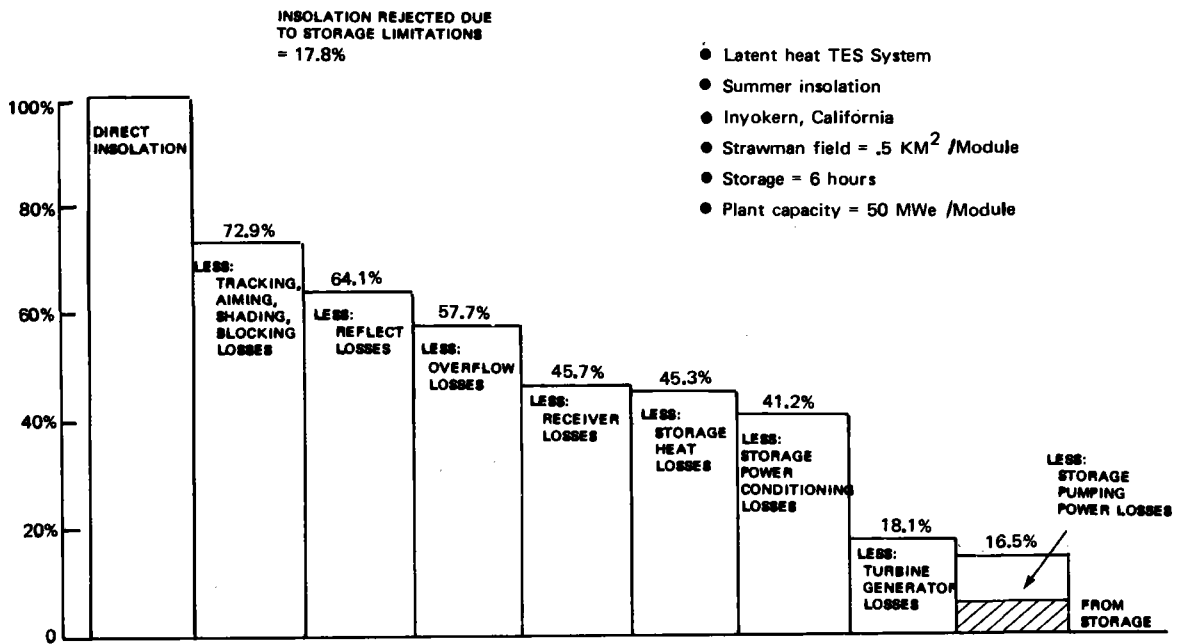
Daily Plant Performance: Closed Cycle Helium

Season	Plant operation (hours)	*Plant efficiency η_p	Max-min generator capacity (MW _e)	Max receiver mass flow (kgm/sec)	Max turbine mass flow (kgm/sec)	Max storage mass flow (kgm/sec)	Charge to discharge ratio	Round trip storage efficiency	Daily storage (hours)
Winter	12.2	30.7, 15.4	58-50	168	195	195	0.58	0.68	3.5
Spring	16.4	31.0, 17.3	66-50	225	195	195	0.76	0.74	6.0
Summer	16.9	30.7, 17.7	67-50	231	195	195	0.74	0.73	6.0
Fall	15.1	30.9, 17.5	62-50	192	195	195	0.64	0.74	6.0

*Plant efficiency definition

$$\eta_p = \frac{\text{Net generator energy}}{\text{Heat energy input to receiver}} = \frac{\text{Net generator energy}}{\text{Specular insolation energy}}$$

Figure 8-5. 4-Day Performance Summary (Sensible Heat TES System)



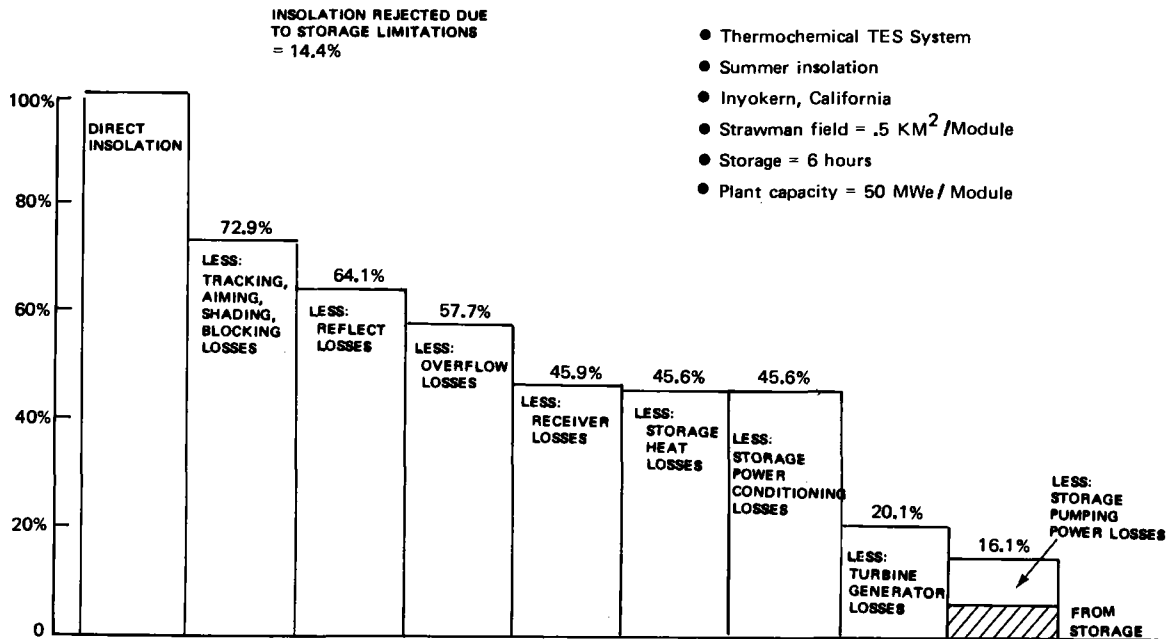
Daily Plant Performance Closed Cycle Helium

Season	Plant operation (hours)	*Plant efficiency η_P	Max-min generator capacity (MW _E)	Max receiver mass flow (kgm/sec)	Max turbine mass flow (kgm/sec)	Max syorage mass flow (kgm/sec)	Charge to discharge ratio	Round trip storage efficiency	Daily storage (hours)
Winter	11.7	29.6, 14.9	63-50	196	195	195	0.49	0.60	3.1
Spring	16.3	29.1, 16.3	70-50	256	195	195	0.72	0.64	6.0
Summer	16.8	28.6, 16.5	71-50	259	195	195	0.72	0.62	6.0
Fall	14.3	29.1, 16.5	67-50	233	195	195	0.63	0.64	5.3

*Plant efficiency definition

$$\eta_P = \frac{\text{Net generator energy}}{\text{Heat energy input to receiver}} = \frac{\text{Net generator energy}}{\text{Specular insolation energy}}$$

Figure 8-6. 4-Day Performance Summary (Latent Heat TES System)



Daily Plant Performance Closed Cycle Helium

Season	Plant operation (hours)	*Plant efficiency η_p		Max-min generator capacity (MW _E)	Max receiver mass flow (kgm/sec)	Max turbine mass flow (kgm/sec)	Max storage mass flow (kgm/sec)	Charge to discharge ratio	Round trip storage efficiency	Daily storage (hours)
Winter	10.6	29.2	14.7	72-50	179	133	92	.55	.56	2.9
Spring	15.8	27.9	15.6	81-50	212	149	92	.76	.58	5.8
Summer	16.9	27.9	16.1	82-50	215	151	92	.78	.57	6.0
Fall	13.8	28.0	15.9	77-50	196	142	92	.66	.57	4.8

*Plant efficiency definition

$$\eta_p = \frac{\text{Net generator energy}}{\text{Heat energy input to receiver}} \quad \frac{\text{Net generator energy}}{\text{Specular insolation energy}}$$

Figure 8-7. 4-Day Performance Summary (Thermochemical TES System)

The next step is to arrive at a levelized, or average, plant cost over its total lifetime. This is done by multiplying the total capital cost by the fixed charge rate, expressed in percent per year. The fixed charge rate takes into account the cost of long-term debt, cost of capital, plant operating lifetime, and local taxes or payments.

8.2.3 Storage/Collector Field Trade Studies

The purpose of these trade studies is to examine the sensitivity of solar power insolation availability to two design parameters: collector area and energy storage limitation.

Collector area (km ²) -2 Modules	1.0
Storage time (hour)	6
Account	
Land	2
Structures and facilities	44
Heliostats*	600
Central receiver/tower/heat exch	209
Storage/tanks** (phase change)	164
Boiler plant	-
Turbine plant equipment	119
Electric plant equipment	20
Misc plant equipment	4
Allowance for cooling towers	15
Total direct cost	1,177
Contingency allowance and spare parts allowance (5%)	59
Indirect costs (10%)	118
Total capital investment (1975)	1,354
Interest during construction (15%)	203
Total cost at year of commercial operation (1975 dollars)	1,559

* Collector cost \$60/m²

** Storage cost Phase change \$16.3/kWh + \$66/kW
Sensible heat \$48.7/kWh + \$44/kW
Chemical \$5.0/kWh + \$442/kW

Figure 8-8. 100 MW_e Solar Power Plant Cost Accounts (\$/kW)

The approach described above was used to conduct the following parametric studies. Varying the storage limit and collector area affects solar availability factor as shown in figure 8-9. The receiver aperture radius is optimally sized for each heliostat field, keeping the receiver capture efficiency constant. These results were obtained by running the plant operation computer model described in section 8.2.1. As can be seen in figure 8-9, the parametric variation was made for three storage schemes: phase change, sensible heat, and chemical.

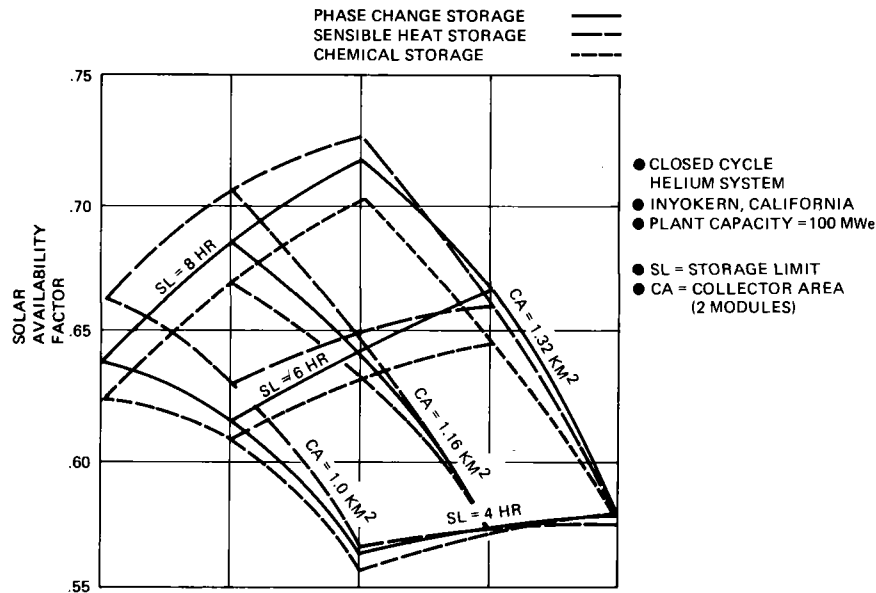


Figure 8-9. Plant Performance Sensitivity

8.2.4 Hybrid Plant Operation

The prior plant operation discussions have been for STC intermediate load as a stand-alone plant with up to 6 hours of storage. Operation as a 100-MW_e hybrid plant (the original study concept) has also been considered. Hybrid plant performance for a summer daily cycle is displayed on figure 8-10. Results show a solar plant power production equivalent to 1,200 MWH_e of fuel displacement.

The performance of a hybrid plant can be compared to that of the stand-alone plant having 6 hours of thermal storage by first integrating the solar mode power production rate over a daily cycle. This determines the total energy that would have to be supplied by a fossil fuel backup heat source. For a summer day, energy to produce approximately 500 MWH_e must be added to match the 1,700 MWH_e of a stand-alone plant operating 17 hours. Energy to produce an additional 540 MWH_e would be required for a winter day to match the 1,170 MWH_e of the stand-alone plant.

8.3 PLANT TRANSIENTS

Solar plant performance and operations are normally cited for steady-state conditions, but there are many important transient (or time dependent) processes that must be considered for the design, implementation, and control of a solar plant. Of specific interest are plant startup and shutdown, responses to partial or total cloud cover, switchover to and from storage, response to variable

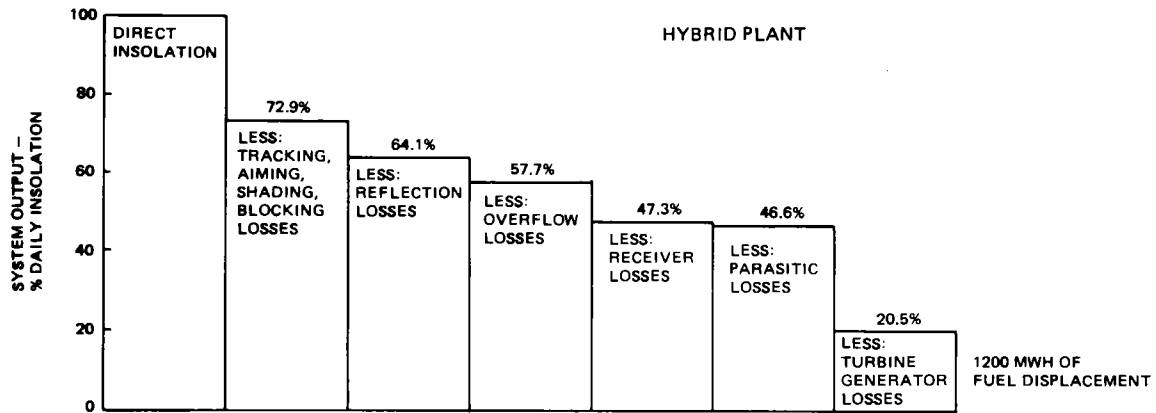


Figure 8-10. Closed Cycle Helium Plant Performance

electrical load demand, and the contingencies associated with equipment failure. Early in the selection of a conceptual design for a commercial plant, consideration should be given to the effect of system transient behavior on performance.

The total plant response chain is shown schematically on figure 8-11. The solid lines represent solar operation including charging of storage. The dotted-line additions show operation from charging only. Conditions not shown are operations from combined solar input from insolation and from charged storage as might apply during the startup mode, partial cloud cover, or solar shutdown. In addition, plant performance has been considered at a constant electrical output, but, from a utility standpoint, the ability to load-follow may be a more important consideration. This would superimpose other transients on the plant.

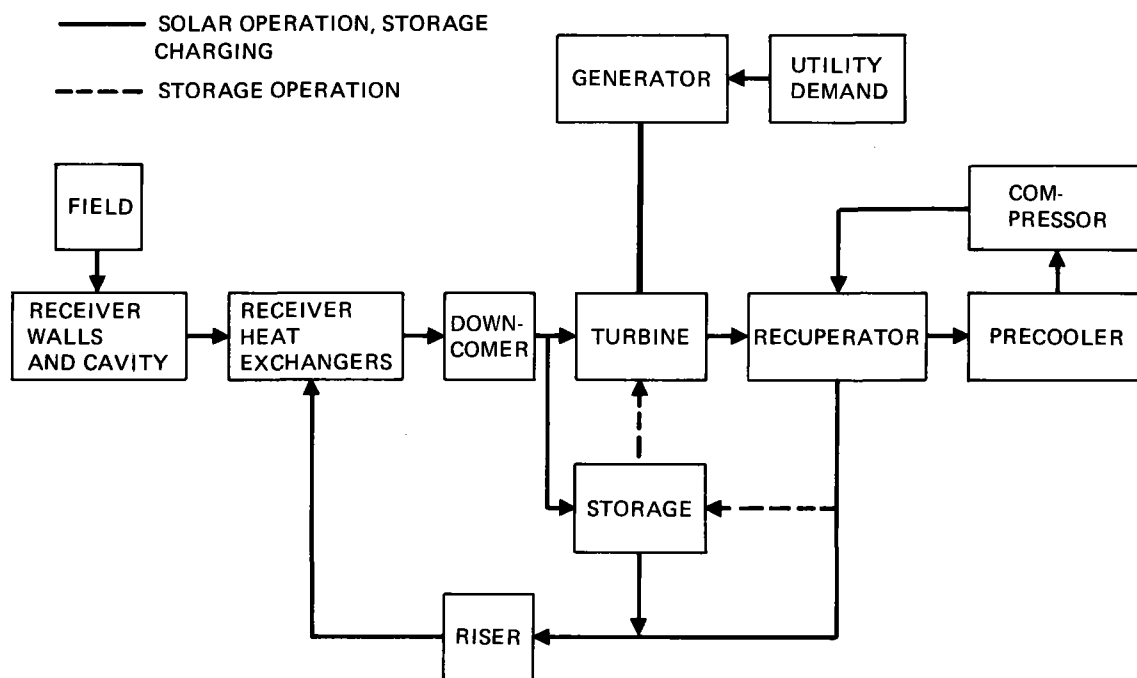


Figure 8.11. Plant Response Chain

8.3.1 Heating and Cooling Transients

Total plant response to input change is determined by summing the individual responses of each plant element in the response chain.

The total effect of heating and cooling changes as they cascade through a plant is a subject requiring more extensive work than was available during the contract period. However, the fundamental transient processes in the receiver heat exchanger tubes and the risers and downcomers were examined to determine how fast their responses would be to input changes. The subsequent paragraphs establish the basic solutions of the prevailing heat transfer equations and then treat the specific designs of the receiver heat exchanger tubes and the long gas lines from the receiver to the turbine.

General Solution for Transients in Long Tubes. The long tubes used in any design of the heat exchanger or heat transport elements of a solar plant requires the following equations to be solved in any transient process for wall temperature, T_w , and fluid temperature, T_f :

$$\frac{\partial T_w}{\partial t} = -c(T_w - T_f) \quad c = h_i C_i / \rho_w C_{mw} \ell_w C_w$$

and

$$\frac{\partial T_f}{\partial t} + v \frac{\partial T_w}{\partial x} = d(T_w - T_f) \quad d = h_i C_i / \rho_f A_f C_f \quad v = \text{velocity}$$

Solutions for these two equations subject to constant temperature initial conditions ($T_{w_i} = T_{f_i}$) and a step change at one boundary to $T_f = T_{ft}$ are available from Boeing analyses outside of this contract. These are

$$T_f(x,t) = T_{f_i} + (T_{f_i} - T_{f_i}) e^{-\frac{xd}{v}} \left\{ e^{-c(L - \frac{x}{v})} \left[I_0 \left(2\sqrt{\frac{xcd}{v}} \left(t - \frac{x}{v} \right) \right) + \sum_{k=0}^{\infty} \left[\frac{v_c \left(t - \frac{x}{v} \right)}{xd} \right]^{\frac{k+1}{2}} I_{k+1} \left(2\sqrt{\frac{xcd}{v}} \left(t - \frac{x}{v} \right) \right) \right] \right\}$$

and

$$T_w(x,t) = T_{w_i} + (T_{f_i} - T_{w_i}) e^{-\frac{xd}{v}} e^{-c(t - \frac{x}{v})} \sum_{k=0}^{\infty} \left[\frac{v_c \left(t - \frac{x}{v} \right)}{xd} \right]^{\frac{k+1}{2}} I_{k+1} \left(2\sqrt{\frac{xcd}{v}} \left(t - \frac{x}{v} \right) \right)$$

with all conditions subject to t greater than x/v to allow the fluid time for its first pass down the tube to reach the pint, x , being calculated I_0 and I_{k+1} are modified Bessel functions of the first kind. Derived forms of these equations were used to calculate the receiver heat exchanger, riser, and downcomer responses to be displayed in subsequent sections. The equations with their infinite series do not display by inspection the widely variant responses obtained by variations of the parameters c , d , x , and v . However, there is a characteristic time, t^* , for which the equations have an instructive, simple closed solution. This is defined by:

$$c \left(t^* - \frac{x}{v} \right) = \frac{wd}{V}$$

At this point, t^* , the above equations reduce to:

$$T_f = T_{f_i} + \frac{(T_{f_i} - T_{f_i})}{2} \left\{ 1 + e^{-2c(t^* - \frac{x}{v})} I_0 \left[2c \left(t^* - \frac{x}{v} \right) \right] \right\}$$

and

$$T_w = T_{w_i} + \frac{(T_{f_i} - T_{w_i})}{2} \left\{ 1 - e^{-2c(t^* - \frac{x}{v})} I_0 \left[2c \left(t^* - \frac{x}{v} \right) \right] \right\}$$

The quantity x/v in the preceding equations is small for the velocities of helium and can usually be ignored. Omitting this x/v and examining the extremes of the second term in the brackets,

$$e^{-2ct^*} I_0(2ct^*) \text{ near } 1; T_f \sim T_{f_t} \text{ and } T_w \sim T_{w_i}$$

which describes the start ($I_0(0) = 1$) and situations at time, t^* , where the heat has not readily transferred to the fluid or the heat capacity of the fluid is so large compared to that of the wall that the fluid temperature has not been substantially affected. The risers and downcomers are more typical of this case. At the other extreme,

$$e^{-2ct^*} I_0(2ct^*) \text{ near } 0; T_f = \frac{T_{f_i} + T_{f_t}}{2} \text{ and } T_w = \frac{T_{w_i} + T_{f_t}}{2}$$

which describes situations where the heat supplied by the wall by time t^* has been readily transferred to the fluid and substantially affects the fluid temperature. The receiver's heat exchangers are more typical of this case.

Receiver Heat Exchanger. The heat exchanger tubes of the receiver have been shown on figure 3-4. The "U-shape" configuration has a steady-state operating temperature distribution that has been approximated by the analytical distributions of figure 8-12. The wall temperature rises rapidly toward 816°C ($1,500^\circ\text{F}$) and then levels off, while the helium temperature has a much more gradual rise to exit at 816°C ($1,500^\circ\text{F}$).

The transient response of a heat exchanger tube was calculated by the equations described using an initial tube temperature of 816°C ($1,500^\circ\text{F}$) subjected to 538°C ($1,000^\circ\text{F}$) helium entering the cool side. The wall heating on the tube exterior was assumed to be instantaneously cut off with no further heat gain or loss to the outside from the tube. The resulting tube temperature and the helium temperature at the exit are shown on figure 8-13, and the temperature difference is small. The temperatures have reduced to about 50% of the total drop value at the characteristic time of $t^* + 0.53$ minute. Figure 8-13 gives a conservatively slow response considering the actual tube temperature distribution in steady state (figure 8-12); the response time coordinate should be reduced about 15% or 0.08 minute at the characteristic time. The tube and helium temperature histories at the "hot" end on startup or restart with an instantaneous heat flux have not been determined, but are predicted to be somewhat faster than the inverse of the curves shown.

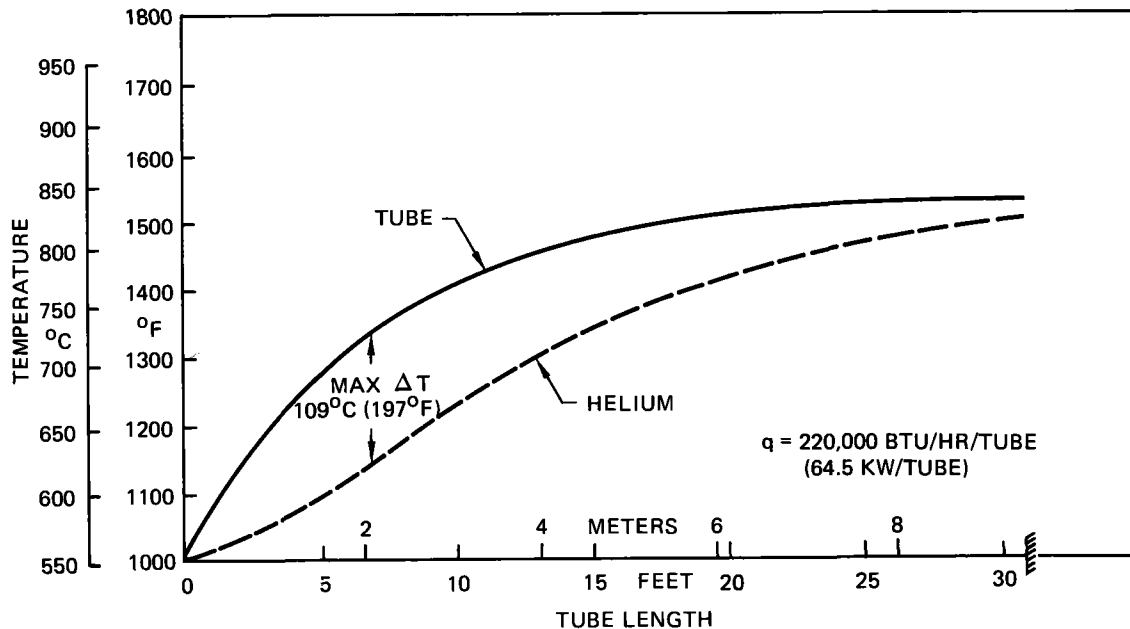


Figure 8-12. Receiver Heat Exchanger Tube and Helium Temperatures in Steady Operation

Risers and Downcomers. The lines that transport the helium between the receiver and the equipment at the base of the tower experience several situations in which transient situations exist. These are: on startup to raise the riser fluid temperature from ambient to 538°C ($1,000^{\circ}\text{F}$) and to raise the downcomer fluid temperatures to 816°C ($1,500^{\circ}\text{F}$); on shutdown to return fluid and wall temperatures from the normal operating temperatures to levels where the equipment may be shut off. Another situation of interest occurs if there is a temporary insolation interrupt and heat from storage must be supplied to maintain continuous power production. This case was examined for the two downcomer lengths.

The downcomer analyses consisted of examining the responses of (1) the approximately 67-meter (220 feet) length from the receiver to the tower top, and (2) the 229-meter (750 feet) length from tower top to bottom. The first situation has two flow tubes dividing the total flow. The main downcomer in the tower contains all the flow. Assuming initial tube and fluid conditions at 816°C ($1,500^{\circ}\text{F}$)

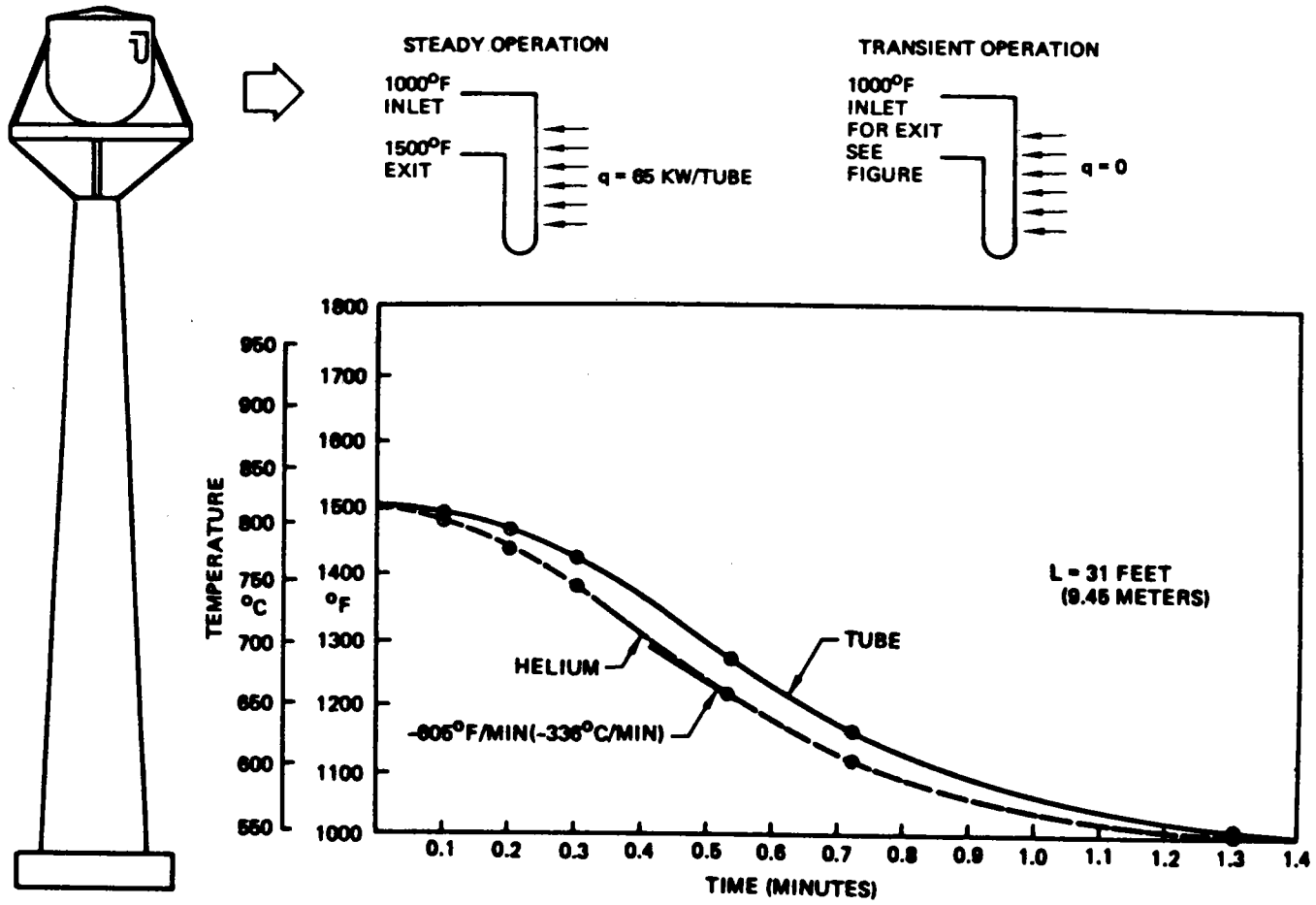


Figure 8-13. Receiver Heat Exchanger Tube Response to Input Heat Removal

and subjecting each downcomer to a rapid fluid temperature decrease to 538°C ($1,000^{\circ}\text{F}$) at their respective inlets, as would occur with the field heat supply interrupted, resulted in data plotted as shown on figure 8-14. The large thermal gradient between helium and wall is caused by the low conductance in the wall material. In the preferred design, the two 67-meter (220-foot) sections supply the 229-meter (750-foot) section. The response at the bottom of the tower for a sudden temperature drop at the receiver (67-meter section inlet) has not been calculated, but the exit fluid temperature would probably drop rapidly to the sum of the individual excesses over 538°C ($1,000^{\circ}\text{F}$) to about 650°C ($1,190^{\circ}\text{F}$) and tail off accordingly.

Figure 8-15 shows the temperature distribution down the length of the 229-meter (750-foot) downcomer at various times. Wall temperatures are fairly uniform, and the helium temperatures have an approximate linear increase with tube length.

Recuperator and Precooler. The other significant heat transfer elements in the system response chain are the recuperator and precooler. Transient analyses are complicated by the presence of two fluids and, in the solar plant case, by the size of the units. Unfortunately, reports on operational experience with units of comparable size have transient data that conflicts. Indications are that cross-responses can range from a few minutes to 10-15 minutes. For the slow cases, prewarming of the heat exchangers may be accomplished from storage prior to collector-field heat supply on plant startup. More work should be done on transients for these integral portions of the plant before establishing operational concepts.

Energy Storage. Response data on charging and discharging for the various energy storage concepts are given in section 6.0. All systems should react quickly for emergency use, such as in a field interrupt. Continued quick reactance with time is a function of the concept (e.g., the thermochemical concept probably sustains longest and the sensible-heat concept the least). In addition to the initial transients of storage systems, their steady-state temperature from storage to the turbine differs from the $1,500^{\circ}\text{F}$ normally supplied from the receiver. This introduces another transient that must be cascaded through the portion of the plant response chain being used.

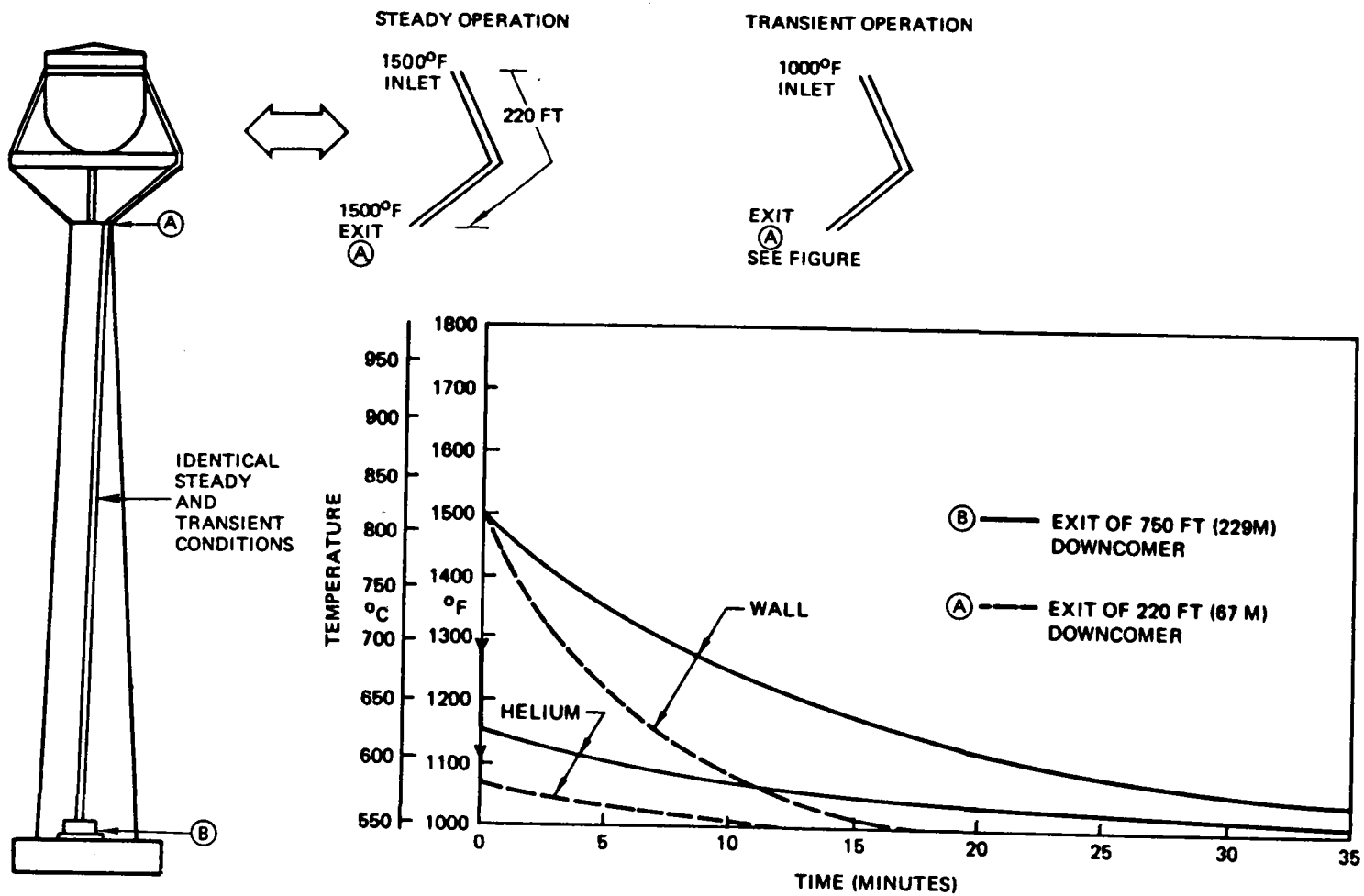


Figure 8-14. Downcomer Responses to Inlet Temperature Drop

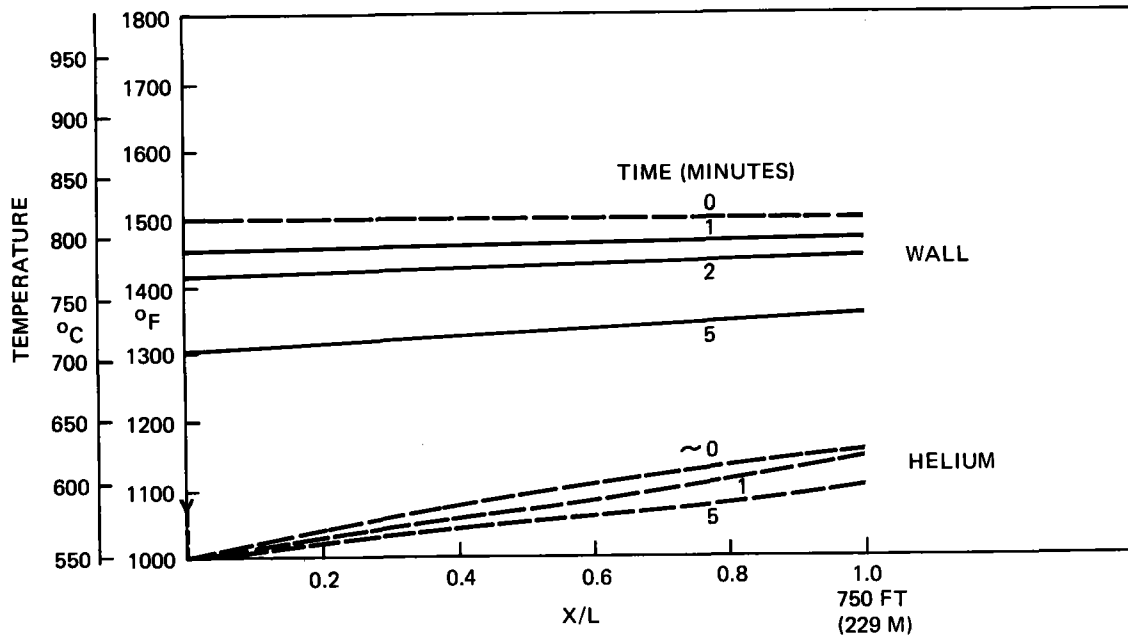


Figure 8-15. Temperature Profiles in 750 Ft (229 M) Downcomer as Response to Sudden Inlet Temperature Drop in Helium

8.3.2 Pressure Transients

Using pressure changes as a means of plant control adds operational flexibility unique to closed-cycle plants. Helium can be introduced or withdrawn from the cycle very rapidly because of the normal operating pressure of 3.45 MN/m^2 (500 psi). Raising helium pressure with a cool supply would introduce a secondary fluid temperature effect into the system.

Attention was given to the problem of sudden loss of receiver pressure and the resultant heating effects on equipment. Pressure loss in an individual receiver heat exchanger tube causes no particular problem for that tube. Adjacent tubes continue to control the temperature level of the starved tube. However, the reduction of fluid mass flow through other tubes in same heat exchanger panel may cause these tubes to overheat. These tubes could take excesses in temperature for a time, as shown by the elevated-temperature rupture tests (reported in section 7.0), but their 30-year lifetime design integrity could be compromised. Other situations would be pressure loss upstream of the receiver proper in the risers or downstream in the downcomers. The former case could cause helium starvation in the receiver and general tube overheating before the field could be scrambled; the latter case could cause a transient pressure shock (in extreme cases, a reverse flow situation) in the turbomachinery. If the depressurization is small,

as should be the case for the amount of mass flow moving through the system, sensing the situation can cause remedial action to be initiated, such as adding from supply until the situation can be controlled.

8.3.3 Turbomachinery Transients

The turbomachinery should react more quickly than other plant elements to transient changes in temperature and pressure. The response to off-nominal conditions requires a full set of turbine and compressor data to determine the effect on system temperatures and power output.

8.4 PLANT COSTS

Previous report sections have discussed costs appropriate to individual plant elements. Section 4.4 has receiver/heat exchanger costs, section 5.3.3 turbomachinery costs, and section 6.2 the storage concept costs. All other costs used for the plant summary are either the itemized amounts in the plant account prescribed by EPRI or are prorated from these items to adapt to use of helium.

One of the major objectives of the continuation study phase was to make comparisons of (1) those account items where the helium system is unique from the EPRI "strawman" items and (2) total plant costs. This has been accomplished in the sense of equating the conceptual helium-plant performance to the same megawatt rating as the "strawman" plant. The results are displayed on figure 8-16 for comparison of intermediate and hybrid plants.

The general comparisons of total costs between the "strawman" plants and the helium plants show that the costs are comparable, with a little more disparity in the hybrid plant. Examining individual stand-alone plant-account items shows some interesting data. The higher efficiency helium system with its receiver sized for direct heat to turbine and storage is more expensive than the steam boiler, but the field costs can be reduced to produce 100 MW_e. The storage account is slightly lower thus verifying the "strawman" plant storage costs. Turbine plant equipment and miscellaneous plant-equipment costs are higher than the steam plant accounts. The miscellaneous plant account includes the tower's helium riser and downcomer costs (\$1.2 million per set). The same cost comparisons hold true for the hybrid plant, except for a wide disparity in the 1/2-hour storage accounts. The "strawman" intermediate-plant-storage cost prorated by storage time to \$15 KW_e represented an economy not possible for the helium plant.

PLANT TYPE	STAND-ALONE		HYBRID	
	STRAWMAN	HELIUM	STRAWMAN	HELIUM
COLLECTOR AREA (KM ²)	1.0	0.84	0.5	0.42
STORAGE TIME (HOUR)	6	6	0.5	0.5
ACCOUNT				
LAND	2	2	1	1
STRUCTURE AND FACILITIES	44	44	51	51
HELIOSTATS*	600	505	300	258
CENTRAL RECEIVER/TOWER**/HEAT EXCHANGER	95	197	68	98
STORAGE TANKS	180***	164	15***	74
BOILER PLANT	-	-	73	73
TURBINE PLANT EQUIPMENT	80	119	80	105
ELECTRIC PLANT EQUIPMENT	21	20	21	20
MISC PLANT EQUIPMENT	4	28	4	16
ALLOWANCE FOR COOLING TOWERS	20	15	20	15
TOTAL DIRECT COST	1,046	1,094	633	711
CONTINGENCY ALLOWANCE AND SPARE PARTS ALLOWANCE (5%)	52	55	32	36
INDIRECT COSTS (10%)	105	109	63	71
TOTAL CAPITAL INVESTMENT (1975)	1,203	1,258	728	818
INTEREST DURING CONSTRUCTION (15%)	180	189	109	123
TOTAL COST AT YEAR OF COMMERCIAL OPERATION (1975 DOLLARS)	1,383	1,447	837	941

*COLLECTOR COST-\$60/M²

**TOWER HEIGHT-260M (2 and 1 TOWER(S), RESPECTIVELY)

***THERMAL STORAGE COST-\$30/KWH

Figure 8-16. Plant Cost Comparisons (\$/kWe)

A comparison of plant costs for various cycle efficiencies within their expected operating range was also made. Figure 8-17 has the summary results. The plant costs cited above are located at 0.36-cycle efficiency for the "strawman" steam plant and at 0.44 for the helium system. The results show the bottoming or cost minimization for helium at the 0.44 design point. Operation of open air and helium are shown also for 980°C (1,800°F), indicating the potential for helium with a solution of the high-temperature materials problem. Open-air receiver costs were based on rough estimates. The general downward slope is a result of reduced field costs for higher efficiencies. The exaggerated ordinate of figure 8-17 tends to show large differences in plant type.

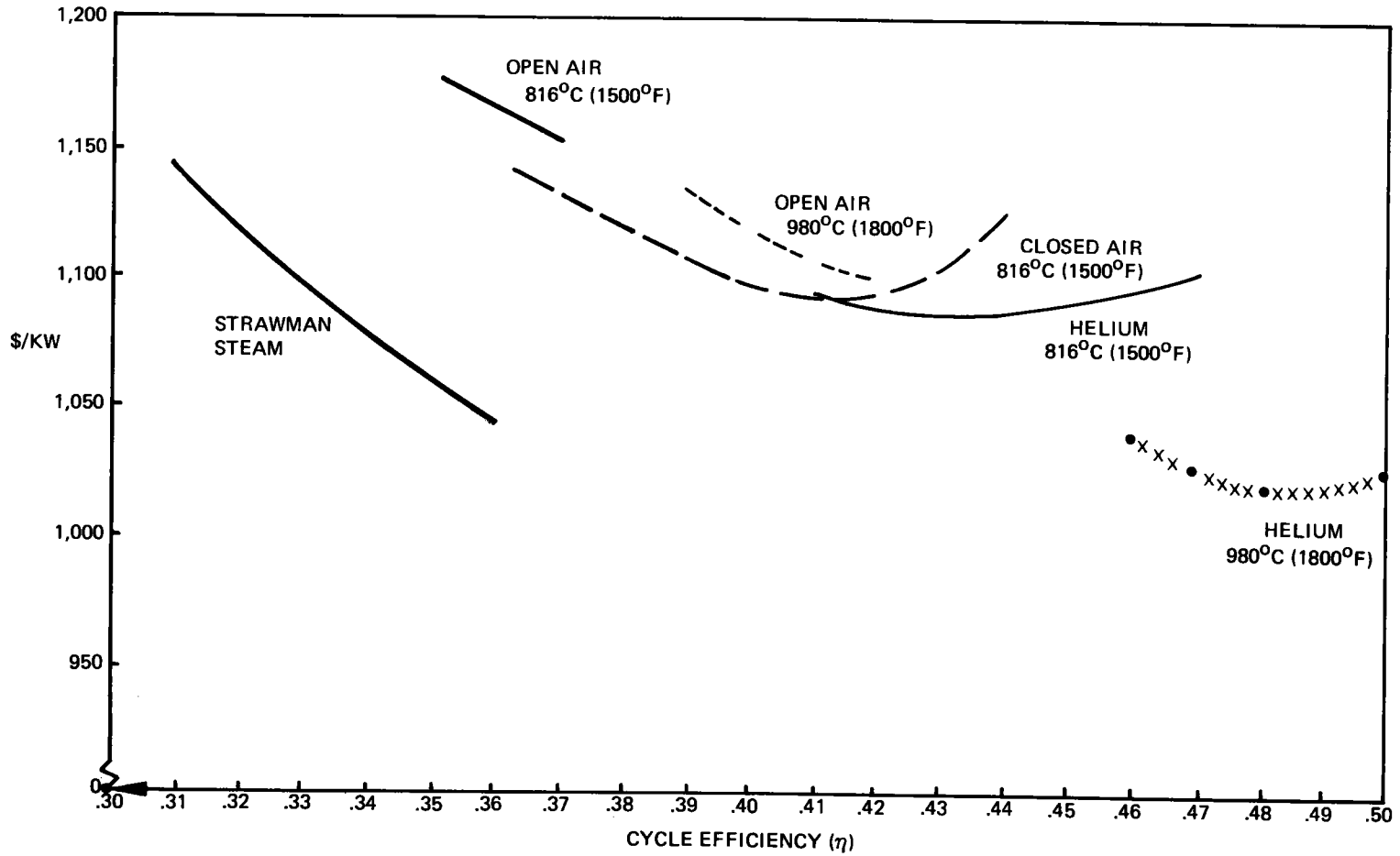


Figure 8-17. 100 MWe Plant Cost

Section 9.0
RECEIVER SCALE MODEL

9.1 INTRODUCTION

The objective of this portion of the high-temperature central receiver study is to develop a conceptual design of a subscale-receiver test bench model and to define an appropriate model testing program. The purposes of the bench model testing are to validate the technology for gas-cooled central-collector powerplants, to verify the design concepts proposed for the commercial size powerplant, and to gain operational experience with the selected high-temperature materials.

High-pressure closed-gas-cycle powerplants have been produced for many years. These plants use fossil-fuel-burning gas heaters. Each of the heater designs is tailored for a particular fuel such as natural gas, pulverized coal, oil, or peat. In each, the general configuration is specialized to accommodate the fuel, but all of these designs utilize gas-in-tube heat exchangers similar to the solar powerplant. The new technology results when these concepts are used with the high-intensity solar flux of the central receiver powerplant.

The materials selected for receiver wall insulation and heat exchanger tubing have been used at these temperatures and at working-stress levels in nonsolar-heated commercial equipment. Their exposure to high-intensity solar flux at these high temperatures is a new application for each of the materials.

An important consideration involved in the prototype receiver design is the analysis of the capability to manage gas temperature with variations in incoming solar flux. Its cavity-wall configuration is designed to trap this entering flux geometrically while reflectively dispersing it to heat the gas-in-tube heat exchangers uniformly. The most sophisticated means of heat transfer analysis have been used in the design. The proof, however, is in the performance of a solar-heated scale model of similar design.

Finally, the design details for high-temperature solar-heated heat exchanger and insulation systems need to be defined and tested under simulated operational conditions. This allows special problem areas to be identified and properly emphasized in on-going development activity for the demonstration powerplant. Therefore, a maximum effort has been expended to define a test model that exhibits all the solar interface functions of the prototype, utilizes as many of the prototype materials and manufacturing processes as possible, and incorporates as many of the prototype design details as practical.

Section 9.2 of this report describes the model receiver, outlines a plan for testing, and defines test facility requirements. The most difficult technical problem in subscale-model thermal design is the matching of heat exchanger tubing temperatures. This subject is discussed and the rationale for other model design choices is presented in section 9.3.

9.2 MODEL RECEIVER CONFIGURATION AND TEST PLAN

The most important features, capabilities, and limitations of the proposed model test program are summarized on figure 9-1.

A design was required that could be tested either at the U.S. ERDA solar thermal test facility, using its north quadrant field, or at the CNRS solar furnace at Odeillo, France. These test facility options established a requirement that other gases such as superheated steam and air be determined as acceptable for subscale thermal modeling of the helium gas in the prototype commercial plant. Furthermore, since other receiver tests in these same facilities require an air supply at 0.943 MN/m^2 (135 psia) and high temperatures, a design was needed that could use a common source of air.

These basic requirements are all fulfilled by the preferred model design shown on figure 9-2. Minor configuration changes are incorporated depending on whether it is tested with an axisymmetric or quadrant field of solar collectors. The quadrant-field option shown was selected for tests at Sandia, Albuquerque. The test receiver is shown on figure 9-3, installed in the ERDA solar thermal test facility. With the aperture location illustrated, the narrow-angle solar input of the 1-MW_{th} ERDA facility directly illuminates the conical back wall, simulating the wide-angle axisymmetric field input through the prototype receiver aperture. Since the insulation-wall surface is a near-perfect diffuser, all past history is lost at first incidence and the reflected/reradiated flux distribution pattern is similar for either field design.

ITEM	STATUS	REMARKS
<u>GENERAL TEST PROGRAM FEATURES</u>		
Solar Collector Test Facility	Yes	1 MW _{th} in size, ERDA or CNRS
Electric Heated Test Facility	Optional	Lower in cost, field flux not simulated
Axisymmetric or north quadrant collector field	Optional	Minor adaptation of basic model configuration required.
Heat transfer medium in model	Air	Superheated steam could be used interchangeably
Model Test Gas Cycle	Open Flow	Additional cost of gas circulation equipment for closed cycle is prohibitive
Part load and transient load testing feasible	Yes	Model incorporates transient thermal response capability of the prototype.
Test capability for off-design distribution of solar input	Yes	Model incorporates off-design temperature balancing features of prototype.
<u>TEST MODEL DETAILS</u>		
Exact geometric match of prototype solar input.	Facility Dependent	CNRS solar input provides near perfect match with prototype solar flux distribution. However, exact match is not required because of minimal direct solar heating of prototype heat exchanger tubing. This condition can be duplicated in either CNRS or ERDA north field installation

Figure 9-1:

FEATURES OF PROPOSED TEST PROGRAM

ITEM	STATUS	REMARKS
<u>TEST MODEL DETAILS</u> (Cont)		
Exact geometric scaling of receiver interior.	Facility Dependent	Aperture size, heat transfer surface areas, and wall insulation properties exactly matched with axisymmetric solar input option (CNRS). Inexact match for aperture relocated for ERDA tests.
Exact matching of prototype materials.	Yes	Tubing and interior wall materials are identical.
Exact matching of prototype insulation wall design.	Yes	Model wall equal to prototype thickness. Verifies design and operation for commercial plant.
Exact matching of prototype convective heat losses.	No	Neither candidate facility offers downward facing aperture. Result is greater convective loss of hot air from model receiver. Not a critical problem.
Exact scale model of prototype heat exchangers.	No	Model tubes 3 times longer than scale and larger than exact scale diameter. Thermal boundary conditions on distorted tubes are nearly identical to prototype. Total surface area exactly scaled.
Modeling of prototype operating characteristics.	Yes	<p>These features are incorporated in the model:</p> <ul style="list-style-type: none"> • Dynamic flow control for eight separate zones of heat transfer panels. This provides local control of gas outlet temperatures and minimizes the effects of solar flux gradients. • Exact matching of transient thermal response rates for insulation walls.

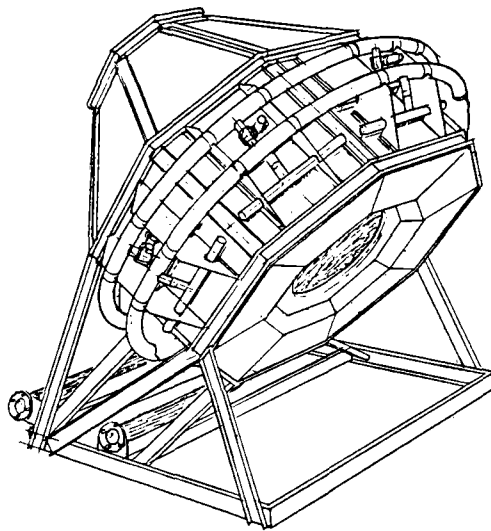
Figure 9-1: (Cont)

FEATURES OF PROPOSED TEST PROGRAM

ITEM	STATUS	REMARKS
<u>TEST MODEL DETAILS (Cont)</u> Exact Prototype Temperatures	No	Part load outlet temperature dynamically controlled. Compromised to allow testing at gas inlet pressure lower than 1.38 MN/m ² (200 psia)

Figure 9-1: (Cont)

FEATURES OF PROPOSED TEST PROGRAM



1 MW_{th} NORTH QUADRANT
U.S. ERDA SOLAR THERMAL TEST FACILITY

Figure 9-2 Test Model Configuration

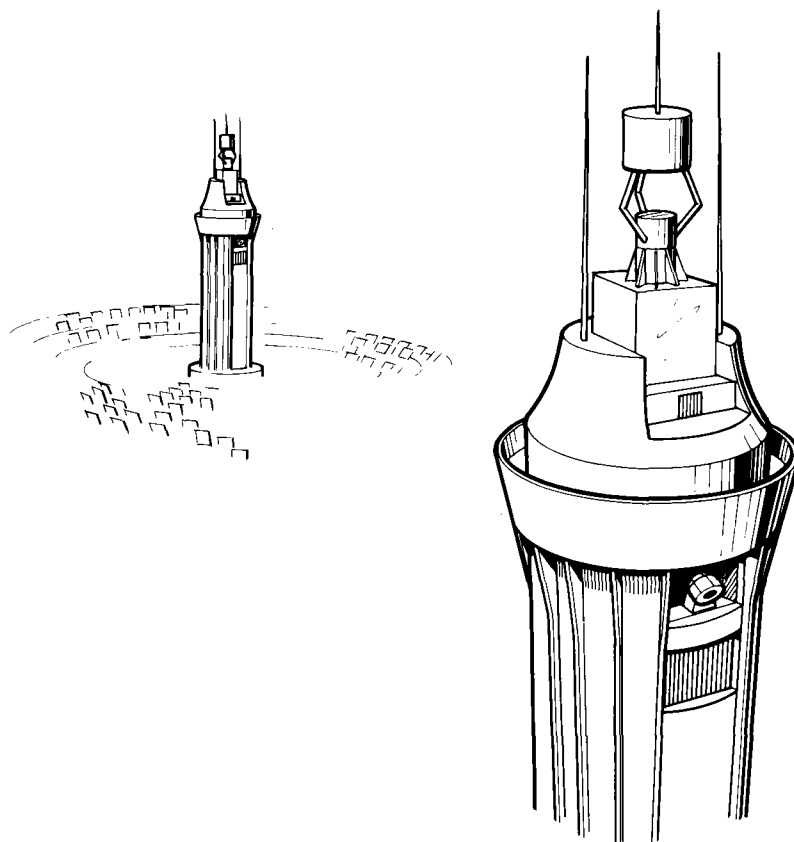


Figure 9-3. Model Configuration for ERDA Solar Thermal Test Facility

The receiver gas flow is shown schematically on figure 9-4. The gas flow rate through each of the eight heat exchanger panels is dynamically controlled. The control valves are high-temperature valves with remote actuators. The outlet temperature of each panel is monitored and valve position adjusted to obtain the correct outlet temperature.

The test program consists of three types of testing:

- System checkout to verify system and instrumentation operation, test facility interfaces, solar radiation patterns at low heat levels, and the test-gas supply system
- Receiver efficiency measurement with various levels and distributions of heat input (These tests determine reflective, radiative, conductive, and convective heat losses.)
- Receiver response tests simulate typical operating and emergency conditions pertinent for the commercial plant. These tests will be used to evaluate the system stability and sensitivity to:
 - Rapid startup and shutdown
 - Loss of gas flow in a portion of the receiver heat exchangers
 - Emergency conditions as may be determined

Because of the slow thermal response of wall insulation, the test model will require 1 to 2 hours to achieve thermal equilibrium. Transient response tests, except startup, will be initiated from an equilibrium state. Therefore, a typical day's testing will require at least 2 hours of nearly steady solar input.

Figure 9-5 shows the testing activities required to accomplish model test program objectives. The activity has been scheduled assuming that adequate solar heat is available on the days it is required. The schedule is preliminary, but it indicates the approximate period of time required with the model in test position in the solar test facility.

Preliminary test facility requirements have also been determined. The test model instrumentation and controls are described on figure 9-6. The other test facility interfaces are shown on figure 9-7. Discussions with the U.S. ERDA test facility design engineers indicate that their preliminary facility design satisfies all the data acquisition and solar energy requirements. The CNRS facility, however, does not have a dedicated test data management system. This would have to be provided along with the test model. The air supply for model testing is not presently available at either of the candidate test sites.

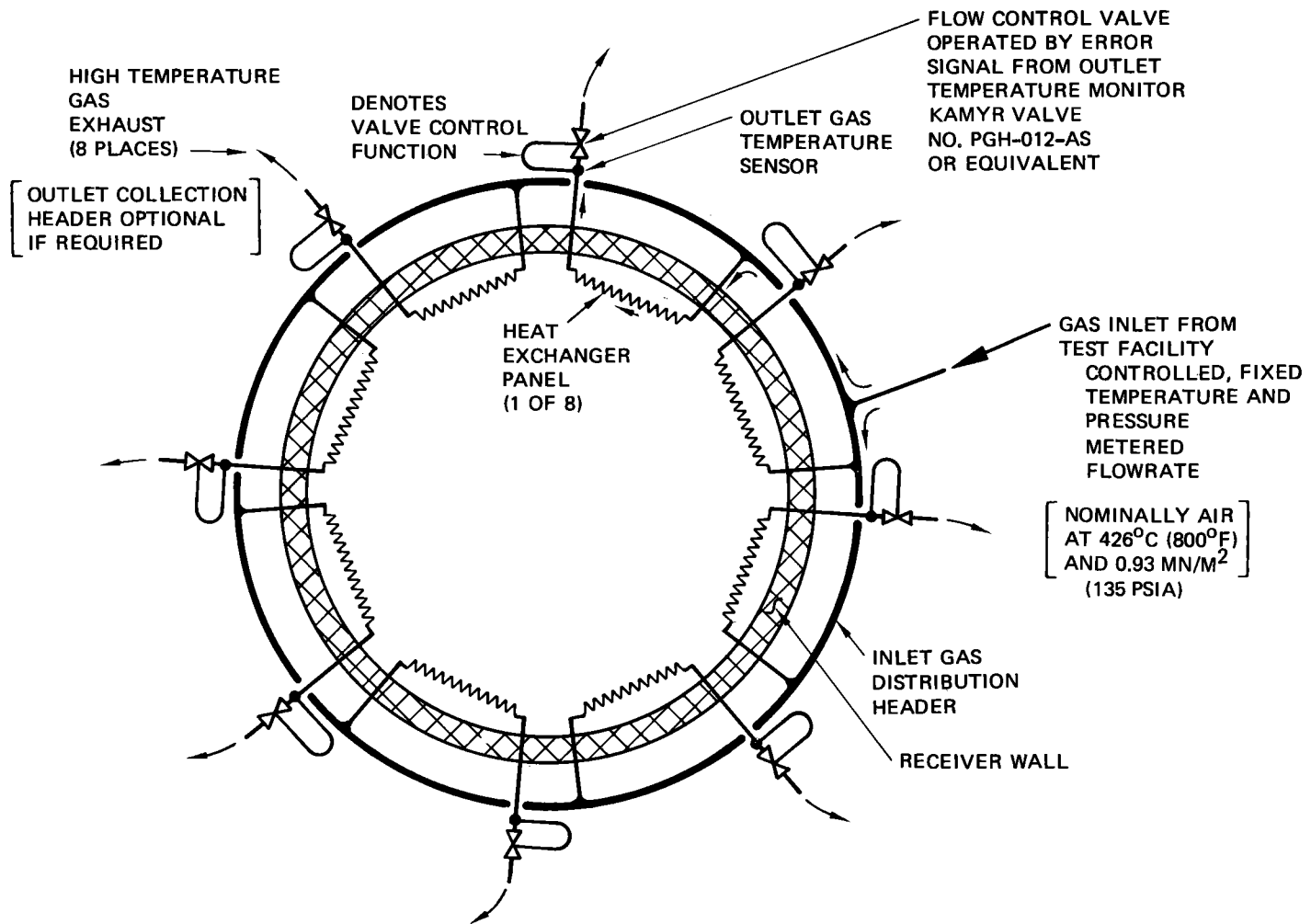


Figure 9-4. Model Test Gas Flow Schematic

TEST DAY

1. Verify temperature instrumentation.
2. Pressurization and verification of strain and pressure sensors.
3. Cold gas flow to verify gas flow instrumentation and controls.
4. Hot gas flow at inlet conditions.
5. Solar heating to verify facility solar collector system operation.

OPERATIONAL TESTS TO EQUILIBRIUM

	Gas Temperature °C, (°F)		Solar Heat KW _{th}
	Inlet	Outlet	
6.	316 (600)	593 (110)	300
7.	426 (800)	704 (1300)	300
8.	538 (1000)	816 (1500)	700
9.	454 (850)	816 (1500)	900
10.	426 (800)	816 (1500)	1000

Each Equilibrium Test Consists of:

- o Initiation of gas flow through model
- o Receiver stabilized at gas supply temperature
- o Gradual increase of solar input to test level
- o Steady operation to thermal equilibrium
- o Gradual reduction of solar input
- o Termination of gas flow

SPECIAL PURPOSE TESTS

	Gas Temperature °C, (°F)		Initial Equilibrium Condition	Final Off-Design Condition
	Inlet	Outlet		
11.	426 (800)	816 (1500)	1000 KW _{th} Solar Input	Terminate East or West half of collector field
12.	426 (800)	816 (1500)	1000 KW _{th} Solar Input	Reduce fluid flow through one heat exchanger panel until, o Tube temp. exceeds 982°C (1800°F) o Average gas outlet temp. exceeds 843°C (1550°F) on remaining panels
13.	426 (800)	704 (1300)	300 KW _{th} Solar Input	Terminate solar input, simulating collector system failure
14.	426 (800)	816 (1500)	1000 KW _{th} Solar Input	Terminate solar input, as above.
15.	426 (800)	816 (1500)	1000 KW _{th} Solar Input	Simulate passage of dis- crete cloud shadow over field.

Figure 9-5: On-Site Test Activity

PARAMETRIC DATA SIGNALS - INTERPRET, DISPLAY, RECORD

<u>ITEM</u>	<u>MAXIMUM VALUES</u>	<u>NUMBER OF CHANNELS</u>	
		<u>Real Time Access</u>	<u>Recorded</u>
Temperature (Thermocouples)	1390°C (2500°F)	25	125
Pressure (strain gage type)	1.36 MN/m ² (200 psia)	3	10
Differential Pressure (Strain Gage Type)	.27 MN/m ² (40 psia)	5	13
Strain	-	0	6
Heat Flux (Calorimeter Signal)	1 MW/m ²	14	28
Flowrates (Type TBD)	4.5 kg/sec (10 lb/sec)	1	10
Control Valve Position (Type TBD)	0-90°	8	8

TEST CONTROLS AND ALARM CIRCUITS

<u>ITEM</u>	<u>FUNCTION</u>
High Temperature Alarm	Monitor 10 temp. channels/signal operator if limit exceeded
Valve Actuator Controls	Monitor 8 temp. channels/provide proportional signal to valve control system
Flow Alarm	Monitor gas flow/Signal operator or scramble heliostats

Figure 9-6: Test Facility Requirements/Test Data Acquisition

Solar Heating

Receiver aperture	1.1 meter (3.6 feet) diameter, oriented in vertical plane for CNRS facility of in plane inclined 37° from vertical for ERDA.
Solar input	Variable 50 to 1000 KW_{th} on above aperture. Heat input calibrated to within \pm TBD percent.

Test Gas Flow

Supply to model	Supply pressure of 0.943 to 1.886 MN/m^2 (135 to 270 psia), regulated during test run within \pm 5 percent, pulsations less than 0.5 percent. Supply temperature adjustable from 316 to 518 $^{\circ}\text{C}$ (600 to 1000 $^{\circ}\text{F}$) and regulated within \pm 11 $^{\circ}\text{C}$ (\pm 20 $^{\circ}\text{F}$) of set point. Mass flow of 0.45 to 2.28 kg/sec (1 to 5 lb/sec) available on demand at supply pressure and temperature, measured \pm 1 percent.
Return from model (if applicable)	Back pressure, regulated at 0.276 MN/m^2 (40 psia) below the supply pressure, independent of flow rate. Return temperature of 650 to 871 $^{\circ}\text{C}$ (1200 to 1600 $^{\circ}\text{F}$)

Figure 9-7: Test Facility Requirements/Model Operation and Control

9.3 MODEL DESIGN

The commercial receiver has a maximum solar heat input of about $300 \text{ MW}_{\text{th}}$, of which about 85% is transferred to the circulating helium gas. The 1-MW_{th} model receiver must be scaled down in size while reproducing thermal efficiency and operating temperatures of the prototype.

The 300:1 power ratio results in a model scale size ratio of 1:17.3. Heat flux per unit area is preserved. This size reduction must be accommodated while retaining all the important functions and characteristics of the prototype. These are described on figure 9-8. Its most important functions are management and optical trapping of entering sunlight, capability to diffuse this flux and provide nearly uniform heating of the gas-in-tube heat exchangers, and effectively absorb and transfer this heat to the circulating helium gas.

The important receiver heat transfer processes to be modeled are the radiative interchange between surfaces inside the receiver enclosure, the convective tube-to-gas heat transfer inside the heat exchanger tubing, and the heat loss through insulation walls.

The radiative and solar heat transfer is preserved in a geometrically scaled receiver having the same solar input flux distribution, the same temperatures, and the same radiant surface properties (materials and coatings) as the prototype. The heat exchanger wall, when viewed from across the receiver interior, takes on the average temperature and properties of the combination of tubes and wall. Therefore, we shall take liberties in the detailed definition of this surface while maintaining average thermal radiative characteristics for the model equal to those in the prototype. For thermal as well as mechanical design reasons, prototype materials are used throughout the model cavity.

Wall-insulation thermal properties of the prototype commercial receiver can be duplicated in the scale model. The heat transfer by conduction through the wall is essentially one-dimensional. Therefore, by retaining the prototype insulation materials and the 0.15-meter wall thickness, the prototype temperatures and heat transfer per unit area are reproduced in the model.

The cavity wall is composed of three layers of different insulation materials:

FUNCTION	MINIMUM APERTURE SIZE	RELIABLE AND EFFICIENT WALL INSULATION MATERIALS	HIGHLY REFLECTIVE MATERIALS	RECEIVER WALL NEAR APERTURE INCLINED TO BIAS FIRST REFLECTION AWAY FROM APERTURE	GAS-IN-TUBE HEAT EXCHANGERS LOCATED OUT OF DIRECT SOLAR REFLECTION	SUFFICIENT HEAT EXCHANGERS TO ASSURE DOMINATION OF TUBE TEMPERATURE BY INTERNAL GAS	METERING OF GAS FLOW IN ZONES TO CONTROL OUTLET GAS TEMPERATURE AND MAXIMUM TUBING TEMPERATURE	GAS TIGHT CAVITY WALLS AND DOWNWARD FACING APERTURE	MINIMUM PRACTICAL HEAT EXCHANGER TUBE SIZE MAXIMIZES HEAT TRANSFER COEFFICIENT	GENEROUS THERMAL SHIELD SURROUNDS APERTURE
TRAPPING OF INCIDENT SUNLIGHT	●		●	●						
ACCOMMODATION OF CONCENTRATED AND VARIABLE DISTRIBUTION OF ENTERING SOLAR FLUX		●	●	●	●					
REDISTRIBUTION OF ENTERING SOLAR FLUX TO LEVELS COMPATABLE WITH GAS-IN-TUBE HEAT EXCHANGERS			●	●	●					
CONTROL OF FREE CONVECTIVE LOSS OF HOT AIR FROM CAVITY	●							●		●
CONTROL OF HEAT EXCHANGER TUBING TEMPERATURES			●		●	●	●		●	
MAINTENANCE OF GAS OUTLET TEMPERATURE AT PART LOAD		●					●			
PROTECTION OF EXTERIOR STRUCTURE FROM SPURIOUS SOLAR FLUX										●

Figure 9-8. Receiver Heat Transfer Functions and Characteristics

an inner-surface layer of Kaowool¹ blanket, a layer of rigid Kaowool block, and an outer layer of mineral-wool block. These are retained by metal standoff studs that attach to a mild-steel outer skin. These insulation panel arrangement and fastening methods have been standardized in the furnace industry. This will be the first known application of the technology for high solar flux. The experience gained here will be a valuable contribution to future efforts.

The modeling of prototype gas-in-tube heat exchangers is a more difficult problem. The governing thermal-scale-modeling criteria were developed, and a number of different model heat exchanger designs are presented on the following pages. The criteria change depending on the assumption of different degrees of similitude (e.g., scale size, temperature matching, and heat flux matching). A number of candidate designs were developed for the model heat exchangers. In particular, the selected design that uses air at an inlet pressure as low as 0.943 MN/m² (135 psia) is studied in detail.

The modeling criteria were developed by consideration of the gas-in-tube heat transfer models shown on figure 9-9 and their related differential equations. Symbols are defined on figure 9-9.

Total heat transfer Q for the cavity is

$$Q = \dot{m} C_p \Delta T_G N \quad (9-1)$$

Similitude requirements for preservation of prototype heat fluxes in the model result in the relationship

$$\frac{Q_{\text{model}}}{Q_{\text{prototype}}} = Q^* = R^2 \quad \text{where } R \text{ is model-to-prototype dimensional scale ratio} \quad (9-2)$$

*denotes model-to-prototype ratio

Then, combining equations in ratio form,

$$Q^* = \dot{m}^* C_p^* \Delta T_G^* N^* = R^2 \quad (9-3)$$

This equation of model-to-prototype ratios must be satisfied for accurate simulation of the prototype heat fluxes in the model.

¹Registered Trademark of Babcock and Wilcox Company

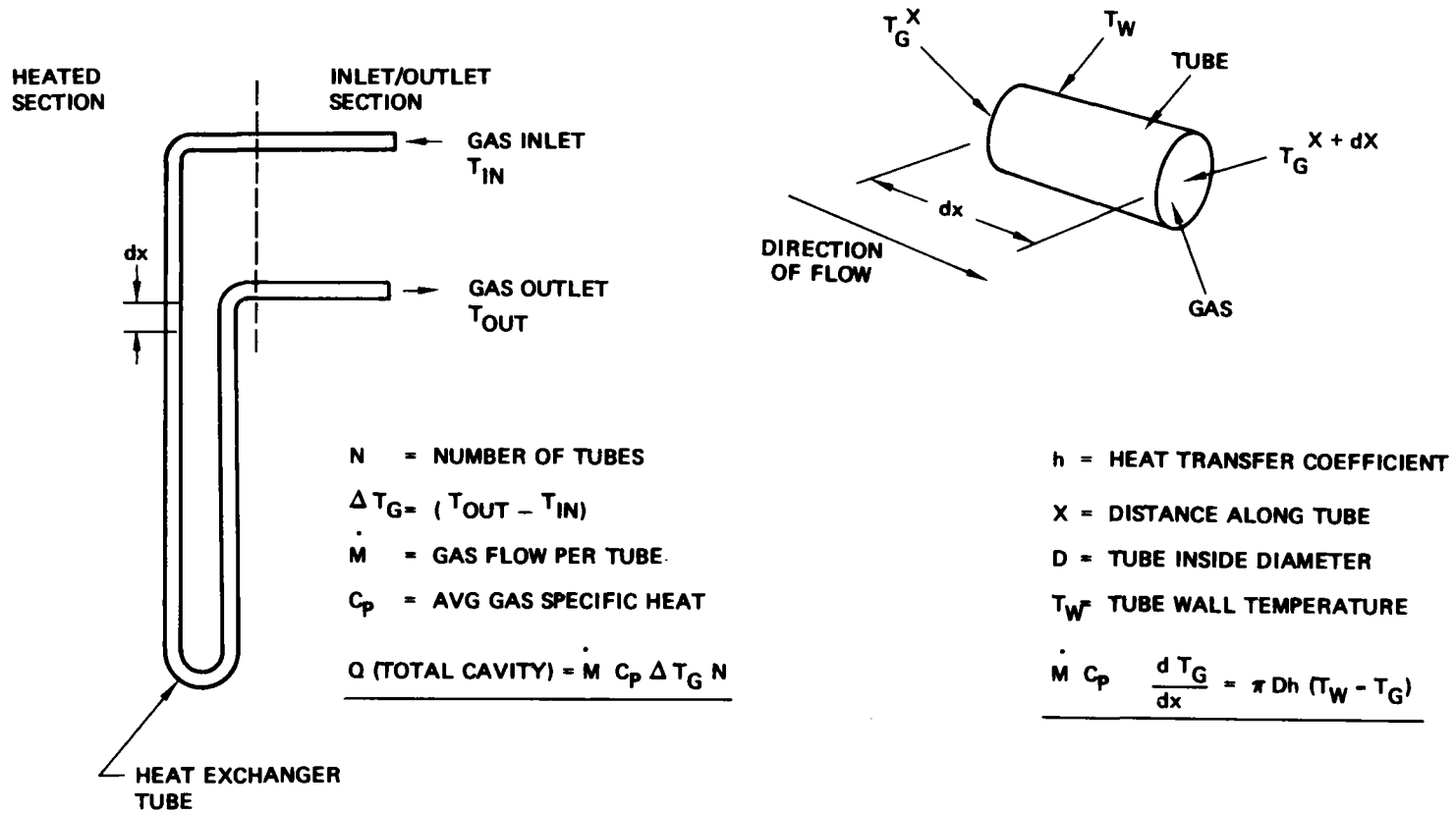


Figure 9-9. Analytical Models, Gas in Tube Heat Transfer

The tube wall-to-gas heat transfer is described, in general, by

$$\dot{m} C_p \frac{dT_G}{dx} = \pi Dh (T_W - T_G) \quad (9-4)$$

(symbols defined on figure 9-9)

or

$$\dot{m} C_p \frac{dT_G}{dx} = \pi KN_u (T_W - T_G) \quad (9-5)$$

$$N_u = \frac{hD}{K}$$

K = gas thermal conductivity

and by substitution of Reynolds and Prandtl numbers, where

$$R_E = \frac{4 \dot{m}}{\pi D \mu}$$

$$P_R = \frac{C_p \mu}{K}$$

μ = gas viscosity

$$\frac{dT_G}{dx} = \frac{4 N_u}{R_E P_R D} (T_W - T_G) \quad (9-6)$$

Integrating for gas temperature change, ΔT_G , and length of tube, ℓ , yields

$$\Delta T_G = \frac{4 N_u}{R_E P_R D} \int_0^{\ell} (T_W - T_G) dx \quad (9-7)$$

and defining an effective tube-to-gas temperature gradient,

ΔT_E , such that

$$\Delta T_E = \int_0^{\ell} (T_W - T_G) dx$$

Equation 9-7 can be rewritten in ratio format as

$$\frac{\Delta T_G^*}{\Delta T_E^*} = \frac{Nu^* \ell^*}{R_E^* P_R^* D^*} \quad (9-8)$$

which is the defining criterion for accurate simulation of gas-to-tube temperature gradients in the subscale model.

The fundamental thermal similitude requirements are defined by equations 9-3 and 9-8. Next, a few types of scale models will be postulated and their physical properties derived by use of these formulas.

First, 9-8 can be simplified by assuming that turbulent flow in the prototype is reproduced in the model heat exchanger. In the range of interest here,

$$Nu = 0.0215 P_R^{0.6} R_E^{0.8} \quad , \quad \pm 10\%$$

or

$$Nu^* = (R_E^*)^{0.8} (P_R^*)^{0.6}$$

Then equation 9-8 reduces to

$$\frac{\Delta T_G^*}{\Delta T_E^*} = \frac{l^*}{(R_E^*)^{0.2} (P_R^*)^{0.4} D^*} \quad (9-9)$$

Case I, Prototype gas at equal temperatures in model and exact scaling of heat exchanger tubes.

$$\text{Where: } P_R^* = N^* = Cp^* = \Delta T_G^* = \Delta T_E^* = \mu^* = 1$$

$$D^* = l^* = R$$

Then, from 9-3,

$$\dot{m} = R^2 \quad \text{so that } R_E^* = R$$

and from 9-9

$$R = 1$$

which shows that exact modeling of temperatures with the prototype gas in the model can only be accomplished at $R = 1$ or full size.

Case II, Prototype gas with exact scaling of tubing dimensions and distorted values of ΔT_E and ΔT_G .

$$\text{Here, } P_R^* = N^* = Cp^* = \mu^* = 1$$

$$D^* = \ell^* = R$$

Then, from 9-3 and 9-9,

$$\Delta T_G^* = \frac{R^2}{\dot{m}^2} \quad \Delta T_E^* = \Delta T_G^* (R_E^*)^{0.2}$$

$$\text{since } \dot{m} = R_E^* \mu^* D^*$$

Combining yields

$$\Delta T_G^* = \frac{R}{R_E^*}$$

$$\Delta T_E^* = \frac{R}{(R_E^*)^{0.8}}$$

This set of conditions is depicted on figure 9-10 for a range of R_E^* . These are dimensionally true scale models using helium gas. The scale size ratio of these model designs is 1:17.3, assuming a 300-MW_{th} prototype and a 1-MW_{th} model. The variable of interest is Reynolds number. The prototype flow is turbulent with a Reynolds number of about 60,000. Turbulent gas flow must be maintained in the model so the minimum feasible ratio of model-to-prototype Reynolds number is about 0.083 (for model Reynolds numbers above 5,000).

As evident, the gas temperature rise in the model cannot be maintained equal to that in the prototype. At the minimum Reynolds number ratios, it is only 70% of the prototype temperature rise. Furthermore, even though the heat flux from the tube to gas is matched (a requirement on figure 9-10), the temperature difference, tube to gas, at this condition is only about 38% of the gradient in the prototype.

Another model design compromise has been investigated that increases the feasibility of using helium gas. The compromise is to distort the tubing size in the

model. Since the heat exchangers form a continuous surface over much of the upper cavity wall, it makes little difference in the overall performance to use tubes slightly different in diameter and two or three times longer than true scale. Viewed from the cavity, the heat exchanger panel exhibits net radiant exchange properties that depend on tube spacing (in relation to tube diameter), tube average temperatures, and radiant surface properties (tube materials) being preserved. The same is true for tubes viewing one another.

Case III, Prototype gas, exact matching of temperatures and heat fluxes, distorted scaling of tubing diameter and length.

$$\text{here, } P_R^* = C_p^* = \Delta T_G^* = \Delta T_E^* = \mu^* = 1$$

and new symbols are needed to define the distortion of diameter and length. For example

$$G = \frac{\text{Tube Length in Model}}{\text{True Scale Model Tube Length}} = \frac{l^*}{R}$$

and

$$H = \frac{\text{Tube Inside Diameter in Model}}{\text{True Scale Model Tube Diameter}} = \frac{D^*}{R}$$

Also preservation of model heat transfer area with distorted tubes requires

$$G H N^* = 1 \quad \text{or} \quad N^* = \frac{R^2}{D^* l^*}$$

This also ensures maintenance of proper spacing between tubes in proportion to tube diameter.

Then, equation 9-3 yields

$$\frac{\dot{m}^*}{l^* D^*} = 1 - \frac{R_E^*}{l^*}, \quad l^* = R_E^*$$

and 9-9 yields

$$l^* = (R_E^*)^{0.2} D^*, \quad D^* = (R_E^*)^{0.8}$$

Then

$$N^* = \frac{R^2}{(R_E^*)^{1.8}}$$

and

$$G = \frac{R_E^*}{R} \qquad H = \frac{(R_E^*)^{0.8}}{R}$$

There are few limitations on distortion of tubing diameter. Length distortions are more restricted. Figure 9-11 describes two types of tube routing modifications that can be used to distort the length of tubes in the model.

The prototype receiver has three tiers of heat exchanger panels. If the number of vertical tiers is preserved, a distortion in scale length for tubes can be accomplished by changing the number of vertical passes per tube. These cases are shown across the top of figure 9-11. This compromise preserves the difference in heat transfer capability exhibited by the three vertical tiers in the prototype that occurs because of the moderate vertical gradient of incident heat flux. However, the radiant interchange between adjacent tubes is not preserved.

If the number of passes (the prototype "U"-shaped tubes) are retained in the model design, the tube length distortion can be accomplished by reducing the number of tiers used in the model. Starting with three tiers in the prototype, the distortion from true model scale that are available are 1.5 and 3.0, as shown vertically on figure 9-11.

This compromise preserves tube-to-tube radiation exchange and average tube-bank temperature, as viewed from the interior of the receiver. However, the effect of vertical incident flux gradients on the three tiers of heat exchanges is masked, particularly if the three tiers are replaced by one.

Tubing distortion by reducing the number of tiers is preferred over changing the number of passes per tube. This provides better reproduction of tubing temperatures. The substitution of fewer tiers of heat exchangers causes only a few percent error in local tubing temperatures while preserving the overall heat transfer to more distant points such as the cavity aperture.

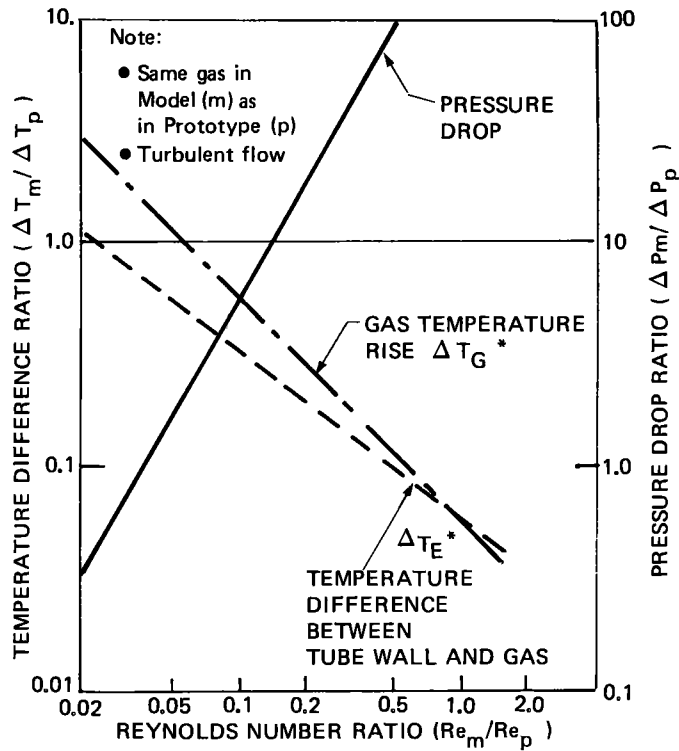


Figure 9-10. Exact Geometric Scaling—Scale Ratio = 0.0577

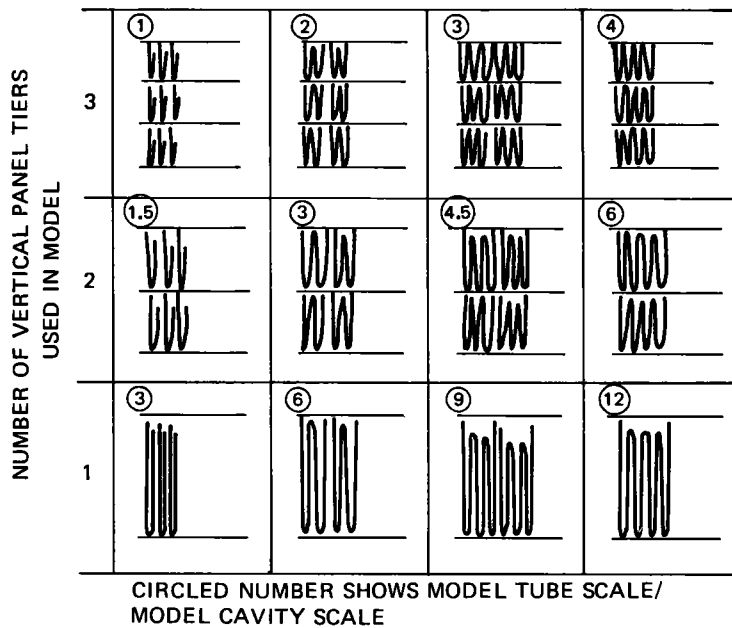


Figure 9-11. Tubing Distortions Considered for Scale Model

Figure 9-12 describes the heat exchanger tubing design requirements for 1-MW_{th} bench model receivers with helium. As developed earlier, the value of L^* , N^* , D^* , and G are functions of Reynolds numbers alone. With these designs, the tube and gas temperatures and the local heat transfer coefficient (tube-to-gas) are the same in model and prototype. The preferred tube size distortions from figure 9-11 are spotted on the figure. Details for these three acceptable helium bench model designs are compared on figure 9-13 with the prototype commercial receiver. The design using one tier of heat exchangers is preferred because the Reynolds number of 11,520 allows operation at significantly lower than maximum flow rate without the onset of laminar flow. The design with three tiers is now acceptable (where it was not on figure 9-10) because the tubing diameter is larger than scale, being 0.099 times the size of the prototype rather than the 0.0577 for the true scale modeling. This results in accurate matching of gas temperatures with the prototype.

Other more readily available working gases can also be used in the 1-MW_{th} model. These require a new evaluation of the basic equations for similitude (9-3 and 9-9).

Case IV. "Alternative Gas, Exact Matching of Temperatures and Heat Fluxes, Distorted Scaling of Tubing Diameter and Length."

Here, $\Delta T_G^* = \Delta T_E^* = 1$

$$G = \frac{l^*}{R}, \quad H = \frac{D^*}{R}, \quad N^* = \frac{R^2}{D^* l^*}$$

Equation 9-3 yields

$$\frac{\dot{m}^* C_p^*}{D^* l^*} = 1$$

and since now $R_E^* = \frac{\dot{m}^*}{\mu^* D^*}$

$$l^* = R_E^* P_R^* K$$

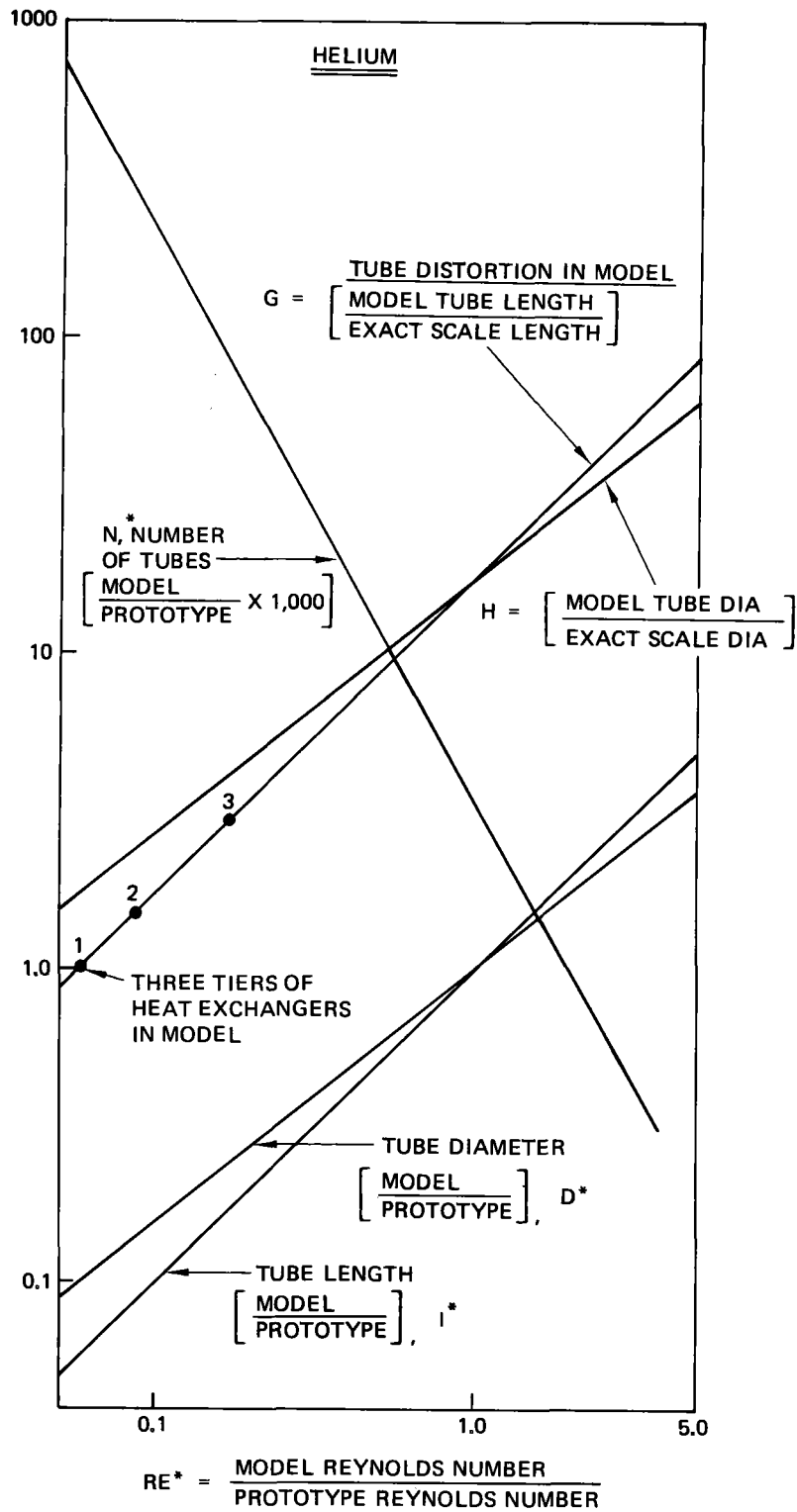


Figure 9-12. Feasible 1-MW_{th} Bench Model Heat Exchanger Designs With Helium

	Commercial 300 MW _T receiver (Three tiers)	1 MW _T helium bench model receivers		
		Three tiers $\frac{\text{Tube scale}}{\text{Cavity scale}} = 1.0$	Two tiers $\frac{\text{Tube scale}}{\text{Cavity scale}} = 1.5$	One tier $\frac{\text{Tube scale}}{\text{Cavity scale}} = 3.0$
Total number of tubes	4,200	2,360	1,135	324
Tube I.D. (CM)	2.22	0.220	0.311	0.537
Tube heated length (M)	9.76	0.565	0.839	1.707
Reynolds number at maximum gas flow	66,600	3,840	5,760	11,520
Vertical height of heat exchangers on receiver wall (M)	16.8	0.97	0.97	0.97

Figure 9-13. Acceptable Designs for the 1-MW_{th} Bench Model Heat Exchanger With Helium

Equation 9-9 yields,

$$L^* = (R_E^*)^{0.2} (P_R^*)^{0.4} D^*$$

And combining equations yields

$$D^* = (R_E^*)^{0.8} (P_R^*)^{0.6} K^*$$

$$N^* = \frac{R^2}{(R_E^*)^{1.8} (P_R^*)^{1.6} (K^*)^2}$$

$$G = \frac{R_E^* P_R^* K^*}{R}$$

The design charts for superheated steam and air have been developed assuming these relationships and utilizing gas thermal properties at an average temperature of 677°C (1,250°F). They are shown on figures 9-14 and 9-15. Acceptable results are summarized on figure 9-16.

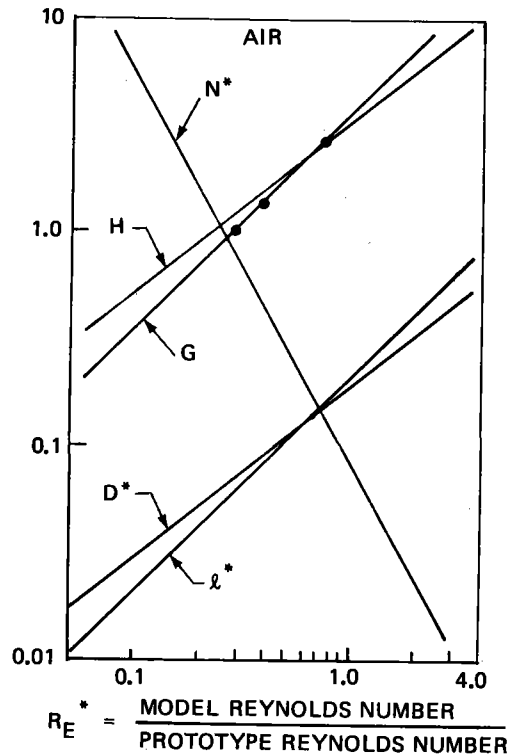


Figure 9-14. Feasible 1-MW_{th} Bench Model Heat Exchanger Designs Using Air, Exact Temperature Matching

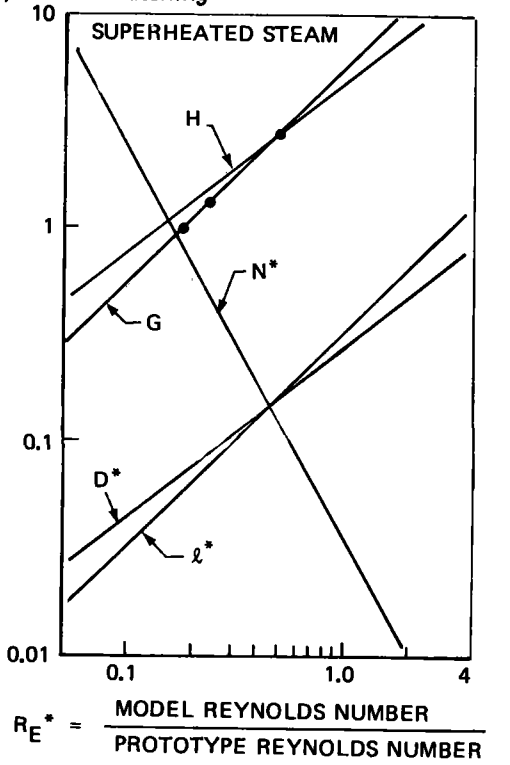


Figure 9-15. Feasible 1-MW_{th} Bench Model Heat Exchanger Designs With 500 psia Superheated Steam

Thus far a total of seven model heat exchanger designs have been identified, all meeting the requirements for thermal similitude, one using helium, three with air, and three with superheated steam. Flow Reynolds number has been used as a design variable and adjusted to provide the correct gas-to-tube heat transfer coefficient. Since Reynolds number can be expressed as:

$$R_E = \frac{(\text{mass flow rate})}{(\text{viscosity})(\text{diameter})}$$

Each of the seven designs are constrained to operate at a specific mass flow rate. From the heat transfer standpoint, there is no restriction on velocity or pressure level except that essentially incompressible flow must be maintained.

One objective described earlier is to define a minimum-cost model suitable for operation using air at a supply pressure of 0.943 MN/m^2 (135 psia). This allows open air flow during testing with the air supply provided by large industrial air compressors.

The one-tier model design described on figure 9-16 has a practical number of tubes (473) of sizes that can be manufactured without special skills. It is selected from among the seven candidates for further investigation.

The gas velocity and pressure losses have been examined for this model when operated at various inlet pressures. The data for model tube size of 0.380-centimeter (0.150-inch) inside diameter are shown on figure 9-17.

The velocity and pressure decreases due to kinetic and friction effects become excessive at the lower pressures examined. The practical lower limit of inlet pressure is about 1.72 MN/m^2 (250 psia).

Therefore, the fundamental equations must be referred to again and the possibility of further modifications examined to achieve acceptable velocity and pressure loss at a 0.943 MN/m^2 (135 psia) inlet pressure. The model tubing diameter will be increased, resulting in a distortion of gas and tube temperature simulation of the prototype. Model tubing lengths will be retained.

Case V. "Air Simulating Helium, Distorted Scaling of Tube Diameter To Accommodate Low Pressure Flow With Matching of Surface Heat Flux on I.D. of Heat Exchanger Tubes by Distortion of Gas Temperatures." Again, as in Case IV,

	Other 1-MW _{th} bench model receivers					
	Air			3.45 MN/m ² (500 PSIA) superheated stream		
	Three tiers	Two tiers	One tier	Three tiers	Two tiers	One tier
Total number of tubes	3360	1598	473	3480	1640	470
Tube I.D. (cm)	0.159	0.218	0.380	0.158	0.218	0.386
Tube heated length (m)	0.566	0.849	1.700	0.556	0.849	1.700
Reynolds number at maximum gas flow	18,950	28,600	56,000	11,850	17,780	35,430
Vertical height of heat exchangers on receiver wall (m)	1.01	0.997	0.991	0.974	0.963	0.958

Figure 9-16. Acceptable 1-MW_{th} Bench Model Designs Using Air or Superheated Steam as Working Fluid

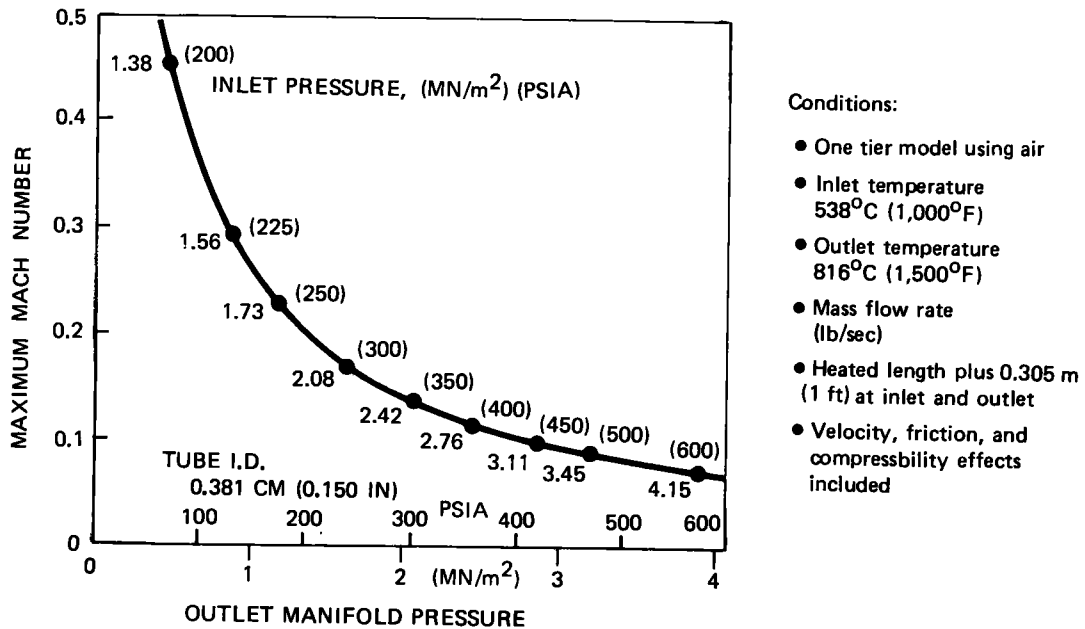


Figure 9-17. Gas Velocity and Pressure Loss for Candidate Heat Exchanger Design

air is used rather than the prototype helium gas.

Preserving surface heat flux requires that

$$N^* = \frac{R^2}{\ell^* D^*}$$

The value of ℓ^* will be maintained constant corresponding to one tier of model heat exchangers. As D^* is increased, the number of tubes will decrease. A new value of D^* will be found that results in acceptable pressure drop. The questions addressed here are: How much do gas temperatures need to be distorted to accommodate the larger tubing size? Also, what is the relationship between distortions of the two temperature gradient ratios ΔT_G^* and ΔT_E^* that satisfies the basic equations 9-3 and 9-9?

Equation 9-3 can be written

$$\Delta T_G = \frac{1}{R_E^*} \text{ (const. I)}$$

$$\text{where (const. I) = } \frac{\ell^*}{\mu^* C_p^*}$$

which are all defined.

Equation 9-9 is

$$\Delta T_E^* = \Delta T_G^* D^* (R_E^*)^{0.2} \text{ (const. II)}$$

$$\text{where (const. II) = } \frac{(P_{R^*})^{-4}}{\ell^*}$$

is also defined.

Combining equations

$$\Delta T_E^* = \frac{D^* (\text{const I}) (\text{const II})}{(R_E^*)^{0.8}}$$

Figure 9-18 describes the values ΔT_E^* and ΔT_G^* as functions of R_E^* and D^* . (The exact temperature-matching case that occurs at $R_E^* = 0.845$ and $D^* = 0.1706$ is noted.)

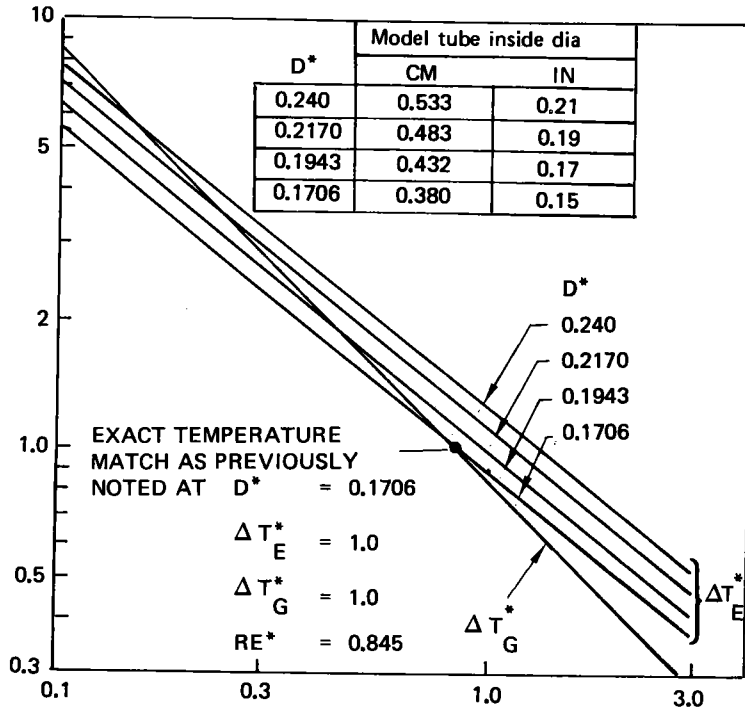


Figure 9-18. Effect of Tubing Distortion for Reduced Pressure Drop on Gas Temperatures and Gradients

Upon selection of a value for D^* , the pair of functions ΔT_E^* and ΔT_G^* vs R_E^* on figure 9-18 define the range of full-power (1-MW_{th}) gas temperatures that occur as functions of mass flow through the model (i.e., R_E^*). Moving to the left with reduced mass flow rates increases gas temperature change, ΔT_G^* , because of the longer time spent in the heated cavity. It also results in larger temperature difference between tube and gas, ΔT_E^* , because of the lower value of heat transfer coefficient at reduced Reynolds number.

The original design, $D^* = 0.1706$, which exhibits exact temperature matching can be operated to the left of $R_E^* = 0.845$. Lower pressure drop will occur because of the reduced gas velocity. It is equally valid to consider the use of larger tubing to accomplish the same purpose. This is advantageous because relief from high gas velocities and excessive pressure drop is achieved with small increases in tube diameter because of the strong dependence of pressure drop on diameter.

A tubing size of 0.483 centimeter (0.190 inch) has been selected for the low-pressure receiver design. Its pressure drop and gas velocity performance is shown on figure 9-19 as functions of gas inlet temperature and pressure. At an inlet pressure of 0.943 MN/m² (135 psi), rather large increases in gas-temperature change (i.e., reduction of inlet temperature) are required to accomplish acceptable gas velocities.

In conclusion, the performance of the prototype helium-in-tube heat exchangers has been reproduced exactly in model heat exchangers that use high pressure inlet gas. Either helium, superheated steam, or air can be used to accomplish nearly perfect matching of the gas and tube temperatures and heat fluxes. The design using air has been further modified to operate at an inlet pressure of 0.945 MN/m² (135 psia) and found to require up to 60% more temperature gradient from tube-to-gas and 40% more gas-temperature change to satisfy the velocity and pressure drop requirements of a prudent design.

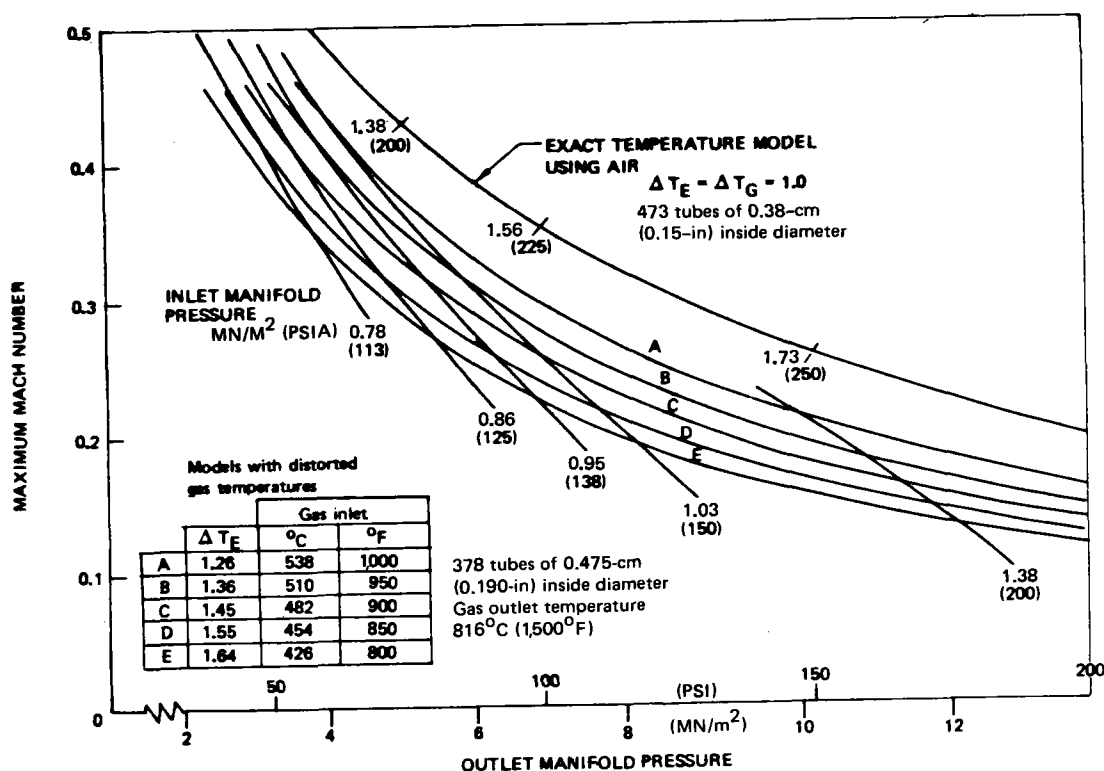


Figure 9-19. Distortion of Model Temperatures To Accommodate Low Pressure Flow

Section 10.0

10-MW_e SCALE PILOT PLANT

The development schedule to a 100-MW_e commercial STC plant should include a closed-cycle pilot plant after completion of the model receiver tests (discussed in section 9.0). A closed-cycle pilot plant would demonstrate the performance and operational capability for the commercial plant at a much reduced investment. To hasten pilot plant development at minimum cost, EPRI advanced the concept of a 10-MW_e-rated plant that would perform all the functions of a 100-MW_e plant, but that would initially use only a quadrant of a field and turbomachinery appropriately rated at approximately 2.5 MW_e. The cost economy of such a rated pilot plant is obvious. Late in the current contract, EPRI requested Boeing to examine the feasibility and adaptability of the 10-MW_e-rated pilot plant concept to the closed-cycle, high-temperature central receiver concept under study. The initial results of the investigation reported in this section are very encouraging.

Section 10.1 discusses the implementation of this concept in the receiver area. A survey of turbomachinery availability and adaptations required to the 10-MW_e-rated plant concept are covered in section 10.2. While the investigation to date has not included implementation of a storage concept(s), the discussions and results reported in sections 6.0 and 8.0 give Boeing confidence that thermal storage could be adapted to the pilot plant. A recommended commercial plant development schedule, with the pilot plant fitted in, is covered in section 10.3.

10.1 CONCEPTUAL DESIGN OF PILOT PLANT RECEIVER

The present commercial-sized receiver design was evolved by means of design trade studies that maximize its operating efficiency and reliability; minimize technical risk, initial cost, maintenance, and service; and, in general, ensure the economic viability of the plant. Some of these factors are of secondary importance for the pilot plant receiver. Also, many design factors are affected by scale size, particularly the relative cost of components such as tower and collector field, and the significance of minimum-cost power production as affected by efficiency and maintenance cost.

There are two main factors, in addition to the reduced importance of power production cost, that result in a pilot plant receiver design significantly different from the commercial design. These factors are: utilization of a quadrant field and the possible incorporation of turbomachinery using air rather than helium as the working fluid.

The bench model receiver designed for use in the 1-MW_{th} ERDA solar thermal test facility uses a quadrant field of solar collectors. The bench model receiver, described in section 9.0, is adapted from the commercial plant design to operate in the quadrant field with rim angles of 18 and 36 degrees rather than the 68-degree angles in the commercial plant. This is accomplished by relocating the aperture at the opposite end of the receiver cavity and orientating the assembly so that the vector normal to the aperture plane is directed toward the center of the collector field quadrant (i.e., the "bullseye aperture"). By this means, the narrow rim angle solar flux continues to impinge first on the bare hemispherically shaped walls of the cavity rather than on the heat exchanger panels. Its diffusion and reflection onto heat exchangers remains identical in principle to the manner in which concentrated solar input flux is managed in the commercial receiver. There are differences in detail, but the conceptual design appears to be feasible and practical to implement. This same approach is proposed for the pilot plant receiver when used with a quadrant field.

A number of receiver design studies have been conducted in conjunction with the investigation of alternative types of closed-cycle turbomachinery for the pilot plant.

If a closed-cycle helium machine is used it will result in the smallest receiver size per unit heat transfer. The helium gas provides higher convective heat transfer between gas and tube. With a higher heat transfer coefficient the tubing temperature is more closely coupled to gas temperature, allowing higher heat flux at equal tubing and gas outlet temperatures. Also, even though the heat transport per unit volume flow is about equal for helium and air at equal pressure and temperature, the sonic velocity of helium is much higher. This allows higher design flow velocity and smaller heat exchangers to be utilized at equal pressure loss.

Air is the alternative working gas, which may be used in the 100-MW_e-rated, 2.5-MW_e-output pilot plant. Data have been prepared that compare the heat transfer

capability of air-in-tube receiver heat exchanger designs with the helium-in-tube baseline design. In particular, the receiver operating pressure is allowed to vary so that different closed-air-cycle gas turbines can be evaluated.

The baseline gas-cooled receiver design accommodates the strong sensitivity of heat exchanger design lifetime to peak tubing temperature. Tubing temperatures are dominated by heat transfer with the coolant gas rather than the cavity environment. A flow control system is provided for dynamic control of gas outlet temperatures and thereby maximum tube temperatures. Even at maximum heat loads, the heat exchanger tubing can be controlled to within 39°C (70°F) of the outlet gas, if helium is used.

Figure 10-1 describes heat exchanger performance at maximum heat load using air as the working fluid. The receiver air pressure is varied along with the temperature difference between outlet gas and the heat exchanger tube. The tube size, routing, and friction pressure loss are equal for all these designs, being equal to the helium gas prototype. Moving to the right on figure 10-1 the tubing temperatures increase significantly and the Mach number approaches limiting values for gas-in-tube flow at these lengths-to-diameter ratios.

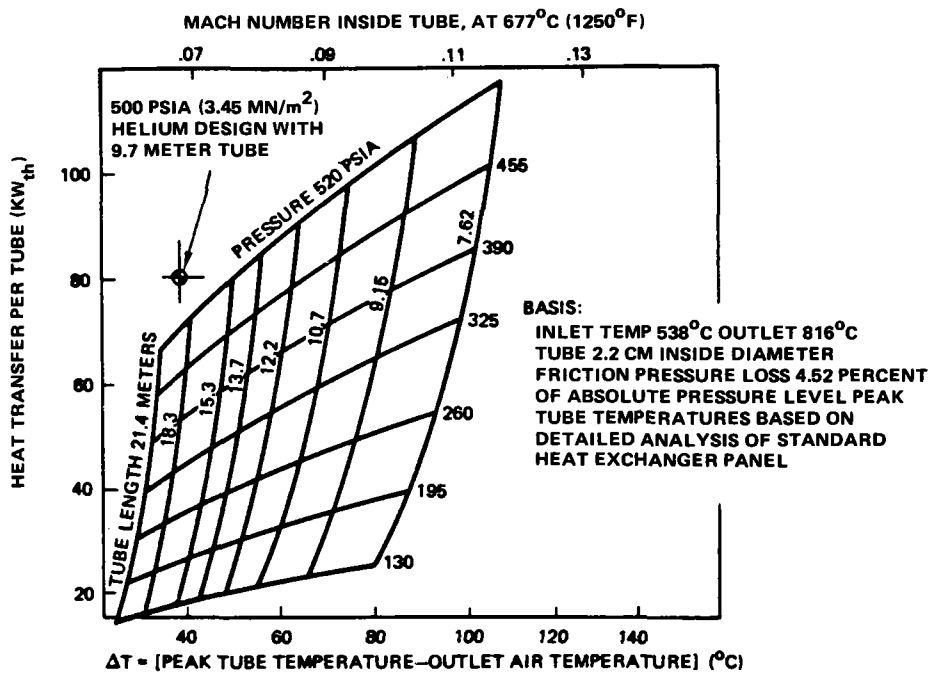


Figure 10-1. Relative Performance of Air-in-Tube versus High Pressure Helium-in-Tube Heat Exchangers

Other tubing diameters were considered, but the total surface area required for equal heat transfer at equal tube excess temperature is not greatly influenced. The heat transfer area requirement increases slightly with increasing tube diameter for equal air-outlet and tubing temperatures.

Figure 10-1 shows two things. First, low-pressure air designs can be accomplished that are compatible with the temperature limits for superalloy tubing. Second, the heat transfer area is twice that required for helium-in-tube heat exchangers at equal gas pressure and temperature and tubing temperature. The area requirement increases dramatically at lower air pressure.

10.2 PILOT PLANT TURBOMACHINERY

Survey and analysis efforts have concentrated on the availability and adaptability of turbomachinery at ratings up to 2.5 MW_e . The major consideration was that the machines either be closed cycle, or adaptable to closing the cycle, as this is an essential part of the pilot plant demonstration. Discussions in section 5.0 show that the same cycle technology can be applied for closed air and helium, so pilot plant test gas selection is less important than adherence to a closed cycle. Results of the investigations with turbomachinery suppliers are separately reported for closed helium and air machines in subsequent paragraphs.

10.2.1 Closed-Cycle Helium Turbomachinery

A request was sent to Brown, Boveri and Co. Ltd. (BBC) for an ROM cost estimate and availability date of a 10-MW_e helium turbine of the same design as the baseline cycle (i.e., maximum pressure of 3.45 MN/m^2 (500 psia) and a turbine inlet temperature of 816°C ($1,500^\circ\text{F}$)). The response from BBC was that the turbogroup could be built and available 3-4 years from an initiation date. Cost would be \$1.3-\$2.0 million as of April 1976. Included with the turbogroup would be a lubrication and sealing system, control equipment, and internal instrumentation. A reduction gear, generator, and starting system were not included in the quotation.

The advantage of the 10-MW_e turbomachinery for the rated pilot plant is that it inherently has full capability and, with an easily-accomplished reduction in pressure level, it can be used for the lower megawatt rating (2.5 MW_e) of an initial quadrant utilization of the plant.

10.2.2 Closed-Cycle Air Turbomachinery

Existing Turbomachinery. A determination was made of the existing turbomachinery of 2.0-2.5 MW_e rating, and letters were sent to the owners requesting information on current disposition of the machines. At contract conclusion, the only response was from the Hokkaido Electric Power Company of Toyotomi, Japan, who owns a high-pressure 2-MW_e closed-cycle air plant. Currently the plant is shut down because of a natural gas shortage. The uncertainty of the problem has caused Hokkaido to delay a decision on the fate of the plant. If it is surplused, the plant would be a prime closed-cycle air candidate for a 10-MW_e plant quadrant. While the plant design point has not been definitely confirmed, it is expected to be within the following limits: 760⁰-816⁰C (1,400⁰-1,500⁰F) turbine inlet temperature and a maximum pressure of 2.07-2.76 MN/m² (300-400 psia). This would give an output of approximately 2 MW_e.

Turbomachinery Adaptable to Closed-Cycle Operation. The potential for closing the cycle of existing open-cycle air machines has been examined, with principal U.S. suppliers of turbomachinery, up to the rating range desired. Summaries of correspondence and discussions carried on with Solar, a division of International Harvester, and AiResearch of Arizona, a division of the Garrett Corporation, in terms of their respective turbomachines, are reported below. Discussions of pressures considerably removed from the 3.45-MN/m² (500-psia) concept baseline should not detract from interest and suitability. The Boeing modeling capability to reduce pressure, discussed in section 9.0 for test receiver applications, is appropriate.

Solar has an open-cycle recuperated Centaur system that could be modified into a low-pressure closed-cycle air system to produce 2.0-2.5 MW_e. The cycle planned for this turbine, after discussions with Solar, would have a turbine inlet temperature of 816⁰C (1,500⁰F) and a maximum pressure of 0.86 MN/m² (125 psia), with the pressure at the compressor inlet being increased to reach the operating pressure. Modifications to the turbomachinery would be minimal; most of the changes occur in the ducting and recuperator. The cost estimate for an unmodified recuperated Centaur system would be \$700-\$750,000.

Garrett AiResearch has several surplus recuperated open-cycle turbomachines, of the Model 831-200 variety, that could be modified into a low-pressure closed-cycle air system producing 0.35 MW_e. The design operation conditions for this

turbine would be 816°C (1,500°F) turbine inlet temperature and 1.21 MN/m² (175 psia), with pressure at the compressor inlet increased to achieve this level. Modification cost estimates from Garrett are about \$260,000. This does not include the price of the surplus equipment. The engine does not produce the desired 2.5 MW_e but it could be used with either a smaller segment of the pilot plant field or with the bench model.

10.3 PILOT PLANT SCHEDULE

A recommended commercial plant development schedule is shown on figure 10-2. The 1-MW_{th} model receiver design and test program is shown as being completed in mid-1978. The 10-MW_e scale pilot plant is shown below it with an extension into full 10-MW_e capability (dotted lines). The 100-MW_e commercial plant schedule is indicated at the bottom of figure 10-2.

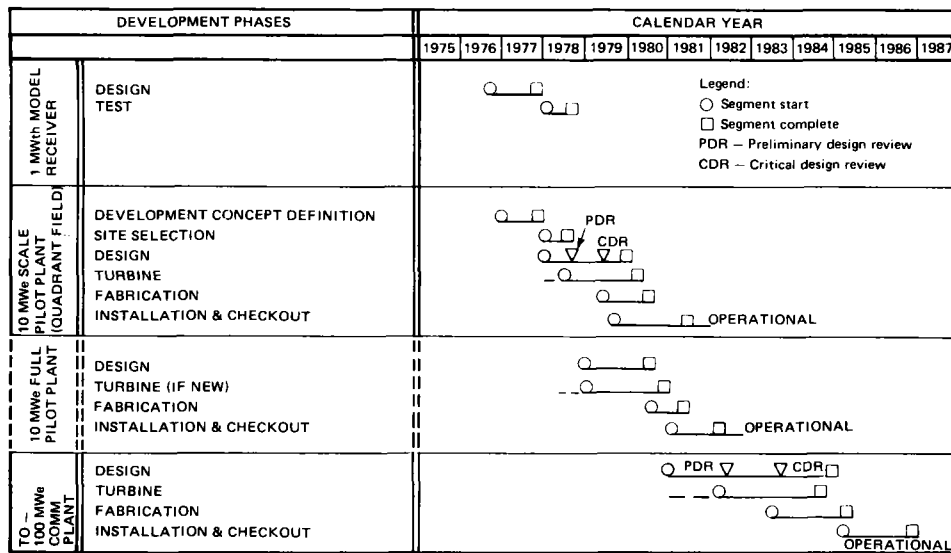


Figure 10-2. Commercial Plant Development Program

Section 11.0

CONCLUSIONS AND RECOMMENDATIONS

The 18-month study of the closed-cycle, high-temperature central receiver and its integration into a 100-MW_e solar plant has confirmed the predicted potentialities of the concept that led to the investigations. Prior sections of this report have discussed the central receiver, the supporting subsystems required for solar plant implementation, and plant operation. Costs have been presented at the subsystem and plant level.

The primary conclusions and recommendations, based on the results reported and an overview of the total study, are presented in this section.

11.1 CONCLUSIONS

Receiver

A closed-cycle, high-temperature central receiver, employing closed-cycle helium, is a promising choice for solar thermal conversion plants, in that:

- Technical feasibility has been exhibited in design, materials, performance, and integration into stand-alone and hybrid commercial plant operations.
- Receiver costs, while slightly higher than steam boilers, are such that overall plant costs are equivalent to that of a steam/Rankine-cycle solar plant due to the effectiveness of the closed cycle.
- The receiver can operate simply and effectively over a wide range of environmental and operational conditions.
- All the required technology for receiver design and implementation currently exists.
- Verification of commercial receiver performance and operation can be obtained in a development program with model and pilot plant phases that preserves the options of test facility and test gas selection.
- Adaptations can be made for use of closed-cycle air in the commercial plant receiver, should that option be desirable for other reasons.

Closed-Cycle Application and Turbomachinery

Utilization of a closed helium cycle in a commercial central receiver solar plant offers very distinct and attractive advantages over other cycle possibilities.

These are listed below:

- The highest efficiency of any cycle can be obtained with helium, which reduces the size and cost of all elements involved in collecting and processing (i.e., collector field, receiver, and storage) the heat to be converted to electrical energy.
- The selected cycle parameters (pressures, temperatures, and recuperator effectiveness) reduce the size of required turbomachinery and associated equipment.
- Closed cycles have a strong advantage over other cycles in the ability to assist and/or provide plant control and responsiveness over the variety of environmental and operational situations inherent in solar plants incorporating storage and load-following capabilities.

Should a closed helium cycle be unattractive to commercial customers, a closed air cycle may be utilized in a similar manner with only slight impact on performance and cost.

High-Temperature Materials

Two potential materials (Inconel 617 and Haynes 188) have been selected and tested successfully for high-temperature applications at 816⁰C (1,500⁰F). The major results are given below.

- Both materials performed excellently in thermal cycling tests simulating 30-year lifetimes of plant operation. Strength properties remained high at combined temperature and pressure levels to be experienced in plant operation. Surfaces were resistant to oxidation and to scaling loss. Dimensions remained relatively true.
- Both materials can sustain prolonged elevated temperature exposure without rupture. Test ruptures were obtained at approximately 1,090⁰C (2,000⁰F) after cyclic exposure at other temperatures. All failures were noncatastrophic, relieving concern for potential safety hazards in use.

Energy Storage

A survey and screening of storage system types shows that source-side (as opposed to load-side) energy storage is the preferred storage method and that with such thermal energy storage concepts these conclusions apply:

- A storage time of 6 hours gives near optimum total energy costs.
- The storage concept of 1/2 hour required for thermal buffering should also be source-side thermal storage.
- High-temperature thermal energy storage (TES) is technically feasible with near-term technology.
- Latent-heat (phase-change) storage and chemical energy storage are longer range technical solutions with significant promise.
- The latent-heat storage concept can become near-term technology with a vigorous development program.
- Latent-heat storage in fluoride salts is the preferred storage system for gas-cooled receivers in terms of size, implementation, and cost.
- All favored concepts (latent heat, sensible heat, and thermo-chemical) can be integrated into plant operation.

Plant Operation, Integration, and Costs

The closed-cycle central receiver concept, the turbomachinery, and storage concepts can be integrated into a commercially operational plant that can perform over the daily and yearly cycles and a variety of conditions. Some general conclusions from the study are:

- Best plant energy economics are achieved with receiver solar multiples of about two.
- Inventory control with closed-cycle gas-turbine operation provides unique and flexible load-following capabilities.
- Closed-cycle gas turbines provide zero generation-capacity loss when operating from storage temperatures below the normal (insolation loaded) turbine inlet temperature.
- Source-side thermal energy storage is an integral part of the solar plant and is involved in every major operating mode.
- A closed-cycle central receiver plant is competitive in cost with a steam/Rankine-cycle central receiver plant.
- A closed-cycle central receiver plant would be more flexible and responsive to controls than plants with other type cycles.
- The "strawman" plant provided by EPRI for comparative purposes served as an effective guide for directing study results.
- A closed-cycle commercial plant development schedule, with receiver model tests and pilot plant demonstrations, can be obtained using designs and technology developed in this study. Flexibility can be retained in these interim developments in model design and test gas selection while retaining the materials technology developed and the overall prototype plant simulation.

11.2 RECOMMENDATIONS

Recommendations for further technology development in certain subject areas may be found in the appropriate report sections. The intent here is to pull together those recommendations that build upon this completed study to bring the closed-cycle, high-temperature central receiver/solar thermal plant closer to commercial reality.

Several related efforts either currently being contracted by EPRI or in their near-term planning will be included in the recommendations to follow and will be noted in the text. These are an advanced thermal energy storage contract with Boeing (EPRI RP-788-1), plans for 1-MW_{th} model tests for competitive gas receivers, and the development concept for a 10-MW_e scale pilot plant.

For the high-temperature receiver, design and modeling verification should come from the 1-MW_{th} test in current EPRI plans. Options on test gas (air, helium, steam) should be carefully preserved until the test facility (ERDA CNRS, or IR) can be scheduled and the facility constraints entered into test model design. Heat exchanger test materials (Inconel 617 and Haynes 188) should be committed early to sustained high-temperature testing at temperatures above 760°C (1,400°F) so they can start to accrue operational time to evaluate material creep properties. The preliminary receiver planning work completed for a quadrant of the EPRI 10-MW_e scale pilot plant should be expanded to consider the direction of growth to a full-scale plant (i.e., should three more directed receivers be added, or one larger receiver with a bottom aperture). These considerations should be extended to gas supply lines, receiver(s) support, and cost trades. In a receiver-related area, the technology and experience gained elsewhere in interior insulation of high-temperature gas lines should be examined for solar plant applications to become more familiar with the practical problems, solutions, and costs extant in such a beneficial concept.

The cycle analysis work should be continued so the technology is available for use in pilot and commercial plants. For both plant types, the relative merits of closed-cycle air and helium in areas of cost, performance, and application should be detailed further so that either option may be selected and the turbomachinery availability options made less of a constraint. This should include comparisons of the cycles at both nominal and off-nominal conditions. The large control advantages of closed cycles over open cycles should be explored in more detail

and applied to plant operational mode switchovers/transients. Progress at the Oberhausen plant in Germany in the helium turbomachinery tests used there should be monitored carefully and their experience reflected in the solar plant's closed-cycle usage. The associated heat exchangers required in each plant cycle need more extensive work with expanded size, effectiveness, and cost trades, as well as concentration on thermal transients. In the 10-MW_e scale pilot plant, the work emphasis should be on the relative merits (and long-lead commitment) of obtaining an ultimate 10-MW_e turbogroup that can be scaled down by pressure control to an early quadrant field use (2.5 MW_e) or the reverse (i.e., obtaining a 2.5-MW_e-rated machine that can be scaled up), or for two separate turbogroups for both applications.

In the thermal energy storage area, it is recommended that an advanced thermal energy storage system development program be carried out in the areas of:

- Technical and economic feasibility
- Experimental verification

The first item is currently in work under EPRI contract RP 788-1 and will be extended with an ERDA contract. The second item, experimental verification, can come initially in two ways: either a test of a selected storage system with an independent heat source or a development schedule to test the storage concept using the model test receiver's waste heat as a source and solving a receiver test problem. Depending upon final selection of the receiver test facility, the test gas, and pressure, it is recommended that such a test be examined for timing and combined test cost sharing. The development program should include preparations for storage inclusion in the 10-MW_e-rated pilot plant.

The commercial plant operations and simulation work should be continued with the following objectives:

- Initiate real-time plant control studies.
- Expand the simulation analysis to include the real operational environment.
- Evaluate specific utility grid operations.

The first objective for real-time plant control studies would put together the transient performances of plant elements to determine the amount of control required for nominal and contingency plant operations. Then the types of control should be determined (pressure, temperature, or field), and the plant loops,

schematics, and operational modes selected to accomplish plant control. The second objective involves examining plant response and operations on an hourly basis and would examine variations (and impact) from the ideal or average day performance presumed in the initial study. The other objective covers specific utility grid applications such as load demands and the plant operations required to supply such loads. The EPRI contract with Westinghouse should be tied to this effort.

The above paragraphs all relate to bringing the receiver/plant studies along in a straight-forward development program. Other areas where additional work is required involves removing some of the constraints imposed on this study. The study considered Inyokern, California, as the plant site. Other study locations where less severe seismic conditions or less favorable yearly insolation profiles exist should be examined, and deltas in performance and cost determined. The study used dry cooling only for the solar plant. The use of available water at other sites to replace the gas-to-air precooler should be examined in terms of performance and costs. In a related area, the use of a bottoming cycle for closed-cycle gases should be examined due to the gain in efficiency possible, and the amortization of costs due to utilization of waste heat determined.

If the technology is developed and verified for ceramic heat exchangers operating at over 980°C ($1,800^{\circ}\text{F}$), then this technology should be applied to the closed-cycle gas systems. The efficiency gain is +4% for helium, for example, for the increased temperature delta reduces plant size and cost. These developments should be watched closely, and preliminary studies completed based on that eventuality.

APPENDIX
RECEIVER/TOWER INTEGRATION

The original concept examined had the turbomachinery located at the tower top to shorten the helium runs. A conventional horizontal installation, such as the concept depicted in figure A-1 was used. A turbomachinery installation as shown will fit within the 19-meter (63-feet) envelope available at the tower top location.

A storage location has also been identified in figure A-1. If storage is for the 6-hour study requirement, a mass of from 4-13 million kilograms (9-30 million pounds) is required, depending on energy storage concept selection. A tower to support this loading is considered impractical in terms of erection, equipment, and overall cost. For this reason, thermal energy storage is located at the base of the tower.

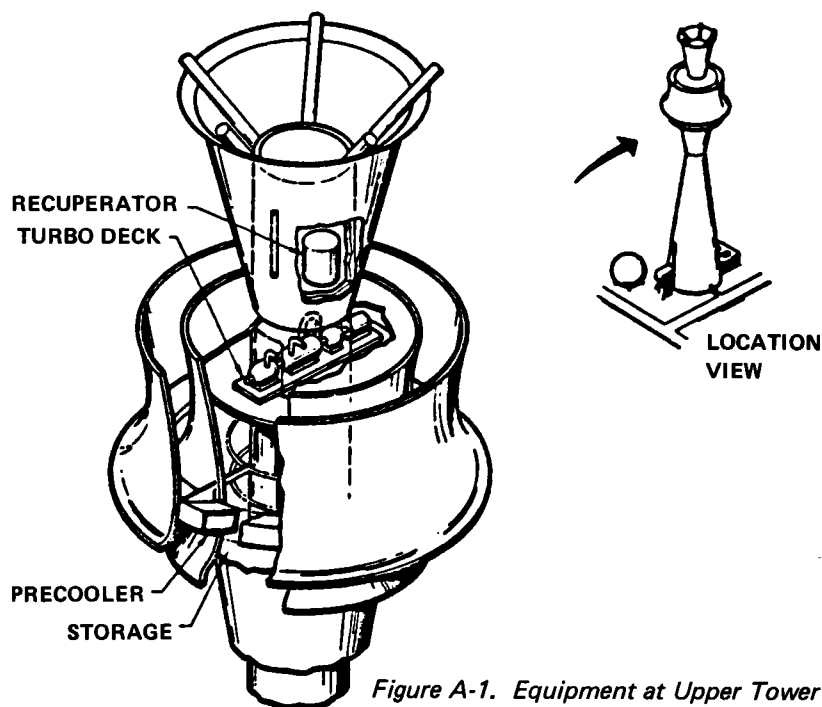


Figure A-1. Equipment at Upper Tower Location

An analysis was made to determine the impact of seismic loading on turbomachinery located at the tower top and to assess the effect on design of the tower shown on figure A-2. The receiver support structure was not modeled in this analysis; instead, the receiver was treated as a lumped mass connected to the concrete tower by a rigid structure.

The weight of the turbogroup shown in figure A-1, with recuperator, is about 400,000 kilograms (900,000 pounds). Precooler weight is another 360,000 kilograms (800,000 pounds). The estimated receiver weight, tabulated in section 3.2.4, is 1,510,000 kilograms (3,320,000 pounds). To place these values in perspective, the weight of a tower to support these elements is 30,000,000 kilograms (86,000,000 pounds) not including the footing.

A seismic analysis of the tower was performed to determine tower response and loads for a selected-design earthquake. The analysis used the response-spectrum method, which is well documented in the literature. Nodal responses were combined by the root-sum-square (RSS) method. Six lateral bending modes of the tower were included in the analysis. The frequencies of these modes are shown in the table below:

<u>Mode</u>	<u>Frequency (Hz)</u>	<u>Period (sec)</u>
1	0.5	2.0
2	1.88	0.53
3	4.74	0.21
4	9.11	0.11
5	1.46	0.068
6	2.10	0.048

The response spectra at the base of the tower were taken from page 13 of reference 1 and are shown in figure A-3. These response spectra are representative of a damage-threshold level and were chosen for design because they include the effect of the San Fernando earthquake of 1971. A damping value of 5% of critical was assumed for the analysis of the tower and is consistent with references 2 and 3. Therefore, the 5% damping response spectrum curve of figure A-3 was used.

The results of the analysis are shown on figures A-4 and A-5. The bending moments and shears of these curves were compared to the results of a standard ACI Code (307-69) analysis, reference 4, and were found to be approximately twice that of the ACI analysis.

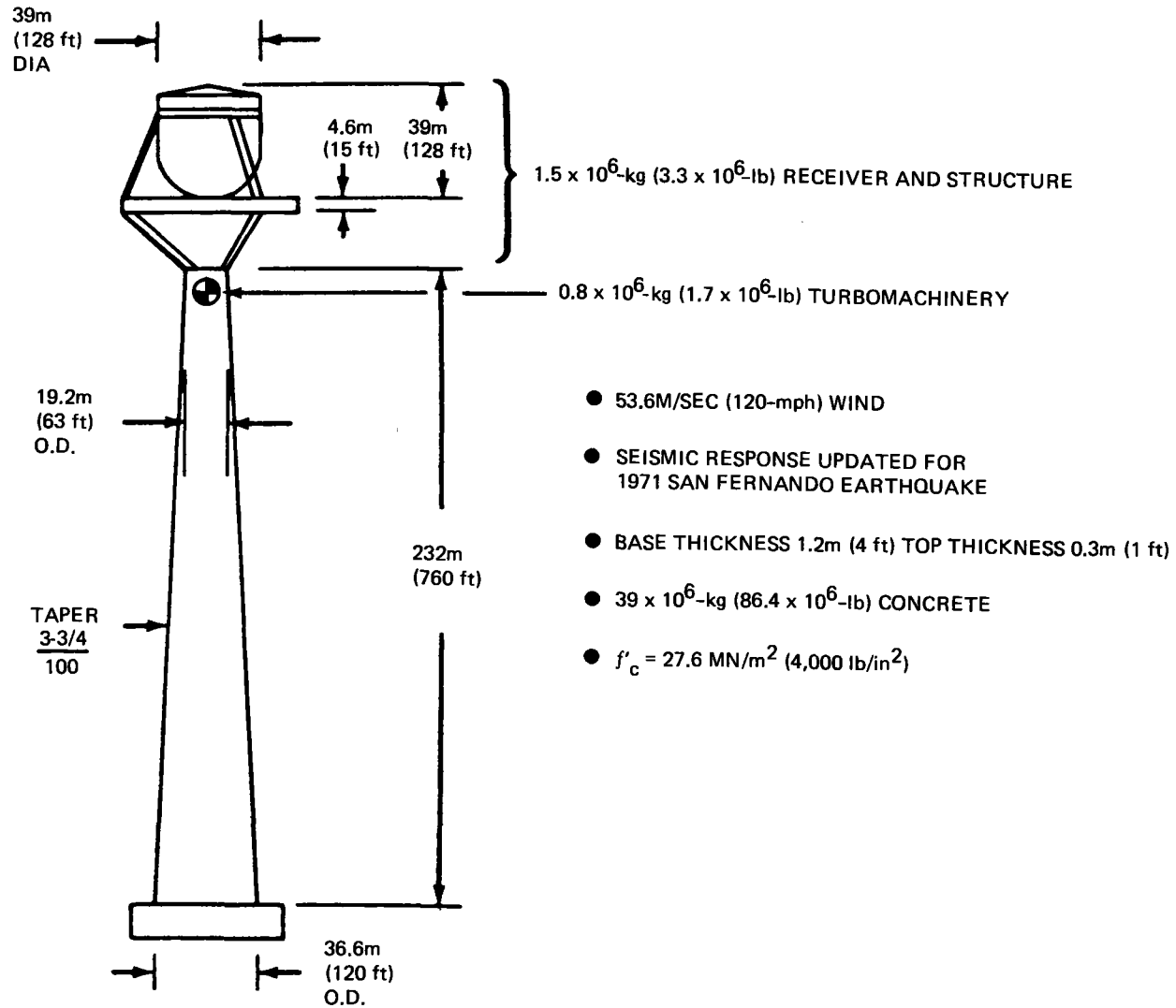


Figure A-2. Tower Configuration

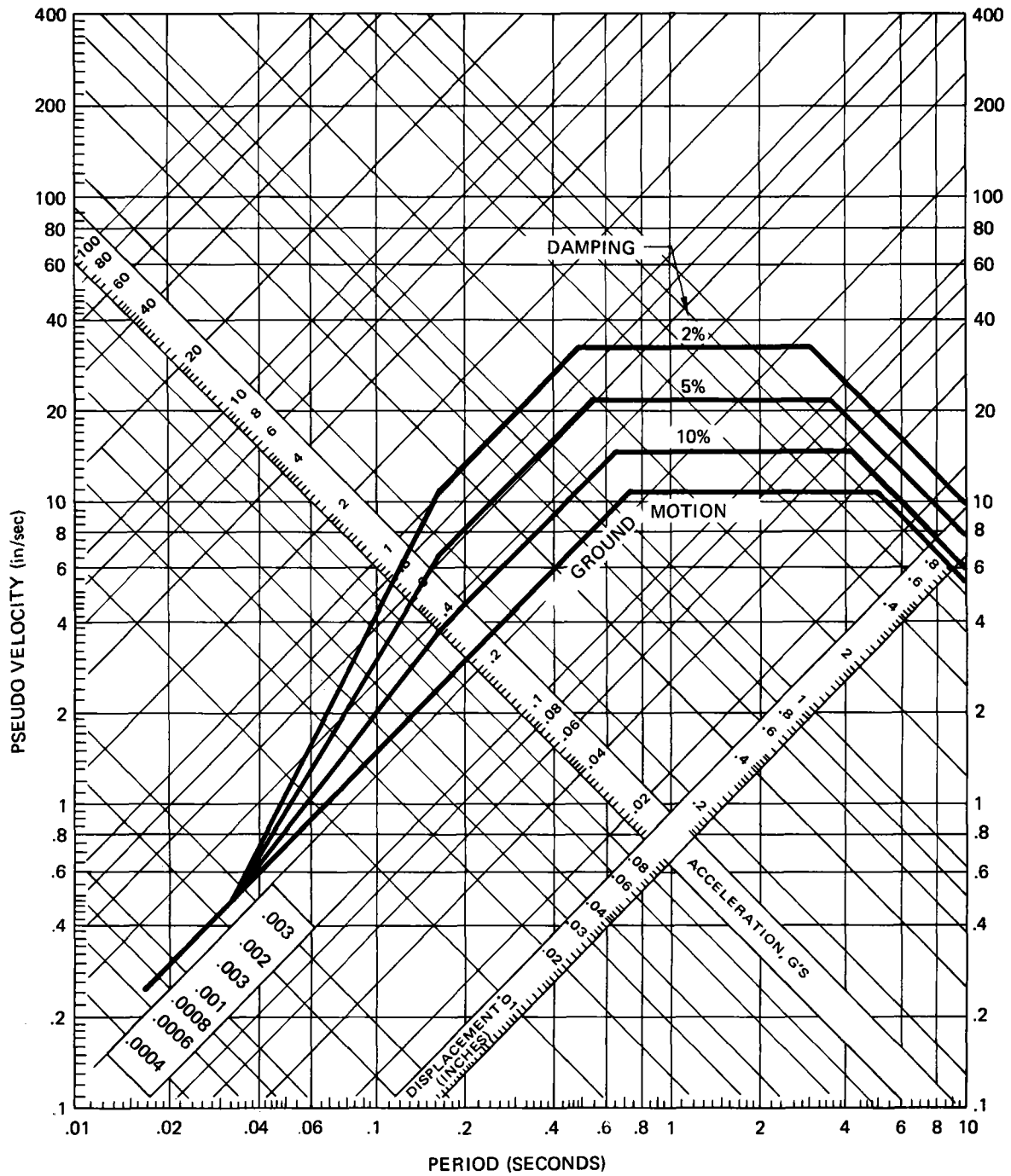


Figure A-3. Seismic Response Spectra

Since the turbomachinery is a small portion of the tower weight, the effect of its location (top or base) on tower loads and deflections is small. Conversely, as evidenced in figure A-4, the tower-top location will subject the turbomachinery to a lg lateral acceleration, which is an abnormal load environment for this type of equipment. Based on the lateral loading in the seismic environment, a base location was selected for the turbomachinery. The choice of ground-level storage necessitated long helium runs the length of the tower; therefore, locating the turbomachinery at the base did not further penalize the system. Figure A-6 shows a conceptual arrangement of the major equipment of a plant using a chemical thermal storage concept (precooler not shown) at the base.

In figure A-5, the wind loading is compared to seismic loads for the tower of figure A-2. Wind loads on the receiver were applied as moment, shear, and dead load at the tower top. Wind pressures were varied as a function of height for the various elements of the model. The pressures were based on a standard of 1,101 N/M² (23 psf) at 9-meter (30-ft) elevation. The seismic load environment is critical for design in Zone 3. In Zone 2, wind and earthquake loading is equally critical, and in Zone 1 the wind-load case prevails for design.

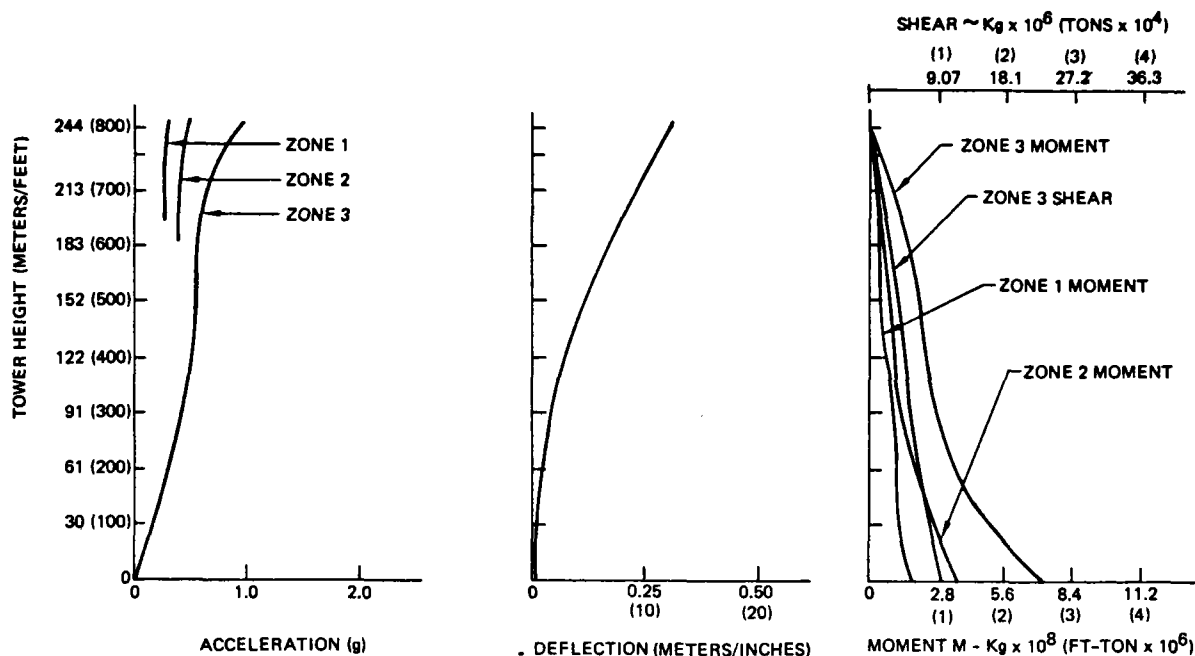


Figure A-4. Tower Seismic Analysis Results

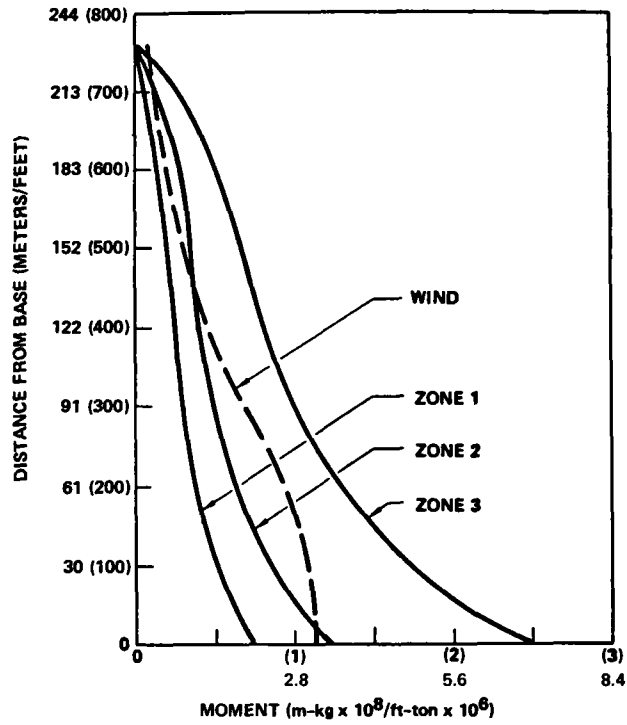


Figure A-5. Seismic and Wind Load Comparisons

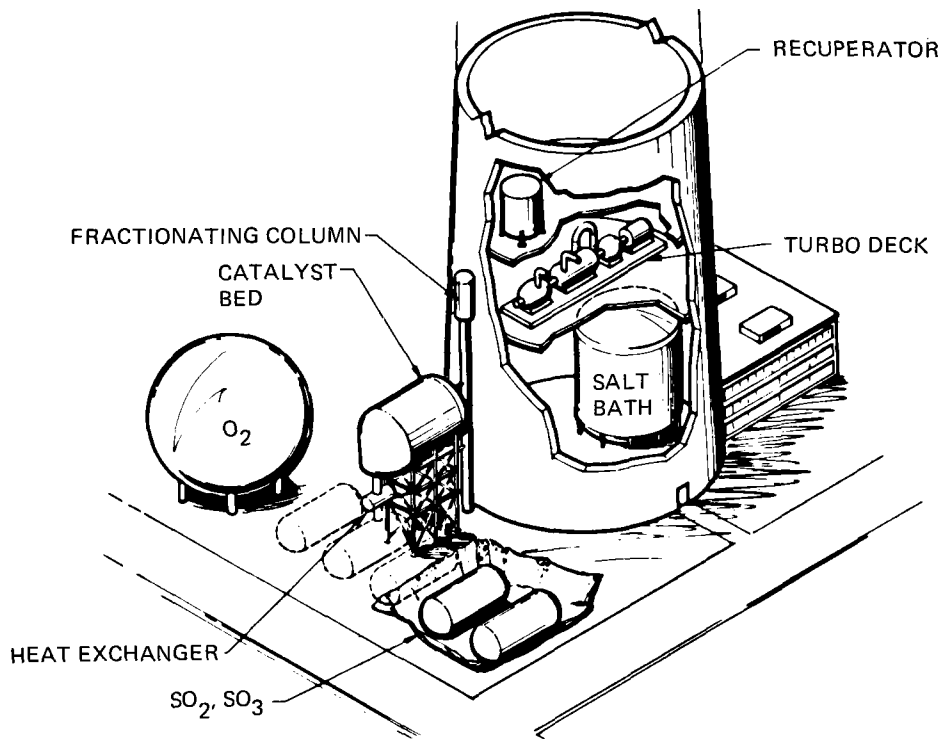


Figure A-6. Equipment at Lower Tower Location

REFERENCES

- A-1 An Evaluation of a Response Spectrum to Seismic Design of Buildings, Applied Technology Council, San Francisco, California, September 1974
- A-2 Rumman, Wadi S., "Earthquake Forces in Reinforced-Concrete Chimneys," Journal of the Structural Division, No. ST6, December 1964, pages 55-70
- A-3 Mauch, Lawrence C., and Rumman, Wadi S., "Dynamic Design of Reinforced-Concrete Chimneys," ACI Journal, September 1967, pages 558-566
- A-4 ACI Manual of Concrete Practice, Part 2-1972, American Concrete Institute, Redford Station, Detroit, Michigan